Development, characterization, and application of a novel scale-down apparatus for the investigation of the scale-up dependent CO_2/HCO_3^- stimulus in *Corynebacterium glutamicum*

DISSERTATION

Von der Fakultät Energie-, Verfahrens- und Biotechnik der Universität Stuttgart zur Erlangung der Würde eines Doktor-Ingenieurs (Dr.-Ing.) genehmigte Abhandlung

Vorgelegt von

Jens Buchholz

aus Hagen

Hauptberichter:	Prof. Dr.-Ing. Ralf Takors
Mitberichter:	Prof. Dr. Peter Neubauer

Tag der mündlichen Prüfung: 17. März 2015

University of Stuttgart
Germany

Institut für Bioverfahrenstechnik

2015

Meiner Familie

In a world of uncertainty
in which nobody knows the right answer,
you need to try out a lot of things
and hope you will find one that works.

Douglass C. North, 2003

DANKSAGUNG

Die Arbeiten zu dieser Dissertation wurden seit Mai 2011 am Lehrstuhl für Bioverfahrenstechnik der Universität Stuttgart durchgeführt. In dieser Zeit haben eine ganze Reihe von Personen auf verschiedenste Weise zum Fortschritt dieser Arbeit beigetragen, denen ich auf diesem Wege herzlich meinen Dank aussprechen möchte.

Mein erster Dank geht an meinen Doktorvater Prof. Dr.-Ing. Ralf Takors für die hervorragende Betreuung und das mir entgegengebrachte Vertrauen in meine Arbeit. Seine Begeisterung für die wissenschaftlichen Fragestellungen dieser Dissertation, seine Tür die stets für Gespräche, Diskussionen und Hilfestellungen „offen stand“, sowie im Besonderen, sein Verständnis und seine Unterstützung gerade in schwierigen Phasen, sind für mich von großer Bedeutung.

Bei Prof. Dr. Peter Neubauer möchte ich mich herzlichst für die Übernahme der Funktion des Zweitberichters und bei Prof. Dr. Thomas Hirth für die Bereitschaft den Prüfungsvorsitz zu übernehmen bedanken.

Ein ganz großes Dankeschön geht an Dr. Bastian Blombach für das „zur Seite stehen“ in den letzten Jahren, seine unzähligen Hilfestellungen und sein offenes Ohr, für die vielen gemeinsamen Versuche, seine ansteckende Faszination und Motivation, seine kritischen Anmerkungen beim Verfassen der Publikationen und dieser Arbeit, sowie im besonderen Maße für seine Freundschaft.

Ein Dankeschön geht auch an Dr. Martin Siemann-Herzberg für die vielen fachlichen Hinweise im Laufe des Projektes.

Bei der Deutschen Forschungsgemeinschaft (DFG) möchte ich mich für die Finanzierung dieses Projektes (TA 241/5–1) bedanken.

Ein herzliches Dankeschön geht an Prof. Dr. Jörn Kalinowksi und Dr. Tobias Busche vom CeBiTeC in Bielefeld für die ausgezeichnete Kooperation bei der Durchführung und Auswertung der Microarray-Experimente.

Vielen Dank an Silke Reu, der „guten Seele“ des IBVT, für ihre unzähligen Versuche mir „schwäbisch Schwätzen“ beizubringen, der Geduld bei der Entgegennahme zahlreicher Paketzustellungen und unzureichender Fähigkeiten meinerseits was das Ausfüllen von Dienstformularen anbelangt, sowie die unzähligen „Motivationsspritzen“ in Form kleiner Kalorienbomben.

Bei allen Festangestellten möchte ich mich für ihre Hilfe und Unterstützung in den vergangenen drei Jahren bedanken. Ein ganz besonderer Dank geht an Andreas Freund für die unzähligen Stunden zum Aufbau und zur Bereitstellung der Reaktoranlage, seiner Kompetenz, Geduld und Hilfsbereitschaft bei der Unterweisung im Technikum, sowie für das anregende „Philosophieren“ über unser gemeinsames Hobby. Ohne ihn wäre ein großer Teil dieser Dissertation in der Form nicht möglich gewesen. Hervorheben möchte ich außerdem Mira Lenfers-Lücker für die angenehme Atmosphäre und Hilfestellung in der Analytik, sowie Salaheddine Laghrami ohne den ich bis heute noch suchend im Technikum umherirren würde.

Ein großes Dankeschön geht an alle Kolleginnen und Kollegen am Lehrstuhl für die angenehme Arbeitsatmosphäre und spannende Zeit, sowie im Besonderen den „Mensarianern“ für schöne Stunden und anregende Diskussionen zur Mittagszeit.

Meinen Mitstreiterinnen im dekorativsten Büro des IBVT, Sarah Lieder und Joana Simen, danke ich sehr für die gemeinsame Zeit und den Zusammenhalt an guten Tagen und an denen die dazwischen lagen – ich werde beide nicht vergessen. Ein dickes Dankeschön geht auch an Maria Rahnert für die turnusmäßigen Erörterungen und konspirativen Diskussionen der allmonatlich aufkeimenden Sachzusammenhänge der Bioverfahrenstechnik, sowie die gegenseitigen, gern gesehenen prokrastinativen Aktivitäten wenn die Stunden im Technikum doch mal wieder länger wurden.

Meinen Studenten Michael Ghosh, Andreas Ulmer und Marina Perich danke ich für die Leistungsbereitschaft und die durchgeführten Arbeiten. Des Weiteren gilt mein Dank in ganz besonderer Weise Michaela Graf für ihren Einsatz in ihrer Abschlussarbeit und darüber hinaus, was nicht unerheblich zum Erfolg dieser Arbeit beigetragen hat, sowie für Diskussionen auf Augenhöhe und das Korrekturlesen meiner Arbeit.

Dr.-Ing. Danielle Dennewald und Dr. Christoph Bendig danke ich für ihre Freundschaft und Unterstützung in den letzten Jahren und ihren Einsatz beim Korrigieren meiner Arbeit.

Ein herzliches Dankeschön geht auch an meine Freunde, insbesondere an Sabrina Witthoff und Florian Baumgärtner, die mich auf vielen meiner Stationen begleitet und unterstützt haben und auf die ich mich auch in schwierigen Zeit uneingeschränkt verlassen konnte.

Nicht zuletzt gilt mein größter Dank Iris und meinen drei Familien! Ihr hattet immer Verständnis für meine Entscheidungen und ohne eure Unterstützung wäre ich nicht da angekommen wo ich heute bin. Euer Vertrauen in mich ist ein großer Rückhalt in meinem Leben, auch wenn fast immer mehrere hundert Kilometer zwischen uns liegen.

Stuttgart, im Juni 2014

Jens Buchholz

CONTENTS

Appendices

LIST OF FIGURES

LIST OF TABLES

NOMENCLATURE

ATCC	American Type Culture Collection
AU	Arbitrary unit
Bo	Bodenstein number
c	Concentration of a compound
C	Carbon
CR	Cascade bioreactor
CBS	Cascade bioreactor system
CDW	Cell dry weight (g)
CER	Carbon dioxide evolution rate ($\mathrm{mol\,L^{-1}\,h^{-1}}$)
CFD	Computational fluid dynamics
CSTR	Continuous stirred tank reactor
$c'(t)$	Normalized signal of tracer over time (AU)
$c(t)$	Signal of tracer over time (AU)
CTR	Carbon dioxide transfer rate ($\mathrm{mol\,L^{-1}\,h^{-1}}$)
D	Tank diameter (m)
d	Impeller diameter (m)
D_{ax}	Longitudinal dispersion coefficient ($\mathrm{m\,s^{-2}}$)
DNA	Deoxyribonucleic acid
e.g.	*exempli gratia*, "for example"
$E(t)$	Exit age function of residence time distribution
et al.	*et alii*, "and other"
F	Feed rate ($\mathrm{L\,h^{-1}}$)

Fig.	Figure
GFP	Green fluorescent protein
$G(s)$	Transfer function
H	Henry's law constant ($\mathrm{mol\,L^{-1}\,atm^{-1}}$)
HPLC	High pressure liquid chromatography
i.a.	*inter alia*, "amongst other things"
i.e.	*id est*, "that is"
k	Number of comparison groups for MAPE calculations
K_1, K_2	Chemical equilibrium constant ($\mathrm{mol\,L^{-1}}$)
k_1, k_2	Reaction rate constant for forward reaction ($\mathrm{h^{-1}}$)
k_{-1}, k_{-2}	Reaction rate constant for reverse reaction $\mathrm{h^{-1}}$)
$k_L a$	Volumetric mass transfer coefficient ($\mathrm{h^{-1}}$)
K_S	Saturation constant concentration ($\mathrm{g\,L^{-1}}$)
m	Mass of a compound (g)
M	Molarity ($\mathrm{mol\,L^{-1}}$)
MR	Main reactor
MAPE	Mean absolute percentage error (%)
$M_{C,X}$	Mass carbon fraction in biomass in % ($\mathrm{g\,g^{-1}}$)
MP	Metering diaphragm pump
mRNA	Messenger RNA
$\dot{n}$	Molar flow ($\mathrm{mol\,h^{-1}}$)
N	Agitation speed ($\mathrm{min^{-1}}$)
n	Molar quantity (mol)
Ne	Newton or dimensionless power number
N_{P_0}	Dimensionless power number
N_{tip}	Impeller tip speed ($\mathrm{m\,s^{-1}}$)
N_T	Number of ideal tanks
OD	Optical density
OTR	Oxygen transfer rate ($\mathrm{mol\,L^{-1}\,h^{-1}}$)
OUR	Oxygen uptake rate ($\mathrm{mol\,L^{-1}\,h^{-1}}$)
P	Power input (Nm)
p	Total pressure (bar)
P^*	Tracer pulse or perturbation

pCO_2	Partial pressure of carbon dioxide (mbar)
PCS	Process control system
PFR	Plug flow reactor
pH	Negative decadic logarithm of the proton concentration
pO_2	Dissolved oxygen saturation (%)
PPP	Pentose phosphate pathway
PTS	Phosphotransferase system
P/V_R	Volumetric power input ($\mathrm{W\,L^{-1}}$)
Q	Volumetric gas flow rate ($\mathrm{L\,min^{-1}}$)
q_{CO_2}	Biomass specific carbon dioxide evolution rate ($\mathrm{mol\,g^{-1}\,h^{-1}}$)
q_{O_2}	Biomass specific oxygen uptake rate ($\mathrm{mol\,g^{-1}\,h^{-1}}$)
Q_P	Volumetric production rate ($\mathrm{g\,L^{-1}\,h^{-1}}$)
q_P	Biomass specific production uptake rate ($\mathrm{g\,g^{-1}\,h^{-1}}$)
qRT-PCR	Quantitative real-time polymerase chain reaction
q_S	Biomass specific substrate uptake rate ($\mathrm{g\,g^{-1}\,h^{-1}}$)
Q/V_R	Volumetric gas flow rate per unit volume of liquid in vvm ($\mathrm{L\,L^{-1}\,min^{-1}}$)
R	Universal gas constant ($\mathrm{J\,mol^{-1}\,K^{-1}}$)
R^2	Coefficient of determination
R_c	Carbon recoveries in % ($\mathrm{mol\,mol^{-1}}$)
Re	Reynolds number of the impeller
RNA	Ribonucleic acid
RQ	Respiratory quotient
RT	Room temperature
RTD	Retention time distribution ($\mathrm{min^{-1}}$)
RV	Regulating valve
s	Parameter of the frequency domain
S^*	Sampling port
S	Substrate concentration ($\mathrm{g\,L^{-1}}$)
SD	Standard deviation
STR	Stirred tank reactor
$\bar{t}$	Mean residence time (min)
T	Temperature (°C)

t	Time (h)
Tab.	Table
t_c	Circulation time (s)
TC	Total carbon
TCA	Tricarboxylic acid cycle
t_d	Doubling time (h)
$\bar{t}_i$	Mean residence time of the individual tank (min)
TIC	Total inorganic carbon
TIS	Tank-in-series reactor model
t_{lag}	Delay or dead time (min)
TOC	Total organic carbon
U	Applied voltage (V)
u	Mean flow velocity ($\mathrm{m\,s^{-1}}$)
v_a	Experimental data for MAPE calculations
v_p	Predicted data for MAPE calculations
(v/v)	Volume to volume proportion
V_E	Volume element
V_R	Reactor volume (L)
(w/v)	Weight to volume proportion
(w/w)	Weight to weight proportion
WT	Wild-type strain
X	Biomass concentration ($\mathrm{g\,L^{-1}}$)
y	Molar exhaust gas fraction
Y_{PS}	Yield coefficient of product per unit substrate ($\mathrm{g\,g^{-1}}$)
Y_{PX}	Yield coefficient of product per unit biomass ($\mathrm{g\,g^{-1}}$)
Y_{XS}	Yield coefficient of biomass per unit substrate ($\mathrm{g\,g^{-1}}$)

Greek letters

α	Alpha
β	Beta
Δ	Difference between two quantities
$\delta(t)$	Delta dirac function

°C	Degree Celsius
η	Dynamic viscosity (Pa s = kg s^{-1} m)
η	Normalization factor
γ^2	Quadratic deviation
λ_i	Molar stoichiometric coefficient of chemical formulae i
μ	Specific growth rate (h^{-1})
μ_{max}	Maximum growth rate (h^{-1})
ν	Circulation flow rate (L min^{-1})
%	Percent
ρ	Density of the medium (kg m^{-3})
σ^2	Variance
σ^2	Variance (min^2)
σ^2_Θ	Dimensionless variance
σ_f	Total uncertainty of a function f
σ^2_θ	Dimensionless variance
τ	Theoretical space time (min)
Θ	Dimensionless residence time
θ	Mixing time (s)

Chemicals

CO_2	Carbon dioxide
CO_3^{2-}	Carbonate ion
H_2CO_3	Carbonic acid
HCO_3^-	Bicarbonate
$C_6H_{12}O_6$	Glucose
dH_2O	Deionized water
K_2HPO_4	Di-potassium phosphate
KIV	2-Ketoisovalerate
KOH	Potassium hydroxide
O_2	Oxygen

Subscripts

0	Process start at $t = 0\,\mathrm{h}$
95	95 %
a, b, c, and d	Molar proportions of respective element
Bal	Balance
circ	Switch from batch to circulation mode
Cor	Coriolis flow meter
g	Gaseous phase
∞	Point in time with $t \longrightarrow \infty$
in	Input
l	Liquid phase
lys	L-Lysine
out	Output
s, n, x, and p_j	Substrate, nitrogen source, biomass, and (by-)products j
t	Time of sampling
TIS	Tanks-in-series
var	Variance

Superscripts

L	Liquid phase
S	Substrate (glucose)
Sys	System (gaseous and liquid phase)

ZUSAMMENFASSUNG

Die industrielle Biotechnologie gilt als Schlüsseltechnolgie für die nachhaltige Produktion von Chemikalien und Treibstoffen aus nachwachsenden Rohstoffen. Daraus folgt unter Berücksichtigung von Degressionseffekten immer häufiger die Verwendung großvolumiger, nicht ideal durchmischter Bioreaktoren mit mehreren hundert Kubikmetern. Somit erfahren die Zellen entlang ihres Strömungspfades kontinuierlich Änderungen in ihrer Mikroumgebung, z.B. CO_2 Partialdruck (pCO_2) Gradienten, was aufgrund der Hydrostatik gerade am Reaktorboden zu erheblichen Mengen an gelöst CO_2/HCO_3^- führt.

In dieser Arbeit erfolgte unter "quasi-stationären" Bedingungen die erstmalige Untersuchung von sehr 'niedrigen' (< 40 mbar) und 'hohen' (≥ 300 mbar) pCO_2 auf die Wachstumskinetik und die transkriptionelle Regulation in *Corynebacterium glutamicum*. Unter 'hohen' pCO_2 wurden neben einer initial erhöhten Biomasseausbeute ähnliche Leistungsparameter für Wachstumsrate und Substrataufnahme, sowie ausgewählte Aktivitäten de-/carboxylierender Enzyme im Vergleich zum Referenzprozess beobachtet. Eine vergleichende Transkriptomanalyse konnte die Bedeutung des globalen Regulators DtxR (51 % der 117 differenziellen Gene) für das Wachstum in Gegenwart 'hoher' CO_2/HCO_3^- Gehalte herausstellen, was durch signifikant langsameres Wachstum der $\Delta dtxR$ Mutante untermauert wurde. 'Geringe' pCO_2 führten zu drei-phasigem Wachstum mit um 50 % reduzierter Wachstumsrate in Phase II. Ein komplexer Regulationsmechanismus in Reaktion auf 'geringe' CO_2/HCO_3^- Gehalte wurde durch die Kombination von Enzymaktivitätsmessungen (zweifache Erhöhung von Glucose-6-phosphat-Dehydrogenase und 6-Phosphogluconat-Dehydrogenase), Nebenproduktbildung (L-Alanin und L-Valin) und Transkriptomanalysen (140 differenzielle Gene) ermittelt. So liegt die Vermutung nahe, dass eine Verstärkung der Expression der Thiaminpyrophosphat (TPP)-Biosynthesegene

erfolgt, um die Aktivität TPP-abhängiger decarboxylierender Reaktionen zu steigern und so die CO_2 Verfügbarkeit in der Zelle zu erhöhen.

Die quantitative Prozessauswertung via Kohlenstoffbilanzen ist für weiterführende Betrachtungen wie z.B. Stoffflussanalysen auch in Gegenwart veränderter CO_2/HCO_3^- Gehalte essentiell. Unter Verwendung eines Kohlenstoffanalysators erfolgte die Etablierung eines Bilanzierungsansatzes, der die Gesamtkohlenstoffspezies sowohl in der Flüssigphase, als auch in der Biomasse berücksichtigt. Neben der vollständigen Bilanzierung zwischen (96–100) % konnten so falsch-negative Unterschätzungen vermieden und Bilanzierungslücken identifiziert und zugeordnet werden. Weiterhin wurde gezeigt, dass sich bereits unter Referenzbedingungen erhebliche CO_2/HCO_3^- Mengen im Medium lösen, was in Verbindung mit ungenauen Biomasse-Kohlenstoffgehalten aus der Literatur dazu führt, dass andernfalls Bilanzlücken von bis zu 24 % im Fermentationsverlauf auftreten.

Grundlage einer rational-getriebenen Verbesserung von Bioprozessen ist u.a. das quantitative Verständnis großvolumiger Produktionsumgebungen. Experimentelle Ansätze verfolgen die Abbildung realer Bioreaktoren in sogenannten „scale-down“ Reaktoranlagen. Hierfür erfolgte die Entwicklung und Etablierung eines neuartigen Kaskadenreaktors bestehend aus einem 100 L Haupt- und zwei 1 L Kaskadenreakoren, die jeweils individuell betrieben und bilanziert werden können. Die erfolgreiche verfahrenstechnische Charakterisierung und Verifizierung über Modell- und Simulationsansätze erlaubte die Abbildung definierter pCO_2 Gradienten (ΔpCO_2 bis zu ≈260 mbar) und Verweilzeiten im Bypass (Kaskadenreaktor 1 und 2) in Abhängigkeit der Misch- und Strömungszustände großskaliger Reaktoren von bis zu ≈4 min. Gleichzeitig wurde gezeigt, dass prozessrelevante Sekundärparameter wie z.B. die Temperatur und der pH im Fermentationsverlauf konstant gehalten werden können. Unter Berücksichtigung einer mittleren Verweilzeit von 3.55 min, erfolgten Fermentationen mit dem *C. glutamicum* Wildtyp und dem L-Lysin Produzenten DM1933 unter Anwendung eines inkrementellen pCO_2 Gradienten von (75–315) mbar. Die phänomenologische Untersuchung ergab, dass die pCO_2 Oszillationen zu keinen signifikanten Inhibitionen von Wachtums-, Substrat,- und Produktkinetik im Vergleich zum Referenzprozess führten. Darüber hinaus veranschaulichten vergleichende Transkriptomanalysen für den Wildtyp-Prozess erstmalig eine schnelle transkriptionelle Antwort als Reaktion auf den applizierten pCO_2 Gradienten. Die resultierende Systemantwort korrelierte (linear) in ihrer Gesamtheit sowohl mit der vorliegenden Verweilzeit der Zellen als auch mit der Intensität des pCO_2 Stimulus. So wurden nach 1.74 min (Δ75 mbar) 15 differenzielle Gene beobachtet, während nach 3.55 min (Δ240 mbar) 66 differenzielle Gene identifiziert werden konnten.

SUMMARY

Industrial biotechnology is regarded as a key technology for the sustainable production of chemicals and biofuels from renewable raw materials. The economy-of-scale principle leads to a more frequent application of large scale, non-ideally mixed bioreactors of several hundred cubic meters. As a result, the cells are subjected to continuously changing micro-environments along their flow path, such as gradients of the CO_2 partial pressure (pCO_2), which results due to the tank hydrostatics in exceptional amounts of dissolved CO_2/HCO_3^- towards the bottom of the reactor.

This thesis covered the first time investigation of "quasi-stationary" 'low' (<40 mbar) and 'high' (≥300 mbar) pCO_2 conditions on the growth kinetics and the transcriptional regulation in *Corynebacterium glutamicum*. Fermentations performed under 'high' pCO_2 levels resulted in initially enhanced biomass to substrate yields and similar total performance parameters as growth rate and substrate uptake, as well as enzyme activities of selected de-/carboxylating enzymes compared to the reference process. A global comparative transcriptional analysis revealed the importance of the global regulator DtxR (51 % of 117 differential genes) for growth in presence of 'high' CO_2/HCO_3^- levels, which was corroborated by the significantly reduced growth rate of a $\Delta dtxR$ mutant. 'Low' pCO_2 led to a bi-level growth behavior with a growth rate reduction of 50 % in phase II. A complex regulatory mechanism in response to 'low' CO_2/HCO_3^- levels was deduced by combining the results of enzyme activity measurements (two-fold increase of glucose-6-phosphate dehydrogenase and 6-phosphogluconate dehydrogenase activity), by-product formation (L-alanine and L-valine), and DNA microarray analyses (140 differential genes). It is therefore assumed that an amplified expression of thiamin pyrophosphate (TPP)

biosynthesis genes occurs to enhance the activity of TPP-dependent reactions to finally increase the availability of CO_2 in the cells.

The quantitative analysis of processes via carbon balancing is essential for advanced considerations such as flux analysis, especially under different CO_2/HCO_3^- conditions. A novel balancing approach was established by using a total carbon analyzer that considers all carbon species in the liquid phase and in the biomass. Besides leading to completely matched balances of (96–100) %, it prevented false-negative underestimations and allowed the identification and assignment of balance gaps. In addition, it could be shown that considerable amounts of CO_2/HCO_3^- dissolved in the culture medium, even under reference conditions, which in combination with inaccurate biomass carbon contents derived from the literature led to balance gaps of 24 % in the course of fermentations.

The quantitative understanding of large scale production environments is an important factor for the rational improvement of bioprocesses. Experimental approaches focus on the abstraction of real bioreactors using specially designed scale-down devices. For this purpose, a novel cascade bioreactor system was developed and established consisting of a 100 L main and two 1 L cascade reactors that can be operated and balanced independently.

The successful technical characterization and the verification by model and simulation approaches allowed the defined application of pCO_2 gradients (ΔpCO_2 up to ≈260 mbar) and residence times in the bypass (cascade reactor 1 and 2) in dependence on the mixing and flow characteristics of large scale reactors up to ≈4 min. At the same time, it could be shown that process relevant secondary parameters such as the temperature and the pH can be kept constant in the course of cultivations. Fermentation experiments were performed using *C. glutamicum* wild-type and the L-lysine producer DM1933 by considering a mean residence time of 3.55 min and an incremental pCO_2 gradient of (75–315) mbar. The phenomenological analysis demonstrated that pCO_2 oscillation did not inhibit growth, substrate, and product kinetics compared to the reference process. Furthermore, comparative transcriptional analysis revealed a fast transcriptional response in reaction to the applied pCO_2 gradient for the first time. The resulting system response correlated (linearly) in its entirety with the residence time of the cells and the intensity of the pCO_2 stimulus. In this regard, 15 differential genes were identified after 1.74 min (Δ75 mbar), whereas 66 differential genes were observed after 3.55 min (Δ240 mbar).

CHAPTER 1

MOTIVATION AND OBJECTIVES

This chapter gives a short overview of the current research status, about the background of this project, and emphasizes important aspects to be addressed in future studies, which were the motivation of conducting this thesis. In general, this project consists of three main working packages as illustrated in Fig. 1.1, which are detailed in the following paragraphs.

Fermentation studies under "quasi-stationary" conditions with varying carbon dioxide/bicarbonate levels

The literature offers a variety of surveys that investigate the sensitivity of bacterial, fungal, and mammalian cells to cultivation environments enriched with high amounts of carbon dioxide (CO_2) and bicarbonate (HCO_3^-) depending on the pH of the system. In many cases, the fermentation processes that were carried out under high CO_2/HCO_3^- levels with model organisms as e.g. Chinese hamster ovary cells (e.g., Zhu et al., 2005), *Penicillium chrysogenum* (e.g., El-Sabbagh et al., 2006), *Saccharomyces cerevisiae* (e.g., Aguilera et al., 2005; Isenschmid et al., 1995), *Bacillus subtilis* (Amanullah et al., 2001), *Escherichia coli* (e.g., Baez et al., 2009), or *Corynebacterium glutamicum* (Bäumchen et al., 2007; Knoll et al., 2007) were characterized with reduced observable growth rates, lower biomass and product yields, or hampered product formation. The general motivation of using these organisms is not only their importance for fundamental research, but also their common property of being platform organisms and production hosts for the biotechnological manufacturing of bulk products as e.g. amino and organic acids,

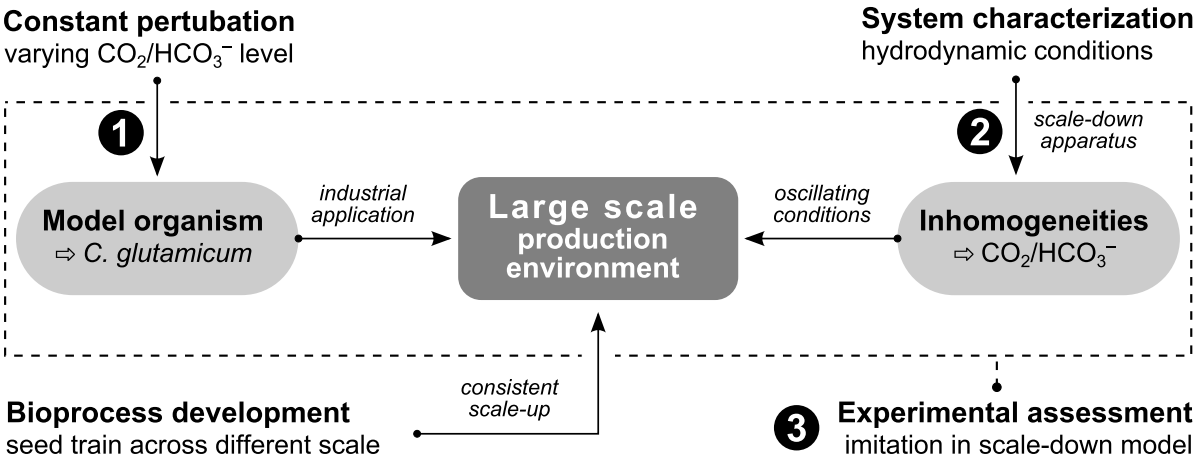

Fig. 1.1: Schematic concept of this thesis, which eventually considers/simulates the interplay of reactor inhomogeneities (i.e. CO_2/HCO_3^- level oscillation) with microorganisms (i.e. *C. glutamicum*) in large scale production environments of several hundred cubic meters. This thesis was separated into three main working packages: **(1)** preliminary application of constantly supplied, varying CO_2/HCO_3^- levels (reference fermentations), **(2)** development and characterization of the scale-down device for the application of variable hydrodynamic conditions and CO_2/HCO_3^- gradients, and **(3)** imitation of large scale conditions by applying defined CO_2/HCO_3^- gradients in the developed scale-down device for fermentations of *C. glutamicum* wild-type and L-lysine producer strain.

vitamins, or antibiotics. As the production of commodities usually follows the economy-of-scale principle, large scale bioreactor facilities with reported capacities as high as (250–750) m^3 are used (Kelle, 2005). However, process conditions at manufacturing scale differ greatly compared to laboratory (lab) systems (Lara et al., 2006a). Geometry driven, reactor heights of several meters implicate hydrostatic pressures up to 2 bar at the bottom of the reactor (Noorman, 2011), which is significantly higher than found in (1–100) L scale systems. Consequently, this does not only lead to (i) observable vertical pressure gradients but also to (ii) increased O_2 and CO_2 gas solubilities and partial pressures, in turn resulting in exceptional amounts of dissolved carbonic species in the culture liquid (McIntyre & McNeil, 1997).

Carrying out CO_2/HCO_3^- sensitivity studies in the context of scale-up is therefore not only driven by a fundamental research-oriented motivation but it is also, from an industrial perspective, a commercial necessity when high CO_2/HCO_3^- levels are connected to the loss of process performance. Initial research focused on the mechanistic understanding of CO_2's toxic effects, revealing its potential to e.g. alter the physico-chemical properties of proteins, acidify the internal pH, disrupt the cell membrane, or regulate virulence and toxin production in pathogens (Bothun et al., 2004; Follonier et al., 2013; Gutknecht et al., 1977; Isenschmid et al., 1995; Jones & Greenfield, 1982; Kuriyama

et al., 1993). This was followed by several phenomenological studies dealing with the detrimental consequences on cell vitality, metabolism, and productivity (Castan et al., 2002; Dixon & Kell, 1989; McIntyre & McNeil, 1997). In recent years, the advances in all "OMICS" technologies were used to gain a more detailed understanding and elucidate potential regulatory effects (e.g., Aguilera et al., 2005; Amoabediny & Büchs, 2010; Amoabediny et al., 2010; Baez et al., 2009, 2011; El-Sabbagh et al., 2006, 2008; Ezraty et al., 2011).

However, despite its industrial importance and its metabolic characteristic, only limited work was carried out on the scale-up dependent impact of different CO_2/HCO_3^- levels on the physiology, metabolism, and regulation in *C. glutamicum*. In contrast to *E. coli* and many other organisms, *C. glutamicum* comprises two anapleurotic reactions as part of the PEP–pyruvate–oxaloacetate node, which is one of the key switch points for carbon flux distribution through several de-/carboxylating reactions (Sauer & Eikmanns, 2005). Due to its complexity and versatility, the physiological function and interaction of the connecting reactions is yet not fully understood and investigated; in particular with regard to varying CO_2/HCO_3^- environments. Initial phenomenological observations were published by Knoll et al. (2007) revealing a general robustness of growth and L-lysine production to CO_2 partial pressures up to 0.6 bar in high density fed-batch cultures ($\gg$200 g L^{-1}), which was generally confirmed in turbidostat processes (Bäumchen et al., 2007). Even though, a profound understanding of the e.g. transcriptional regulation is still missing. Therefore, the first objective of this study was the systematic analysis and the experimental assessment of varying CO_2/HCO_3^- levels on the growth kinetics and regulatory consequences in *C. glutamicum* as illustrated in Fig. 1.1. Besides investigations using *C. glutamicum* wild-type (WT), growth studies with corresponding deletion mutants should contribute to a better understanding. A detailed description of the individual aspects and requirements for that purpose is given in the following:

- Development of a reference fermentation process using *C. glutamicum* WT and determination of e.g. seed-train and culture medium.
- Accomplishing characteristic reference fermentations under defined conditions to provide representative (biomass) samples to establish project-relevant measurement techniques for the determination of enzyme activities and transcriptional analysis (DNA microarrays).

- Characterizing the reference fermentations and determining macrokinetic parameters of *C. glutamicum* WT such as growth and substrate kinetics, and by-product formation.
- Accomplishing preliminary fermentations under different, "quasi-stationary" CO_2/HCO_3^- levels, subsequently determining the physiological consequence and metabolic response, as well as analyzing the corresponding transcriptional regulation.
- Comparison of provided *C. glutamicum* single deletion mutants of anaplerotic/gluconeogenic reactions to the WT under equivalently varying CO_2/HCO_3^- levels.
- Establishment of a measurement protocol for the quantification of total carbon (i.e. all carbonic species) in the culture liquid and thus carbon balancing of the fermentations.

Development and characterization of a novel scale-down bioreactor system

As already introduced above, large scale bioreactors are characterized as highly heterogeneous environments. In addition to the aforementioned pressure distribution influencing the partial pressure of dissolved gases, limitations in energy input and mixing lead to the formation of various other gradients (temperature, pH, nutrients, etc.) to which the cells are subjected to during the cultivation process (Junker, 2004; Schmidt, 2005). This might ultimately lead to a reduced process performance (Lara et al., 2006a) and results in two major challenges: (i) consistent and efficient bioprocess development (e.g. seed-train) from lab over pilot to production scale (scale-up) at least with equal performance (Noorman, 2011) and (ii) the development of methodologies and tools for the description and understanding of large scale environments. The latter is facilitated by computational methods or specifically developed bioreactor system at lab scale (scale-down).

Traditional approaches of biotechnological scale-up and process transfer commonly focus on physical criteria with conclusion by analogy (Garcia-Ochoa & Gomez, 2009; Gill et al., 2008; Hewitt & Nienow, 2007; Junker, 2004; Neubauer et al., 2013; Schmidt, 2005). Even though research has been focusing on a more in-depth and direct process comparison of lab vs. large scale conditions (Bylund et al., 1998; Enfors et al., 2001; Hewitt et al.,

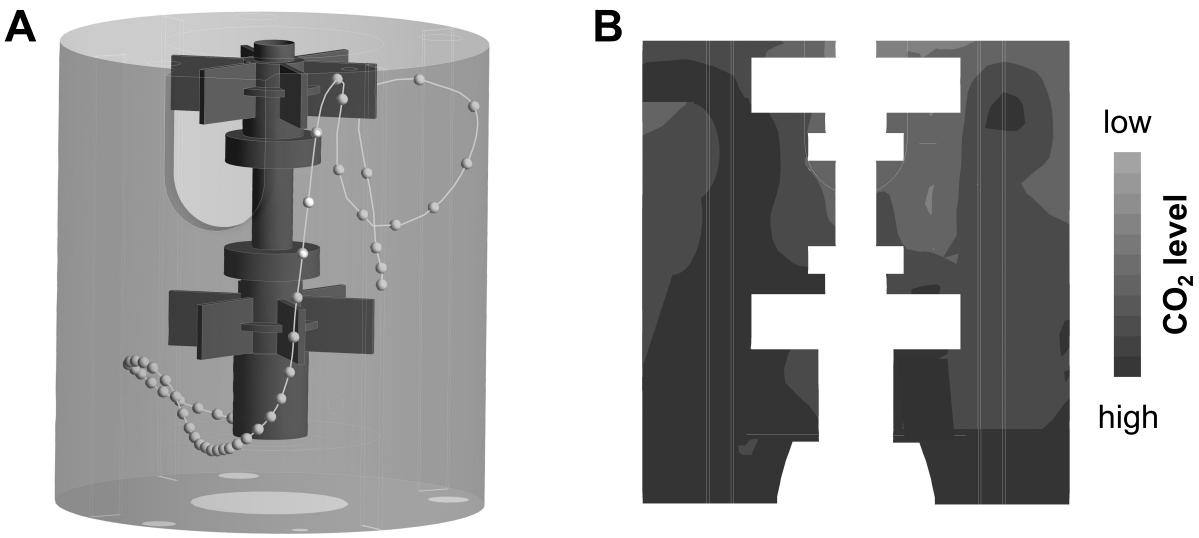

Fig. 1.2: (A) Exemplary illustration of a hypothetical cellular flow path through a bioreactor derived from computational fluid dynamics. **(B)** Schematic representation of the inhomogeneous CO_2 distribution within large scale bioreactors. Figure courtesy of Johannes Wutz, Institute of Biochemical Engineering, University of Stuttgart.

2000; Larsson & Enfors, 1988) and advances of computational approaches trying to link fluid dynamics to cell kinetics were reported (Lapin et al., 2004, 2006; Schmalzriedt et al., 2003; Vrábel et al., 2001), a holistic and profound understanding of large scale conditions, or the *a priori* prediction of process performance cannot be accomplished (Takors, 2012). In this regard, various scale-down devices were developed in the last two decades that aim at the abstraction of (large scale) bioreactor heterogeneities, usually focusing on the application of one or more distinct gradients in a fermentation scenario, and the integration of the dynamic and multi-level cellular response (Neubauer & Junne, 2010; Takors, 2012). For that purpose, the apparatuses ought to provide a first abstraction of the flow path of the cells through the heterogeneous environment (Fig. 1.2) by applying a (stress) stimulus and adjusting the residence time according to the large scale mixing and flow behavior (Junne et al., 2011; Lara et al., 2006a; Takors, 2012). Published setups vary greatly from one to multi-compartment systems: mostly using stirred tank (STR) or plug flow reactors (PFR). The complexity of the approaches differs significantly, and thus does the degree of flexibility and large scale imitation capacity. However, to provide a basis of advanced analysis as labeling experiments, (carbon) balancing, and distinct decoupling of scale-up impacts as dissolved CO_2/HCO_3^- gradients from secondary process variables, a novel, multi-compartment system used to capture the dynamic cellular response had

to be developed and systematically characterized (Fig. 1.1). A detailed description of the individual aspects and requirements for that purpose is given in the following:

- Implementation and evaluation of system components to establish a novel multi-compartment, cascade bioreactor platform (scale-down device) that represents characteristic volume elements of a large scale bioreactor to abstract the flow path of a cell through CO_2/HCO_3^- gradients.
- Implementation of the total system setup (bioreactors, valves, pump, mass flow meter, etc.) into the process control system (LabVIEW®).
- Configuration of the final system setup, performing stability tests, and establishing working routines necessary for all standard operations.
- Performing the process technical characterization of the system by determining the hydrodynamic constitution (e.g. residence time distributions and mixing times) and define the operational range of the system.
- Validation of the cascade bioreactor platform by accomplishing test fermentations.

Final application of the scale-down bioreactor system to imitate oscillating carbon dioxide/bicarbonate conditions

The main application of so far reported scale-down studies was the analysis of the cellular metabolic and physiological response, e.g. growth, biomass yield, substrate uptake, and (by-)product formation, when subjected to typical large scale inhomogeneities as O_2, pH, or substrate concentrations (Amanullah et al., 2001; Hewitt et al., 2007; Junne et al., 2011; Sandoval-Basurto et al., 2005). These phenomenological investigations were extended in recent years by advanced analyses of all "OMICS" technologies to unravel potential regulatory effects (Delvigne et al., 2009, 2010, 2011; Käß et al., 2013, 2014; Lara et al., 2006b; Schweder et al., 1999). Similar to the aforementioned CO_2/HCO_3^- studies, *C. glutamicum* was only rarely addressed despite its versatile industrial applicability (Schilling et al., 1999). Most investigations were performed with *E. coli* (e.g., Lara et al., 2006b; Neubauer et al., 1995a; Onyeaka et al., 2003; Sandoval-Basurto et al., 2005; Soini et al., 2011), consequently also providing the only study available that addresses

CO_2/HCO_3^- oscillations (Baez et al., 2011). Only recently, Käß et al. (2013, 2014) put *C. glutamicum* more into focus by using a STR-PFR scale-down device for fermentations with *C. glutamicum* WT and an L-lysine producer strain. However, both studies focus again on the application of substrate and O_2 gradients, meaning that so far, CO_2/HCO_3^- oscillations as found at large scale have not been investigated in *C. glutamicum* cultures.

The main objective of the last working package of this thesis was therefore the first time application of *C. glutamicum* under dissolved CO_2/HCO_3^- gradients in the previously mentioned, newly designed scale-down reactor (see working package II; Fig. 1.1). The phenomenological evaluation of the process performance should be followed by the determination of the transcriptional response in context to the preliminary studies under "quasi-stationary", different CO_2/HCO_3^- levels (see working package I). A detailed description of the individual aspects and requirements for that purpose is given in the following:

- Transfer of process characteristics obtained under "quasi-stationary" CO_2/HCO_3^- conditions to design representative cascade fermentations with total circulation under CO_2/HCO_3^- gradients.
- Accomplishment of *C. glutamicum* WT fermentations in the scale-down system and determination of the physiological consequences and metabolic response, as well as the comparison of the transcriptional regulation to the reference condition.
- Determination of characteristic response times of the system by coupling the interaction of CO_2/HCO_3^- gradients with the dynamic metabolic and/or transcriptional response of the cells.
- Determination of the impact of oscillating CO_2/HCO_3^- conditions on L-lysine formation using the producer strain *C. glutamicum* DM1933.
- Development of a systematic understanding of the scale-up dependent influence of dynamic CO_2/HCO_3^- oscillations on *C. glutamicum* and deduce, when possible, a biologically-motivated scale-up criterion.

CHAPTER 2
THEORETICAL BACKGROUND

This chapter summarizes the theoretical background of this thesis dealing with the application of *C. glutamicum* in the industrial context and the various scale-up /-down questions of microbial processes.

2.1 Model organism: *Corynebacterium glutamicum*

C. glutamicum is a rod-shaped, Gram-positive facultative anaerobic organism originating from soil, which grows on a variety of different sugars, organic acids, and alcohols (Eggeling & Reyes, 2005; Liebl, 1991; Nishimura et al., 2007; Takeno et al., 2007). Being generally regarded as safe (GRAS status), *C. glutamicum* belongs to the well-known organisms under study and thus has proven to provide significant industrial capabilities. *C. glutamicum* is known as an industrial workhorse for commercial production of amino acids (Leuchtenberger et al., 2005; Takors et al., 2007), such as the food and feed additives L-glutamate and L-lysine, which have reached a world-wide capacity of > 2.5 Mio. and > 1.9 Mio. tons per year, respectively (Ajinomoto Co., 2013; Eggeling & Reyes, 2005; Takors et al., 2007).

2.1.1 Industrial relevance

Numerous studies exist that demonstrate the potential or applicability of *C. glutamicum* as a versatile production host for other commodities than amino or organic acids (Wieschalka et al., 2013): e.g. biofuels (Blombach & Eikmanns, 2011; Blombach et

al., 2011; Inui et al., 2004; Smith et al., 2010), diamines for synthetic polymers in textile and automotive industry (Kind et al., 2010a,b; Schneider & Wendisch, 2010a,b, 2011; Schneider et al., 2012), xylitol for the nutrition industry (Sasaki et al., 2010), polyhydroxybutyrate as bio-derived and biodegradable plastics (Song et al., 2013), as well as ectoine and carotenoids for health care and cosmetics industries (Becker et al., 2013; Heider et al., 2012, 2014).

This was possible due to sophisticated knowledge about pathway regulation, systems biology approaches on all "OMICS" levels, and improvement of metabolic engineering strategies [overviews given in Becker & Wittmann (2012), Becker et al. (2011), Burkovski (2008), Eggeling & Reyes (2005), Kirchner & Tauch (2003), Sauer & Eikmanns (2005), Takors et al. (2007), Teramoto et al. (2011), and Vertès et al. (2012), and Wendisch et al. (2006)]. The central and common precursor of most aforementioned products is pyruvate and optimizing its availability is therefore a promising target to improve microbial production processes. Amongst many other (metabolic) engineering approaches, the adjustment of promoter activity by promoter engineering instead of directed gene deletion or amplification was demonstrated as a suitable strategy to improved precursor supply, reduced by-product formation, and ultimately into enhanced accumulation of the desired bio-based product. In this regard, studies using *C. glutamicum* illustrate the application for e.g. L-lysine and L-valine production (Becker et al., 2005, 2007, 2011; Holátko et al., 2009).

2.1.2 Central carbon metabolism

When grown aerobically on sugars, *C. glutamicum* utilizes the glycolysis and the pentose phosphate pathways (PPP) (Bott, 2007; Eikmanns, 2005), connected to the tricarboxylic acid cycle (TCA) by several C_4-decarboxylating and C_3-carboxylating enzymes that are involved in the PEP–pyruvate–oxaloacetate node (Fig. 2.1), which is one of the key switch points for carbon flux distribution and precursor supply for amino acid production (Sauer & Eikmanns, 2005). In contrast to many other organisms, *C. glutamicum* comprises two anapleurotic reactions that are able to replenish TCA intermediates, the phosphoenolpyruvate (PEP) carboxylase (PPC) and the pyruvate carboxylase (PYC). Flux studies performed under non-gluconeogenic conditions by Klapa et al. (2003) and Petersen et al. (2001) revealed that the main carbon flux of about 90 % is channeled through PYC, whereas PPC operates in quasi-parallel mode with a contribution of less than 10 %. It is therefore thought that the existence of both enzymes facilitate the ability

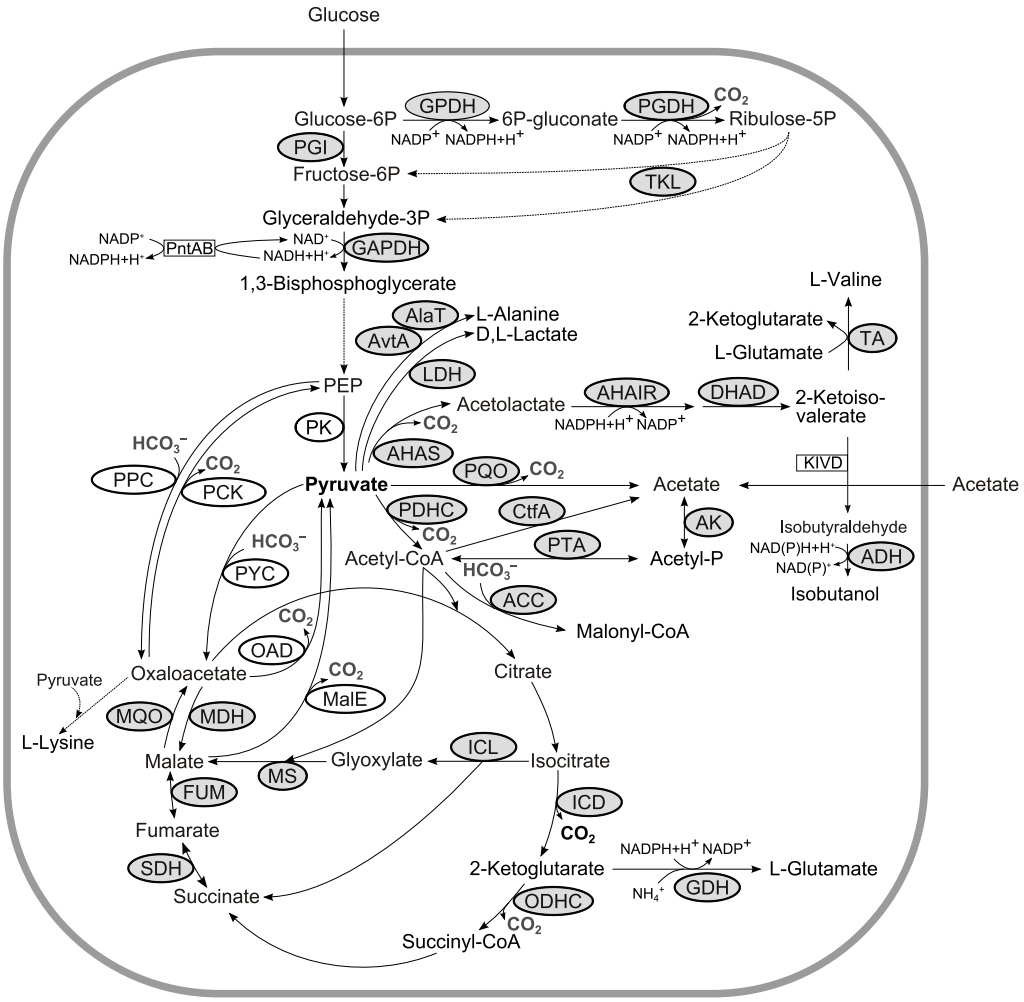

Fig. 2.1: Overview of the central metabolism of *C. glutamicum* with indicated production pathways of pyruvate, 2-ketoisovalerate, succinate, L-lysine, L-valine, and isobutanol (non-native). Native enzymes of *C. glutamicum* are illustrated as ellipses (shaded in gray), heterologous enzymes as rectangles. Enzymes of the PEP–pyruvate–oxaloacetate node are additionally indicated (shaded in white). Abbreviations are as follows with coding genes given in parentheses: ADH (*adhA*), alcohol dehydrogenase A; AHAIR (*ilvC*), acetohydroxyacid isomeroreductase; AHAS (*ilvBN*), acetohydroxyacid synthase; AK (*ack*), acetate kinase; AlaT (*alaT*), alanine aminotransferase; AvtA (*avtA*), valine-pyruvate aminotransferase; CtfA (*cat*), CoA transferase; DHAD (*ilvD*), dihydroxyacid dehydratase; FUM (*fum*), fumarase; GAPDH (*gapA*), glyceraldehyde-3P dehydrogenase; GDH (*gdhA*), glutamate dehydrogenase; GPDH (*zwf*, *opcA*), glucose-6P dehydrogenase; ICD (*icd*), isocitrate dehydrogenase; ICL (*aceA*), isocitrate lyase; KIVD (*kivD*), 2-ketoacid decarboxylase from *Lactococcus lactis*; LDH (*ldhA*), L-lactate dehydrogenase; MalE (*malE*), malic enzyme; MDH (*mdh*), malate dehydrogenase; MQO (*mqo*), malate:quinone oxidoreductase; MS (*aceB*), malate synthase; ODHC (*odhA*, *aceF*, and *lpd*), 2-ketoglutarate dehydrogenase complex; OAD (*odx*), oxaloacetate decarboxylase; PYC (*pyc*), pyruvate carboxylase; PDHC (*aceE*, *aceF*, and *lpd*), pyruvate dehydrogenase complex; PEP phosphoenolpyruvate; PCK (*pck*), PEP carboxykinase; PPC (*ppc*), PEP carboxylase; PGDH (*gnd*), 6P-gluconate dehydrogenase; PGI (*pgi*), phosphoglucose isomerase; PK (*pyk*), pyruvate kinase; PntAB (*pntAB*), membrane bound transhydrogenase from *E. coli*; PQO (*pqo*), pyruvate:quinone oxidoreductase; PTA (*pta*), phosphotransacetylase; SDH (*sdhABC*), succinate dehydrogenase; TA (*ilvE*), transaminase B; TKL (*tkt*), transketolase. The illustration was modified after Eikmanns & Blombach (2014).

of *C. glutamicum* to adept to different substrates and CO_2/HCO_3^- environments (Sauer & Eikmanns, 2005).

Besides the ability to (oxidatively) decarboxylate pyruvate to acetyl-CoA by the pyruvate dehydrogenase complex (PDHC), which can be potentially bypassed by the decarboxylation to acetate by pyruvate:quinone oxidoreductase (PQO) and the subsequent reactions of the acetate kinase (AK) and phosphotransacetylase (PTA), three C_4-decarboxylating enzymes (MalE, OAD, and PCK) facilitate the backward reaction of oxaloacetate (OAA) or malate to PEP or pyruvate. With fully functional gluconeogenesis required, e.g. when grown on acetate and lactate, PEP is only provided by PEP carboxykinase (PCK) from the TCA (Petersen et al., 2001), which cannot functionally be replaced by malic enzyme (MalE) or oxaloacetate decarboxylase (OAD) (Riedel et al., 2001). The absence of a functional PEP synthetase was argued beforehand (Peters-Wendisch et al., 1998). Contradictory studies were published regarding oxaloacetate/malate fluxes to pyruvate. While Petersen et al. (2000, 2001) did not identify a direct OAD-mediated carbon flux, Klapa et al. (2003) attributed high pyruvate formation rates in a L-lysine producer solely to OAD. MalE, which catalysis the decarboxylation reaction of malate to pyruvate is due to its NADPH generation hypothetically associated with NADPH/NADH cycling (with PYC, PPC, and malate dehydrogenase), was completely inactive under the conditions tested. While Netzer et al. (2004) reported that the growth phenotype of weakly growing *C. glutamicum* Δ*pyk* strains on acetate can be successfully complemented by *malE* overexpression, Klaffl & Eikmanns (2010) illustrated the same effect of cells with high OAD activity, proving the *in vivo* decarboxylation of OAA. However, despite intensive studies [reviewed in Sauer & Eikmanns (2005)], the complex interplay of *C. glutamicum's* anaplerosis is still not completely understood; especially with respect to HCO_3^- and CO_2 that serve as educt and product of the aforementioned de-/carboxylating reactions, respectively.

Since CO_2 is not only highly soluble in liquids, but in contrast to HCO_3^- also in the lipid layer of the cell membrane, free diffusion out of the cells can occur (Gutknecht et al., 1977). With a rather slow interconversion rate of CO_2 to HCO_3^- (Kern, 1960), depletion of the latter can be circumvented by carbonic anhydrase activity (CA), which catalyzes the reversible hydration in water to maintain favorable intracellular CO_2/HCO_3^- levels. Mitsuhashi et al. (2004) identified two genes encoding for putative β-type and γ-type carbonic anhydrases in *C. glutamicum*. However, only β-type enzyme was shown to excerpt essential functionality under normal growth and ordinary atmospheric conditions.

In summary, the physiological function or the cycling/interaction of the connecting reactions is yet not fully understood. Obviously, the PEP–pyruvate–oxaloacetate node is a key factor of the adaption of *C. glutamicum* to variable environmental conditions. Due to its versatility, it remains open whether different CO_2/HCO_3^- levels have an effect on the de-/carboxylating reactions or trigger regulatory changes of the gene expression. In line with this project, the relevance of the PEP–pyruvate–oxaloacetate node and corresponding enzymes is going to be elucidated not only with the *C. glutamicum* WT, but also with existing deletion and over-expression *C. glutamicum* mutants.

2.2 Scale-up of microbial processes

Industrial biotechnology is regarded as one of the key technologies of the 21st century with a world-wide market volume that is expected to rise to more than $300 billion by 2030 (Neubauer, 2011) for microbial, non-biopharmaceutical products (Festel, 2010; Neubauer, 2011). Due to the economy-of-scale principle that applies for the manufacturing of commodity high volume/low price products, large scale bioreactor capacities as high as (250–750) m^3 are essential (Kelle, 2005). Consequently, great effort is spent on efficient bioprocess design and development (including high-throughout miniaturization and parallelization) to provide cost-competitive production platforms (Betts & Baganz, 2006; Neubauer et al., 2013; Schäpper et al., 2009; Weuster-Botz, 2005). However, strategies for process establishment and improvement (e.g. metabolic engineering or synthetic and systems biology) commonly focus on lab scale environment; the same fact applies for many economical decisions regarding novel investments. Therefore, a successful process transfer (scale-up) without reduction of the performance across all scales of the seed train finally resulting in the manufacturing plant is of utmost importance (Garcia-Ochoa & Gomez, 2009; Hewitt & Nienow, 2007; Junne et al., 2012; Neubauer et al., 2013; Schmidt, 2005). Amongst others, Lara et al. (2006a) provide a summary of documented large scale-associated performance losses concerning biomass/product titer, quality, and yields. On the contrary, beneficial effects as e.g. increased viability reported by Enfors et al. (2001) can only rarely be found. Deterioration effects and symptoms occurring in plant or production scale were generically circumscribed as “scale-up-deteriorated production syndrome” (Okada & Iwamatu, 1997).

Thereby, these studies practically emphasize the fundamental differences between the "ideal" (model-like) lab scale environment and manufacturing conditions. In general, these so called scale-up impacts can be classified into (Takors, 2012):

(i) Biological factors: Increasing the final bioreactor capacity during scale-up consequently leads to an expansion of the seed train. The process itself becomes therefore more complicated and the cells are faced with multiple changes of their environment requiring a stable recombinant production host. More upon, the generation number increases significantly, which in turn may interfere with e.g. plasmid stability and inoculum development or increase the mutation probability and contamination vulnerability (Junker, 2004).

(ii) Chemical factors: The increase of the cultivation dimension might also indirectly influence the medium preparation or medium composition: e.g. the titration scheme might has to be adapted to potential downstream processing requirements. In addition, the solubility of process gases (O_2 and especially CO_2) is directly affected by higher hydrostatic (reactor height) and operating pressures (see physical factors), which in turn also influences the total amounts of all carbonic species (see section 2.3.3) and the buffering capacity. Medium stability might also be an issue due to increased heat-up and cool-down times during sterilization (Junker, 2004).

(iii) Physical factors: Naturally, the increase of bioreactor dimensions goes along with a fundamental change of the physical properties of the cellular environment. As mentioned before, given reactor heights of large scale facilities of several hundred cubic meters implicate hydrostatic-dependent, vertical pressure gradients that easily exceed 1 bar. The latter are superimposed by technical gas transfer limitations due to high metabolic activities of microbial cells that lead to radial gradients. In addition, heat removal becomes challenging and the mixing quality of the bulk liquid reduces significantly resulting in blend times of up to 240 s (Junker, 2004; Mayr et al., 1994). As a consequence, reactor inhomogeneities also apply for other relevant process parameters as e.g. substrate/nutrients, pH, and temperature distribution (Amanullah et al., 2001; Bylund et al., 1998; Caspeta et al., 2009; Enfors et al., 2001; Langheinrich & Nienow, 1999; Onyeaka et al., 2003).

As a result, cells in large scale bioreactors are continuously exposed to inhomogeneous conditions and thus subjected to significant micro-environmental changes. These

heterogeneities of reaction conditions and, consequently, the induction of stress gene expression are believed to lead to a completely altered physiology and a constant metabolic shift (Enfors et al., 2001; Schmidt, 2005). In turn, the probability of amino acid mis-incorporation increases, which affects the product quality and yield in productions at larger scales due to inherent inaccuracy of the translation machinery (Schweder et al., 1999). Equally important for production hosts is the stable propagation of plasmids to daughter cells, considering the higher number of generations (larger volumes) and longer inoculation chains. Again, plasmid stability is not only influenced by the plasmid and genetic properties itself, or by the strain stability characteristics of its host, but also by the process parameters and potential gradients (Lin & Neubauer, 2000).

The latter might therefore interfere with the attempt to transfer production processes from ideally mixed lab scale vessels to manufacturing scale. On that account, the literature provides several, typically physical scale-up criteria to manage a scale transfer. Under the common principle, one factor is maintained constant across the different scales: the most frequently applied are (i) geometric similarity, (ii) (volumetric) power impact (P/V_R), (iii) volumetric mass transfer coefficient (k_La), (iv) the mixing (Θ_{95}) or circulation time (t_c), (v) impeller tip speed (N_{tip}), (vi) Reynolds number (Re) of the impeller, and (vii) oxygen uptake rate (OUR) or dissolved oxygen pressure (pO_2) (Garcia-Ochoa & Gomez, 2009; Gill et al., 2008; Junker, 2004; Schmidt, 2005).

However, the linear increase of all dimensions cannot (always) be facilitated since other variables of the three-dimensional system rise on the linear scale with different exponents; from negative to three or higher (Oldshue, 1966). As an example, many strategies lead to dramatically increased power inputs (industrially unmanageable), also with enormous cooling costs as side effect. In turn, maintaining equivalent values for the power input will lead to considerable longer mixing times. Therefore, approaches were developed that focused on dimensionless coefficients as i.a. dimensionless power number (N_{P_0}) or Re (Schmidt, 2005). Even though, most solutions were empirically developed and cannot be regarded as generally applicable. Furthermore, so far no successful and functional universal scale-up concept has been derived or published that directly relates the physical parameters based on the reactor heterogeneities to the biological response as cellular dynamics (Hewitt & Nienow, 2007).

However, initiatory studies document the expression of stress genes and metabolite determination in response to varying conditions. In the broader sense, the maintenance of constant pO_2 values within the process by variation of stirrer speed and aeration rate is a common method to transfer fermentation process in scale and design (Schmidt,

2005). Besides, the only valid fool-proof scale-up method is to increase the production capacity by simply multiplying the number of lab and pilot scale, maintaining the overall performance of each reactor. Naturally, the latter cannot be applied in reality in terms of production and service costs (Villadsen et al., 2011).

For all these reasons, research has been focusing on a more in-depth process comparison of lab vs. large scale conditions studying the effect of e.g. substrate and O_2 gradients in STRs up to 22 m^3 on *E. coli* cultures (Bylund et al., 1998, 1999; Enfors et al., 2001; Hewitt et al., 2000; Larsson & Enfors, 1988). These process heterogeneities were shown to inhibit growth and cause increased by-product (acetate) formation. Interestingly, Hewitt and coworkers found with flow cytometry measurements that the oscillation of substrate and O_2 supply finally resulted in higher observable cell viabilities. Besides, advances of the computational tools during the last decades, as in fluid dynamics (CFD) helped significantly to improve the simulation of bioreactor hydrodynamics and mass transfer (Kelly, 2008). Initial CFD approaches by Oosterhuis & Kossen (1983) were complemented by multi-phase compartment models (Reuss et al., 2000), which were then further extended by the incorporation of microbial kinetics reflecting the activity of the (central) metabolism (Lapin et al., 2004, 2006; Schmalzriedt et al., 2003; Vrábel et al., 2001). Alternatively, stochastic mixing and circulation models were used to simulate and describe large scale bioreactors (Delvigne et al., 2006).

However, as indicated before, an *a priori* estimation of large scale performance of microbial production processes is impossible. It has been highlighted that a profound understanding of the cellular metabolism is essential to get an idea of the complex, multi-level response to the extracellular heterogeneity (Hewitt & Nienow, 2007). STRs with capacities significantly larger than 1 m^3 available for basic research are the rare exception. Therefore, and as an alternative to computational approaches, scale-down devices mimicking large scale conditions at lab scale became popular within the last two decades and are therefore addressed in the following section.

2.3 Scale-down of microbial processes

The central and common objective of the various scale-down devices presented so far is the integration of simulated reactor heterogeneities occurring at industrial scale with the dynamic and multi-level cellular response. For that purpose, several bioreactor designs were developed that ought to abstract the flow path of the cells through the

heterogeneous environment by adjusting the residence time in the compartment with step-change appropriately. The concepts were recently reviewed (Junne et al., 2011; Lara et al., 2006a; Takors, 2012) and vary greatly in complexity and applicability (Fig. 2.2). They generally distinguished between one- and two-compartment devices that can be classified as follows:

(i) Single-compartment STR with feeding/pulse regime and (optional) sampling device, or oscillatory feeding/pulse regime

(ii) Single-compartment STR using cylindrical discs between stirrer blades to realize different mixing zones and effects

(iii) Multi-compartment setups with two STR in parallel mode (STR-STR) or a STR that is connected to a PFR with and without static mixers (STR-PFR)

In the beginning of the research field of "scale-down studies" about 30 years ago, experimenters predominantly focused on the physiological and metabolic consequences that arose from the perturbation experiments. One of the first approaches to assess the influence of environmental gradients on the culture performance was carried out with a two-compartment STR-STR setup revealing the detrimental impact of high residence times (about 180 s) in combination with O_2 gradients/fluctuations on gluconic acid production by *Gluconobacter oxydans* (Oosterhuis, 1984; Oosterhuis et al., 1985). Later on, the concept was then taken up by e.g. Sweere et al. (1988), Sandoval-Basurto et al. (2005), or Lara et al. (2006b) to investigate the influence of pO_2 gradients on *Saccharomyces cerevisiae* and proinsulin producing *E. coli* by circulating the culture between anoxic and aerobic conditions, respectively. It could be shown that the oscillation lead to reduced biomass and increased by-product formation in the first case, whereas increased glucose uptake and organic acid formation rates, plus a significant decrease in product yield was observed for the *E. coli* cultures.

The STR-PFR is the most frequently used concept in the past two decades (Lara et al., 2006a), widely applied (Bylund et al., 2000; Neubauer et al., 1995a,b; Schweder et al., 1999), and originally published with and without static mixers by George et al. (1993) and Larsson & Enfors (1988). The system was recently extended to simulate substrate and pO_2 gradients leading to increased by-product formation and a general metabolic shifting in *Bacillus subtilis* (Junne et al., 2011). Therefore, the PFR was equipped with multiple pH/O_2 probes and sampling ports to firstly record time- and place-dependent cultivation

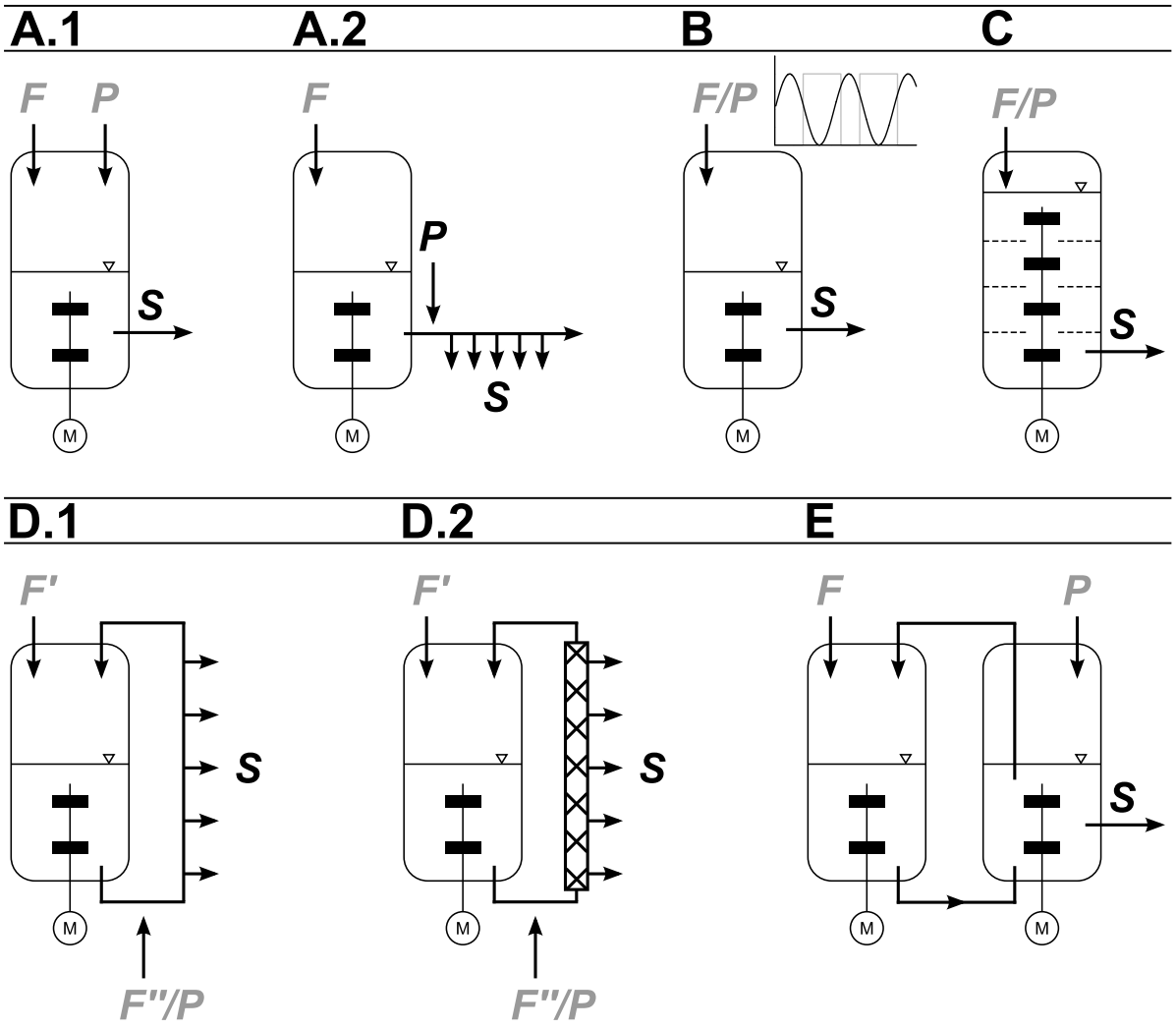

Fig. 2.2: Simplified overview of published one- **(A–C)** and two- **(D–E)** compartment scale-down concepts that were used to simulate large scale conditions by applying various bioreactor inhomogeneities. **(A.1)** Rapid sampling after perturbation of a single-compartment bioreactor (Schaefer et al., 1999). **(A.2)** Perturbation at the entry position of a stopped-flow sampling device (Lara et al., 2009). **(B)** Rapid sampling of a single-compartment bioreactor after application of various feeding regimes (homogeneous oscillation, step function, etc.) as demonstrated in e.g. de Jonge et al. (2011). **(C)** Compartmentalization of the bioreactor by perforated disks between stirrer blades (Schilling et al., 1999). **(D.1)** Two-compartment system connecting a stirred tank bioreactor (STR) to a plug-flow reactor (PFR) that serves as by-pass (Larsson & Enfors, 1988). **(D.2)** Enhancement of the original STR-PFR setup through static mixers (George et al., 1993) and advanced process control via measurement probes or aeration (Junne et al., 2011). **(E)** Two-compartment STR-STR setup as firstly demonstrated by Oosterhuis (1984) and Oosterhuis et al. (1985). Abbreviations are as follows: F, (optional) feed addition with multiple entry sites where applicable; P^*, tracer pulse or perturbation; S^*, common sample port(s) position(s). The illustration was modified after Junne et al. (2011) and Lara et al. (2006a).

profiles in the PFR. Slightly different approaches were followed by developing the STR-PFR concepts "BioCurve" (Aboka, 2008; Aboka et al., 2006) and "BioScope" (Lara et al., 2009; Mashego et al., 2006; Visser et al., 2002). Whereas the "BioScope" device can only be used to study non-stationary (pulse) perturbation effects, "BioCurve" facilitates well-mixed conditions (high recycle flow) with O_2/CO_2 online measurements (Aboka et al., 2006). However, both assemblies share the common feature of two hemispherical channels (liquid flow and gas exchange) with a two-dimensional serpentine/loop geometry, milled in a Perspex block, and separated by a silicone membrane permeable to O_2 and CO_2 (Lara et al., 2009; Mashego et al., 2006). Both systems were applied to study very fast metabolic responses (by-product formation) of *E. coli* to glucose pulses.

Relatively simple designs are realized with one-compartment STRs, applying sudden or oscillating perturbations to trigger (short term) metabolic responses of cells that were previously in (pseudo) steady-state (Takors, 2012). Rapid sampling after the pulse and immediate inactivation of the metabolism are essential (Oldiges & Takors, 2005; Oldiges et al., 2007). Different concepts were introduced as reviewed in Schädel & Franco-Lara (2009), ranging from automatic sampling devices (Magnus et al., 2006; Oldiges et al., 2007; Schaefer et al., 1999) to a stopped-flow technology enabling the stimulus outside the bioreactor in the sampling device itself (Buziol et al., 2002; Mauch et al., 2000). Eventually, all short-term perturbation studies aim to unravel basic metabolic control mechanisms (Reuss et al., 2007).

However, these one-compartment-based methods have their pitfalls concerning potential culture changes after the stimulus and general repeatability (Neubauer & Junne, 2010). Additionally, not every perturbation concept associated with large scale reactor inhomogeneities can be examined, e.g. as fluctuating dissolved gas concentrations or partial pressures are limited by the slow response time of such systems due to slow adsorption and desorption rates (Lara et al., 2006a). Even though, the latter was just recently applied to investigate penicillin production using an intermittent feeding regime in a (pseudo) scale-down study with simulated substrate oscillations reducing the overall productivity (de Jonge et al., 2011).

In summary, various scale-down studies were reported applying a multitude of different gradients on prokaryotic and eukaryotic organisms. Within the last couple of years, initial phenomenological investigations were complemented by advanced methods from all "OMICS" technologies (e.g. transcriptomics) to get further insights on the complex regulatory response of the cells. Schweder et al. (1999) were one of the first using transcriptional analysis to report rapid stress gene expression in response to O_2

and glucose gradients in a comparative experimental setup of *E. coli* fermentations in an industrial-type 30 m^3 STR and a STR-PFR scale-down device. Recently, the initial findings were taken up presenting a summary of stress- and nutrient limitation-specific marker genes that indicate the physiological status of the bacterial production hosts *Bacillus subtilis*, *B. licheniformis*, and *E. coli* (Schweder, 2011). Similarly, Lara et al. (2006b) used a previously published STR-STR device (Sandoval-Basurto et al., 2005) to simulate pO_2 gradients with an *E. coli* green fluorescent protein (GFP) producer strain and reported a fast transcriptional adaption to the aerobic and anaerobic compartments, the up-regulation of genes coding for mixed acid metabolism (plus by-product formation), as well as a reduced final product titer compared to reference conditions. Alternatively, direct coupling of GFP to reporter genes, e.g to the stress response associated *rpoS* gene (Delvigne et al., 2009), was used to demonstrate the impact of extracellular perturbations or artificially reduced bioreactor mixing efficiency, thereby establishing a platform approach for the lab scale validation of industrial-like conditions, which can also be coupled to flow cytometry measurements (Brognaux et al., 2013; Delvigne et al., 2010, 2011; Han et al., 2013; Hewitt et al., 2007) or dynamic single cell analysis in general (Delvigne & Goffin, 2014).

2.3.1 Flow characterization of (scale-down) bioreactors

One fundamental implication of the scale-down devices presented in Fig. 2.2 (concept C–E), is the alteration of the (overall) system geometry or, more importantly, of the flow behavior. Originating from an ideal lab scale single-compartment STR with perfect mixing, this allows the experimenter to apply artificial gradients or the abstraction of the flow path of the cells at large scale with multi-compartment devices. As detailed above, cells are subjected to various environmental stimuli and the time of exposure is usually carefully designed, often correlating to manufacturing scale mixing conditions (section 2.2). Therefore, the accurate determination of the (mean) residence time (of the cells) for the given experimental setup (or compartment) is essential and commonly carried out by tracer experiments. Subsequently, the determination of the probability function of the residence time, i.e. the residence time distribution (RTD), provides the required information for the development of suitable models that represent the flow pattern, which usually lies between the two extremes of plug and mixed flow, or facilitate the comparison to prevalent models of the literature (Levenspiel, 2012).

Common experimental practice is the use of tracing agents (chemically inert or non-reactive) as e.g. fluorescent dyes or salt solutions for conductivity changes, which are injected into the system following step or pulse functions. The latter is mostly the method of choice and also termed as Delta Dirac function $\delta(t)$, which is mathematically defined as:

$$\delta(t) = \begin{cases} 0, & t \neq 0 \\ \infty, & t = 0 \end{cases} \qquad [2.1]$$

with

$$\int_{-\infty}^{\infty} \delta(t)dt = 1 \qquad [2.2]$$

Due to experimental limitations of the injection procedure, a common practical orientation is given in reference to the average space time of the system τ, aiming to yield a pulse duration of: $\Delta t \approx 0.01\,\tau$.

Two frequently used approaches for the representation of flow patterns of compartment systems in chemical (reaction) engineering are the dispersion and tank-in-series (TIS) model. The former is frequently applied to distinguish between the existence of ideal plug flow (flat velocity profile) and dispersed plug flow (longitudinal fluctuations) in PFR or PFR-like reactors. The mass balance (after tracer injection) for a volume element (V_E = constant) considering the summation of convection and diffusion is defined as:

$$\frac{\partial c}{\partial t} = -u\,\frac{\partial c}{\partial z} + D_{ax}\,\frac{\partial^2 c}{\partial z^2} \qquad [2.3]$$

with D_{ax} as longitudinal dispersion coefficient (in $\mathrm{m^2\,s^{-1}}$), u as mean flow velocity (in $\mathrm{m\,s^{-1}}$), c as (tracer) concentration (in $\mathrm{mol\,L^{-1}}$), and z as coordinate (in m). Standardization of Eq. 2.3 using the dimensionless factors $\zeta = z/L$ with L as length of the section (in m), $C = c/c_0$ with c_0 as initial (tracer) concentration, and $\Theta = t/\bar{t} = t\,u/L$ with $\bar{t}$ as mean residence time of passage, results in:

$$\frac{\partial C}{\partial \Theta} = -\frac{\partial C}{\partial \zeta} + \frac{1}{\mathrm{Bo}}\,\frac{\partial^2 C}{\partial \zeta^2} \qquad [2.4]$$

where Bo is defined as Bodenstein number, a dimensionless quantity indicating the ratio between the flow of the bulk liquid (convection) and the axial dispersion with:

$$\mathrm{Bo} = \frac{L\,u}{D_{ax}} \tag{2.5}$$

Both extreme flow environments (ideal reactors) can therefore be obtained depending on the approximation of:

$$\mathrm{PFR}: \quad \mathrm{Bo} \longrightarrow \infty \tag{2.6}$$

$$\mathrm{STR}: \quad \mathrm{Bo} \longrightarrow 0 \tag{2.7}$$

In the literature, an experimental verification of Bo > 10 is considered sufficient for proven PFR behavior (George et al., 1993). For the dispersion model the dimensionless residence time distribution $E(\Theta)$ is defined as:

$$E(\Theta) = \frac{1}{2}\sqrt{\frac{\mathrm{Bo}}{\pi\,\Theta}}\,e^{-\frac{\mathrm{Bo}}{4\Theta}(1-\Theta)^2} \tag{2.8}$$

Alternatively, the TIS model considers a series of equally sized tanks in series. Each of the N_T reactors behaves as an ideal continuous stirred tank reactor (CSTR) with a steady flow ν (in $\mathrm{L\,min^{-1}}$) into and out of the tank. The residence time distribution $E(t)$ of a single CSTR is found to be:

$$E(t) = \frac{1}{\bar{t}}\,e^{-\frac{t}{\bar{t}}} \tag{2.9}$$

When using more than one compartment, the input signal $c_{in}(t)$ of the first will be modified according to its flow and $E(t)$, producing an output signal $c_{out}(t)$ that will in turn serve as input signal for the next compartment as depicted in Fig. 2.3. The convolution integral relates the input and output signal as follows:

$$c_{out}(t) = \int_0^t c_{in}(t-t')\,E(t')dt' = \int_0^t c_{in}(t')\,E(t-t')dt' \tag{2.10}$$

where t' is the time of the tracer molecule entering the system before leaving the reactor after $t - t'$.

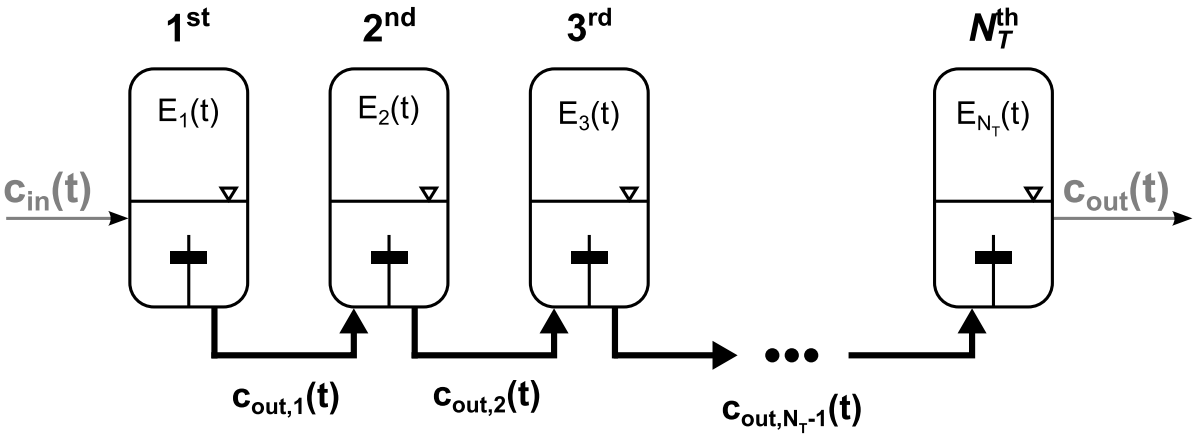

Fig. 2.3: Schematic drawing of the tank-in-series model, which considers a number of N_T ideal continuous stirred tank reactors. The input signal $c_{in}(t)$, a tracer pulse, injected into the first tank distributes according to the individual residence time distribution $E(t)$ for each individual tank as indicated, and results in the global output signal $c_{out}(t)$.

With the help of Laplace transforms, $E(t)$ for N_T number of ideal, identical tanks can be derived as firstly published by MacMullin & Weber (1935) as follows:

$$E(t) = \frac{1}{\bar{t}} \left(\frac{1}{\bar{t}} \right)^{N_T - 1} \frac{N_T^{N_T}}{(N_T - 1)!} e^{-\frac{t\, N_T}{\bar{t}}} \qquad [2.11]$$

Accordingly, the dimensionless representation is given by:

$$E(\Theta) = N_T \frac{(N_T\, \Theta)^{N_T - 1}}{(N_T - 1)!} e^{-N_T\, \Theta} \qquad [2.12]$$

When plotting Eq. 2.12 for increasing ideal tanks as depicted in Fig. 2.4 one can derive that the RTD for a reactor cascade approaches ideal plug flow behavior for $N_T \longrightarrow \infty$. For the characterization of the given experimental setup, the estimation of N_T according to the TIS therefore helps to determine the corresponding number of ideal tanks.

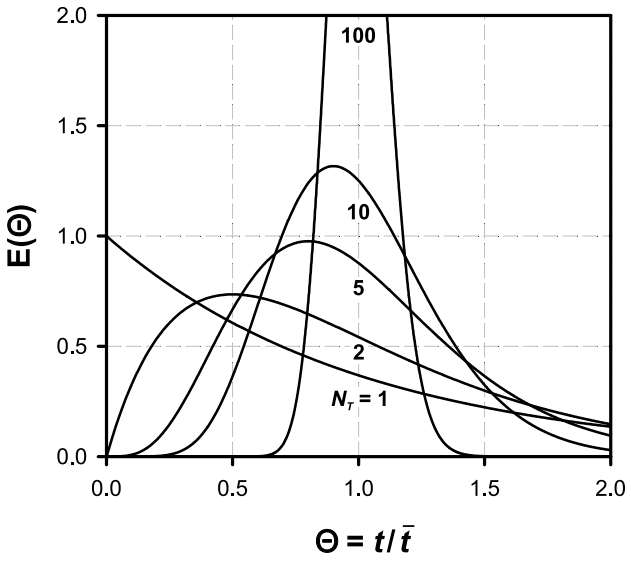

Fig. 2.4: Normalized residence time distribution curves $E(\Theta)$ for the tank-in-series model calculated for the indicated number of ideal tanks N_T according to Eq. 2.12. The figure was modified after Levenspiel (1999) and illustrates the approximation to plug flow behavior for a series of ideal continuous stirred tank reactors with $N_T \longrightarrow \infty$.

2.3.2 Inhomogeneity studies using *Corynebacterium glutamicum*

Despite the significance of *C. glutamicum* for the biotechnological industry, only few studies have been dealing with the investigation of its scale-down characteristics. The first reference is given by Schilling et al. (1999) who used a compartmented single STR setup (Fig. 2.2) on an L-lysine production process to artificially reduce the mixing quality. However, a detailed gradient characterization was not provided and critically remarked (Lara et al., 2006a). Therefore, the reported physiological consequences of overall reduced growth, substrate uptake, and product formation compared to reference conditions remain questionable. While the study of Chamsartra et al. (2005) documented the relatively low impact of fluid mechanical stress on *C. glutamicum* in an excursion of scale-up related questions on process performance, further scale-down investigations were only recently published. Thereby, fermentations with *C. glutamicum* WT and the L-lysine producer strain *C. glutamicum* DM1933 in a previously published STR-PFR system (Junne et al., 2011) revealed the general robustness of the bacterium to common bioreactor inhomogeneities (via most technologies of the complete "OMICS" spectrum) imitated by intensive pO_2 and substrate oscillations with residence times in the PFR of up to 2.8 min (Käß et al., 2013, 2014).

2.3.3 Scale-up/down implications of varying carbon dioxide/bicarbonate levels

As indicated in section 2.1.2, the major source of CO_2 found in (microbial) fermentation processes derives from cellular respiration. Enforced by an about 30-fold increased solubility compared to O_2 at 30 °C (Carroll et al., 1991; Weiss, 1970), high amounts of CO_2 not only leave the bioreactor as exhaust gas ($CO_{2,g}$) but also dissolved in the cultivation medium ($CO_{2,l}$). The concentration of the latter can be related to the CO_2 partial pressure of the surrounding gas atmosphere ($CO_{2,g}$) according to Henry's law, defined as:

$$CO_{2,l} = H \times pCO_{2,g} \quad [2.13]$$

with H as Henry's law constant (in $mol\,L^{-1}\,atm^{-1}$) being strongly temperature and solvent dependent (Jones & Greenfield, 1982; Stumm & Morgan, 1996). However, the dissociation equilibrium of CO_2, or rather of all carbonic acid species is complex and depends in actual experimental processes not only on the applied cultivation medium and bioreactor environment (absorption and desorption rates), but also on the pH of the cultivation liquid (Stumm & Morgan, 1996). Under physiological conditions e.g. at pH 7.4, HCO_3^- is the predominant species followed by CO_2 with a ratio larger than 10 : 1 (Fig. 2.5 A and section C.1). Nevertheless, to consider all species is essential for advanced process analyses as e.g. carbon balancing, in which the cumulative determination of the total inorganic carbon (TIC) amount is necessary (Ho et al., 1987):

$$TIC = CO_{2,l} + H_2CO_3 + HCO_3^- + CO_3^{2-} \quad [2.14]$$

Following from the equilibrium constants (K_1 and K_2) of the carbonic acid distribution (Stumm & Morgan, 1996), Eq. 2.14 derives to:

$$TIC = CO_2 \left(1 + \frac{K_1}{[H^+]} + \frac{K_1 K_2}{[H^+]^2}\right) \quad [2.15]$$

which can then be used to calculate the individual and total species concentrations for an aqueous carbonate equilibrium as depicted in Fig. 2.5 B.

However, CO_2/HCO_3^- may not only serve as co-substrate/-product for enzymes, but has also the potential to alter physico-chemical properties of proteins, acidify the internal pH, and regulate virulence and toxin production in pathogens (Follonier et al.,

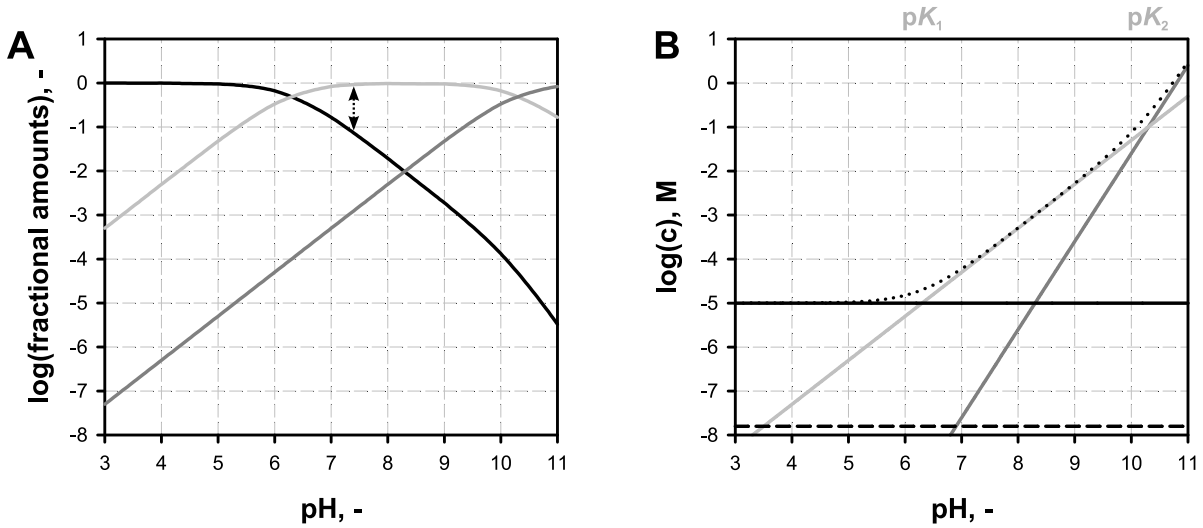

Fig. 2.5: (A) Distribution of the carbonate species in an aqueous solution of a closed system. The fractional amounts of CO_2 (—), HCO_3^- (—), and CO_3^{2-} (—) are indicated for the complete pH range at chemical equilibrium constants of $K_1 = 10^{-6.3}\,\mathrm{mol\,L^{-1}}$ and $K_2 = 10^{-10.3}\,\mathrm{mol\,L^{-1}}$ (refer to section C.1). Indication of the dominating species ($HCO_3^- : CO_2 > 10 : 1$) at physiological pH conditions during *C. glutamicum* fermentations at pH 7.4. **(B)** Aqueous carbonate equilibrium with air as atmosphere and ambient CO_2 concentration. The logarithm of the species concentrations [$\log(c)$] is exemplarily illustrated for a system at $T = 25\,°C$; with H_2CO_3 (- - -) and the total inorganic carbon (TIC; ····) according to Eq. 2.15.

2013). CO_2 freely diffuses through the cellular membrane (Gutknecht et al., 1977) and might accumulate in the same (Bothun et al., 2004; Jones & Greenfield, 1982; Kuriyama et al., 1993). This can increase its fluidity and permeability eventually leading to potentially lethal "anaesthesia effects" (Isenschmid et al., 1995). In addition, detrimental consequences of high CO_2 pressures, as might occur at large scale, were reported on vitality, growth, metabolism, and productivity of many industrially relevant bacteria and fungi (Amoabediny & Büchs, 2010; Amoabediny et al., 2010; Baez et al., 2009; Castan et al., 2002; Dixon & Kell, 1989; El-Sabbagh et al., 2006, 2008; Jones & Greenfield, 1982; McIntyre & McNeil, 1997), being advantageous for emerging non-thermal pasteurization methods of foodstuffs (Ballestra et al., 1996; Garcia-Gonzalez et al., 2007; Spilimbergo & Bertucco, 2003).

Despite its physiological impact and its prevalence under large scale conditions, only limited work has been carried out on the scale-up dependent CO_2/HCO_3^- impact by scale-down studies (Aguilera et al., 2005; Baez et al., 2009, 2011). Regarding *C. glutamicum*, Bäumchen et al. (2007) firstly revealed that the impact of CO_2-enriched environments depends strongly on the applied culture conditions: where CO_2 partial pressures above (200–300) mbar (in exhaust gas) led to maximum growth rates in turbidostat cultures on

glucose, enhanced biomass formation was detected with lactate as carbon source. These statements were further confirmed in a series of high pressure fermentations up to 10 bar, revealing that growth of *C. glutamicum* in fed-batch cultures (specific growth rate set to $0.16\,h^{-1}$) to very high densities of $226\,g\,L^{-1}$ are not inhibited by maximum CO_2 partial pressures of 0.6 bar (Knoll et al., 2005, 2007).

Thereupon, constant elevated partial pressures of $pCO_2 > 150$ mbar were shown to trigger an acid stress response in *E. coli* cultures (Baez et al., 2009). In a further study, Baez et al. (2011) utilized the concept described by Sandoval-Basurto et al. (2005) and implemented pCO_2 monitoring and control. The latter is in fact the first publication that tries to determine the effect of oscillatory pCO_2 gradients on microbial fermentations by scale-down simulation. It could be shown that when considerably high t_c of 375 s are applied, the (specific) growth rate and productivity (GFP) decreases, whereas by-product formation was stimulated. In addition, pCO_2 fluctuations were followed on transcriptional level by analyzing glutamate decarboxylase and 2-oxoglutarate dehydrogenase genes by quantitative real-time PCR (qRT-PCR). It has to be noted that the detrimental effects on growth and yields with lower t_c were less prominent since *E. coli* could rapidly adept their metabolism and reestablish homeostasis. Taken together, Baez et al. (2011) conclude the overall effect (t_c = 170 s and 375 s and pCO_2 of 213 mbar at maximum) on protein production in this particular study as generally not significant.

CHAPTER 3
MATERIALS AND METHODS

This chapter summarizes materials and methods that have been used throughout this study. Some sections of this chapter have been published or submitted partially or in detail in the manuscripts I–IV (appendices A–D). Cross references are provided when applicable.

3.1 Bacterial strains, media, and cultivation systems

The WT strain *C. glutamicum* ATCC13032 obtained from the American Type Culture Collection (ATCC, Manassas, VA, USA), its derivatives *C. glutamicum* Δ*dtxR* (Brune et al., 2006) kindly provided by the Kalinowski lab (CeBiTeC, Bielefeld, Germany), *C. glutamicum* Δ*ppc*, Δ*malE*, Δ*pyc*, and Δ*pck* (Blombach et al., 2013), the L-valine and 2-ketoisovalerate producers *C. glutamicum aceE* A16 Δ*pqo* Δ*ppc* (pJC4 *ilvBNCE*) and *C. glutamicum aceE* A16 Δ*pqo* Δ*ppc* Δ*ilvE* (pJC4 *ilvBNCD*) (Buchholz et al., 2013), as well as the L-lysine producer *C. glutamicum* DM1933 (Blombach et al., 2009a), were used in this study. Detailed information about the cryogenic, pre- and main culture media, as well as about the corresponding cultivation systems, culture and process conditions can be found as follows:

(i) Fed-batch fermentations with *C. glutamicum aceE* A16 Δ*pqo* Δ*ppc* (pJC4 *ilvBNCE*) and *C. glutamicum aceE* A16 Δ*pqo* Δ*ppc* Δ*ilvE* (pJC4 *ilvBNCD*) were carried out in 3 L scale bench-top bioreactors according to section A.2.3 (manuscript I).

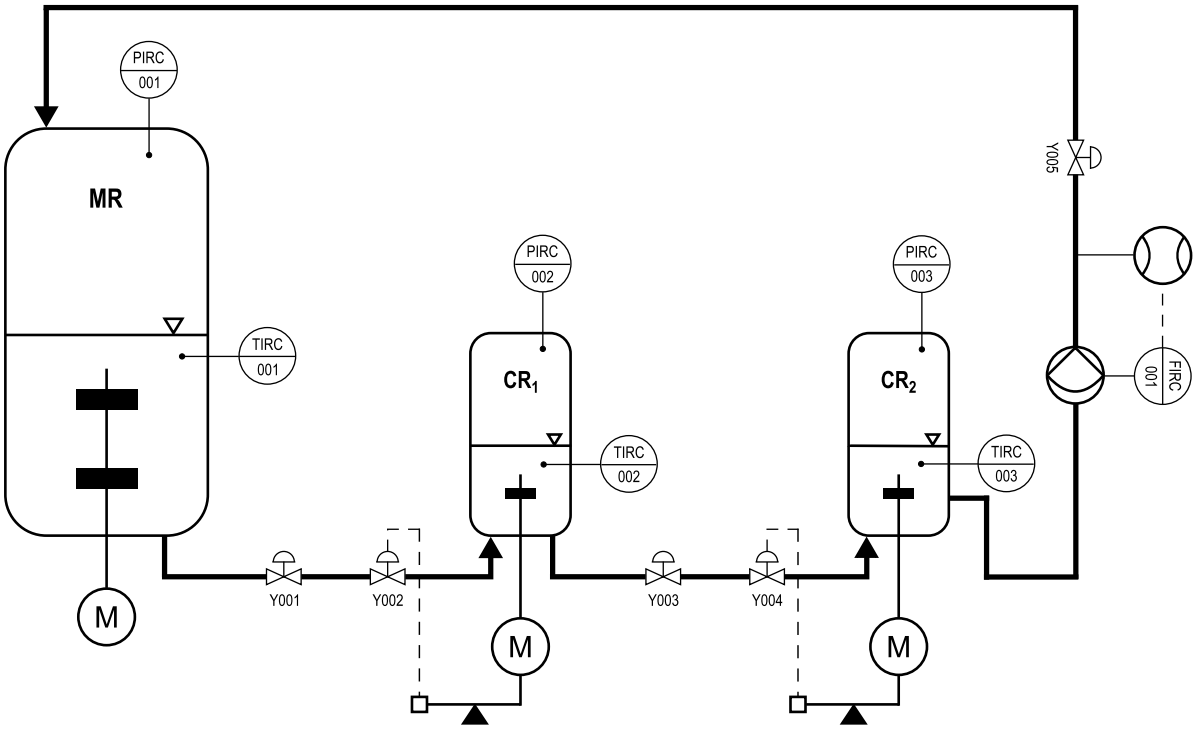

Fig. 3.1: Flow sheet of the cascade bioreactor system (CBS) consisting of a 100 L scale main (MR) and two 1 L cascade reactors (CR) put in series. Forward liquid transport (MR ⇒ CR_1 ⇒ CR_2) is facilitated by a pressure gradient (PIRC) and total recirculation by a diaphragm metering pump controlled by a mass flow meter (FIRC). Volumetric level control of both CRs was performed gravimetrically and through regulating valves (Y) as indicated. During cascade cultivations, secondary process parameters as e.g. the temperature were kept constant (TIRC). The figure was modified after from Fig. D.1.

(ii) Batch fermentations with *C. glutamicum* WT, Δ*dtxR*, Δ*ppc*, Δ*malE*, Δ*pyc*, and Δ*pck* were carried out in 1 L scale bench-top bioreactors according to section B.2.1 and section B.2.2 (manuscript II).

(iii) Batch fermentations using *C. glutamicum* WT and *C. glutamicum* DM1933 were carried out at 100 L scale and in the newly developed cascade bioreactor system (CBS) according to section C.2.1 (manuscript III), section D.2.2 and section D.2.3, respectively (manuscript IV).

Detailed information regarding the bioreactor dimensions of the 1 L and 100 L bioreactor are schematically depicted in the appendix (Fig. DS.1 and Tab. DS.3). For scale-down processes, a newly developed CBS consisting of the 100 L scale main reactor (MR) and two 1 L scale cascade reactors (CR) set in series was used. The corresponding flow sheet of the experimental setup is given elsewhere (Fig. 3.1), whereas a photograph

is provided in Fig. 4.10. Further details on the description of the construction can be found in section D.2.3.

The general working procedure based on the application of a pressure gradient (Δp = 0.4 bar) between the individual STRs (MR ⇒ CR_1 ⇒ CR_2) and a subsequent diaphragm metering pump that is responsible for the back flow into the MR. Constant circulation flows between (0.58–3.95) L min^{-1} can be facilitated, enabling a constant liquid distribution by gravimetrically-based level control of both CRs. To establish CO_2/HCO_3^- gradients during the cultivation process, CO_2 was proportionately added to the inlet gas flow (air) followed via pCO_2 probes in the liquid phase. However, all other process parameters were kept constant.

3.2 Analytical methods

References to detailed information about the analytical methods including the determination of the optical density (OD), biomass (X), as well as amino and organic acid analysis via high pressure liquid chromatography (HPLC) can be found in the following. Where applicable, information about the transcriptional analysis by DNA microarray and total carbon (TC) analysis are also provided:

(i) Analytical procedures for the fed-batch fermentations with *C. glutamicum aceE* A16 Δ*pqo* Δ*ppc* (pJC4 *ilvBNCE*) and *C. glutamicum aceE* A16 Δ*pqo* Δ*ppc* Δ*ilvE* (pJC4 *ilvBNCD*) are described in section A.2.6 (manuscript I).

(ii) General analytical methods for batch fermentations with *C. glutamicum* WT, Δ*dtxR*, Δ*ppc*, Δ*malE*, Δ*pyc*, and Δ*pck* is given in section BS.1.4 and section BS.1.5, whereas information about the DNA microarray experiments are provided in section BS.1.7 (manuscript II).

(iii) General and TC-specific analytical methods for batch fermentations using *C. glutamicum* WT and *C. glutamicum* DM1933 are given in section C.2.2 (manuscript III).

(iv) General, TC-specific, and information about the DNA microarray experiments for CBS fermentations are described in section D.2.4 (manuscript IV).

3.3 Quantification of fermentations and data analysis

3.3.1 Bacterial growth kinetics

The inoculation of cells into fresh media as part of the seed train might be followed by an adaption phase to the new environment (e.g. different substrates, temperature, pH, etc.) with no or only little growth. This phase is designated as "lag phase" and the consequence of altered gene expression and/or enzyme production essential for growth under the new conditions. The length of this period depends on many factors as e.g. cell type and age, cell number, or the type of medium. After adaption of the cells to the new conditions, the specific growth rate μ (in h^{-1}) increases moderately and biomass formation follows a specific time course under the limitation of one substrate, which is schematically depicted in Fig. 3.2. The following phase is characterized by a constant, maximum growth rate μ_{max} (in h^{-1}), thus termed "exponential phase". Afterwards, the substrate concentration becomes limiting and growth declines ("decelerating phase") finally leading to the "stationary phase" when substrate is completely consumed. Without sufficient energy supply, homeostasis and maintenance functions cannot be sustained, leading to cell destruction and death ("declining phase").

In a closed system, μ can be obtained from the mass balance of the biomass in a batch process following:

$$\frac{dm_X}{dt} = \mu X V_R \qquad [3.1]$$

with m_X as amount of biomass (in g), X as biomass concentration (in $g\,L^{-1}$), and V_R as working volume of the bioreactor (in L). Given $m_X = X V_R$ and V_R = constant for a batch process ($dV_R/dt = 0$), Eq. 3.1 simplifies to:

$$\mu = \frac{1}{X}\frac{dX}{dt} \qquad [3.2]$$

Upon integration of Eq. 3.2, the time required for the given cell mass or number to double is given by the doubling time t_d (in h) defined as:

$$t_d = \frac{\ln 2}{\mu} \qquad [3.3]$$

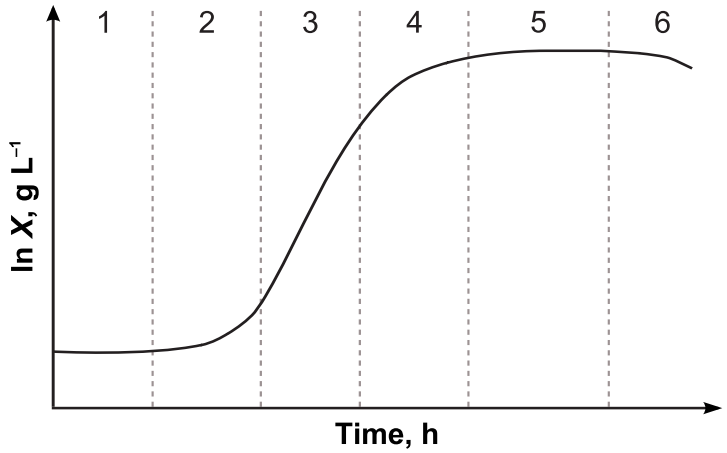

Fig. 3.2: Typical growth curve of bacterial cells in a batch culture on one substrate. After an initial "lag phase" of the cells due to adaption to the new environment **(1)**, the growth increases in the "accelerating phase" **(2)**. A constant, maximum growth rate is obtained in the "exponential growth" phase **(3)**, before substrate limitation causes cell growth to decrease in the "decelerating phase" **(4)**. Finally, growth and death rate become equal resulting in a constant cell concentration in the "stationary phase" **(5)**, eventually leading to self-destruction and cell death characteristic for the "declining phase" **(6)**. Modified after (Katoh & Yoshida, 2009).

For batch cultivations with only one limiting substrate as illustrated above (Fig. 3.2), growth is considered as an unstructured (black box) model in which balanced growth as proposed by Monod (1949) is defined as:

$$\mu = \mu_{\max} \frac{S}{K_S + S} \qquad [3.4]$$

with S as limiting substrate concentration (in $\mathrm{g\,L^{-1}}$) and K_S as saturation constant concentration (in $\mathrm{g\,L^{-1}}$). Given the case that $S >> K_S$ applies, which is justified for *C. glutamicum* for $S >> 0.36\,\mathrm{g\,L^{-1}}$ (Lindner et al., 2011), Eq. 3.4 simplifies to:

$$\mu = \mu_{\max} \qquad [3.5]$$

in the exponential phase. Unless otherwise stated, all growth rates in this study are thus indicated as μ, correspond to $\mu_{\max}$, and were obtained by linear regression and least squares fitting of $\ln X(t)$ courses of the constant (exponential) phase (μ = constant). Alternatively, the integration of Eq. 3.2 results in:

$$X_t = X_0\, e^{\mu t} \qquad [3.6]$$

which was used for the calculation of μ between two biomass time points ($t = 0$ and t).

As stated above, cell growth under unlimited conditions (as in batch mode) resembles inevitably μ_{max} (Eq. 3.4). To deal with the undesired overflow metabolism, and with the significant oxygen demand of high cell densities while regarding the oxygen transfer capabilities of the bioreactor (Eq. 3.17), fed-batch processes are typically carried out in the industrial context (e.g. section 2.1.1). Applying substrate limiting conditions by distinct feeding profiles is a common strategy to control μ during the fermentation process. Derived from substrate mass balancing of a fed-batch process given with:

$$\frac{dm_S}{dt} = F\,S_{in} + q_S\,X\,V_R \qquad [3.7]$$

with F as feed rate (in $\mathrm{L\,h^{-1}}$), S_{in} as substrate concentration of the feed (in $\mathrm{g\,L^{-1}}$), and q_S as biomass specific substrate uptake rate described below (in $\mathrm{g\,g^{-1}\,h^{-1}}$). After insertion of Eq. 3.6 and integration, an exponential feeding regime can be obtained for the desired μ, given the corresponding feed rate at time point t as follows:

$$F(t) = \frac{\mu}{Y_{XS}}\,\frac{1}{S_{in}}\,X_0\,V_0\,e^{\mu t} \qquad [3.8]$$

given that $q_S = \mu/Y_{XS}$, whereas X_0 and V_0 denote for the biomass concentration and the liquid volume of the bioreactor at feed start, respectively.

3.3.2 Substrate uptake, product formation, and yield coefficients

Similar to the mass balance of the biomass (Eq. 3.1), the mass balances for the substrate and product in closed (batch) systems are defined as:

$$\frac{dm_S}{dt} = -q_S\,X\,V_R \qquad [3.9]$$

$$\frac{dm_P}{dt} = q_P\,X\,V_R \qquad [3.10]$$

with m_S being the amount of substrate (in g), m_P of the product (in g), and q_P the biomass specific production rate (in $\mathrm{g\,g^{-1}\,h^{-1}}$). Under the assumption of $m_S = S\,V_R$,

$m_P = P\,V_R$, and V_R = constant, Eq. 3.9 and Eq. 3.10 simplify to:

$$q_S = -\frac{1}{X}\frac{dS}{dt} \qquad [3.11]$$

$$q_P = \frac{1}{X}\frac{dP}{dt} \qquad [3.12]$$

In the following, q_S is defined and indicated positive throughout this thesis. The total volumetric production rate Q_P (in $\mathrm{g\,L^{-1}\,h^{-1}}$) was derived from linear regression and least squares fitting of product concentrations over time (V_R = constant). By relating the specific growth rate to the specific production and uptake rate, one can calculate the differential (Y_{XS}, Y_{PS}, or Y_{PX}) biomass or product yields (in $\mathrm{g\,g^{-1}}$), respectively:

$$Y_{XS} = \frac{dX/dt}{dS/dt} = \frac{dX}{dS} = \frac{\mu}{q_S} \qquad [3.13]$$

$$Y_{PS} = \frac{dP/dt}{dS/dt} = \frac{dP}{dS} = \frac{q_P}{q_S} \qquad [3.14]$$

$$Y_{PX} = \frac{dP/dt}{dX/dt} = \frac{dP}{dX} = \frac{q_P}{\mu} \qquad [3.15]$$

Alternatively, integral biomass or product yields were determined between $t = 0\,\mathrm{h}$ (at process start) and t, and obtained from linear regression and least squares fitting. Within the exponential phase, q_S and q_P were calculated according to Eq. 3.13 and Eq. 3.15, respectively, if μ and the corresponding yield coefficient are constant. In that case, and where applicable, the determination of the standard deviation (SD) of that function was based on the uncertainties of the individual factors (assuming uncorrelated errors) by Gaussian error propagation. Let $f(x, y)$ be a function of two variables (quantities), one then obtains the total uncertainty σ_f of f as follows:

$$\sigma_f = \sqrt{\left(\frac{\partial f}{\partial x}\right)^2 \sigma_x^2 + \left(\frac{\partial f}{\partial y}\right)^2 \sigma_y^2} \qquad [3.16]$$

3.3.3 Respiration rates and exhaust gas analysis

The supply of oxygen is one of the key factors for aerobic cultivations. The oxygen transfer rate OTR (in $\mathrm{mol\,L^{-1}\,h^{-1}}$) is proportional to the volumetric mass transfer coefficient $k_L a$ (in $\mathrm{h^{-1}}$) and the concentration driving force for mass transfer defined as:

$$\mathrm{OTR} = k_L a \left(c^*_{\mathrm{O_2}} - c_{\mathrm{O_2}}\right) \quad [3.17]$$

with $c^*_{\mathrm{O_2}}$ (in $\mathrm{mol\,L^{-1}}$) as oxygen concentration in the liquid at the gas-liquid interface, and $c_{\mathrm{O_2}}$ (in $\mathrm{mol\,L^{-1}}$) as oxygen concentration in the bulk liquid. The accumulation ($dc_{\mathrm{O_2}}/dt$) of oxygen in the liquid (well-mixed) relates the OTR (from the gas to the liquid phase) and the consumption by the microorganism by the oxygen uptake rate OUR (in $\mathrm{mol\,L^{-1}\,h^{-1}}$):

$$\frac{dc_{\mathrm{O_2}}}{dt} = \mathrm{OTR} - \mathrm{OUR} \quad [3.18]$$

The OUR is directly derived from the mass balance of oxygen and V_R according to:

$$\mathrm{OUR} = \frac{\Delta \dot{n}_{\mathrm{O_2}}}{V_R} \quad [3.19]$$

with $\Delta \dot{n}_{\mathrm{O_2}}$ as absorbed oxygen mass flow (in $\mathrm{mol\,h^{-1}}$) calculated from the incoming ($\dot{n}_{\mathrm{O_{2,in}}}$) and outgoing ($\dot{n}_{\mathrm{O_{2,out}}}$) amount of oxygen of the inlet and exhaust gas by:

$$\Delta \dot{n}_{\mathrm{O_2}} = \dot{n}_{\mathrm{O_{2,in}}} - \dot{n}_{\mathrm{O_{2,out}}} \quad [3.20]$$

Inserting the ideal gas law into Eq. 3.20, which is defined as:

$$p\,\dot{V}_g = \dot{n}\,R\,T \quad [3.21]$$

with $\dot{V}_g$ (in $\mathrm{L\,h^{-1}}$) as volumetric gas flow rate, R as universal gas constant (in $\mathrm{J\,mol^{-1}\,K^{-1}}$), T as absolute temperature (in K), y as molar O_2 and CO_2 fractions of the inlet and outlet, and p as pressure (in Pa), assuming isobaric and isothermal (inlet to outlet), and providing the inert gas balance, the OUR can be calculated as:

$$\mathrm{OUR} = \frac{p}{RT}\,\frac{\dot{V}_{g,\mathrm{in}}}{V_R}\left(y_{\mathrm{O_{2,in}}} - y_{\mathrm{O_{2,out}}}\left[\frac{1 - y_{\mathrm{O_{2,in}}} - y_{\mathrm{CO_{2,in}}}}{1 - y_{\mathrm{O_{2,out}}} - y_{\mathrm{CO_{2,out}}}}\right]\right) \quad [3.22]$$

In analogy to the determination of the OUR, the carbon dioxide evolution rate CER (in $\mathrm{mol\,L^{-1}\,h^{-1}}$) was derived from:

$$\mathrm{CER} = \frac{p}{RT}\frac{\dot{V}_{g,\mathrm{in}}}{V_R}\left(\left[\frac{1 - y_{\mathrm{O_{2,in}}} - y_{\mathrm{CO_{2,in}}}}{1 - y_{\mathrm{O_{2,out}}} - y_{\mathrm{CO_{2,out}}}}\right] y_{\mathrm{CO_{2,out}}} - y_{\mathrm{CO_{2,in}}}\right) \quad [3.23]$$

The volumetric respiration rates (Eq. 3.22 and Eq. 3.23) are related to X in order to obtain the biomass specific oxygen uptake rate $q_{\mathrm{O_2}}$ and carbon dioxide evolution rate $q_{\mathrm{CO_2}}$ (both in $\mathrm{mol\,g^{-1}\,h^{-1}}$) according to:

$$q_{\mathrm{O_2}} = \frac{\mathrm{OUR}}{X} \quad [3.24]$$

$$q_{\mathrm{CO_2}} = \frac{\mathrm{CER}}{X} \quad [3.25]$$

When applicable, $q_{\mathrm{O_2}}$ and $q_{\mathrm{CO_2}}$ were derived from linear regression and least squares fitting. From the exhaust gas analysis, the dimesionless respiratory quotient RQ can be readily derived from the volumetric or biomass specific respiration rates as follows:

$$\mathrm{RQ} = \frac{\mathrm{CER}}{\mathrm{OUR}} = \frac{q_{\mathrm{CO_2}}}{q_{\mathrm{O_2}}} \quad [3.26]$$

3.3.4 Carbon balancing

The methodology for carbon (C-) balance calculations is specified in detail in the appendix (section C.2.3) and bases on the quantification of C-species in the gas and liquid phase of the bioreactor as summarized in Fig. 3.3.

As illustrated, the C-distribution of the liquid phase distinguishes between an organic (e.g. biomass, substrate, etc.) and an inorganic fraction of all carbonic species (see Eq. 2.14), which results in the total carbon (TC) determination by: $\mathrm{TC} = \mathrm{TOC} + \mathrm{TIC}$. In this study, C-recoveries R_c [in % ($\mathrm{mol\,mol^{-1}}$)] were generally calculated by balancing all relevant quantities (n) in C-mole. Integral substrate (S) based recoveries (R_c^S) regarding the consumed glucose of the time interval $t = 0\,\mathrm{h}$ to t, were calculated according to:

$$R_c^S = \frac{\Delta n_{X_{t-0}} + \Delta n_{TIC_{t-0}} + \Delta n_{other_{t-0}} + \Delta n_{\mathrm{CO_{2,g}}} + \left(\Delta n_{lys_{t-0}}\right)}{\Delta n_{S_{0-t}}} \times 100 \quad [3.27]$$

with C-mole fractions of the liquid phase found in X, TIC, other (by-products), and L-lysine (*lys*) in respective production processes. The integral C-amount from the exhaust gas analysis according to Eq. 3.23 was then calculated by:

$$\Delta n_{\mathrm{CO_{2,g}}} = \int_0^t (\mathrm{CER}(t)\, V_R)\, dt \qquad [3.28]$$

C-recovery determination by TC analysis that referenced the complete balance system R_c^{Sys} on the scale basis of TC amounts at process start $n_{TC_{t=0}}$, considered $n_{\mathrm{CO_{2,g}}}$ and the liquid phase to $n_{TC_{sample}} = n_{TOC_t} + n_{TIC_t}$ of each individual sample at t:

$$R_c^{Sys} = \frac{n_{TC_{sample}} + n_{\mathrm{CO_{2,g}}}}{n_{TC_{t=0}}} \times 100 \qquad [3.29]$$

Calculations of C-recoveries of individual samples considered the liquid phase only R_c^L, setting the scale basis to the TC value of the corresponding sample equivalently withdrawn from the system $n_{TC_{sample}}$:

$$R_c^L = \frac{n_{X_t} + n_{S_t} + n_{TIC_t} + n_{other_t} + \left(n_{lys_t}\right)}{n_{TC_{sample}}} \times 100 \qquad [3.30]$$

with 'other' indicating the sum of C-mole found in by-products and antifoam.

3.4 Characterization of bioreactors

Some excerpts of this section are presented in the manuscript III (section D). A detailed description of the methodology that was applied for the characterization of the mixing time, residence time distribution, and simulation is given in the following.

3.4.1 Determination of the mixing time

Blend times θ (in s) were calculated for the individual bioreactors (MR and CR) by varying the agitation speed N (in $\mathrm{min^{-1}}$) of the bioreactors within the operational range [(300–1,500) $\mathrm{min^{-1}}$ in CR and (25–388) $\mathrm{min^{-1}}$ in MR], as previously published (Brown et al., 2004). Response curves $c(t)$ (in arbitrary units; AU) from tracer pulse experiments using a 3 M di-potassium phosphate (K_2HPO_4) solution were recorded with conductometers (LF 521, WTW Wissenschaftlich-Technische Werkstätten GmbH, Weilheim, Germany). The tracer was rapidly injected within 25 ms via a pulse unit (p = 6 bar) into the bioreactor

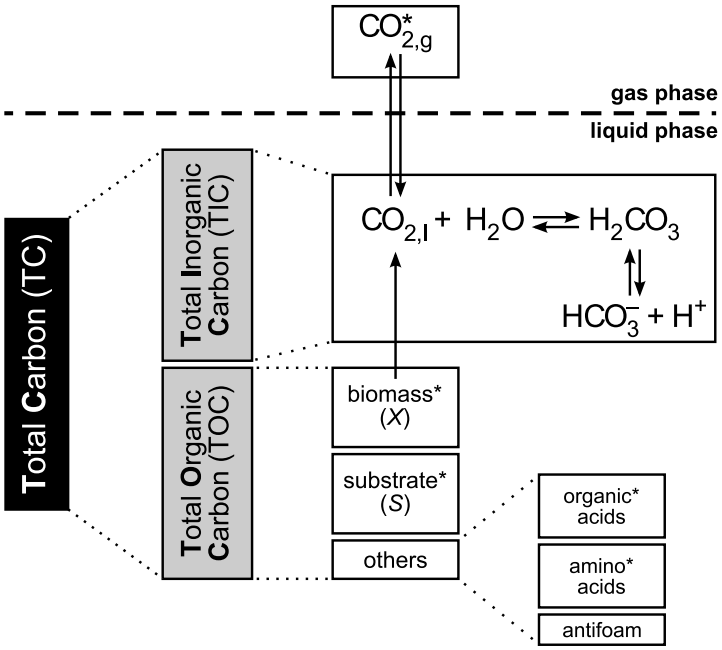

Fig. 3.3: Schematic overview of the hierarchy of the different carbon (C-) species in the gas and liquid phase used to determine C-balances for fermentations processes. The * indicates commonly detected quantities. The figure was modified after Fig. C.2.

containing deionized water (dH_2O) at a fixed temperature of 24 °C and constant V_R according to fermentation conditions (Fig. 3.4). Equivalently, mixing experiments were performed in the complete CBS, thereby setting the agitation speed to 1,500 rpm and 350 rpm in CRs and MR, respectively, and varying the corresponding flow rate of the system between (0.58–3.95) L min^{-1} to obtain θ for the various operation modes.

For all experiments, the normalized response $c'(t)$, as exemplarily depicted in Fig. 3.5 A, was retrieved from the initial zero c_0 (t = 0 h) and final stable c_∞ ($t = \infty$) signal as follows:

$$c'(t) = \frac{c(t) - c_0}{c_\infty - c_0} \qquad [3.31]$$

Due to the exponential decay of the signal fluctuations and for simplification of the blend time detection, the quadratic deviation γ^2 was derived from $c'(t)$ by:

$$\gamma^2 = (c'(t) - 1)^2 \qquad [3.32]$$

The time required for the system to reach a 95 % degree of uniformity θ_{95} (in s), i.e. ±5 % of the final equilibrium level after tracer injection, was then determined after the

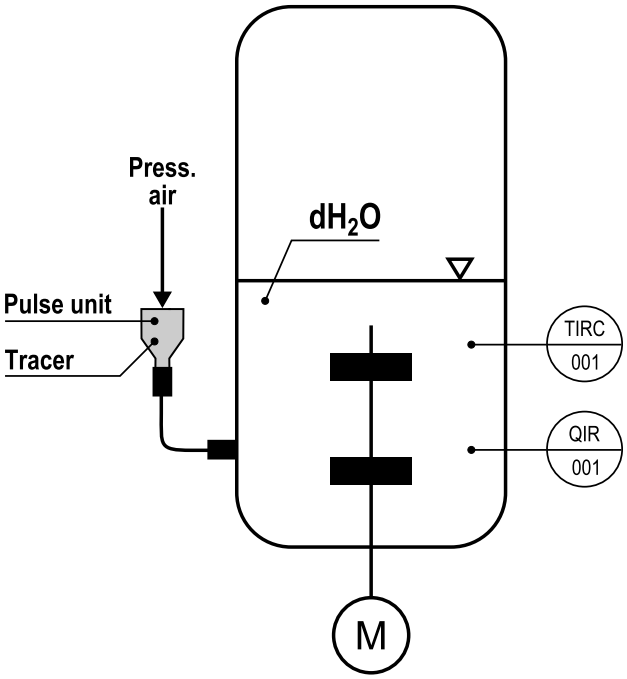

Fig. 3.4: Exemplified setup for the experimental determination of mixing times in the main (MR) and cascade reactors (CRs). 3 M K_2HPO_4 was used as a tracer solution provided in a pulse unit under overpressure (p = 6 bar) for rapid injection (25 ms). During the experiment, the temperature was controlled (TIRC) and the tracer response recorded through a conductivity prove (QIR). Mixing times were determined within the operation range of the bioreactors, applying (300–1,500) min^{-1} in CRs and (25–388) min^{-1} in MR, respectively.

permanent crossing below $\log(\gamma^2) = -2.6$ derived from semi-log plotting of Eq. 3.32 over time (Fig. 3.5 B). Average mixing times with indicated SD were derived from at least five technical replicates per experimental condition. The circulation time t_c (in s) defined as the time necessary for a fluid element to return to a fixed position after circulation through the bioreactor for fully turbulent flow (Palomares et al., 2009), can be estimated from θ according to:

$$t_c = \frac{\theta}{4} \qquad [3.33]$$

and is, in some cases, regarded as equivalent to the space time defined in Eq. 3.42.

The experimental results were contrasted to the empirical characteristics of baffled STR in the turbulent regime ($n\,\theta$ = const) published by (Mersmann et al., 1975):

$$\frac{P\,\theta^3}{\rho\,D^5} = 300 \qquad [3.34]$$

with ρ (in $\mathrm{kg\,m}^{-3}$) as mass density of the bulk liquid, D (in m) as tank diameter, and P (in Nm) as power input given with:

$$P = \mathrm{Ne}\,\rho\,n^3\,d^5 \qquad [3.35]$$

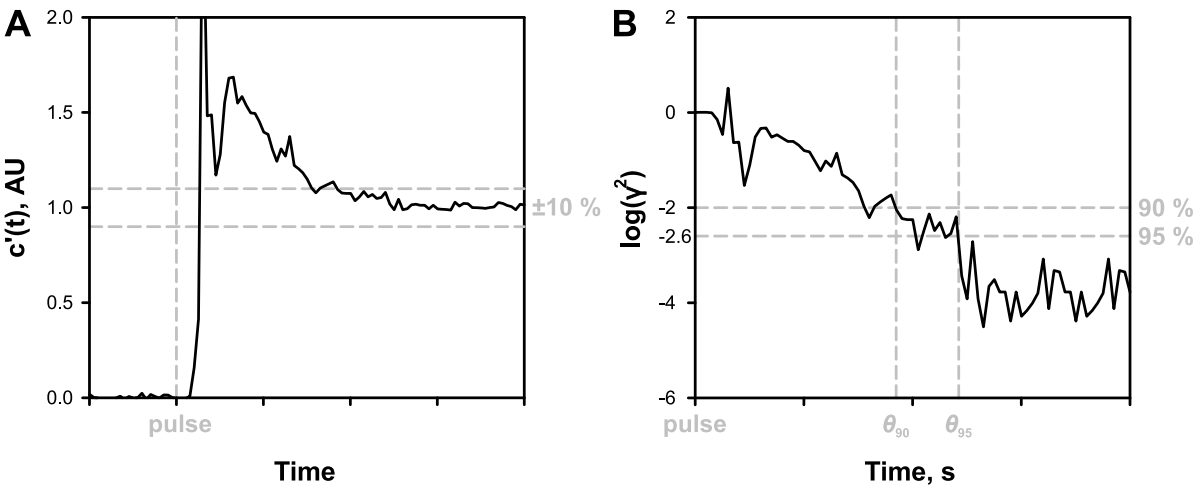

Fig. 3.5: Determination of bioreactor mixing times (θ) from tracer pulse experiments detailed in setup Fig. 3.4. **(A)** Response signals $c(t)$ obtained after the pulse were normalized from initial zero and final stable values yielding $c'(t)$ (Eq. 3.31), indicating e.g. θ_{90} by ± deviation of 10 % from 1 (final signal). **(B)** Semi-log plotting of the quadratic deviation γ^2 of $c'(t)$ (Eq. 3.32) results in the determination of θ_{90} and θ_{95} after final crossing of -2.0 and -2.6, respectively.

where Ne is defined as dimensionless power number of the impeller in dependency of the Reynolds number, set to $\mathrm{Ne} = f(\mathrm{Re}) = 5$ for baffled STR with Rushton turbines at $\mathrm{Re} > 10^4$ (Bates et al., 1963; Kraume, 2012) and d (in m) as stirrer diameter. Combining Eq. 3.34 and Eq. 3.35 finally leads to the correlation:

$$\theta = \frac{6.7}{n}\left(\frac{d}{D}\right)^{-\frac{5}{3}} \mathrm{Ne}^{-\frac{1}{3}} \qquad [3.36]$$

Contrasting of the model and experimental values was performed by calculating the mean absolute percentage error MAPE (in %) as a measure of the accuracy of the prediction, which is defined as:

$$\mathrm{MAPE} = \frac{1}{k}\sum_{t=1}^{k}\left|\frac{v_a - v_p}{v_a}\right| \times 100\% \qquad [3.37]$$

with k as number of comparisons, v_a as actual experimental and v_p as predicted data point.

3.4.2 Determination of the residence time distribution

Equivalent to the mixing studies above, tracer experiments with 3 M K_2HPO_4 were performed to determine the residence time distribution (RTD) $E(t)$ (in min^{-1}) of

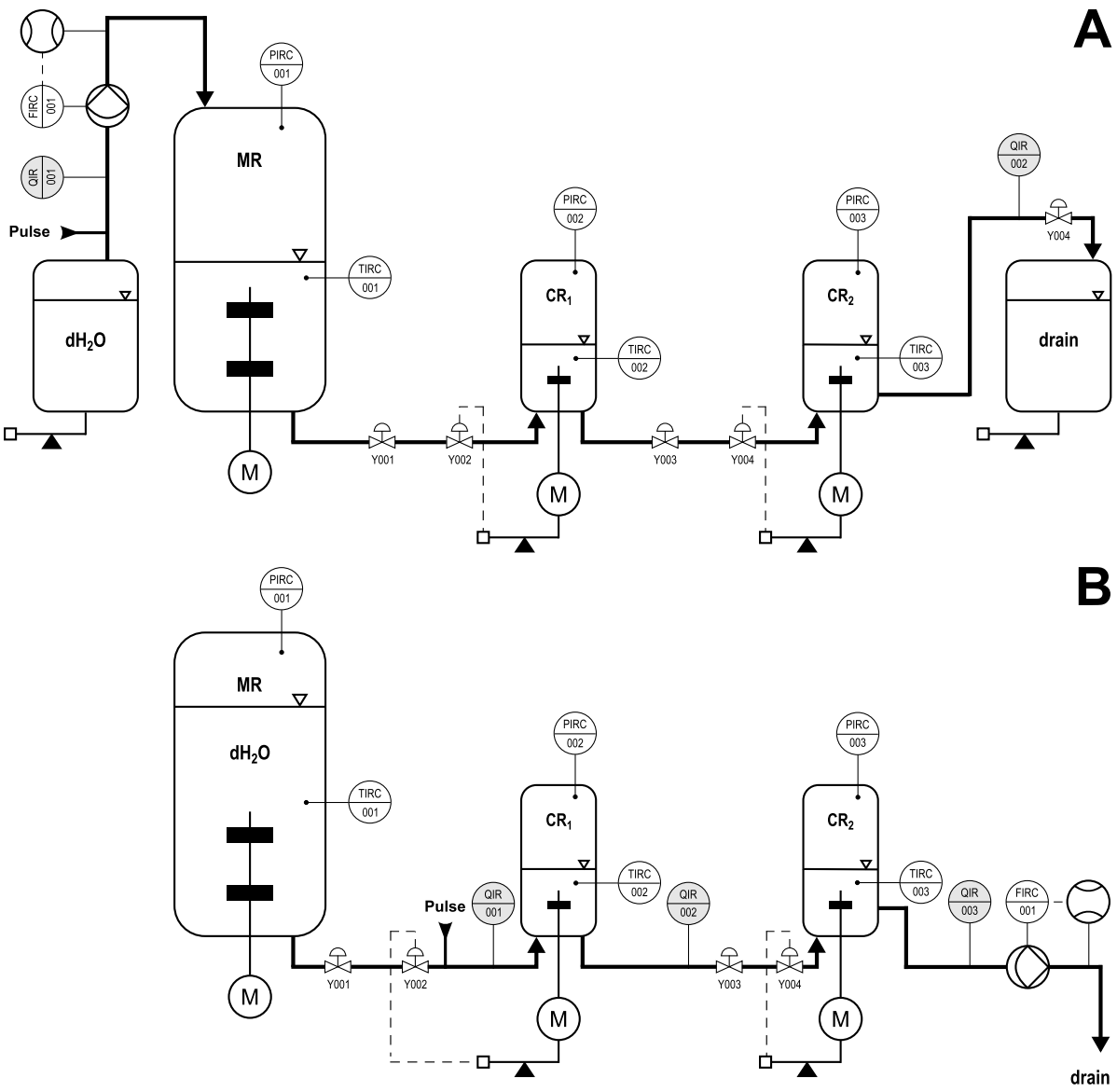

Fig. 3.6: Setup of the cascade bioreactor system (CBS) for the experimental determination of **(A)** open CBS and main reactor (MR) residence time distributions (RTD), as well as **(B)** for the cascade reactor 1 (CR_1) and 2 ($CR_1 \Rightarrow CR_2$). 3 M K_2HPO_4 solution was used for tracer pulse injection as indicated and recorded by conductivity probes (QIR). Equivalently to fermentation conditions, liquid transport was facilitated by the diaphragm metering pump and the applied pressure gradient (compare to Fig. 3.1). Mean residence times were calculated from RTD for varying circulation rates between (0.58–3.95) L min^{-1}.

(i) the open CBS (MR ⇒ CR_1 ⇒ CR_2), (ii) the cascade section (CR_1 ⇒ CR_2), or (iii) the individual reactors (MR, CRs), respectively. The corresponding experimental setup is illustrated in Fig. 3.6. Injection of the tracer was either carried out manually (via syringe) or by using a peristaltic pump. In analogy to the determination of θ_{95} (section 3.4.1), V_R was kept constant according to fermentation conditions, T was set to 24 °C and N to 300 rpm and 1,500 rpm for the MR and CRs, respectively. Further process parameters as the pressure gradient between the individual bioreactors was set to Δ0.6 bar (section 3.1). For the characterization of the system, various circulation rates ν between (0.58–3.95) L min^{-1} with at least three technical replicates per experimental condition were applied.

The determination of $E(t)$ (and subsequent parameters) was performed according to Levenspiel (1999) and Levenspiel (2012) from the response signal $c(t)$ after tracer pulse according to:

$$E(t) = \frac{c(t)}{\int_0^\infty c(t)\,dt} \approx \frac{c(t)}{\sum c(t)\,\Delta t} \qquad [3.38]$$

given that

$$\int_0^\infty E(t)\,dt = 1 \qquad [3.39]$$

The average residence time $\bar{t}$ (in min) can be derived from the first moment of $E(t)$ as:

$$\bar{t} = \int_0^\infty t\,E(t)\,dt \qquad [3.40]$$

Introducing Eq. 3.38 into Eq. 3.40 results then in:

$$\bar{t} = \frac{\int_0^\infty t\,c(t)dt}{\int_0^\infty c(t)dt} \approx \frac{\sum t\,c(t)\,\Delta t}{\sum c(t)\,\Delta t} \qquad [3.41]$$

which can be compared to the theoretical space time τ (in min) of the given system and experimental conditions defined as:

$$\tau = \frac{V_R}{\nu} \qquad [3.42]$$

with ν (in L min^{-1}) as circulation flow rate. For systems without dead zones, the effective reactor volume V_R is equal to the total active volume, $\tau = \bar{t}$ follows. The second moment

of $E(t)$ indicates the variance σ^2 (in min) as degree of dispersion around the mean:

$$\sigma^2 = \int_0^\infty (t - \bar{t})^2 \, E(t) \, dt \qquad [3.43]$$

In analogy to Eq. 3.41, introducing Eq. 3.38 into Eq. 3.43 leads to:

$$\sigma^2 = \frac{\int_0^\infty t^2 \, c(t) dt}{\int_0^\infty c(t) dt} - \bar{t}^2 \approx \frac{\sum t^2 \, c(t) \, \Delta t}{\sum c(t) \, \Delta t} - \bar{t}^2 \qquad [3.44]$$

with the dimensionless variance σ_Θ^2 derived from the dimensionless residence time $\Theta = t/\bar{t}$ according to:

$$\sigma_\Theta^2 = \frac{\sigma^2}{\bar{t}^2} \qquad [3.45]$$

Similar to the approximation of the flow pattern using Bo from the dispersion model as introduced in section 2.3.1, the value of σ_Θ^2 indicates the mixing behavior of the reactor system, distinguishing between ideal PFR and STR conditions according to:

$$\text{PFR}: \quad \sigma_\Theta^2 \longrightarrow 0 \qquad [3.46]$$

$$\text{STR}: \quad \sigma_\Theta^2 \longrightarrow 1 \qquad [3.47]$$

As mentioned before, the extremes are practically non-existent with actual reactor setups usually showing a mixing behavior characterized with $0 < \sigma_\Theta^2 < 1$ (Nauman, 2002).

For the determination of the RTD and mixing behavior of developed CBS, the TIS model defined in Eq. 2.11 was considered. As illustrated in Fig. 2.4, the model reduces to the exponential $E(t)$ distribution of a single reactor for $N_T = 1$ and approaches the delta distribution of piston flow with $N_T \longrightarrow \infty$ (Nauman, 2002). By fitting $E(t)$ (Eq. 2.14) to the experimental data using the method of least squares the number of ideal CSTRs N_{TIS} is derived. Alternatively, N_T correlates to σ_Θ^2 by:

$$N_{var} = \frac{1}{\sigma_\Theta^2} = \frac{\bar{t}^2}{\sigma^2} \qquad [3.48]$$

or can directly be derived from the mean residence time of the individual tank $\bar{t}_i$ (in s) by $N_T = \bar{t}/\bar{t}_i$.

3.4.3 Simulation of residence time distributions

The relation between $c_{in}(t)$, $c_{out}(t)$, and $E(t)$ was introduced through the convolution integral in Eq. 2.10 and can therefore serve to model the response curves for tracer experiments of the MR, the CRs, and the CBS. Additionally, it also provides the ability to estimate $c_{out}(t)$ when the CBS is operated in total circulation and direct output signal measurements for individual cycles are not possible. Using the convolution operator $*$ the syntax can be simplified to:

$$c_{out}(t) = c_{in}(t) * E(t) \quad [3.49]$$

In control theory, the control path in the time domain $E(t)$ is referred to as transfer function $G(s)$ in the frequency domain using Laplace transformation, which therefore leads to the writing:

$$c_{out}(s) = c_{in}(s)\, G(s) \quad [3.50]$$

For the evaluation of RTDs and modeling of individual CBS cycle $c_{out}(t)$, transfer functions available in the literature for common reactor geometries and flow patterns are used. For ideal conditions with perfect mixing in a CSTR or piston flow in a PFR, Hopkins et al. (1969) proposed the following concepts:

$$G(s) = e^{(-\bar{t}\, s)} \quad [3.51]$$

$$G(s) = \frac{1}{1 + \bar{t}\, s} \quad [3.52]$$

with $\bar{t}$ of the individual CSTR as system pole. On the basis of the latter, Eq. 3.52 was extended to fit the experimental setup of the CBS consisting of three STR in series (Fig. 3.1). The overall $G(s)$ then corresponds to the product of the individual reactors. Transformation of the denominator to the zero-pole-gain model yields:

$$G(s) = \frac{1}{(1/\bar{t}_{MR} + s)(1/\bar{t}_{CR_1} + s)(1/\bar{t}_{CR_2} + s)} \quad [3.53]$$

To account for the lag time t_{lag} between the pulse and the response, a dead time element $e^{(-t_{lag}\, s)}$ was introduced following Eq. 3.51. In addition, the normalization factor η was

added to account for Eq. 3.39, finally leading to:

$$G(s) = e^{(-t_{lag}\,s)} \frac{\eta}{(1/\bar{t}_{MR} + s)(1/\bar{t}_{CR_1} + s)(1/\bar{t}_{CR_2} + s)} \qquad [3.54]$$

In analogy to the lab experiments, a Delta Dirac function (Laplace transforms) was used as input signal to simulate the $c_{out}(s)$ profiles for the MR, the CR, and the CBS, which were then compared to the experimental results. For CBS operation with total recycle, the methodology described above can equivalently be transferred. However, $c_{out}(s)$ of the first cycle becomes $c_{in}(s)$ of the following. Each cycle response can thus be distinguished by:

$$\begin{aligned}
&1. \quad c_{out,1}(s) = c_{in,0}(s)\, G(s)^1 \\
&2. \quad c_{out,2}(s) = c_{in,0}(s)\, G(s)^2 \\
&\qquad\qquad \vdots \\
&j. \quad c_{out,j}(s) = c_{in,0}(s)\, G(s)^j
\end{aligned} \qquad [3.55]$$

with j as total number of cycles through the system. After back transformation to the time domain, the modeled signals were compared to the experimental data after summation of the individual cycle responses according to:

$$c_{out}(t) = \sum_{i=1}^{j} c_{out,i}(t)$$

The methodology for the RTD simulation as described above was implemented in a MATLAB® routine, which was part of a Master thesis conducted under supervision of this study (Graf, 2014).

CHAPTER 4
RESULTS AND DISCUSSION

This chapter summarizes the important results of this thesis that have been partially published or submitted. Where applicable, cross references are given to detailed descriptions or supplementary information found in the appendix (A–D).

4.1 L-Valine and 2-ketoisovalerate production

C. glutamicum is one of the workhorses in industrial biotechnology and the literature provides many reports on its applicability for bio-based products ranging from amino acids to biofuels in the last decades (section 2.1.1). This development was possible due to extensive knowledge about metabolism and pathway regulation, and steady improvement of systems biology and metabolic engineering approaches (Becker et al., 2011; Burkovski, 2008; Eggeling & Reyes, 2005; Kirchner & Tauch, 2003; Sauer & Eikmanns, 2005; Takors et al., 2007; Teramoto et al., 2011; Vertès et al., 2012; Wendisch et al., 2006). In this regard, promoter engineering was demonstrated as a valuable tool for the fine tuning of carbon flux through metabolic pathways and a suitable alternative to directed gene deletion or plasmid encoded over-expression (Becker et al., 2005, 2007, 2011; Holátko et al., 2009). Regarding the metabolism, one important target is pyruvate since it is the precursor of many *C. glutamicum*-derived production processes and central element of the main carbon flux between glycolysis and TCA (Fig. 2.1). To improve the availability of pyruvate, several strategies were employed (e.g., Bartek et al., 2008; Radmacher et al., 2002). In particular, the identification and characterization of the E1p subunit of

the PDHC (encoded by the *aceE*) by Schreiner et al. (2005) was used to generate the common basis of PDHC-deficient strains. Originating from *C. glutamicum* Δ*aceE*, the improved precursor supply led to high product titers of 48.3 g L^{-1} L-valine (Blombach et al., 2008), 21.8 g L^{-1} 2-ketoisovalerate (KIV) (Krause et al., 2010b), 45 g L^{-1} pyruvate and 38.9 g L^{-1} succinate (Wieschalka et al., 2012; Wieschalka et al., 2013), as well as 13 g L^{-1} isobutanol (Blombach et al., 2011) and improved the production of L-lysine (Blombach et al., 2007a).

However, the common characteristic of all strains with completely abolished PDHC activity is the inability to grow on glucose, pyruvate, and lactate as sole carbon and energy source (Schreiner et al., 2005). Obviously, bypassing of the PDHC activity for acetyl-CoA formation via pyruvate:quinone oxidoreductase (PQO), acetate kinase, and phosphotransacetylase is not sufficient, which makes acetate or ethanol supplementation essential (Blombach et al., 2009b). In addition, all strains exhibit growth-decoupled production: during co-metabolization of acetate and glucose, exponential growth is only observed as long as acetate is present in the medium, whereas product secretion is initiated not until acetate depletion. Further studies demonstrated the overcoming of the growth-decoupled phenotype either by deletion of the transcriptional regulator SugR, which represses *ptsG* encoding the glucose-specific phosphotransferase system (PTS) enzyme II in presence of gluconeogenic carbon sources, as e.g. pyruvate, citrate, and acetate (Blombach et al., 2009c; Engels & Wendisch, 2007), replacement of acetate by ethanol (Blombach et al., 2009c), or by using the non-PTS sugar maltose (Krause et al., 2010a). However, the triggered increase of ptsG expression and consequently improved glucose consumption only lasted as long as maltose was present in the medium.

To address the necessity of acetate as co-substrate for growth in minimal medium, the native *aceE* promoter was substituted with a previously generated *dapA* promoter library by Vasicová et al. (1999) (see section A.2.4). The replacement with a set of mutated promoter variants led to a series of *C. glutamicum* strains exhibiting gradually reduced PDHC activities and growth rates on medium containing glucose as sole carbon source as illustrated in Fig. A.2. Upon over-expression of the L-valine biosynthetic pathway genes (carried on pJC *ilvBNCE*), the most promising variant, *C. glutamicum aceE* A16 (pJC *ilvBNCE*), exhibited the highest L-valine yield of $Y_{PS} = (0.37 \pm 0.01)$ mol mol^{-1} (Tab. A.2). Interestingly, the derivate A16 also showed the highest PDHC activity after the WT (79 % lower) as depicted in Fig. A.2 A and was finally selected for further strain improvement due to its highest Y_{PS} as shown before. Furthermore, the cumulative deletion of *pqo* and *ppc* led to a slight improvement of about 14 %, resulting in (0.42 ± 0.02) mol mol^{-1}. *C. glu-*

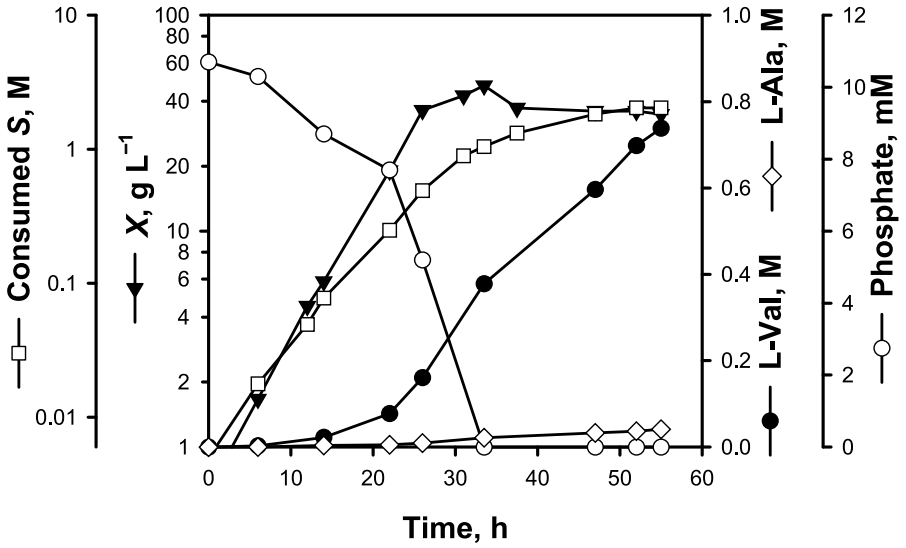

Fig. 4.1: Representative fed-batch fermentation for L-valine production of *C. glutamicum aceE* A16 Δ*pqo* Δ*ppc* (pJC4 *ilvBNCE*) in CGXII medium on glucose. The figure was modified after Fig. A.4.

tamicum aceE A16 Δ*pqo* Δ*ppc* (pJC4 *ilvBNCE*) was applied in fed-batch fermentations in minimal medium on glucose as sole carbon source as described in section A.2.3 yielding a μ of 0.15 h^{-1} as depicted in Fig. 4.1. After phosphate limitation at 33.5 h of cultivation, a maximum cell density of X = 47.4 g L^{-1} was reached that slightly decreased throughout the stationary phase. Concurrently, glucose was still metabolized and L-valine produced, finally reaching a maximum product titer of (0.71 ± 0.02) M at Y_{PS} of (0.33 ± 0.01) mol mol^{-1} within 55 h.

Further experiments should demonstrate the applicability of the aforementioned production platform for KIV production. Therefore , the transaminase B (encoded by *ilvE*) was deleted in *C. glutamicum aceE* A16 Δ*pqo* Δ*ppc* yielding the final strain by transformation with pJC4 *ilvBNCD*. Equivalently to the L-valine process described above, fed-batch fermentations were carried out in minimal medium on glucose initially supplemented with 1 % (w/v) yeast extract, and 10 mM L-valine, L-isoleucine, and L-leucine (Fig. A.5). During the process, a constantly decreasing growth rate was observed yielding a maximum X of about 25.2 g L^{-1} after 29 h, even though all supplements were not exhausted. This effect might be caused by a KIV-mediated inhibition and illustrates the advantage of the PDHC-deficient process for toxic products (growth-decoupled production). However, glucose consumption and product excretion continued until the end of the fermentation, resulting in a final KIV titer of (0.29 ± 0.01) M with a Y_{PS} of (0.21 ± 0.04) mol mol^{-1} after 44 h of cultivation.

Tab. 4.1: Final product titers, substrate specific product yields (Y_{PS}), and volumetric production rates (Q_P) of fed-batch fermentations of *C. glutamicum* L-valine and 2-ketoisovalerate producers with either abolished or attenuated PDHC activity. Values represent the arithmetic mean ±SD of at least three independent experiments. The table was modified after Tab. A.4.

Production process and strain	Titer, M	Y_{PS}, mol mol^{-1}	Q_P, g L^{-1} h^{-1}
L-Valine			
C. glutamicum Δ*aceE* Δ*pqo* (pJC4 *ilvBNCE*)[‡]	0.21 ± 0.02	0.23 ± 0.02	0.5 ± 0.1
C. glutamicum aceE A16 Δ*pqo* Δ*ppc* (pJC4 *ilvBNCE*)	0.71 ± 0.02	0.33 ± 0.01	1.5 ± 0.1
2-Ketoisovalerate (KIV)			
C. glutamicum Δ*aceE* Δ*pqo* Δ*ilvE* (pJC4 *ilvBNCD*)[*]	0.19 ± 0.03	0.26 ± 0.02	0.5 ± 0.1
C. glutamicum aceE A16 Δ*pqo* Δ*ppc* Δ*ilvE* (pJC4*ilvBNCD*)	0.29 ± 0.01	0.21 ± 0.04	0.7 ± 0.1

[‡] Data taken from Blombach et al. (2008)
[*] Data taken from Krause et al. (2010b)

Due to the difficulties in predicting the effects of promoter engineering, the *dapA* variants were randomly chosen to replace the native *aceE* promoter. The most promising strain, *C. glutamicum aceE* A16, exhibited the highest Y_{XS} and Y_{PS}, while still possessing the comparatively highest PDHC activity (reduced by 79 %), suggesting that other promoters with activities between *dapA*-A16 and WT might be even more suitable for L-valine and KIV production. Moreover, the modulation of the translation initiation or deletion of activation/repression binding sites might provide further potential for the adjustment of the PDHC activity and subsequent carbon flux into product formation.

In summary, Tab. 4.1 illustrates the production capacity of both optimization strategies. In both cases, a reduction of the PDHC activity as shown in this study significantly improves the final product titer and volumetric production rates Q_P (in g L^{-1} h^{-1}) compared to the PDHC-deficient strains (Blombach et al., 2008; Krause et al., 2010b). For L-valine overproduction, P and Q_P were more than three-fold higher, whereas both parameters increased by about (40–50) % for KIV production, respectively. Both concepts are therefore highly competitive or superior when compared to previously reported aerobic production processes with 61 g L^{-1} L-valine in *E. coli* (Park et al., 2011) and 48 g L^{-1} in *C. glutamicum* (Blombach et al., 2008), as well 22 g L^{-1} KIV (Krause et al., 2010b). Taken together, *C. glutamicum* with attenuated PDHC activity was demonstrated

to be powerful platform for several pyruvate-based products as L-valine, KIV, and also L-lysine (section A.3.6) and was recently reviewed by Eikmanns & Blombach (2014).

4.2 Carbon balancing of fermentations by total carbon analysis

The determination of respiration rates by exhaust gas analysis is common practice for (microbial) fermentation processes. Thereby, the monitoring of OUR and CER provides not only valuable information regarding the physiological state of the culture, e.g. derived from the RQ (Eq. 3.26), it might also indicate the performance of the process, and offers the application for fermentation (feedback) control strategies (e.g., Jenzsch et al., 2006a,b; Junker & Wang, 2006; Yamuna Rani & Ramachandra Rao, 1999). Additionally, both parameters might have significant influence on the outcome of the fermentation since both promoting and inhibiting influences are described (e.g. section 2.3.3). The accurate calculation or estimation of both parameters is therefore essential. The solubility of O_2 in the fermentation broth is usually very small ($dc_{O_2}/dt \longrightarrow 0$). Hence, OUR and OTR are practically considered as equal (Eq. 3.18); i.e. OUR can be directly derived from the exhaust gas analysis (Eq. 3.22). For aerobic growth on glucose ($C_6H_{12}O_6$) as only substrate one considers the aerobic respiration to CO_2 and H_2O as follows (Nielsen et al., 2003):

$$C_6H_{12}O_6 + 6\,O_2 \longrightarrow 6\,CO_2 + 6\,H_2O \qquad [4.1]$$

which should ultimately lead to a balanced RQ around unity (see Eq. 3.26) during the process.

Initial batch fermentations in this study were carried out at 1 L scale using *C. glutamicum* WT on CGXII minimal medium with 4 % (w/v) glucose under described conditions (section B.2). An exemplary process is illustrated in Fig. 4.2 A, revealing that O_2 can sufficiently be introduced (pO_2 set >20 %) via a stepwise increase of N until reaching X of about $10\,g\,L^{-1}$ (data not shown). Despite aerobic growth on glucose, the calculated RQ was observed to rise in the course of the fermentation without exceeding 0.4–0.6 during an applied Q/V_R of 0.1 vvm. In the following, subsequent Q/V_R step-ups were directly followed by increased RQ values, which indicates the stripping of dissolved CO_2 from the culture liquid into the gas phase. Obviously, disproportional q_{O_2} and q_{CO_2}

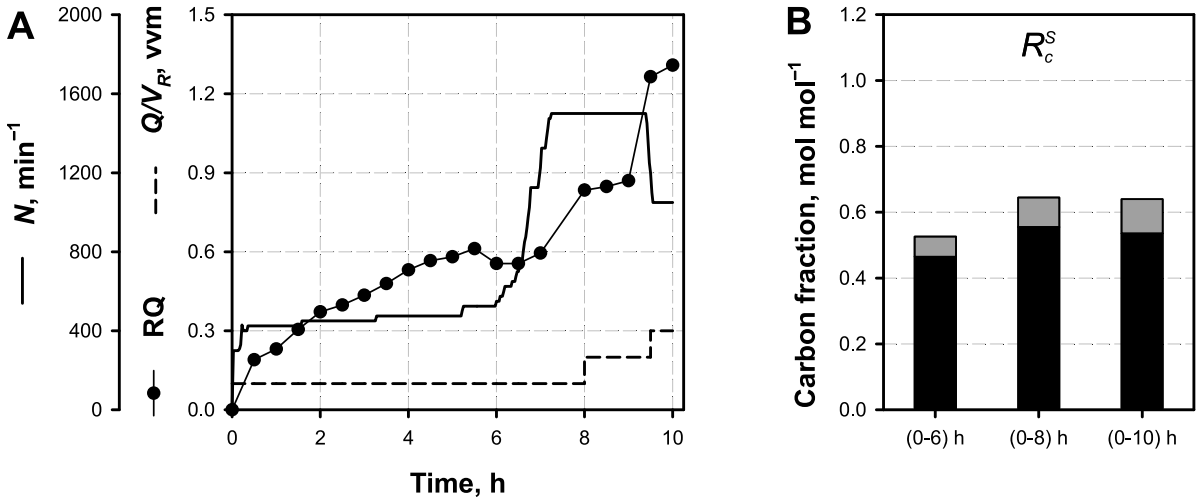

Fig. 4.2: Exemplary batch fermentation of *C. glutamicum* WT on 4 % (w/v) glucose at pH 7.4 carried out at 1 L scale under described conditions (section B.2). **(A)** Summary of selected process parameters in the course of the fermentation. Depicted are the agitation speed (N), the volumetric gas flow rate (Q/V_R), and the respiratory quotient (RQ). **(B)** Carbon balance (R_c^S) calculated for recovered carbon found in biomass (■) and exhaust gas (■) on the basis of introduced glucose (see Eq. 3.27).

were derived from exhaust gas analysis of a standard batch cultivation of *C. glutamicum*, which also has been observed in the literature before (Royce, 1992; Royce & Thornhill, 1991).

This effect is attributed to the high solubility of CO_2 in the fermentation broth (see section 4.3), which is reinforced by the carbonic acid equilibrium and correspondingly, constant titration of the pH. Additionally, under highly dynamic, non-steady state conditions (as given by batch processes), chemical and physical transfer limitations for CO_2 can further complicate the attempt to differentiate between CO_2 transfer (CTR) and actual CER as illustrated by Royce (1992) as in Eq. 4.2. In order to overcome these limitations, efforts have been spent into the reconstruction of exhaust gas dynamics and the incorporation of the CO_2/HCO_3^- interconversion with mathematical models (Bloemen et al., 2003; Kovács et al., 2007; Spérandio & Paul, 1997; Wu et al., 2003); both methods are, however, not always applicable for routine analysis and therefore cannot substitute direct measurements.

$$\begin{array}{c} \text{Cells} \\ \Big\downarrow \text{CER} \\ \end{array}$$

$$CO_{2,g} \xleftarrow[\text{CTR}]{} CO_{2,l} \rightleftharpoons H_2CO_3 \rightleftharpoons H^+ + HCO_3^- \qquad [4.2]$$

The consequences of inadequate CER quantification (amplified by difficulties in balancing small volumes and gas flows) becomes evident after consideration of the C-recovery calculations as depicted in Fig. 4.2 B. Integral balancing of the process was performed on the basis of introduced glucose (see Eq. 3.27) for defined time periods from process start ($t = 0\,\mathrm{h}$) until 6 h, 8 h, and 10 h as indicated. However, summing up the matched C-fractions that were identified in X and $CO_{2,g}$ (by-products were not detected) resulted in very low total R_c^S with a maximum of 65 % at the end of the process. Therefore, by quantifying the conventional C-species for C-recovery calculations as also highlighted in Fig. 3.3, one third of the introduced carbon remains unattributed. From the chemical equilibrium of carbonic acid for aqueous solutions (see section 2.3.3), one can derive that HCO_3^- (nonvolatile) is the dominating species at physiological pH (fermentation conditions of this study) with a surplus larger than ten-fold compared to CO_2 (Fig. 2.5). Applying favorable process and cultivation conditions for the dissolution of CO_2, as e.g. low Q/V_R or high p, makes the quantification of all (dissolved) carbonic species (Eq. 2.14 and Fig. 3.3) thus essential.

4.2.1 Impact of the biomass carbon content on carbon recoveries

One key element for C-balancing of fermentation processes is the accurate quantification of the biomass. Especially for WT cultivations as illustrated above, it is not unusual for n_X to account for about (50–60) % of the TC considered. However, one usually relies on literature references to derive the latter from the CDW detection. For *C. glutamicum* WT, Liebl (1991) reports $M_{C,X}$ to be in the range of (40.8–41.6) % with a rather large SD of 15 %. However, detailed information about the cultural state or sampling details are not provided. Therefore we carried out TC analysis to quantify the C-content of the biomass in the course of fermentations under defined conditions (see section C.2.2). The results of two *C. glutamicum* WT batch fermentations on 4 % (w/v) glucose at 100 L scale as described in section C.2.1 are illustrated in Fig. 4.3.

As can be derived, $M_{C,X}$ remains constant throughout the fermentation and was calculated to be 51.4 %, therefore being about 25 % larger than previously reported (Liebl, 1991). This leads to the fact that the biomass share, as part of the C-recovery calculation, would be significantly underestimated if the particular content of the given strain under the applied conditions is not accurately detected (see below).

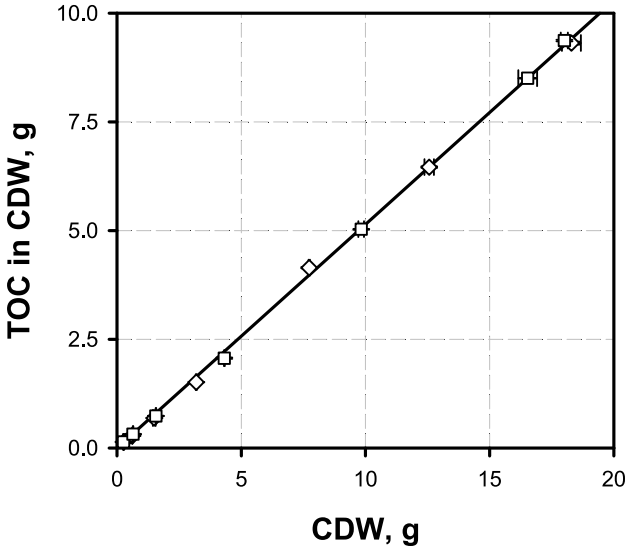

Fig. 4.3: Correlation between the concentrations of total organic carbon (TOC) measured in washed biomass samples over the corresponding dried biomass (CDW) in the course of two *C. glutamicum* WT standard batch fermentation replicates (□/◇). The resulting mass fraction was determined to $M_{C,X} = 51.4\,\%$ and is indicated by the regression line (R^2 = 0.999). Error bars indicate the standard deviation of at least three technical replicates. The figure was modified after Fig. C.4.

4.2.2 Development and application of total carbon analysis

The quantification of the C-content was extended to cover not only the biomass, but also the liquid phase of the system (see section C.2.2), which consists of a TIC and a TOC fraction (Fig. 3.3). The high amounts of dissolved CO_2/HCO_3^- in the cultivation broth require a rapid treatment of the sample, which minimizes the air contact time to prevent the outgassing of $CO_{2,l}$ due to equilibration with the environment. Highly concentrated KOH was therefore quickly added to the sample to increase the basicity (pH >11) and shift the carbonic distribution towards HCO_3^-/CO_3^{2-} (nonvolatile). From multiple TC measurements of H_2O equilibrated with 30 % CO_2, it could be shown that the base addition stabilizes the sample leading to an accurate TC recovery of $(100 \pm 1)\,\%$ as depicted in Fig. 4.4 A. If the sample remains untreated, continuous outgassing can be observed with a relative loss of TIC of about 7 % on average per injection into the TC analyzer (Fig. 4.4 B). The illustrated effect is certainly concentration- and composition-dependent but adequately illustrates the significance of KOH addition.

4.2.3 Improvement of the carbon balance by total carbon analysis

When working with rather small V_R in batch approaches as given in Fig. 4.2, the difficulty of balancing a highly dynamic system is additionally superimposed by further inaccuracies of the detection facilities due to rather small deviations of uptake and production rates. To counteract this limitation and, more importantly, fit the bioreactor environment to

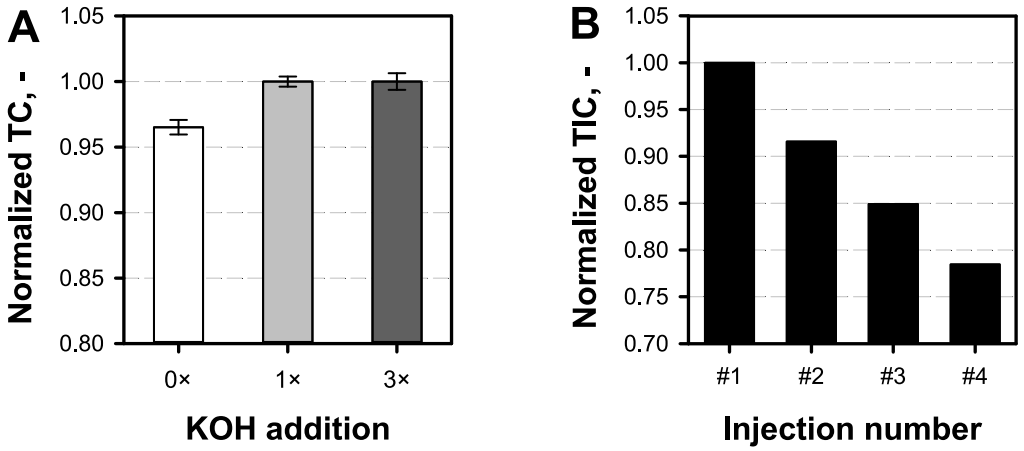

Fig. 4.4: Determination of the sample stability in dependency of the sample treatment. **(A)** Calculation of the total carbon (TC) recovery after equilibration of H_2O with air containing 30 % CO_2, indicated with (number of times of 70 µL) and without KOH treatment according to the protocol given in section C.2.2. **(B)** Illustration of the $CO_{2,l}$ outgassing from the sample (without KOH addition) in the course of four continuous injections into the TC analyzer during total inorganic carbon (TIC) quantification.

the conditions used for CBS fermentations as detailed in the appendix (section D), batch fermentations were carried out at 100 L scale in the following. Comparable to the process analysis illustrated above (Fig. 4.2), C-balancing was performed on a standard batch fermentation using *C. glutamicum* WT carried out under similar conditions with exception of the total V_R being 25 L (Fig. 4.5). R_c^S was determined for two time intervals, depicting the balance after mid-phase and for the total process, respectively. Quantification of the conventional C-fractions found in X, $CO_{2,g}$, and by-product resulted in C-closures of 63 % and 78 %, respectively. In the following, the measurement protocol for $M_{C,X}$ and TIC as summarized above was successively incorporated into the analysis, leading to significantly improved recoveries. The cumulative application resulted in a final R_c^S of (92–94) %, which corresponds to a relative increase of about 20 % and 47 %, respectively, and a final C-gap of clearly below 10 %.

Notably, the relative enhancement of R_c^S decreased by increasing the time periods considered as given in extracts for (0–6) h and (0–10) h, respectively. This effect could clearly be attributed to the amount of the carbon found in the TIC fraction (Fig. 4.5 A) and implicates the high amount of dissolved carbonic species over a broad range of the process (compare RQ in Fig. 4.2 and Fig. 4.6). This observation goes along with the illustration of total molar C-fraction found in $CO_{2,g}$ and TIC in the course of the fermentation (Fig. 4.6 A). Even though the cumulative proportion of $n_{CO_{2,g}}$ and n_{TIC} was consistently identified as (30–34) %, C-shares in TIC dominantly contribute to R_c^S

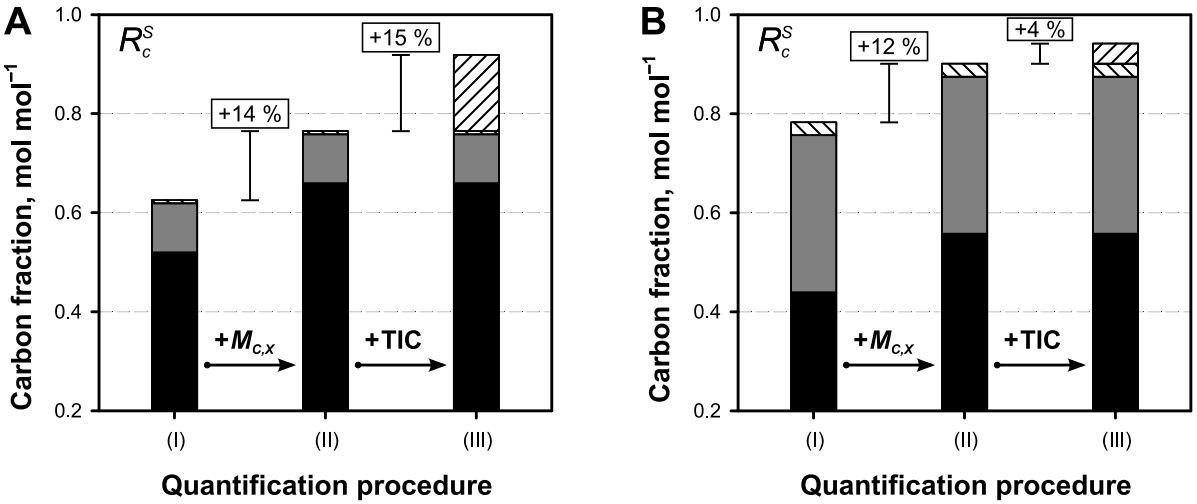

Fig. 4.5: Illustration of increasing the carbon (C-)recovery by detecting the C-content of the biomass ($M_{C,X}$) and the total amount of inorganic carbon (TIC) for an exemplary batch fermentation using *C. glutamicum* WT at 100 L scale on 4 % (w/v) glucose. Illustrated are integral C-recoveries (R_c^S) calculated between **(A)** (0–6) h (mid-phase) and **(B)** (0–10) h (total process period). The quantification procedure for the identification of C-fractions is defined as follows: (I) biomass (■) with $M_{C,X}$ derived from the literature (Liebl, 1991), exhaust gas (▬), and by-products (▨); (II) as in (I) but with $M_{C,X}$ directly derived from TC analysis; (III) as (II) but with additional quantification of TIC (▨). The improvement of obtained R_c^S from each additional quantification step is indicated.

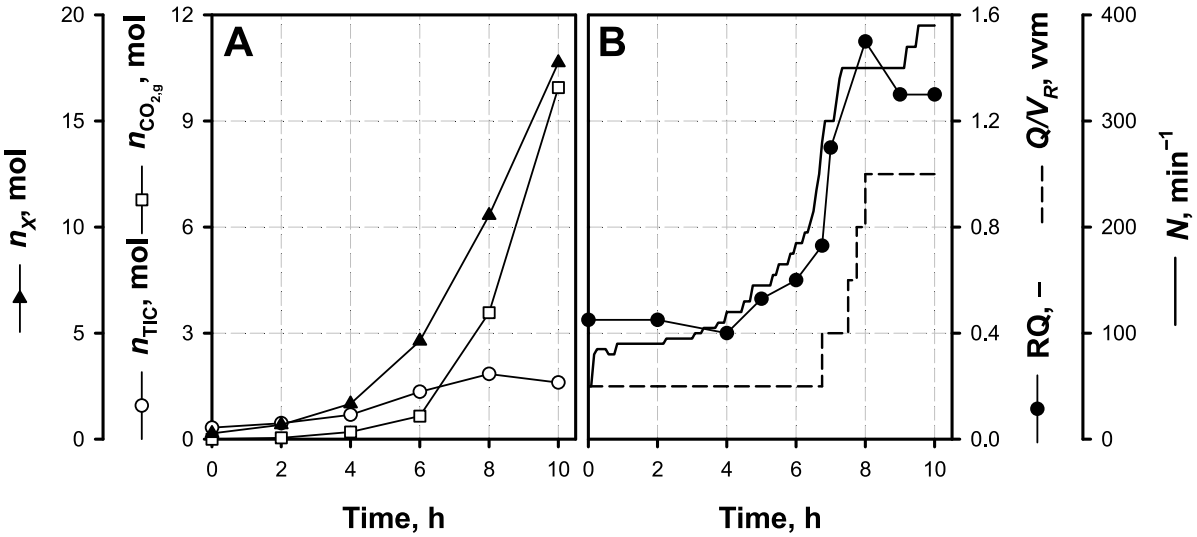

Fig. 4.6: Illustration of selected process parameters of an exemplary 100 L scale *C. glutamicum* WT batch fermentation on 4 % (w/v) glucose at pH 7.4 performed under described conditions (section C.2.1). **(A)** Total molar carbon quantities (n) derived from biomass (n_X), total inorganic carbon (n_{TIC}), and exhaust gas analysis ($n_{CO_{2,g}}$). **(B)** Depiction of the volumetric gas flow rate (Q/V_R), agitation speed (N), and respiratory quotient (RQ). The figure was modified after Fig. C.4.

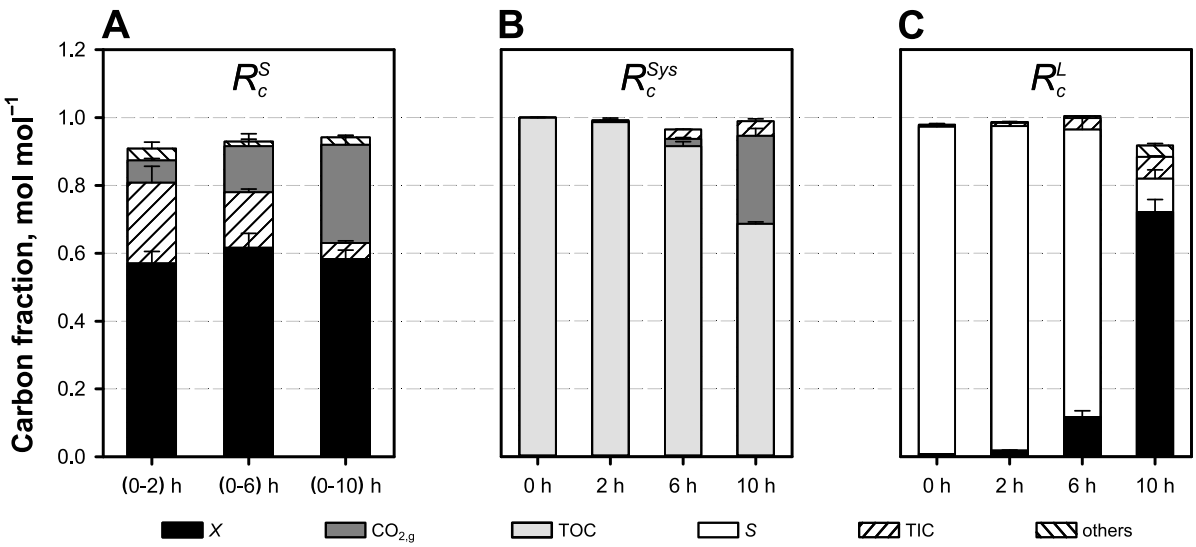

Fig. 4.7: Carbon balancing calculated for two batch fermentations performed under described conditions. Recovery fractions obtained from both cultivations were averaged with error bars indicating the absolute deviation of the experimental measurements to the arithmetic mean (total range of measurements). **(A)** Balance (R_c^S) determined for recovered carbon found in biomass (X), exhaust gas ($CO_{2,g}$), total inorganic carbon (TIC), and by-products (others) on the basis of introduced substrate (glucose). **(B)** Carbon balance based on initially introduced total carbon (TC; R_c^{Sys}) of the complete system for recovered carbon found in total organic carbon (TOC), TIC, and exhaust. **(C)** Recovery calculated for the liquid phase (R_c^L) on the basis of TC. Carbon fractions were recovered in X, substrate (S), TIC, and others (by-products and antifoam). The figure was modified after Fig. C.6.

with (16–24) % during the first 6 h of cultivation (Fig. 4.7 A). Afterwards, n_{TIC} declines considerably compared to $n_{CO_{2,g}}$, which is reflected by the RQ due to the increase of N and Q/V_R (Fig. 4.6 B).

However, despite enhancing the conventional C-balance approach by TC measurements, about 6 % of all carbon remains unattributed. The scope of TC analysis was therefore extended to integrate the TC distribution in the liquid (organic and inorganic species) and gaseous phase of the complete system, calculating R_c^{Sys} according to Eq. 3.29. As a result, high overall C-closures of 99 % were obtained for all detected time points (Fig. 4.7 B) corroborating the accurate integration of the data analysis and general capture/detection of carbon in the system. The latter also excludes the imprecision of the $CO_{2,g}$ quantification as reason for the observed C-gap of the R_c^S balance.

The subsequent focus of the analysis was therefore shifted to the liquid phase of the system only (Fig. 4.7C). As can be derived, the calculation of R_c^L after Eq. 3.30 revealed closed balances between (98–100) % until 6 h of cultivation, subsequently showing a recovery loss of about 8 % at the end of the process. This corresponds to the data

obtained from R_c^L detection (Fig. 4.7 A) and allows the conclusion that imprecise C-detection in biomass, substrate, and by-product fractions are the source of the gap.

In addition, the very same balancing concepts (including the corresponding $M_{C,X}$ determination) were successfully applied to the L-lysine producer *C. glutamicum* DM1933 (Fig. C.7). Thereby, it could also be demonstrated that the quantification of all carbon species, and especially the amounts of dissolved CO_2, prevents the overreached misinterpretation of false-negative, unattributed carbon to e.g. unidentified by-products. Taken together, it could be shown that the determination of the actual $M_{C,X}$ for the given strain and experimental condition is essential for the accurate assignment of the C-fraction as it might deviate significantly from literature values. In addition, the application of all TC measurements can be used to verify and double-check the conventional quantification procedure and is therefore a valuable contribution for process analysis and data interpretation. This even applies for short and/or dynamic experiments that do not benefit from high substrate/biomass quantities as given for high cell density fed-batch or continuous cultivations (see section C).

4.3 Fermentation of *Corynebacterium glutamicum* under different carbon dioxide/bicarbonate levels

The industrial application of *C. glutamicum* for biotechnological commodities entails that the manufacturing processes are carried out in heterogeneous, large scale bioreactors (section 2.2). Consequently, the cells are exposed to varying CO_2/HCO_3^- levels and both, fermentations carried out under (very) high and low CO_2/HCO_3^- conditions have been reported to show detrimental consequences on growth and production (section 2.3.3). Nevertheless, only limited work has been carried out to improve the understanding of the physiological and regulatory effects. In relation to the few initial studies on *C. glutamicum* published so far (Bäumchen et al., 2007; Knoll et al., 2007), the following sections systematically analyze the kinetic and transcriptional impact of different "quasi-stationary" CO_2/HCO_3^- environments also detailed in the appendix (section B).

4.3.1 Effect on growth kinetics and by-product formation

The development of reference conditions for the seed train, the medium, and the fermentation process were part of the cultivation experiments that were conducted to establish the TC analysis and C-balance calculation described above (section 4.2). Details on the individual aspects are provided in section B.2. At first, batch fermentations were performed under 'standard' conditions at $p = 1.5\,\text{bar}$, $T = 30\,°\text{C}$, pH 7.4, and initial Q/V_R of 0.1 vvm in modified CGXII minimal medium on 4 % (w/v) glucose in order to determine the characteristic pCO_2 profile that should serve as the reference condition. Fig. 4.8 A illustrates a distinctive exponential increase (in accordance to the biomass formation) of the pCO_2 signal, reaching a maximum of about 180 mbar in the late exponential phase. Based on the results of the reference ('standard') condition, variation of the bioreactor aeration facilitated the application of artificial low and high CO_2/HCO_3^- environments as follows:

(i) The addition of a significant CO_2 portion of 20 % in the inlet gas flow resulted in high initial pCO_2 values of 300 mbar that increased in the course of the fermentation to maximum 380 mbar (condition termed as 'high'). By approximation of the 'standard' batch approach (pCO_2 and X course; Fig. 4.8), this amount was estimated to represent a realistic scenario of high cell density fed-batch, or large scale conditions and corresponds to previous studies (Baez et al., 2009; Knoll et al., 2007).

(ii) On the contrary, the application of stripping conditions by setting the Q/V_R to 3 vvm successfully counteracted the overall CO_2 accumulation in the medium in the course of the fermentation. Hence, maximum pCO_2 values did not exceed 40 mbar even at the late exponential phase with $X > 15\,\text{g}\,\text{L}^{-1}$ (condition termed as 'low').

The resulting growth curves are depicted in Fig. 4.8 B and readily illustrate that biomass formation is not inhibited under 'high' CO_2/HCO_3^- conditions. For the exponential phase, μ was determined with $(0.41 \pm 0.01)\,\text{h}^{-1}$, which is identical to the 'standard' condition (see Tab. 4.2 and Fig. B.2 A). This observation coincides with fed-batch and turbidostat studies reported by Bäumchen et al. (2007) and Knoll et al. (2007), both revealing mostly unaffected biomass formation in environments up to 300 mbar CO_2. Even though substrate consumption is also not affected by the latter (Tab. 4.2), significantly enhanced Y_{XS} were obtained during the first half of the fermentation (Fig. B.2 B), which

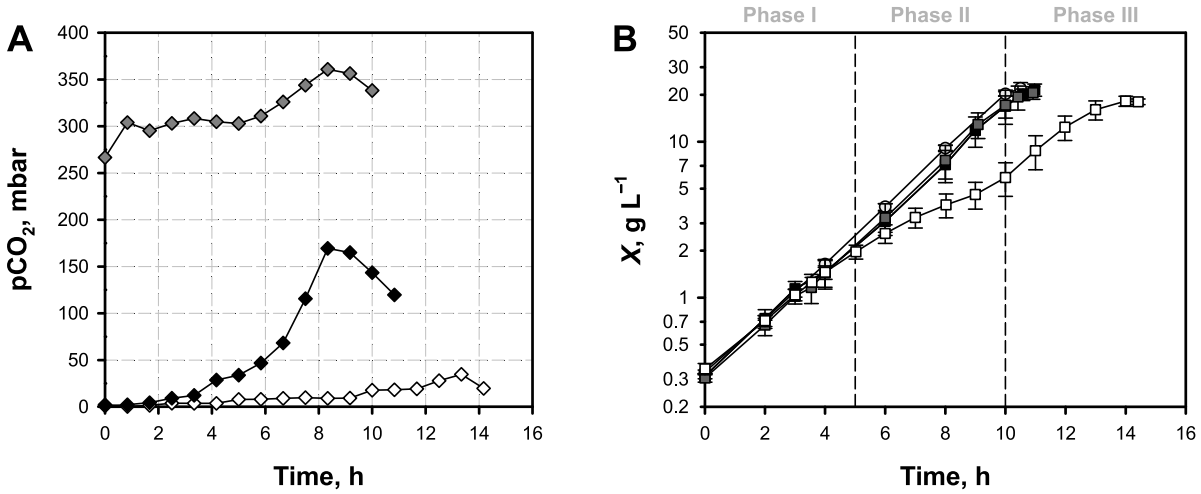

Fig. 4.8: Illustration of of *C. glutamicum* WT batch fermentations carried out at p = 1.5 bar at 1 L scale in modified CGXII minimal salt medium containing 4 % (w/v) glucose. **(A)** Evolution of the pCO_2 under variable process conditions defined as follows: standard/reference fermentations with Q/V_R of 0.1 vvm (◆), elevated CO_2/HCO_3^- levels using 0.5 vvm with 20 % CO_2 in the inlet gas flow (◈), as well as low CO_2/HCO_3^- levels by stripping with 3 vvm (◇). **(B)** Growth curves were obtained from fermentation under the following conditions: standard/reference conditions (■), elevated CO_2/HCO_3^- levels (▩), low CO_2/HCO_3^- levels (□), and complemented conditions with high volumetric gas flow rates (Q/V_R = 3 vvm) and 20 % CO_2 in the inlet gas flow (○), respectively. At least three independent experiments were performed showing the statistical mean with error bars that represent ±SD. The figure was modified after Fig. B.1.

might hint at elevated CO_2/HCO_3^- incorporation rates. On this account, Y_{XS} is increased by 63 % between (0–6) h compared to 'standard' conditions, which eventually equalizes for the total process to result in a final surplus of about 9 % with $(0.61 \pm 0.02)\,\mathrm{g\,g^{-1}}$ vs. $(0.56 \pm 0.02)\,\mathrm{g\,g^{-1}}$, respectively.

On the contrary, high CO_2 stripping as observed under the 'low' condition prevents *C. glutamicum* from regular, exponential growth ($\mu \neq$ constant), revealing a three phasic growth curve as indicated (Fig. 4.8 B). Even though the detected μ resembles 'standard' and 'high' conditions in phase I, a reduction by almost 50 % to $(0.19 \pm 0.03)\,\mathrm{h^{-1}}$ occurs in phase II, which is ultimately followed by a re-increase in phase III; but not to the original level (Tab. 4.2). The inhibition of $\mu_{\max}$ went along with an overall reduction of the final X by 19 % compared to the 'standard' approach, which is in agreement with *E. coli* studies reporting a growth inhibiting effect when sparging the culture with CO_2 depleted air (Kozliak et al., 1995). The latter could be counteracted by supplementing organic acids (e.g. 2-ketoglutarate), leading to the conclusion that the lack of CO_2/HCO_3^- interferes with the precursor supply for biomass formation due to limitations of anaplerotic reactions. While the three phasic growth with the lowest μ in

Tab. 4.2: Summary of process characteristics in CO_2-relevant batch cultivations of *C. glutamicum* WT under 'standard', 'high', 'low' or complemented CO_2/HCO_3^- levels. Aeration conditions, compositions, and corresponding process phase(s) are indicated. Fermentations were carried out at $T = 30\,°C$, pH = 7.4, $p = 1.5\,bar$ at 1 L scale in modified CGXII minimal salt medium containing 4 % (w/v) glucose. Values represent the statistical mean ±SD of at least three independent experiments.

Condition	'Standard'	'High'	'Low'			Complemented
Gas	Air	Air, 20 % CO_2	Air	Air	Air	Air, 20 % CO_2
Q/V_R, vvm	0.1	0.5	3	3	3	3
Process phase	I–III	I–III	I	II	III	I–III
μ_{max}, h^{-1}	0.40 ± 0.02	0.41 ± 0.01	0.35 ± 0.01	0.19 ± 0.03	0.30 ± 0.04	0.42 ± 0.00
Y_{XS}, $g\,g^{-1}$	0.56 ± 0.02	0.61 ± 0.02	0.71 ± 0.10	0.32 ± 0.03	0.50 ± 0.03	0.56 ± 0.01
q_S, $g\,g^{-1}\,h^{-1}$	0.71 ± 0.03	0.68 ± 0.04	0.48 ± 0.05	0.64 ± 0.03	0.60 ± 0.04	0.74 ± 0.01

phase II was also characterized by a reduced Y_{XS} (Tab. 4.2 and Fig. B.3), it showed the highest substrate consumption of $(0.64 \pm 0.03)\,g\,g^{-1}\,h^{-1}$ comparable to 'standard' and 'high' cultures with $(0.68–0.71)\,g\,g^{-1}\,h^{-1}$. As typical for aerobic growth of *C. glutamicum*, by-product formation could not be detected under 'standard' and 'high' conditions. However, beginning with the transition from phase I to II, secretion of L-alanine and L-valine was observed reaching the highest concentrations after 10 h of cultivation with about 1 mM and 4 mM, respectively (Fig. B.4 B).

In the following, two sets of control experiments were conducted to verify that the 'low' CO_2/HCO_3^- level is the only cause of the observed bi-level growth phenotype and not a consequence of high gas flow rates or a oxidative stress: (i) applying stripping conditions (3 vvm) in combination with elevated CO_2 fractions in the inlet gas flow of 20 % and (ii) substituting about 97 % of the initial air volume with N_2 while maintaining the same pO_2 level throughout the process. Providing excessive CO_2 during stripping conditions resulted in the complementation of the bi-phasic growth phenotype yielding μ, Y_{XS}, and q_S comparable to 'standard' and 'high' conditions (Fig. 4.8 and Tab. 4.2). Contrary, fermentations performed with the main portion of the air volume replaced by N_2 exhibited the same, 'low'-typical growth phenotype as seen before (data not shown). Both controls therefore clearly demonstrate that the lack of CO_2/HCO_3^- availability is the cause for the observed growth inhibition.

Even though the PEP–pyruvate–oxaloacetate node is a key factor for the adaption of *C. glutamicum* to variable environmental conditions (Sauer & Eikmanns, 2005), it is yet not fully understood and the effect of different CO_2/HCO_3^- levels on the de-/carboxylating

reactions or regulatory changes cannot be predicted. Therefore, further experiments characterized the growth of single deletion mutants covering selected reactions of the anaplerotic node. *C. glutamicum* Δ*malE*, Δ*pck*, Δ*ppc*, and Δ*pyc* were cultivated under 'standard', 'high', and 'low' CO_2/HCO_3^- conditions and were compared to the results obtained from the equivalently performed WT experiments (Tab. BS.1). Under 'standard' and 'high' CO_2/HCO_3^- levels, constant exponential growth was observed for all mutant strains, which was, however, significantly decreased compared to the WT on average by 20 % and 10 %, respectively (Tab. BS.1). Obviously, the interplay of anaplerotic and gluconeogenic reactions within the PEP–oxaloacetate–node represents a sensible and tightly balanced network. As indicated, even the introduction of a single deletion apparently causes an imbalance of the complete metabolism. The determined Y_{XS} were comparable under all conditions tested. Bi-phasic growth curves equivalent to the WT with similar growth rates were observed for all mutants except for *C. glutamicum* Δ*pyc*, which exhibited a significant reduction of μ by 50 % in phase II. This suggests that the PYC is a predominant enzyme to replenish oxaloacetate under limiting CO_2/HCO_3^- levels. Additionally, it corroborates previous studies that indicate the major importance of PYC for growth on glucose since *C. glutamicum* Δ*pyc* showed reduced μ and Y_{XS} in shake flasks (Peters-Wendisch et al., 1998).

4.3.2 Effect on enzyme activities and comparative transcriptional analyses

The determination of growth-associated kinetic parameters was followed by the detection of enzyme activities of de-/carboxylating reactions mediated by PPC, PCK, PYC, ICD, GPDH, and PGDH (Fig. 2.1). Samples were consistently withdrawn at defined time points corresponding to X = 1.2 g L^{-1} (phase I), 4.5 g L^{-1} (phase II), and 12.3 g L^{-1} (phase III) for all three fermentation conditions (Fig. B.4). Applying the significance criterion of a 1.5-fold increase, most activities remained unchanged. However, under 'low' CO_2/HCO_3^- levels, the activities of both PPP-associated enzymes GPDH and PGDH doubled from phase I to phase II, while remaining high during phase III.

Due to the steady, 'standard'-like growth obtained under 'high' conditions throughout the process (phase I–III), transcriptional analyses by DNA microarrays were performed from samples withdrawn during phase I and compared to the reference condition at the same time point and X. In total, 117 differently expressed genes showing a minimum mRNA fold-change of 2 were detected and, where possible, functionally assigned to the

regulons e.g. DtxR/RipA, AcnR, LtbR, and respiration-specific genes (Tab. BS.2). Notably, a significant overall activation of most genes belonging to the DtxR/RipA regulon was observed that constitute to more than 50 % of all observed genes. In this regard, DtxR is known as a dual transcriptional master regulator involved in the iron homeostasis in *C. glutamicum* and controls, amongst others, the expression of siderophore uptake systems, as well as the transcriptional regulator *ripA* (Fig. 4.9 A). Being active under iron excess conditions, DtxR is described to repress *ripA* (about six-fold decreased; Tab. DS.3), which in turn leads to the de-repression of several genes encoding iron-containing proteins: e.g. aconitase and catalase (Brune et al., 2006; Wennerhold & Bott, 2006). The same regulatory response was detected under 'high' CO_2/HCO_3^- levels in this study (Fig. 4.9), whereas the over-expression of *katA* (catalase) might point to oxidative stress conditions. However, the latter is described to occur (i) under low pH, iron limiting environments (Follmann et al., 2009) and (ii) due to increased TCA flux and respiration leading to higher death rates by exacerbated H_2O_2 (oxidative) stress as shown in *E. coli* (Ezraty et al., 2011). However, extracellular acid stress was not installed in our experiments (pH = constant) and in contrast to Follmann et al. (2009), we observed a transcriptional pattern similar to iron excess conditions, thereby excluding the occurrence of intracellular acidic stress caused by the 'high' CO_2/HCO_3^- environment. Even though, a slightly increased activity of ICD (Fig. B.4) and significantly higher mRNA levels under 'high' CO_2/HCO_3^- conditions of genes encoding succinate dehydrogenase, succinate-CoA ligase, aconitase, nitrate reductase, and cytochrome C oxidase were observed (Tab. BS.2). However, genes known to be involved in the SigM/SigH-dependent (Schröder & Tauch, 2010) or OxyR-related [*C. glutamicum* R; Teramoto et al. (2013)] oxidative stress response were not differently expressed. Taken together, the transcriptional response obtained under 'high' CO_2/HCO_3^- levels, in combination with the control experiment illustrated above, contradicts this indication. Subsequently, the functional correlation of DtxR to 'high' CO_2/HCO_3^- conditions was further verified in fermentations with the deletion mutant *C. glutamicum* $\Delta dtxR$ and its corresponding WT (Fig. B.5 B). The results clearly show that without functional DtxR, growth is significantly inhibited, resulting in a reduced μ by 40 % compared to the WT.

Even though the phenotypic responses of *C. glutamicum* WT via growth kinetics (slightly increased Y_{XS}) and enzyme activities (no change) to 'high' CO_2/HCO_3^- are limited (see above), a complex transcriptional adaptation, different from so far reported studies in the literature, is disclosed. Unlike the regulation regimes specified for *E. coli* and *P. putida* (Baez et al., 2009; Follonier et al., 2013), differential expression of genes

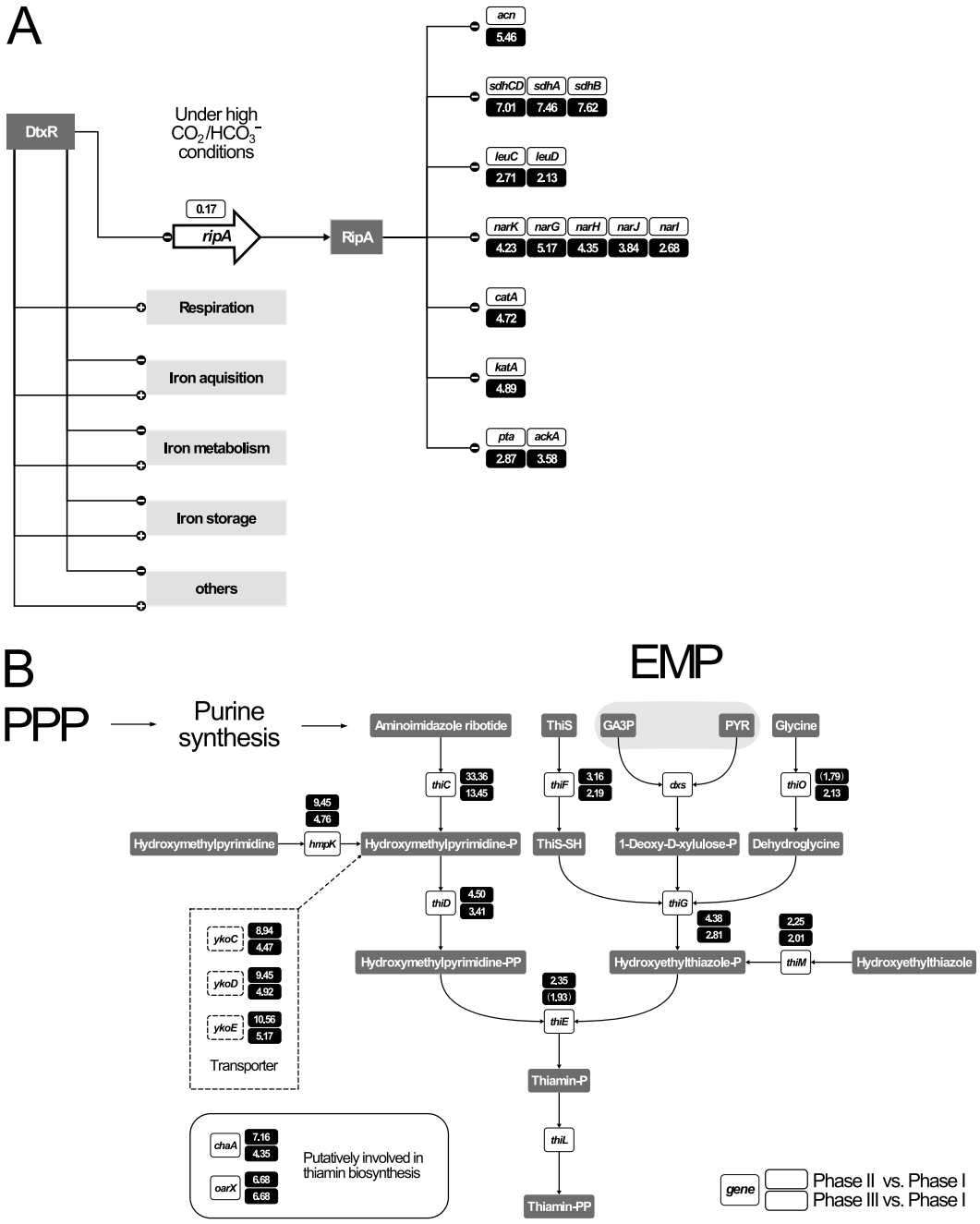

Fig. 4.9: **(A)** Schematic presentation of the DtxR/RipA regulon. Transcriptional activation (+) and repression (−) are indicated. **(B)** Schematic presentation of thiamin biosynthesis deduced from the genomic information of *C. glutamicum* WT. **(A/B)** Numbers in boxes give expressional changes (filled black box, increased mRNA level; open box, decreased mRNA level) of relevant genes identified by DNA microarray analysis from cells grown under 'high' **(A)** and 'low' **(B)** CO_2/HCO_3^- conditions in comparison to the 'standard' approach, respectively. Both figures represent a snapshot of the complete analysis. The detailed summary of all genes showing significantly altered expression was published in Tab. BS.2–Tab. BS.5. The design for the DtxR/RipA regulon was modified after Wennerhold et al. (2005). For abbreviations and the original figure see Fig. B.5.

(i) encoding de-/carboxylating reactions (except for *mez*) and (ii) mediating acid or the general sigma factor-dependent stress response (see above) were not significantly affected (Tab. BS.2). However, a disproportionate high fraction of 28 % (of all differential genes) were identified to code for membrane proteins, which is higher than the annotated number found in the total genome [22 %; Kalinowski et al. (2003)]. This observation is in line with recent studies of high pressure/elevated CO_2/HCO_3^- fermentations (Follonier et al., 2013) and might potentially hint at the cellular response regarding membrane permeability or fluidity changes.

Due to the initial transcriptional comparison between 'low' and 'standard' pCO_2 levels in phase I revealing only three, barely significant, differentially expressed genes (Tab. BS.3), both transcriptional states were considered as equal. Therefore, the ongoing analysis considered phase I of the 'low' condition as new reference point. In the comparison of transcript patterns of phase II vs. phase I, 140 differently expressed genes that were functionally assigned to the regulons e.g. Zur, McbR, Lrp, AcnR, PdxR, NrtR, ArnR, ArgR, AmrR, and respiration specific genes were detected (Tab. BS.4). In addition, most genes assigned to the thiamin biosynthesis pathway were found, showing increased mRNA levels as illustrated in Fig. 4.9 B. Comparing transcript levels of phase III vs. phase I, the same thiamin biosynthesis-associated genes were still present, however, with an overall reduced expression level. In total this comparison revealed 102 differently expressed genes that were grouped into the regulons e.g. Zur, McbR, SsuR, CysR, and respiration specific genes (Tab. BS.5).

It is noteworthy to mention that the expression changes obtained under 'low' CO_2/HCO_3^- levels (phase II) do also include a significant number of membrane proteins (33 % of the total number of altered genes), which indicates that also the lack of sufficient CO_2/HCO_3^- supply causing a growth perturbation might affect the membrane properties similar to 'high' conditions (Fig. BS.1). On that account, it is reported that high interchange rates from $CO_{2,l}$ to HCO_3^- are required to meet the cellular demand for carboxylating reactions during the exponential growth in *C. glutamicum* and *E. coli* (Merlin et al., 2003; Mitsuhashi et al., 2004). However, the transcript levels *bca* and *gca* were neither differently expressed under 'low' nor under 'high' CO_2/HCO_3^- levels, which hints at a constitutive expression independent of CO_2/HCO_3^- availability.

As detailed above, the highest q_S was obtained in growth phase II under low CO_2/HCO_3^- levels, which is also characterized by revealing the lowest μ and Y_{XS}. Concomitantly, this goes along with the excretion of L-alanine and L-valine, which indicates that carbon is at least fractionally re-routed from biomass formation to amino

acid production during that phase. At the same time period, the two-fold increased activities of GPDH and PGDH (Fig. B.4 A), as well as the over-expression of almost all thiamin biosynthesis genes are reported (Tab. BS.4 and Tab. BS.5). Altogether, these results therefore suggest an increased flux into the PPP to improve the precursor supply for the purine synthesis branch of the thiamin biosynthesis (Fig. 4.9 B). Besides CO_2 production, this would lead to the disproportionate formation of NADPH (via GPDH and PGDH), which can be readily converted via the formation of L-alanine and L-valine (Fig. 2.1), which was observed in growth phase II (Fig. B.4 B). The drain towards L-alanine and L-valine also suggests an increased pyruvate pool that also serves as a precursor for thiamin production via the EMP branch. Consequently, by improving the thiamin or thiamin pyrophosphate (TPP) availability, it might be concluded that TPP-dependent reactions as the acetohydroxyacid synthase, pyruvate and 2-ketoglutarate dehydrogenase complex, and pyruvate:quinone oxidoreductase are reinforced. Notably, all of these enzymes catalyze decarboxylating reactions that release CO_2, which might therefore be regarded as a general response mechanism of *C. glutamicum* to counteract the lack of CO_2/HCO_3^- supply and facilitate re-increased growth as finally seen in phase III (Fig. 4.8).

4.4 Process technical characterization of the cascade bioreactor system

One central objective of this thesis was the development, characterization, and application of a novel scale-down apparatus to facilitate the thorough investigation of oscillating CO_2/HCO_3^- levels in *C. glutamicum* for the first time. Therefore, the CBS was designed as a three-compartment STR system consisting of the MR and two CRs (see flow sheet in Fig. 3.1 and photograph in Fig. 4.10) that can be operated in total recycle. All three reactors were fully equipped for standard and advanced process monitoring (T, pH, p, pO_2, and pCO_2) and, notably, can be operated independently from each other during circulation processes. This relates not only to the standard process conditions during the fermentation, but especially to the application of different CO_2/HCO_3^- conditions in each individual compartment (STR). The latter are considered as distinct volume elements of a large scale bioreactor, which permits the abstraction of a hypothetical cellular flow path at large scale and mimics the continuous exposure to heterogeneous (CO_2/HCO_3^--specific) culture environments. Material testing, assembly, programming,

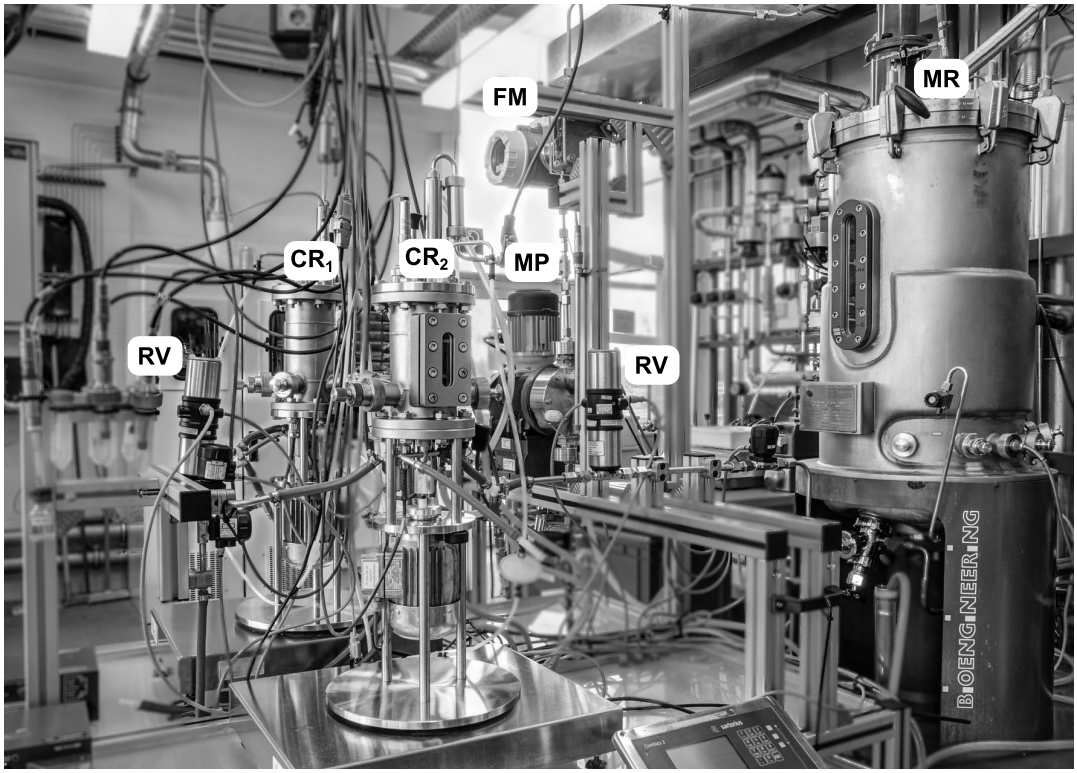

Fig. 4.10: Photograph of the three-compartment cascade bioreactor system (CBS) corresponding to the technical setup described in section D.2.3 and schematically depicted in Fig. 3.1. Abbreviations are as follows: CR, cascade reactor; FM, flow meter; MP, metering diaphragm pump; MR, main reactor; RV, regulating valve.

and parametrization of the CBS was performed on the basis of the preliminary work of Andreas Freund (Institute of Biochemical Engineering, University of Stuttgart) on the relevant engineering drawings, construction, and electrotechnical implementation. A detailed summary of the final setup is supplementary provided in section D.2.3.

The description and results of the technical characterization, which is required to (i) apply defined CO_2/HCO_3^- gradients and (ii) adjust the residence times of the cells under exposure, precede the application of the CBS and are illustrated in the following sections (see also section D.3.1).

4.4.1 Mixing time analysis

In order to evaluate the mixing efficiency of the individual STRs that constitute the CBS, tracer pulse experiments using conductivity measurements were performed. For all vessels, θ_{95} blend times were derived by setting a 95 % homogeneity criterion of the bulk liquid

and detected for the operational range of the STR during the fermentation processes. Since sufficient oxygen transfer in *C. glutamicum* cultivations in this study is mainly facilitated by the agitation until considerable biomass concentrations of $X = 10\,\mathrm{g\,L^{-1}}$ (compare e.g. Fig. 4.6), N was varied in full scope between (50–390) $\mathrm{min^{-1}}$ in the MR, and between (300–1,500) $\mathrm{min^{-1}}$ in the CR (Fig. 4.11 A, B).

The results clearly show that θ_{95} follows an exponential decay function with increasing stirrer speed, observable for both STRs. At the beginning of fermentation processes, minimum N of $50\,\mathrm{min^{-1}}$ and $300\,\mathrm{min^{-1}}$ were applied in the MR and CR, respectively, corresponding to maximum obtained θ_{95} of (16.50 ± 0.43) s and (2.15 ± 0.18) s. On the contrary, highest agitation rates of $390\,\mathrm{min^{-1}}$ and $1{,}500\,\mathrm{min^{-1}}$ accounted for minimum θ_{95}, resulting in (2.60 ± 0.36) s and (0.53 ± 0.05) s, respectively (Fig. 4.11 A, B). As illustrated, a continuous increase of N would only marginally led to higher mixing qualities indicating that θ_{95} becomes independent of the power input and might further only be influenced by diffusive processes. In addition, both correlations showed a good agreement to model assumptions as given by the empirical characteristics of baffled STRs in the turbulent regime [$N\,\theta$ = constant at $\mathrm{Re} > 10^4$; Mersmann et al. (1975)]. The conformity between all experimental and theoretical values expressed by the MAPE was calculated to 5 % (MR) and 9 % (CR). Based on these results, the goodness of the mixture can now directly be derived from the correlation and set according to the requirements of the experimental setup. This becomes especially important for the determination of residence times in the CBS (see section 4.4.3): perfect mixing in the individual compartments is desired to minimize the influence on the distribution of the cells through the apparatus and therefore the time of exposure to the applied CO_2/HCO_3^- gradient.

Equivalent tracer pulse experiments were conducted in the CBS with total recycle to determine the relaxation time of the system and provide a basis for advanced analysis as labeling experiments in the future (Fig. 4.11 C). The experimental response time of the system depended in this case on the applied circulation flow rate (ν) and, similarly to the MR/CR results, follows an exponential decay function with increasing ν. Within the operational range of the CBS between (0.58–3.95) $\mathrm{L\,min^{-1}}$, (1.17–8.00) min passed until the system returns to a homogeneous state. Under optimal conditions, sufficient mixing in the CBS takes at least 25 times longer than in the MR, which demonstrates that blending solely depends on the fluid circulation rate. However, in coincidence to the results obtained for the individual STRs, the potential of reducing θ_{95} by increasing ν is limited. With the help of the RTD simulations in the CBS, which are described

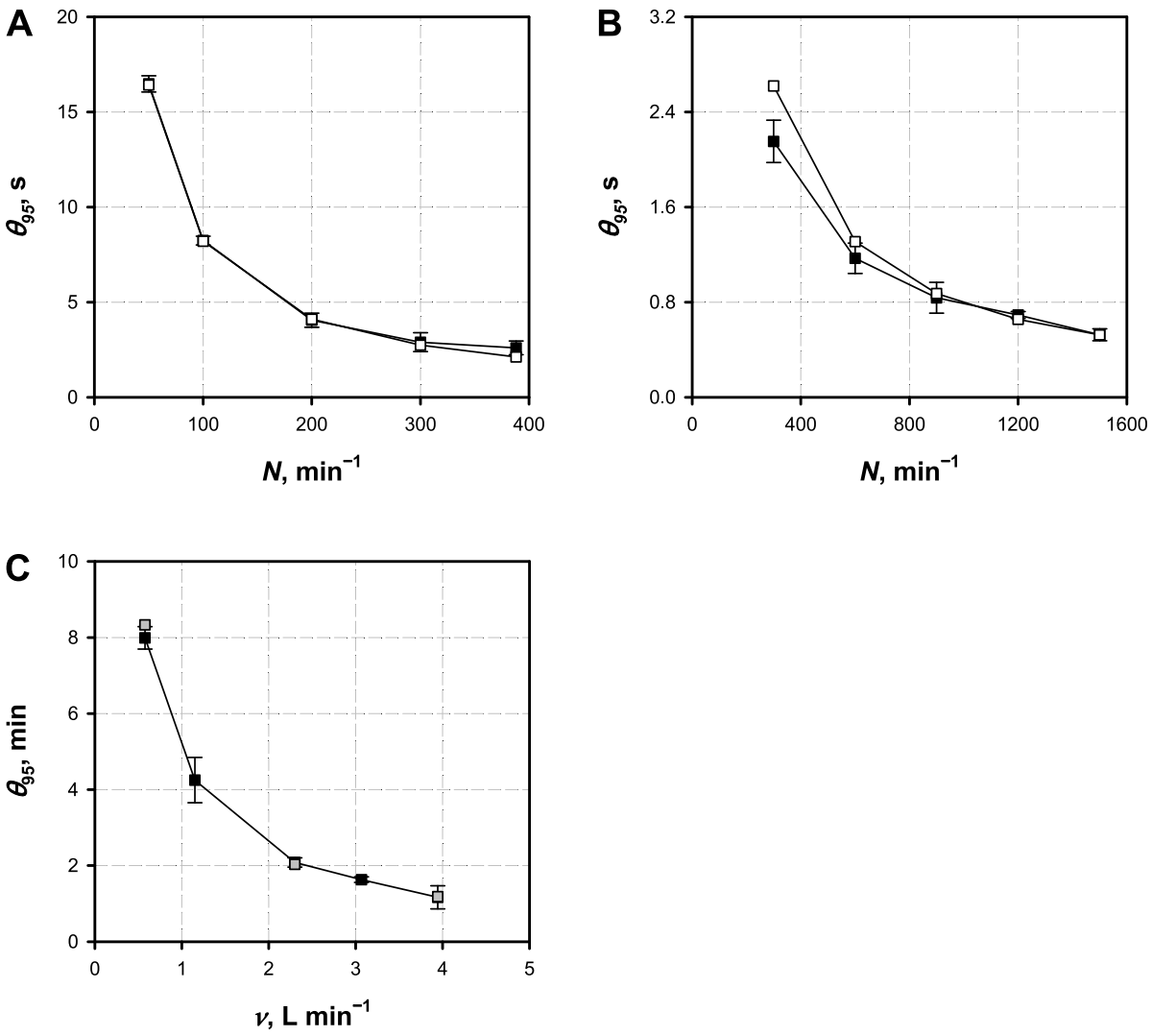

Fig. 4.11: Determination of the mixing time (θ_{95}) reaching a 95 % homogeneity criterion (■) after tracer pulse experiments. θ_{95} was detected in dependency of the agitation speed (N) for the main **(A)** and cascade reactor **(B)**, additionally indicating the theoretical blend time (□) derived from the empirical model introduced by Mersmann et al. (1975). **(C)** Illustration of θ_{95} derived for the cascade bioreactor system (CBS) at various circulation flow speeds (ν) representing distinct residence times in the cascade section. Additionally indicated are the simulated mixing times (▨) of the CBS as illustrated elsewhere (Fig. 4.20). **(A–C)** Values are given as statistical mean from at least four independent experiments ±SD. The conformity between experimental and theoretical/simulated results expressed as mean absolute percentage error was determined to 5 %, 9 %, and 3 %, respectively. The figure was modified after Fig. D.2.

and discussed in detail below (section 4.4.4), θ_{95} were predicted for the three boundary conditions of 0.58 L min^{-1}, 2.3 L min^{-1}, and 3.95 L min^{-1}. As indicated, the estimation that was performed by the simulation was very accurate and accounts for a MAPE of 3 % on average for all conditions.

4.4.2 Configuration and evaluation of the cascade bioreactor system

Further characterization experiments as for the determination of the RTD were not only performed in the individual STRs of the CBS, but also in the complete system. This required fully functional circulation facilitated by the interplay of the diaphragm metering pump and the (gravimetric) CRs level control via RVs, as well as the overall implementation into LabVIEW® as process and control system (PCS; e.g.Fig. 4.12).

In the first step, characteristic curves of the diaphragm metering pump and RVs were determined within the operating range of the CBS (see appendix section E) and then used to identify the appropriate settings under working conditions. In addition, a general control scheme was developed and implemented (Fig. E.3) to facilitate the temperature and pH control in fermentations or characterization experiments that require the use of one or two independent control elements. All parameters used for regulation and control of relevant system conditions, including those derived after design and optimization of the PID controller (T and p), were summarized in Tab. E.8.

All functions that were required to adjust, control, and monitor the circulation process were implemented into an overall circulation-specific front panel in LabVIEW® to simplify the operation as depicted in Fig. 4.12. Most options and settings work indicatively and important routine functions are programmed for fast and automatic execution. The four most important modules are (i) the adjustment and control of the circulation speed, (ii) the fill-up of the CRs from the MR via the 'transfer sequence', (iii) the initiation of the circulation via the 'autostart sequence', and (iv) the fast and safe termination of the circulation progress via the 'shut-down sequence'. All LabVIEW® block diagrams are supplementary provided (section E) with detailed information on the corresponding structure.

Fig. 4.13 visualizes a complete process start-up and indicates relevant circulation parameters as CRs fill levels (V_{CR}), ν, and the corresponding setpoints. The beginning of the characterization and fermentation experiments was commonly initiated by the liquid transfer from the MR into the CRs. For security reasons, the filling process is automatically terminated after reaching 90 % of the given setpoint. In turn, the latter itself is initially reduced if V_{CR} is operated close to the maximum. As soon as the transfer to both CRs is completed, all relevant process parameters are immediately adjusted (T, pH, pO_2, N, etc.) and the autostart sequence executed. In this regard, the results of the pump and RV characteristics were directly implemented (predefined value selection)

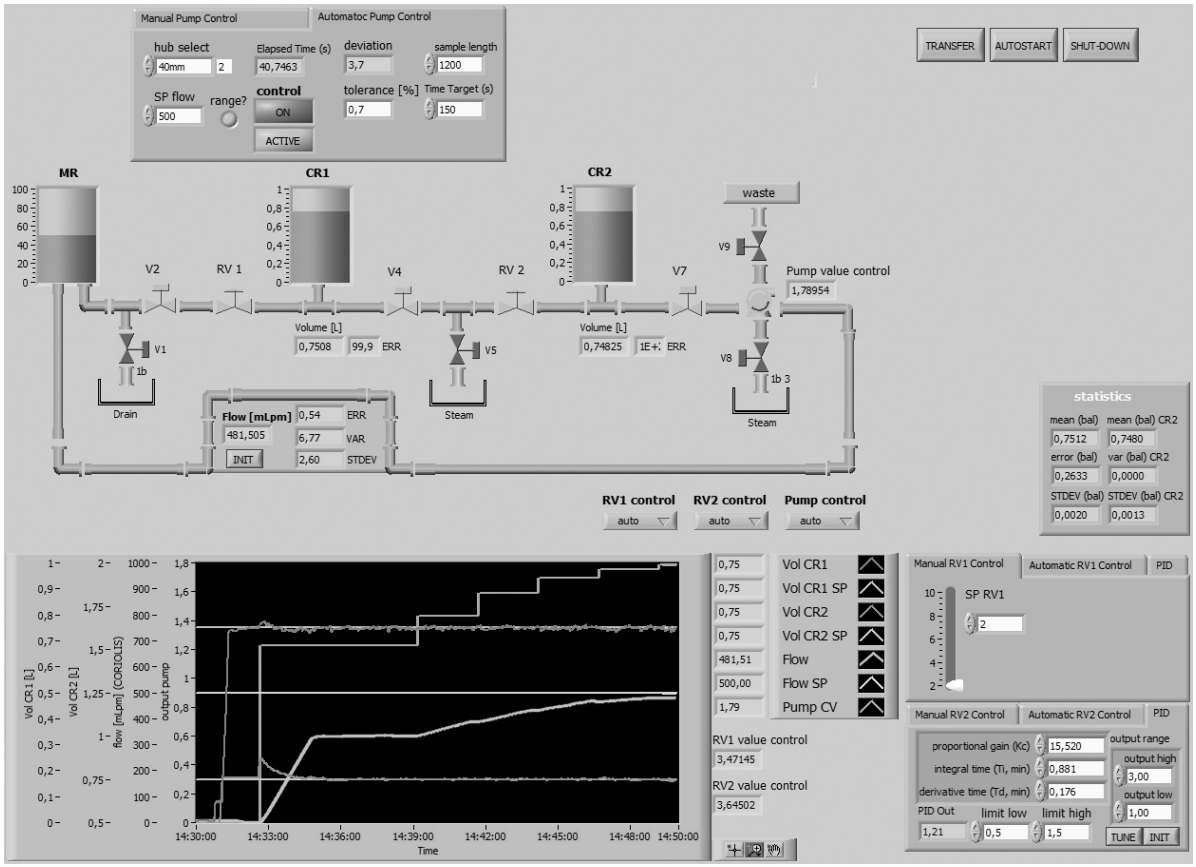

Fig. 4.12: Overview of the LabVIEW® front panel functionality to facilitate circulation control in the cascade bioreactor system (CBS). Indicated are the flow sheet of the individual reactors (including volume level display) of the CBS with switchable (regulating) valves (RV) for regular flow, waste, steam sterilization, and diaphragm metering pump. Pump control settings with optional manual or automatic control are given on the upper left hand side. Correspondingly, settings for the manual and automatic mode of the RVs are placed on the lower right hand side. All relevant process information including setpoints and actual values are given in the overview display, whereas program routines as liquid 'transfer' (initial filling of the reactors), 'autostart' or 'shut-down' automation are located on the upper right hand side. Further details can be found in the appendix (section E).

and set in dependency to the selected flow speed to facilitate circulation conditions close to the setpoint. Level regulation and control is initiated automatically, whereas the pump regulation and setpoint control can be switched on separately. The initiation process of the circulation was then followed by the incremental enhancement of the V_{CR} setpoints until reaching the desired level: the stepwise increase prevents the imbalance of the system, which is further simplified when only small deviations of the pumping rate occur. As indicated in Fig. 4.13, ν rises slowly after each stepwise increase of the pumping setpoint. However, the slow response is only the result of the relatively large averaging of the flow indicator (reaction of the pump and application of the new flow

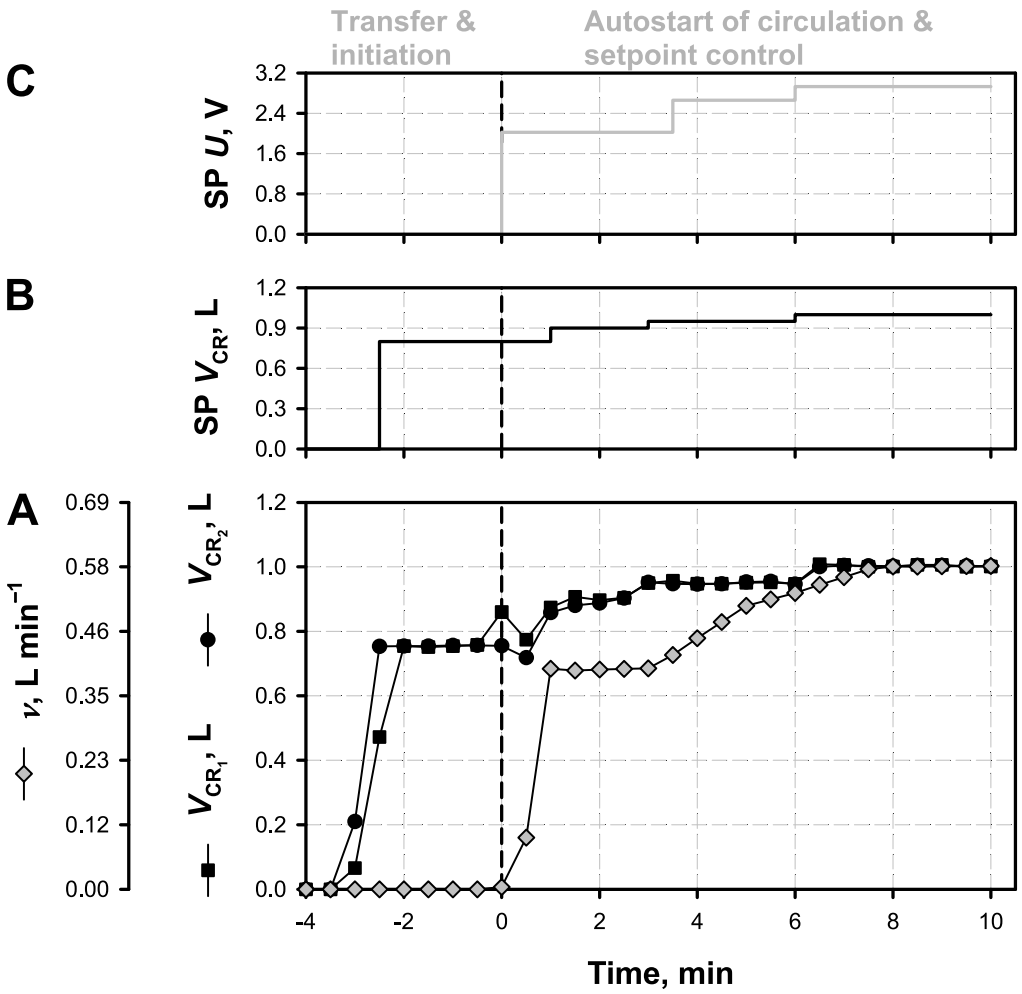

Fig. 4.13: Illustration of an exemplary initiation process for circulation experiments in the cascade bioreactor system (see Fig. 4.12). **(A)** The procedure starts by executing the liquid 'transfer sequence' to fill both cascade reactors (CR) from the main reactor. **(B)** The fill level setpoint (SP) of both CRs (V_{CR}) is set to 90 % of the final value. After initiation and adjustment of all relevant process parameters in both CRs, the circulation can be started ('autostart sequence'). **(C)** Therefore, the pump is switched on by applying the the characteristic voltage (U) for the selected flow rate (ν; see Fig. E.1), which is followed by the V_{CR} level regulation and control (initiated automatically). Finally, SP control for the desired V_{CR} and ν results in a stable process after about (5–8) min.

rate is immediate), which helps to result in smooth and stable circulation rates (compare pump control in Fig. E.4). By using the described procedure and control loop indication, stable process conditions were (visually) reached after (5–8) min, which can be shortened by a couple of minutes if the visualization of ν is reinitialized after each step change for instance.

The agitation of the individual STRs is a pre-requirement for all characterization and cultivation experiments that use the CBS in total recycle. In combination with the

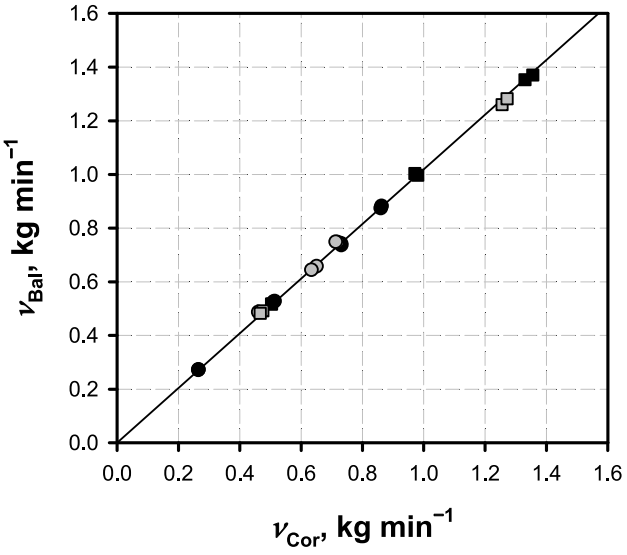

Fig. 4.14: Determination of the flow meter accuracy between the flow path from cascade reactor 2 (CR_2) to the main reactor (MR). The following hydrodynamic conditions were applied to the CR_2 to simulate fermentation conditions: agitation of $N = 500\,\mathrm{min}^{-1}$ with volumetric gas flow rates of $Q/V_R = 0.1$ vvm (black symbols) and $1{,}000\,\mathrm{min}^{-1}$ with 1 vvm (gray symbols). The overall flow (ν) was facilitate with diaphragm metering pump at a stroke setting of 20 mm (circles) or 40 mm (rectangles) and detected either gravimetrically (Bal) or via Coriolis flow meter (Cor). The resulting flow ratio (ν_{ratio}) was determined with <1.02, as indicated by the regression line ($R^2 = 0.999$.)

applied aeration and, due to the circulation itself, gas bubbles are circulated through the system next to the cultivation broth. Nonetheless, the accurate detection of ν is required throughout the (fermentation) process to ensure constant circulation and residence times within the CBS. To evaluate the accuracy of the flow meter under various hydrodynamic conditions, control experiments were performed as indicated in Fig. 4.14. Two fermentation-similar conditions, resembling the first and second half of a standard cultivation process (equivalent to e.g. Fig. 4.6), were applied to the CR_2. The liquid was then transferred through the mass flow meter into the MR with flow rates of about $(0.25–1.4)\,\mathrm{kg\,min}^{-1}$. A flow ratio ($\nu_{ratio}$) was finally derived from the flow rate detected gravimetrically from the supply of CR_2 and from the flow meter. As a result, ν_{ratio} accounted for less than 1.02 by linear regression, which indicates that the gas interference of the detection is negligible within the scope of the applied conditions.

The subsequent characterization of the CBS to determine RTDs for various ν was also performed by conductivity measurements similar to the mixing time analysis (section 4.4.1) with the exception that the conductivity probes were positioned directly in the intersections between the STRs. Therefore, control experiments were conducted to verify the (indirect) influence of the flow condition by ν through the transfer tubing and pipes on the measurement signal of the conductivity probe (Fig. 4.15). The experimental setup consisted of a continuously mixed salt solution that was transferred through the CBS intersection tubing at flow rates in the range of $(0.5–3)\,\mathrm{kg\,min}^{-1}$. Subsequently, the conductivity signal was correlated to ν by linear regression yielding a coefficient of determination of $R^2 < 0.0001$. This result clearly confirms that no physical relation

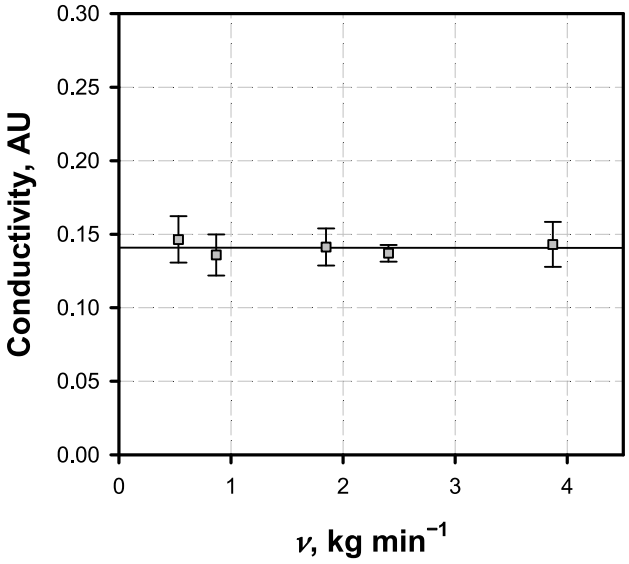

Fig. 4.15: Illustration of the correlation between the conductivity measurement of a defined tracer solution on the pumping rate (ν) applied through the detection position of the probe (cascade bioreactor system tubing). Values represent the statistical mean ±SD of at least three measurements per condition. The results were fitted by linear regression ($R^2 < 0.0001$) as indicated with a given slope of the curve of 3×10^{-5}.

between ν and the size of measurement signal exists and that the detection itself is not influenced by the applied flow pattern essential for the following RTD analyses.

4.4.3 Residence time analysis

The evaluation of the CBS configuration and conductivity measurements, as well as the final implementation of the PCS in LabVIEW® as presented previously were taken up to determine the RTDs under various conditions. Theoretically, the residence time of a particle (or a cell) in a vessel (e.g. bioreactor) can be described by the space time (τ; see Eq. 3.42) underlying the assumptions of e.g. steady state in- and outflux and uniform distribution of the particles through the system. However, actual experimental setups often violate one or more of these constrains, which might eventually lead to a deviation between τ and the mean residence time $\bar{t}$ that is derived from the first moment of the RTD curve. To minimize biased RTD analyses from the mixing condition in the three STRs of the CBS itself, the results of the θ_{95} experiments were directly applied to the CBS configuration. Consequently, all experiments were performed with agitation rates of (1,000–1,500) min^{-1} in the CRs and 300 min^{-1} in the MR to assure adequate mixing.

In the first instance, $\bar{t}$ was determined for the complete CBS, which was opened according to Fig. 3.6 to form a classical STR cascade used in chemical engineering. The repeatedly described pulse experiments were performed for the three boundary conditions with ν set to 0.58 L min^{-1}, 2.3 L min^{-1}, and 3.95 L min^{-1}. These settings do not only represent the maximum working conditions of the CBS (data not shown),

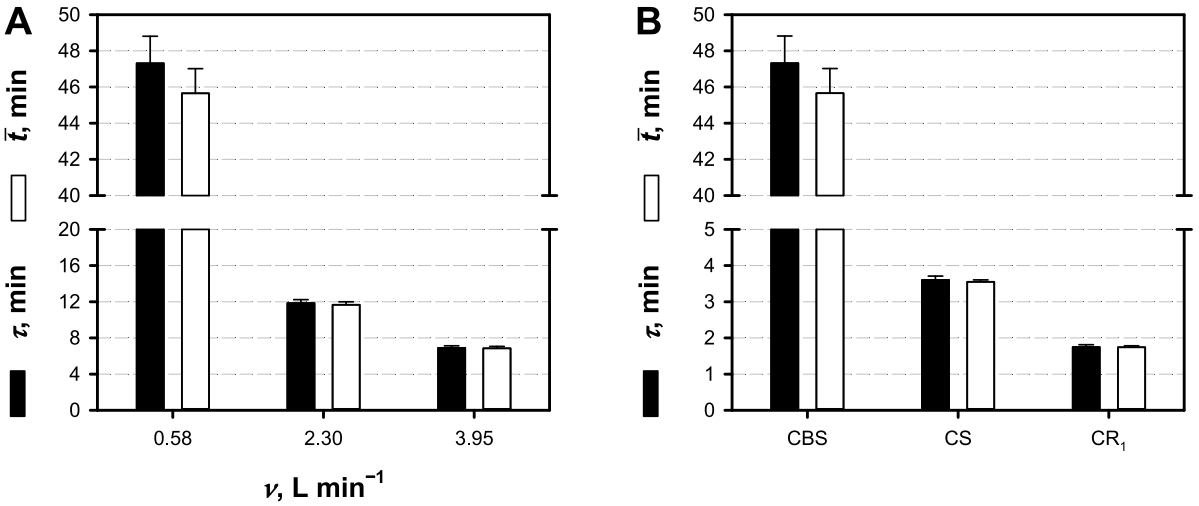

Fig. 4.16: Determination of the mean residence time ($\bar{t}$) after tracer pulse experiments and indication of the space time (τ) of each experimental setup. **(A)** Analysis performed for the cascade bioreactor system (CBS) for various circulation flow rates (ν) as indicated. **(B)** Analysis performed under fermentation conditions ($\nu = 0.58\,\mathrm{L\,min^{-1}}$) for the CBS and the cascade reactor 1 (CR_1), also indicating the cascade section (CS; $CR_1 \Rightarrow CR_2$) used for the application of CO_2/HCO_3^- gradients in this study. Results are given as statistical mean from at least four independent experiments ±SD. SD of τ was derived from error propagation assuming 1 % and 3 % error for the system volume and ν.

but also potential cultivation conditions that correspond to a broad range of residence times similar to large scale mixing conditions. Considering a maximum working volume of the cascade section (CS; $CR_1 \Rightarrow CR_2$) of 2.3 L, theoretical τ of 4 min, 1 min, and 0.58 min can be deduced for (0.58–3.95) $\mathrm{L\,min^{-1}}$. As can be derived from Fig. 4.16 A, the detected residence time correspondingly decreases with increasing ν, resulting in $\bar{t}$ of (45.66 ± 1.37) min, (11.68 ± 0.34) min, and (6.89 ± 0.20) min. The results shown were in good agreement with the theoretical estimation accounting for only a minor decrease compared to τ by 2 % on average.

All CBS fermentations in this study were performed at ν of $0.58\,\mathrm{L\,min^{-1}}$ (see section 4.5). On this regard, further experiments focused on the extended characterization of this condition analyzing CS and CR_1 as depicted in Fig. 4.16 B and Tab. 4.3. Once again, the determination of $\bar{t}$ could be shown to correspond very accurately to the preliminary estimation, resulting in a congruence to τ by 99 %. Therefore, both analysis reveal that the total available volume of the considered configurations was apparently active ($\tau \cong \bar{t}$) suggesting that no dead or stagnant zones exist that would be indicated by so called “early means” (Levenspiel, 2012).

To investigate the hydrodynamic mixing behavior of the CBS and its derived configurations under fermentation conditions at $\nu = 0.58\,\mathrm{L\,min^{-1}}$, the dimensionless

Tab. 4.3: Residence time analysis for the bioreactor setups used in this study. Experiments were performed with a flow rate of about $\nu = 0.58\,\mathrm{L\,min^{-1}}$. Mean residence times ($\bar{t}$) , theoretical space times (τ), dimensionless variances (σ^2_Θ), and ideal tank numbers derived from the latter (N_{var}) or tank-in-series (TIS) fitting (N_{TIS}) are indicated. Results are given as statistical mean from at least four independent experiments ±SD. SD of τ was derived from error propagation assuming 1 % and 3 % error for the system volume and ν, respectively. The table was modified after Tab. D.6.

System	τ, min	$\bar{t}$, min	σ^2_Θ, –	N_{var}, –	N_{TIS}, –
Cascade bioreactor system					
MR ⇒ CR_1 ⇒ CR_2	47.31 ± 1.50	45.66 ± 1.37	0.67 ± 0.03	1.50 ± 0.04	1.49 ± 0.02
Cascade section					
CR_1 ⇒ CR_2	3.60 ± 0.11	3.55 ± 0.05	0.48 ± 0.01	2.08 ± 0.06	1.99 ± 0.03
Cascade reactor					
CR_1	1.75 ± 0.06	1.74 ± 0.04	0.91 ± 0.05	1.10 ± 0.06	1.12 ± 0.01

variance σ^2_Θ was determined from the second moment of the RTD curve (Tab. 4.3). Under ideal conditions, it distinguishes perfectly mixed or plug flow conditions with $\sigma^2_\Theta \longrightarrow 1$ and $\sigma^2_\Theta \longrightarrow 0$, respectively, as detailed in section 3.4.2. For the three-compartment CBS, σ^2_Θ was determined with 0.67 ± 0.03, which decreased to 0.45 ± 0.01 when only the CS is considered. This coincides with the theoretical estimation of the RTD by the TIS model depicted in Fig. 2.4, which demonstrates that the RTD for a series of volumetrically identical, ideal CSTR approximates that of an ideal PFR. On the contrary, σ^2_Θ approaches unity 0.91 ± 0.05 for CR_1 as single reactor system (Tab. 4.3) and was shown to increase in the CBS in conjunction with the enhancement of ν from $0.58\,\mathrm{L\,min^{-1}}$ to $3.95\,\mathrm{L\,min^{-1}}$ to a final value of about 0.74 ± 0.02 (data not shown).

Obviously, the difference in size of the MR ($V_{MR} = 25\,\mathrm{L}$) compared to both CRs ($V_{CR} = 1\,\mathrm{L}$) superimposes this principle, which can also be derived from the calculations of the ideal tank numbers N_{var} defined as the inverse of σ^2_Θ. N_{var} accounted for 2.08 ± 0.06 and 1.10 ± 0.05 for the CS and CR_1, respectively, both values slightly above the actual N_T of the configuration. While this might be a direct consequence of the configuration and measurement setup with intersections pipes between the STRs, the detected N_{var} of the three-compartment CBS was found to be decreased to 1.50 ± 0.04.

Alternatively, N_T was determined by fitting the TIS model to the experimentally obtained RTDs as depicted in Fig. 4.17. It could be shown that the results of N_{TIS} were generally in good agreement to the previous calculation of N_{var} showing only minor deviations of 2 % on average. Both approaches therefore characterize the total CBS as 1.5 ideal tanks. This number was compared to the theoretical estimation considering the sum of the volumetric contribution of the CS and N_T of the MR detailed in Fig. DS.2. It could

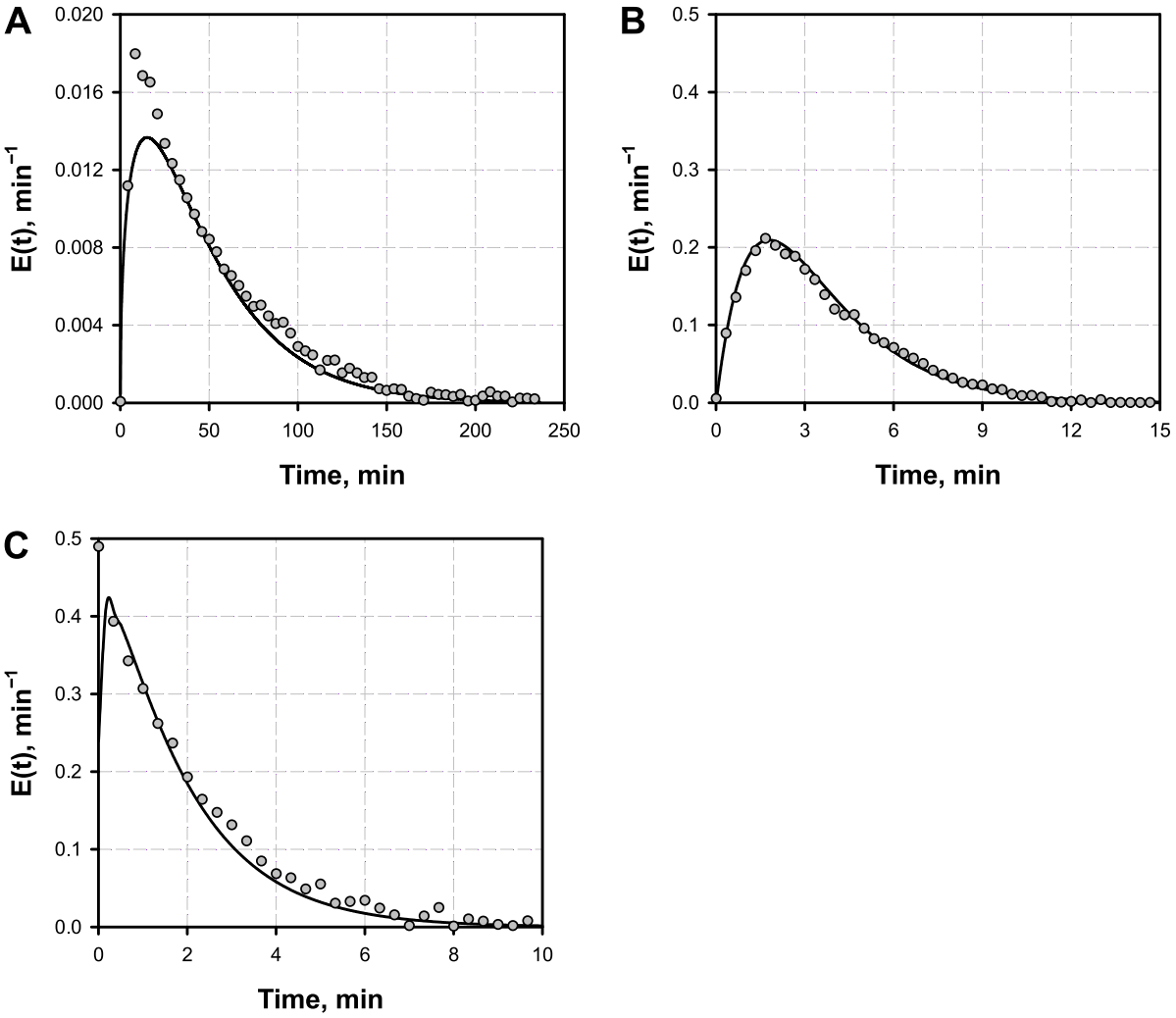

Fig. 4.17: Exemplary determination of the ideal tank number N_{TIS} by fitting the tank-in-series model (—) to the experimental residence time distributions $E(t)$ (●) derived for **(A)** the cascade bioreactor system, **(B)** the cascade section consisting of the cascade reactor 1 and 2 (CR), and **(C)** the CR_1 at a flow speed of $\nu = 0.58\,\mathrm{L\,min^{-1}}$.

be shown that the hydrodynamic impact of the CS is significantly larger (>25 %) than anticipated from the volumetric compartment-ratios within the CBS. Even though the maximum CS-to-CBS ratio that can be applied under working conditions does not exceed 8.4 %, which is at the lower end of previously published scale-down models (Sandoval-Basurto et al., 2005) but qualitatively comparable to CFD estimations (Enfors et al., 2001; Noorman, 2011), the results indicate an advantageous applicability of (CO_2/HCO_3^-) gradients for scale-down studies supported by the hydrodynamic constitution.

4.4.4 Simulation of residence time distributions

The previous sections have shown that the hydrodynamic conditions occurring in the CBS could successfully be described by the experimental θ_{95} and RTD determination. Even though these results are essential for the understanding and characterization of the system, they base on the CBS operated as a classical STRs cascade. However, the transfer of the measurements and calculations to describe the CBS operated in total recycle cannot directly be accomplished (see section 3.4.3 for details). Therefore, an analytical solution was established via transfer functions in the Laplace domain to finally simulate the output signal of the system after pulse experiments (Hopkins et al., 1969).

The resulting response curves of the (open) CBS, the CS, and the CR_1 from experimental and simulative analyses are illustrated in Fig. 4.18. As can be seen, the overall experimental response of the systems can already be acceptably described when using τ of the individual bioreactors as parameter for the system poles (Tab. F.1). In addition, manual adjustment of the poles led to a further improvement of the fit, especially for the important (see below) early response phase of the systems.

As a result, each transfer function serves as a sufficient representation of the signal distribution within the bioreactor configurations. Due to the fact that the latter was still determined without loop, it corresponds to one cycle through the systems. Consequently, the fitted analytical transfer functions were used to calculate the consecutive system response for a number of j cycles. The analytical solution of the response curves for five cycles through the CBS under fermentation conditions of ν = 0.58 L min^{-1} is exemplary provided in Fig. 4.19. It visualizes the transformation of the initial pulse with the RTD characteristic of the CBS for every cycle and finally permits to obtain the overall system response from the superimposition of the individual signals. The simulation was performed for all three circulation conditions between (0.58–3.95) L min^{-1} as mentioned previously and finally compared to the experimental response curves of the tracer experiments in the CBS with total recycle as discussed in the following.

As shown in Fig. 4.20, the response profiles of the CBS resemble classical saturation curves without oscillatory behavior that is usually indicated for STR cascades as in the TIS model by Levenspiel (2012). Similar to the observations of the ideal tank number and fitting of the system poles of the transfer functions illustrated above, this effect is attributed to the (volumetric) dominance of the MR. Therefore, circulation simulations of the CS (volume-identical configuration) are provided in the appendix (Fig. F.1) that

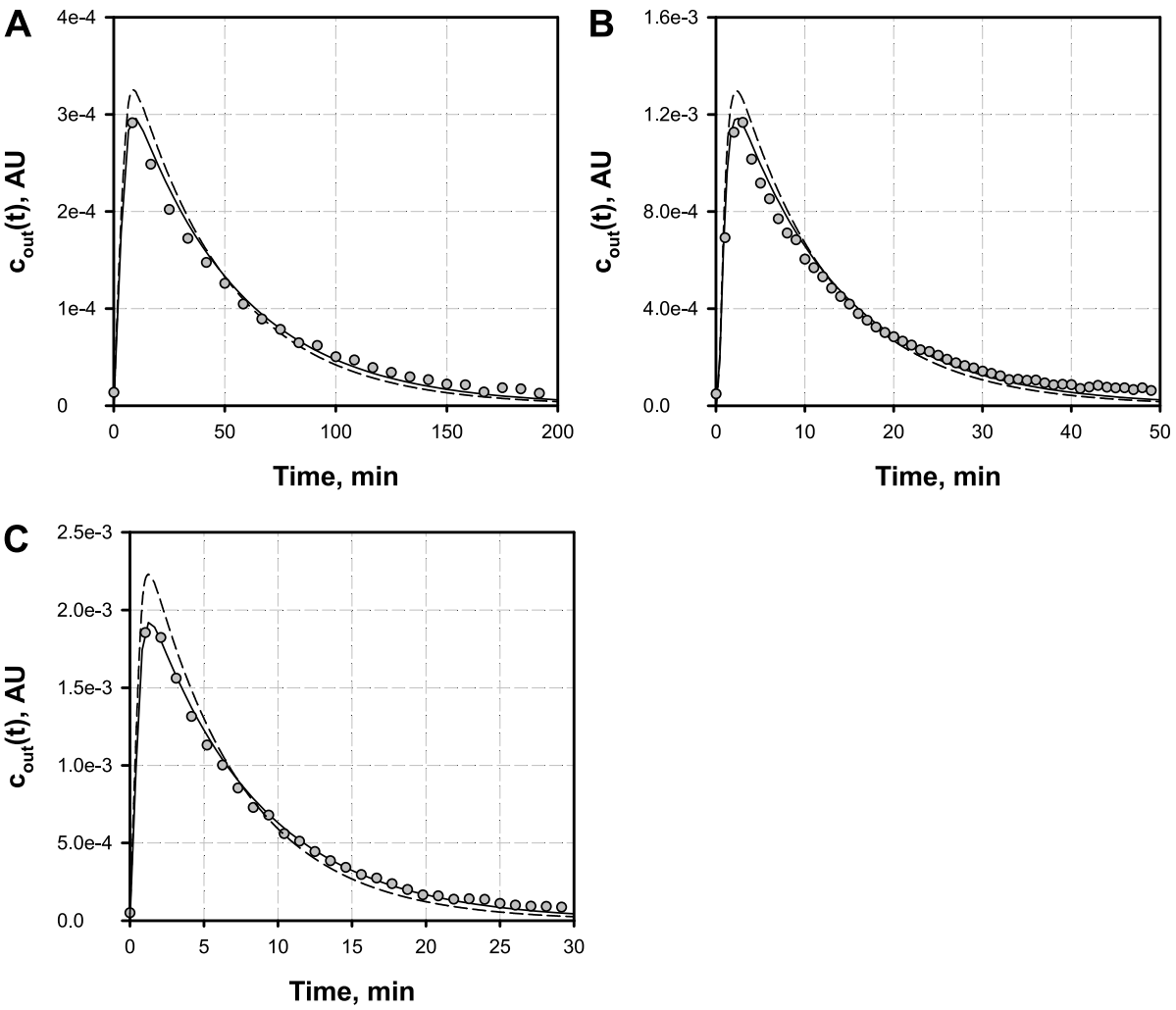

Fig. 4.18: Exemplary illustration of simulated and experimental (●) response curves [$c_{out}(t)$] after pulse experiments applied to **(A)** the cascade bioreactor system, **(B)** the cascade section consisting of the cascade reactor 1 and 2 (CR), and **(C)** the CR_1 at a flow speed of $\nu = 0.58\,\mathrm{L\,min^{-1}}$. Simulated curves were either obtained by fitting the systems poles of the transfer functions to the experimental results (**——**) or by inserting the theoretical space time of the given reactor (**- - -**). All relevant system parameters are supplementary provided (Tab. F.1).

show that the oscillation itself does not only depend on N_T, but also on the length of the intersection (modeled by t_{lag}).

The simulation shown in Fig. 4.20 nicely reproduced the mixing behavior of the CBS at the lowest flow rate of $0.58\,\mathrm{L\,min^{-1}}$ throughout the course of the experiment. With increasing circulation rates, deviations between the experimental and modeled response curves were observed that concentrate mainly on the initial phase of the experiment right after tracer injection. However, the transition phase prior steady state conditions is adequately estimated showing a good congruence to the experimental data for $2.3\,\mathrm{L\,min^{-1}}$

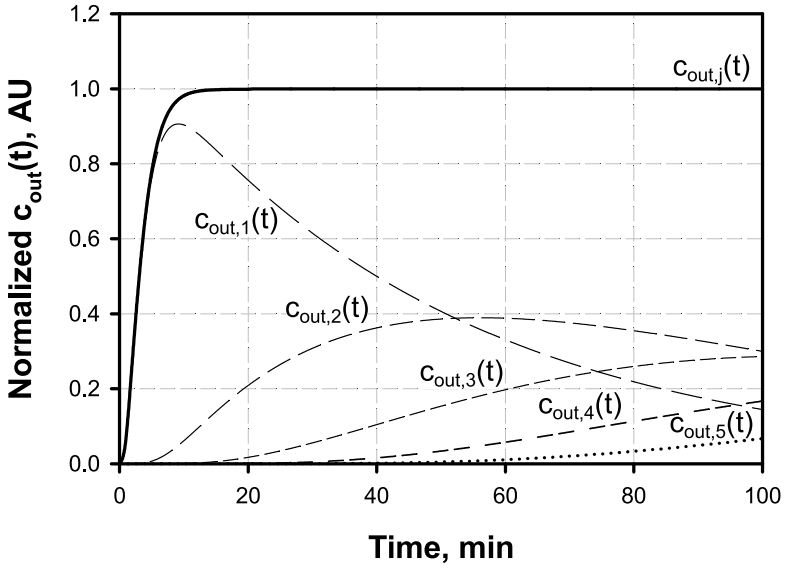

Fig. 4.19: Simulated response curves $[c_{out}(t)]$ after tracer pulse experiments in the cascade bioreactor system under fermentation conditions using a flow rate of $\nu = 0.58\,\mathrm{L\,min^{-1}}$. The final response $[c_{out,j}(t)]$ was obtained after summation of the individual signals after j cycles. The figure exemplary indicates the first five responses.

and $3.95\,\mathrm{L\,min^{-1}}$, respectively. This observation suggests that high ν, which in turn lead to considerable liquid velocity rates, somewhat interfere with the accurate capture of the tracer pulse. Most presumably, this effect is caused by the pulsating flow profile of the diaphragm metering pump and, concluding, multiple measurements of the same tracer particle due to the high frequency of the pump strokes. Nevertheless, the overall sufficient performance of the simulation was demonstrated in the CBS mixing experiments as illustrated before (section 4.4.1). Thereby, a low average MAPE of about 3 % on the overall prediction for all three conditions (Fig. 4.11) verified that the performed characterization and simulation experiments successfully established the relation between the hydrodynamic behavior of the CBS with and without recycle loop.

Taken together, the previous sections demonstrate the successful implementation of the CBS and the subsequent evaluation of the cascade setup and functions to facilitate the accurate circulation process. It further highlights the successful technical characterization of the system and its configurations, and provides the necessary understanding of the mixing and flow conditions inside the system. Therefore, all required steps were accomplished to use the CBS for the abstraction of the cellular flow path through a heterogeneous environment. Compared to previously published STR-PFR scale-down devices, the flexible design of the system offers the applicability of a broad range of

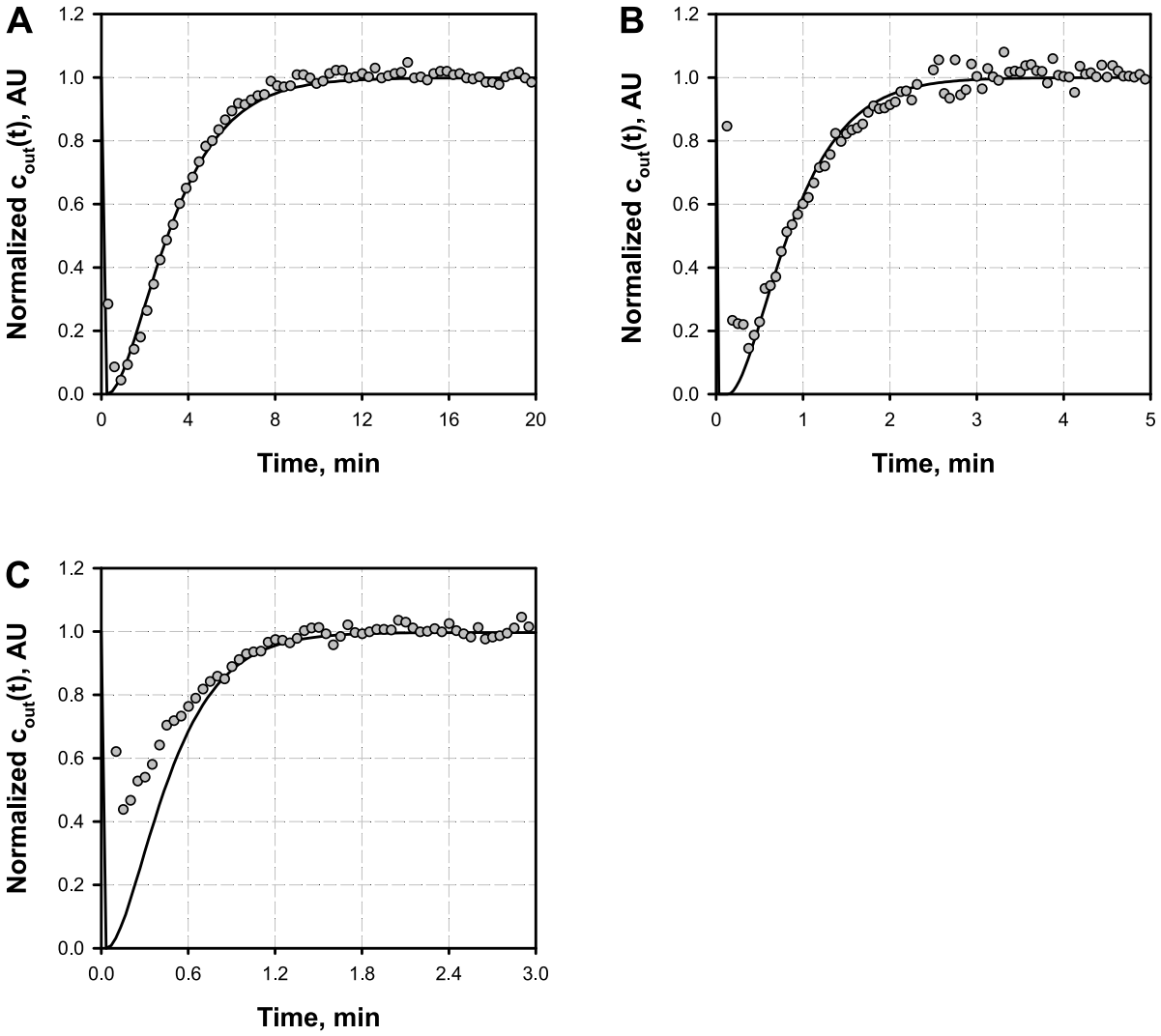

Fig. 4.20: Comparison of simulated (—) and experimental (◉) response curves $[c_{out}(t)]$ after tracer pulse experiments in the cascade bioreactor with total recycle performed with circulation rates of **(A)** $0.58\,\mathrm{L\,min^{-1}}$, **(B)** $2.3\,\mathrm{L\,min^{-1}}$, and **(C)** $3.95\,\mathrm{L\,min^{-1}}$, respectively.

large scale equivalent residence times in the CS of up to 4 min. Therefore, the following sections illustrate the application of defined CO_2/HCO_3^- gradients in the CBS and the capture of the cellular responses following up on the results of the "quasi-stationary" CO_2/HCO_3^--related experiments and results presented before (section 4.3).

4.5 Scale-down analysis of *Corynebacterium glutamicum* under carbon dioxide/bicarbonate inhomogeneities

It has been outlined throughout this thesis that despite the relevance of *C. glutamicum* for industrial biotechnology and the awareness of general growth and production sensitivity towards (large scale-typical) high CO_2/HCO_3^- levels, studies focusing on the combination of both aspects are scarcely available or of rather preliminary extend. Therefore, the investigation on the kinetic and transcriptional impact of "quasi-stationary" CO_2/HCO_3^- environments on *C. glutamicum* as presented before (section 4.3) has shown to provide valuable insights on the general understanding of the cellular response. However, fermentations performed under constantly 'high' or 'low' CO_2/HCO_3^- levels do not represent typical large scale manufacturing conditions. To overcome this limitation, the successful technical characterization and establishment of the CBS as presented in the last section provides a valuable framework for closing this important knowledge gap of scale-down analysis by applying oscillating CO_2/HCO_3^- levels under defined residence times.

4.5.1 Preliminary analyses, system evaluation, and experimental design

As part of the aforementioned work on the characterization and implementation of the CBS, test fermentations with total circulation were performed to address important aspects in the following prior to the final application. Firstly, it should be investigated if the CO_2 absorption/desorption that has been reported to be a limiting factor in one-compartment scale-down devices (Lara et al., 2006a), is sufficient for the intended CO_2/HCO_3^- gradient application. Furthermore, the stability of the CBS under fermentation conditions should be validated with respect to the impact of expectable system dynamics as e.g. biomass and foam formation on the continuous circulation, regulation, and control. Equally important for aerobic fermentations in the CBS is the question of sufficient oxygen introduction. Due to the fact that no O_2 supply is provided in the intersection pipes connecting the three STRs, this aspect is of particular relevance. The time until O_2 becomes depleted depends not only on the amount of O_2 that is dissolved into the medium before leaving the corresponding reactor, but also on the q_{O_2} (i.e. X), as well as on the residence time of the cells in the intersections (i.e. applied ν). To prevent

anaerobic conditions during the circulation process, a simple PFR model combined with Monod kinetics was used to estimate the time until total O_2 consumption (further mass transfer neglected) after transition into the PFR-like intersections (Fig. F.2). With relatively high ν of (2.3–3.95) $L\,min^{-1}$ and corresponding flow velocities of (0.8–1.3) $m\,s^{-1}$, O_2 availability should not be an issue even at high cell densities of 40 $g\,L^{-1}$. However, for cultivation aiming at residence times of about 4 min in the CS (ν = 0.58 $L\,min^{-1}$), pO_2 levels larger than 35 % were applied in the CS compartments as a precaution; in particular for CR_2 as it is followed by the longest intersection.

To cover the two foremost aspects, a first test run with ν of 0.58 $L\,min^{-1}$ was designed to intentionally bring the CBS to its limits regarding process system stability and CO_2 transfer. Therefore, the highest CS-to-CBS volume ratio was selected (Tab. F.2), providing 'high' pCO_2 levels in the CR_1 that ought subsequently to be removed from the culture broth by excessive stripping in CR_2 (data not shown). With the interplay of high CO_2 portions of (50–70) % (v/v) in the inlet gas flow of the first, and Q/V_R of 4 vvm in the second CR, a consecutive pCO_2 gradient of Δ260 mbar was established (compare Tab. F.2) within a $\bar{t}$ of about 1.81 min ($CR_1 \Rightarrow CR_2$) as shown in Tab. 4.3. This reveals a considerable degree of freedom regarding the possibilities for CO_2/HCO_3^- adjustments between the individual compartments. In the following, a second test run was performed that relates to the results obtained under 'low' CO_2/HCO_3^- "quasi-stationary" conditions, motivated by the distinctive bi-level growth phenotype that was observed previously (Fig. 4.8). High stripping conditions with increasing intensities of up to 5 vvm were applied along the CS that could keep the pCO_2 levels below 140 mbar (CR_1) and 75 mbar (CR_2) with a final maximum cell density of about 16 $g\,L^{-1}$. Notably, the intensive sparging of both CRs compartments, which are equal to only 5.5 % of the total V_{CBS}, led to a three phasic growth behavior similar to the single reactor studies (data not shown). Compared with the STR experiments, this is of particular interest, since each cell statistically resides about 94 % of its time in the MR compartment with a 'standard'-similar pCO_2 evolution (data not shown). Even though, the re-establishment of ordinary growth was not observed in this experiment, which hints at a significant stress perturbation that might provoke a similar long-term response or adaption as seen before.

However, both test run conditions have caused intensive foaming soon after initiation of the recycling through the CS loop, which required the addition of considerable amounts of anti-foam agent and the reduction of the CR working volumes (Tab. 4.4). While the described observation is certainly of great interest, further validation experiments

Tab. 4.4: Summary of process parameters obtained for the circulation experiments (test run 1–2 and number 1–3) in the cascade bioreactor system. Indicated are the CO_2/HCO_3^--specific cultivation conditions referred to as 'standard' (S), 'high' (H), and 'low' (L) levels (section 3.1), as well as the corresponding fill levels of the cascade reactors (V_{CR}), and the applied circulation flow rate (ν). Values were calculated as average over the circulation time, and compared to the setpoint to derive the corresponding uncertainty. The average relative errors of V_{CR} and ν correspond to about 1 % and 3 %, respectively. The volume of the main reactor was set to 25 L, yielding a total system volume of 27.3 L in all experiments.

Experiment[†]	Condition[‡]	Parameter[*]	Experimental value	Setpoint	Relative error
Test #1	S–H–L	V_{CR_1}, L	1.00 ± 0.01	1.00	1.25 %
		V_{CR_2}, L	0.70 ± 0.03	0.70	4.06 %
		ν, L min^{-1}	0.58 ± 0.02	0.58	4.02 %
Test #2	S–L–L	V_{CR_1}, L	0.75 ± 0.01	0.75	0.82 %
		V_{CR_2}, L	0.75 ± 0.00	0.75	0.58 %
		ν, L min^{-1}	0.57 ± 0.01	0.58	1.63 %
#1	S–H–H	V_{CR_1}, L	1.00 ± 0.01	1.00	0.75 %
		V_{CR_2}, L	1.00 ± 0.01	1.00	0.82 %
		ν, L min^{-1}	0.58 ± 0.03	0.58	4.86 %
#2	S–H–H	V_{CR_1}, L	1.00 ± 0.00	1.00	0.38 %
		V_{CR_2}, L	1.00 ± 0.00	1.00	0.21 %
		ν, L min^{-1}	0.57 ± 0.01	0.58	2.05 %
#3	S–H–H	V_{CR_1}, L	1.00 ± 0.00	1.00	0.45 %
		V_{CR_2}, L	1.00 ± 0.01	1.00	0.76 %
		ν, L min^{-1}	0.57 ± 0.02	0.58	2.80 %

[†] The circulation experiments 'test run 1–2' and 'number 1–2' were performed with *C. glutamicum* WT and 'number 3' with the L-lysine producer *C. glutamicum* DM1933

[‡] Condition applies to the order MR–CR_1–CR_2. Further details on the applied CO_2/HCO_3^- levels and further culture conditions can be found in Tab. F.2

[*] Deviation of the compartment volumes includes perturbation due to bioreactor sampling

with an adapted process and control strategy are required to counteract the foaming problematics, confirm the data, and elucidate the growth phenomenon. Even though, valuable information regarding the stability and robustness of the system could be

obtained. Despite the extreme process conditions in the form of the application of high CO_2/HCO_3^- gradients (i.e. pH titration in CSTRs) or stripping conditions (foaming), flow and level control were sufficiently stable throughout the course of the experiment with relative errors of 3 % and 1 % on average over all CBS fermentations, respectively (Tab. 4.4). It could therefore be demonstrated that functional circulation under defined conditions can be maintained under fermentation conditions (see also the detailed example in Fig. 4.21) up to considerable cell densities. In addition, it shows that desired residence time of the cells and therefore their time of exposure to the applied gradients can be ensured and adequately adjusted.

To improve the cross comparability between the different CBS fermentations, all experiments were designed to share a common batch phase in the MR only, switching from STR to CBS mode at a pCO_2 threshold of 50 mbar, which corresponds to about $X = (1.1 \pm 0.3)\,g\,L^{-1}$. The following results concentrate on the application of 'high' oscillating CO_2/HCO_3^- levels in the CS of the CBS, which relates to the previous investigations under "quasi-stationary" conditions, and therefore represent the next level on mimicking realistic large scale CO_2/HCO_3^- bioreactor conditions.

However, the accurate estimation of actual CO_2/HCO_3^- concentration profiles during industrial bioprocesses is extremely difficult; up to now, the literature does not provide large scale models or quantitative data sets that can be used directly as a reference for the design of scale-down experiments. In the industrial context, severe sensing and sampling restrictions unfortunately interfere with the local determination of spatial gradients (Noorman, 2011). On the contrary, the alternative in form of advanced CFD simulations faces the tremendously complex challenge to model the interplay of e.g. p gradients, inhomogeneous pH distribution, CO_2 mass transfer, non-equilibrium conditions of the open system, and cell kinetics. For the experimental design of CO_2/HCO_3^- oscillations presented in the following, we considered an initial pCO_2 gradient after initiation of the circulation from 75 mbar (MR) over 150 mbar (CR_1) to 315 mbar (CR_2) as starting condition. This corresponds to previously published studies (Baez et al., 2009, 2011; Knoll et al., 2007, and section D) and permits the determination of characteristic cellular responses via metabolic or transcriptional analyses dependent on the residence time of the cells along the applied gradient.

4.5.2 Application of high oscillating carbon dioxide/ bicarbonate levels

In the first instance, *C. glutamicum* WT CBS cultivations applying 'high' CO_2/HCO_3^- level oscillations, according to the methodologically described above, were performed and compared to reference fermentations under 'standard' levels in the MR and CR only. Corresponding S and X courses are exemplary illustrated in Fig. D.3 and Fig. F.3, respectively and reveal a similar (constant) exponential growth behavior for both conditions and all dimensions tested, permitting the cross comparability of the approaches later on. Detailed process parameters on the MR and CBS experiments are further provided in Tab. 4.5, corroborating the phenomenological observations by similar growth kinetics (μ = (0.40–0.43) h^{-1}), biomass yields (Y_{XS} = 0.48 g g^{-1}), and substrate uptake (q_S = (0.84–0.88) g g^{-1} h^{-1}). Selected process and circulation parameters are summarized in Fig. 4.21 and reflect the promising results of the characterization from above by demonstrating (i) the applicability of desired individual pCO_2 levels in the CBS, (ii) the accuracy of the flow characteristics, V_{CR} level control, and stability, as well as (iii) the ability to maintain constant secondary operating factors as pH, T, or p.

The determination of all CBS-specific parameters (Tab. 4.5) was accomplished from samples withdrawn from the MR. Consequently, individual mass balancing of S and X flows through the MR, CR_1, and CR_2, respectively, were performed on the basis of TC analysis presented in section 4.2 to evaluate potential compartment-specific impacts of the applied CO_2/HCO_3^- gradients (see Fig. DS.3). Recoveries were determined at both (comparative) DNA microarray analyses time points (TP 1, 2; section D.2.4): after initiation of the circulation with highest ΔpCO_2 of 75 mbar ($CR_1 \Rightarrow$ MR) and 240 mbar ($CR_2 \Rightarrow$ MR), and right before level equilibration (Δt = 10 min) between the MR and the CR_1 at 15 mbar and 170 mbar, respectively (see Fig. 4.22). Even though differential biomass formation or substrate consumption was not observed, mass balancing could successfully be demonstrated with fully matched carbon recoveries in both cases.

The full length transcriptional responses of both CRs determined in reference to the MR were obtained by simultaneous sampling at TP1 and TP2, and can be found in Tab. DS.2 to Tab. DS.6. Additionally, MR transcript levels were compared between TP2 and TP1 (Tab. DS.7). The design of the experiment enables therefore the (i) quantification of the short-term transcriptional response as a function of the residence time within each compartment, (ii) the correlation between the transcriptional response to the CO_2/HCO_3^- oscillation, i.e. the gradient intensity, and (iii) a potential

Tab. 4.5: Process parameters obtained in batch fermentations using the *C. glutamicum* WT and L-lysine producer *C. glutamicum* DM1933 under 'standard' and oscillating 'high' CO_2/HCO_3^- levels. Single reactor reference cultivations were performed in the main reactor (MR) only and were compared to the cascade bioreactor system (CBS) for initial pCO_2 levels of about 75 mbar, 150 mbar, and 315 mbar in the MR, CR_1 and CR_2, respectively. The circulation flow was set to about $\nu = 0.58\,\mathrm{L\,min^{-1}}$. Where applicable, values represent the arithmetic mean of two replicates ± total measurement range. The table was modified after Tab. D.7.

Strain	System	$\mu, \mathrm{h^{-1}}$	Y_{XS}, $\mathrm{g\,g^{-1}}$	$q_S, \mathrm{g\,g^{-1}\,h^{-1}}$	Y_{PS}, $\mathrm{g\,g^{-1}}$	Y_{PX}, $\mathrm{g\,g^{-1}}$	$q_P, \mathrm{g\,g^{-1}\,h^{-1}}$
C. glutamicum ATCC13032	MR	0.43 ± 0.00	0.48 ± 0.00	0.88 ± 0.01	—	—	—
	CBS	0.40 ± 0.01	0.47 ± 0.01	0.84 ± 0.04	—	—	—
C. glutamicum DM1933	MR	0.24	0.37	0.65	0.16	0.41	0.10
	CBS	0.22	0.35	0.63	0.15	0.42	0.09

resetting of the transcriptional state due to equalized CO_2/HCO_3^- environments (inter MR comparison).

As can be derived from the schematic overview provided in Fig. 4.22, the intensity of the transcriptional response can be linked directly to the strength of the ΔpCO_2 stimulus and the time of cellular exposure (Fig. 4.22 and Tab. DS.2). The highest number of 66 differently expressed genes was therefore found for the comparison between CR_2 and MR at TP1 ($\Delta pCO_2 = 240$ mbar), which gradually decreased to 55 genes at TP2 ($\Delta pCO_2 = 170$ mbar). Notably, the transcriptional response was observed after an average residence time of (3.55 ± 0.05) min. When considering the transcript levels of CR_1, $\bar{t}$ reduces by about 50 % together with the applied pCO_2 gradient (75 mbar at TP1 and 15 mbar at TP2), and the observable number of differently expressed genes (15 and 10), respectively. Due to the high CO_2 levels applied to the CRs, CO_2 accumulation in the MR could directly be followed after initiation of the circulation. Consequently, a similarly low number of 11 genes showing a significant mRNA fold-change were observed for the MR comparison (Fig. 4.22).

Unlike the scale-down studies of Baez et al. (2009, 2011) that applied constantly or dynamically high pCO_2 levels of up to 300 mbar to an *E. coli* GFP producer, detrimental effects on growth or increased by-product formation (acetate) were not observed in this study. In equivalence to the previous results obtained under constantly 'high' conditions (section 4.3), differential expression of general or acid stress genes were also not detected. However, by using a STR-STR scale-down device, Baez et al. (2011) had to drastically

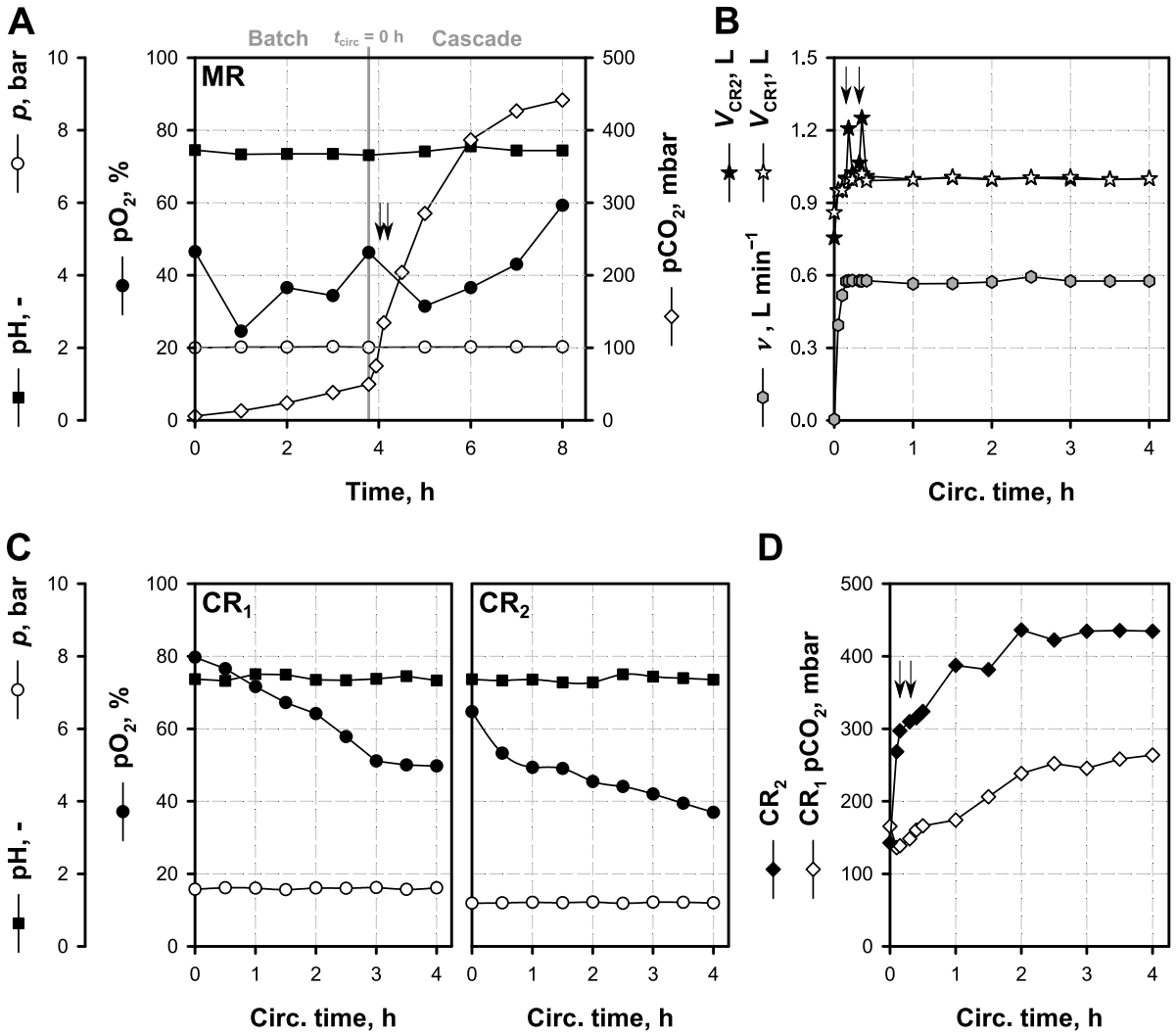

Fig. 4.21: Overview of the selected process parameters pH, total pressure (p), dissolved O_2 and CO_2 (pO_2, pCO_2), obtained from an exemplary cascade bioreactor cultivation using *C. glutamicum* WT with 1 % (w/v) glucose. **(A)** Fermentation process in the main reactor (MR) indicating the switch from batch to cascade mode (t_{circ} = 0 h) with **(B)** relevant circulation characteristics as circulation flow rate (ν) and controlled cascade reactors (CRs) volume levels (V_{CRs}). **(C/D)** Corresponding process parameters in the CRs during time of circulation are indicated. Additionally, both time points for DNA microarray analyses (TP1, 2) are illustrated (arrows). Figure was modified after Fig. D.4

increase $\bar{t}$ to more than 6 min in combination with a very high volume ratio (1.5 to 1) compared to the reference compartment to obtain this effect. The *E. coli* study and our own results therefore demonstrate the adaptive potential of the microbial strains to oscillatory CO_2/HCO_3^- conditions, which was recently confirmed by Käß et al. (2013, 2014) in *C. glutamicum* WT and *C. glutamicum* DM1933 STR-PFR fermentations under intensive pO_2 and S oscillations. Despite maximum $\bar{t}$ of up to 2.8 min in the un-aerated

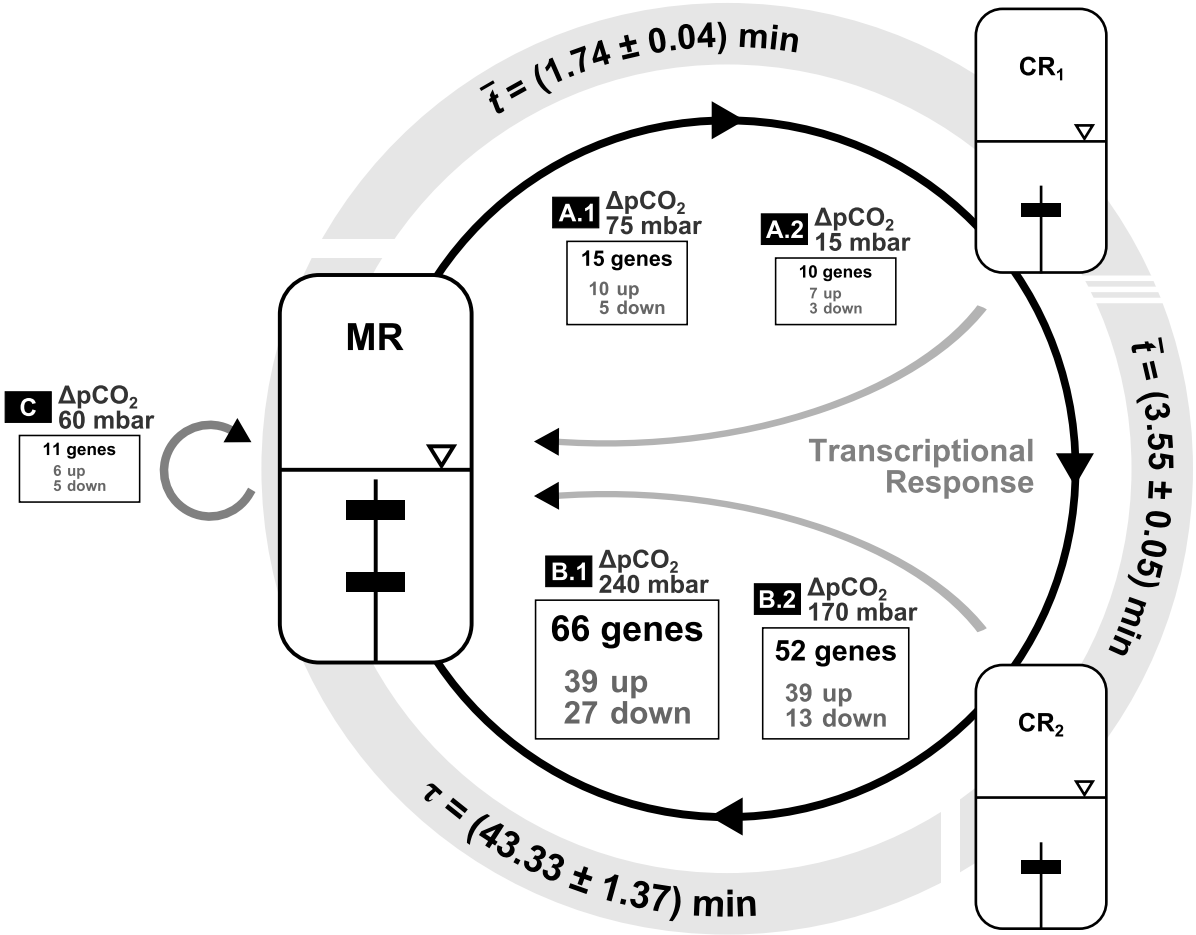

Fig. 4.22: Illustration of the transcriptional short-time response of *C. glutamicum* WT during the batch fermentation in the cascade bioreactor system as a result of the exposure to the applied CO_2/HCO_3^- gradients as described. Mean residence ($\bar{t}$) and space times (τ) are indicated for the corresponding sections of the system (see Tab. 4.3). DNA microarray analyses for cascade reactor 1 (CR_1, A) and CR_2 (B) both referenced to the main reactor (MR), were performed after (i) cascade initiation, and (ii) before pCO_2 level equilibration (MR to CR_1) given a Δt of 10 min. ΔpCO_2 gradients between MR and the individual CRs are indicated. Additionally, transcript differences were measured comparing MR samples between time points A and B (C). The figure was modified after Fig. D.5.

PFR compartment, the comprehensive analysis of the proteome, metabolome, and transcriptome did not reveal a significant impact on growth and subcelluar regulation. On the contrary, biomass formation, yield coefficients, and L-lysine secretion remained unaffected, which once again emphasizes the general robustness and insensitivity of *C. glutamicum* to environmental inhomogeneities.

Subsequent CBS cultivations of *C. glutamicum* WT under identical 'high' pCO_2 conditions were also performed with *C. glutamicum* DM1933 and complete this picture

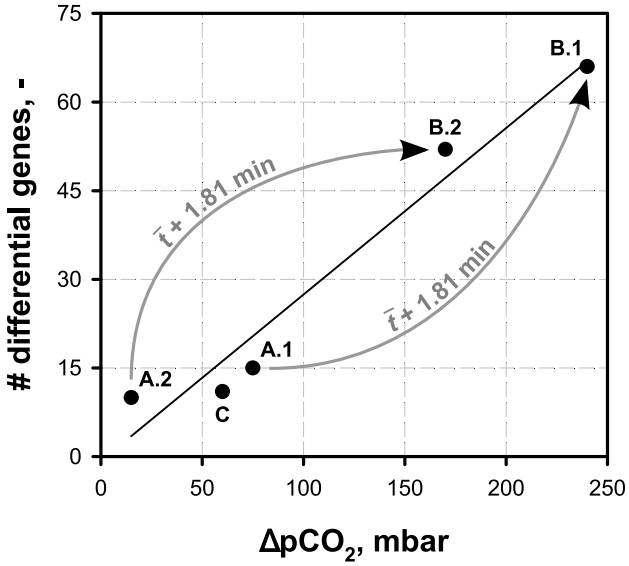

Fig. 4.23: Total number of differentially expressed genes as a function of the imposed ΔpCO_2 gradients (see also Tab. DS.3 to Tab. DS.7) in the cascade bioreactor system fermentations using *C. glutamicum* WT (Fig. 4.22). A, B, and C refer to the corresponding DNA microarray comparison groups, and time points 1 and 2 as indicated in Fig. 4.22 and summarized in Tab. DS.2. Cells flowing from CR_1 to CR_2 are subjected to an additional residence time ($\bar{t}$) of about 1.81 min, which is indicated by arrows. The proportionality of gene expression and ΔpCO_2 stimulus is further indicated by linear regressions. The figure was modified after Fig. D.6.

since growth and production kinetics were highly similar to the reference cultivation in the MR (Tab. 4.5). Interestingly, even though equal total (integral) L-lysine production rates (Q_P = (0.26–0.28) g L^{-1} h^{-1}) were calculated for both processes, higher productivities were detected in the backflow to the MR ($Q_P = (0.27 \pm 0.03)$ g L^{-1} h^{-1}) than in the MR itself ($Q_P = (0.21 \pm 0.03)$ g L^{-1} h^{-1}) within 48 min after cascade start. Considering the fact that pCO_2 levels in the MR reached maximum values not before 2 h after cascade start and that the total CBS residence time was about 47 min (Tab. 4.3), one may conclude that cells flowing back were already adapted to high pCO_2 levels while those still resting in the MR were not yet. However, more detailed studies are certainly necessary to further elucidate these findings by providing reliable statistics and data.

Taken together, the comparative transcriptional analysis of *C. glutamicum* WT under 'high' oscillating conditions revealed a fast transcriptional response already after 1.74 min in the CR_1 that was amplified about five times by doubling the applied pCO_2 level and the $\bar{t}$ of the cells (Fig. 4.22). On that account, a direct correlation of the number of differentially expressed genes with the gradient intensity and time of stimuli exposure can be identified as depicted in Fig. 4.23. A total number of 29 differentially expressed genes collectively changed (CR_2 vs. MR) at TP1 and TP2 (Fig. DS.4), with a majority of 62 % being up-regulated by an average factor of 2.14 and 1.83, respectively (further details in section D.4). Moreover, a gradual expression pattern was identified, showing a reduction of the transcript level by 15 % on average for 83 % of all collectively amplified genes with decreasing ΔpCO_2 levels from TP1 to TP2. In addition, the overall

equalization of the pCO_2 levels obviously led to a restoration of the transcriptional state in the MR as only a small amount of genes were found at TP2.

In summary, the fast and reproducible up-regulation in response to the oscillating CO_2/HCO_3^- environments observed in this study is in agreement with previous scale-down studies on spatial O_2 and S gradients using qPCR (Lara et al., 2006b; Schweder et al., 1999). Experimentally derived gene amplification numbers were compared to and in agreement with theoretical estimations on the basis of *E. coli* RNA polymerase elongation rates (Bremer & Dennis, 1996) and the average gene length of *C. glutamicum* (Fig. DS.5). This therefore suggests a quick (transcriptional) reaction to the reactor inhomogeneity faced by the cells, which can be intensified by ΔpCO_2 and $\bar{t}$ as detailed above. However, a transcriptional regulation pattern as observed under "quasi-stationary" 'high' CO_2/HCO_3^- conditions could not be detected. Thus, further studies are required to elucidate the interplay between short- and long-term response on a transcriptional level.

CHAPTER 5

CONCLUSIONS AND FUTURE PERSPECTIVES

This chapter summarizes the results that were achieved in the course of this thesis and provides conclusions under consideration of the objectives and motivation as presented before. Additionally, some perspectives are highlighted that might be of use for future and continuous work.

Fermentation studies under "quasi-stationary" conditions with varying carbon dioxide/bicarbonate levels

In the first part of this thesis, a systematic understanding of the response of *Corynebacterium glutamicum* wild-type (WT) to different CO_2/HCO_3^- levels was developed to provide the first structural and systematic analysis on the regulatory consequences for growth and transcription.

An experimental design under batch conditions was established to compare significantly de- or increased pCO_2 levels to reference conditions. While the impact of 'high' pCO_2 levels (≥300 mbar) on the detected macrokinetic parameters of *C. glutamicum* WT was solely restricted to an increased biomass-to-substrate yield by 63 % in the first half of the fermentation, stripping conditions with high volumetric gas flow rates of 3 vvm resulted in a distinct growth phenotype and successfully reduced pCO_2 profiles to maximum 40 mbar in the course of the fermentation. The biomass formation under these 'low' conditions was characterized by distinct bi-level growth curves compared to 'standard' conditions, showing a significant reduction of the (maximum) specific growth rate of 50 % within the transition phase.

The transcriptional response was analyzed for both fermentation conditions by comparative DNA microarray analysis in reference to the 'standard' process. In case of 'high' CO_2/HCO_3^- levels, the transcriptional analysis revealed the complete activation of the DtxR/RipA regulon, which controls the iron homeostasis in *C. glutamicum*, and obviously exhibits a key function under excessive CO_2/HCO_3^- levels for maintaining ordinary growth as was shown by further deletion mutant studies. However, the relation between the increased availability of CO_2/HCO_3^- and DtxR as one of the master regulators in *C. glutamicum* is currently not yet fully understood. Future studies might therefore concentrate on the molecular or regulatory interlink to unravel the interplay between the environmental stimuli and transcriptional patterns. The fact that detrimental consequences as reduced yields or by-product formation on the culture performance were not observed emphasizes the general robustness of the microorganism towards high pCO_2 levels, which, hypothetically, hints at undisturbed applicability in industrial large scale applications. To elucidate this hypothesis, future studies using the e.g. L-lysine producer *C. glutamicum* DM1933 might be useful.

A comprehensive regulatory response was observed, which coincided with the transition phase of the observable growth phenotype in case of 'low' CO_2/HCO_3^- application. The combination of the results from the DNA microarrays, enzyme kinetics, and metabolic analysis, hint at a potential strategy to counteract the lack of sufficient CO_2/HCO_3^- levels by triggering thiamin pyrophosphate (TPP)-depended, decarboxylating reactions. In this regard, the observable transcriptional activation of the TPP biosynthesis genes might be linked to enhanced pentose phosphate pathway flux for precursor supply, which is indicated by increased enzyme activities of glucose-6-phosphate dehydrogenase and 6-phosphogluconate dehydrogenase. In turn, the regeneration of the resulting reducing equivalents $NADP^+$ might be reflected by the L-alanine and L-valine secretion during that phase. Coping with reduced CO_2/HCO_3^- supply obviously poses a great challenge for *C. glutamicum* WT, which, most likely, would be even more pronounced for e.g. L-lysine producer strains requiring high anaplerotic fluxes. Therefore, it would be of great interest to evaluate the question whether a critical pCO_2 level exists that distinguishes between standard-like or impaired growth. A possible strategy might thus focus on the application of continuous cultures to perform stability analyses under gradually decreasing pCO_2 levels. This might potentially lead to the identification of a lower pCO_2 level boundary that can be considered for the design of production processes and strategies. Further investigations on the regulatory aspects of the transcriptional

activation of the thiamin/TPP biosynthesis in the context of 'low' CO_2/HCO_3^- would be highly interesting.

To evaluate the relevance of the PEP–pyruvate–oxaloacetate node as key factor for the adaption potential of *C. glutamicum* to environmental changes of varying CO_2/HCO_3^- levels, pCO_2 fermentations equivalent to the WT were performed by using selected single deletion mutants of anaplerotic reactions. The obtained results corroborate previous literature reports on the importance of pyruvate carboxylase for ordinary growth. Besides, all strains exhibited a significantly reduced (maximum) growth rate compared to the WT, independent of the process strategy. However, further insights into the complex interplay of anaplerotic and gluconeogenic reactions, or the identification of regulatory changes under different CO_2/HCO_3^- were not obtained, which suggests the analysis of multi-deletion mutants for further clarification of these dependencies.

It could further be demonstrated during the CO_2/HCO_3^--specific experiments that significant amounts of CO_2 dissolve in the culture medium, which interferes with the accurate balancing of C-recoveries. At physiological pH, most dissolved CO_2 further reacts to bicarbonate, which then remains in the liquid phase without leaving the bioreactor via the exhaust gas. To circumvent mostly exhaust gas-based detection limitations, a total carbon (TC)-based balancing approach (including all carbon species in the liquid phase) was successfully established and demonstrated to significantly improve the carbon closure of fermentations, leading to fully matched recoveries. In addition, it was highlighted that the determination of the carbon content in the biomass, in combination with total inorganic carbon quantification, is indispensable for process interpretation and analysis, successfully preventing the false-negative underestimation of the total balance. Moreover, it could be shown that the concept of TC-based balancing provides the ability to identify the source of missing carbon gaps, which was finally applied to and exemplified for an L-lysine production process.

Development and characterization of a novel scale-down bioreactor system

The second part of this thesis dealt with the development, implementation, and characterization of a novel three-compartment scale-down bioreactor to abstract inhomogeneous, large scale conditions via the application of oscillating CO_2/HCO_3^- gradients. Therefore, different pCO_2 conditions were applied to each individual compartment, which represent

specific volume elements or bioreactor regions at large scale to model a hypothetical cellular flow path through the heterogeneous environment.

The cascade bioreactor system (CBS) was designed as a series of three fully equipped stirred tank reactors (STR) consisting of the 100 L scale main reactor (MR) and two 1 L cascade reactors (CR), facilitating total recirculation by the interplay of an applied pressure gradient between the STRs and a diaphragm metering pump for the back-transport. Notably, all three STRs can be operated and controlled independently from each other, which enables the application of defined gradients while maintaining all other process factors constant. Regulation, control, and working routines that are required for the defined adjustment of the flow rate and therefore of the residence times within the system were successfully implemented into the process control system (LabVIEW®).

After final installation of the setup, evaluation experiments were performed to determine the operational range of the CBS and demonstrated the accuracy and stability of critical performance parameters (e.g. flow rate and level control) under fermentation conditions. This was followed by the technical characterization of the system by using tracer experiments to assess the mixing efficiencies of the individual STRs and determine the flow pattern by residence time distributions (RTD). The latter is required for the application of defined CO_2/HCO_3^- gradients to adjust the time of exposure of the cells to the mixing and flow conditions of large scale environments. The process setup of the CBS is flexible and can be adjusted to the experimental requirements with a broad circulation flow range between (0.58–3.95) L min^{-1}. Due to the dimensions of the system, a maximum volumetric proportion of the complete cascade section (CS; $CR_1 \Rightarrow CR_2$) to the MR of 8.4 % can be obtained with mean residence times in the CS of up to 3.55 min. The comparison to the theoretical space times showed a high level of congruence in all cases and further RTD analysis including the fitting to a multi-compartment model (tank-in-series) revealed that the CBS is characterized by 1.5 ideal tanks. In comparison to the theoretical estimation from the volumetric contribution of the CS to CBS, a 25 % increased hydrodynamic impact of the system was determined that emphasizes the applicability of the system for scale-down studies.

Subsequently, RTDs were successfully simulated by using transfer functions in the Laplace domain to counteract the experimental limitation to distinguish individual response curves while operated in total recycle. Application of the analytical functions retrieved the individual output functions, deducing the overall system response by superimposition of all signals. The latter was finally compared to experimental mixing time studies in the CBS with total circulation. This revealed a high congruence level of

the data sets with a low mean average percentage error of 3 %, which demonstrates the hydrodynamic understanding of the system obtained by the technical characterization. Depending on the applied flow rate between (0.58–3.95) L min^{-1}, relaxation times in the range of (1.17–8.00) min were obtained before reaching the new homogeneous state after perturbation. In future studies, these information are required for the normalization of the labeling distribution after pulse injection, if sampling occurs prior to reaching a new "steady-state".

Final application of the scale-down bioreactor system to imitate oscillating carbon dioxide/bicarbonate conditions

The objective of the third part of this thesis was to bridge the results obtained from the initial CO_2/HCO_3^--related cultivations under "quasi-stationary" conditions with the information of the technical characterization of the CBS to provide a more realistic representation of large scale condition under defined pCO_2 oscillations and residence times.

Initially, test cultivations were carried out that validated the CBS stability in regard to continuous regulation and control under fermentation conditions with high system dynamics such as biomass and foam formation. Regardless of the applied process conditions, the overall CBS performance of the flow and level control was satisfactory showing only minor mean average percentage errors of 3 % and 1 %, respectively. Combining high CO_2 fractions in the inlet gas flow in one CR and high stripping rates in the other resulted in considerable ΔpCO_2 of 260 mbar within a mean residence time of 1.81 min and demonstrated a high degree of adjustable CO_2 gradients within the system. In a further experiment, high stripping conditions were applied to both CRs to refer to the results of the 'low' CO_2/HCO_3^- experiments reported under "quasi-stationary" conditions. Notably, while the CS section has a volumetric portion on the CBS of merely 8.4 % and the MR-specific residence time accounted for about 92 % of the total process period, the CO_2 removal from the medium was obviously sufficient to lead to the previously obtained bi-level growth phenotype. However, the experiment was characterized by intensive foaming, which led to the addition of quite large amounts of antifoam. Nevertheless, further validation experiments are required to counteract the antifoam addition and elucidate the growth defect. In this context, further comparative DNA microarray experiments would offer a novel opportunity to directly compare the

transcriptional responses under dynamic and "quasi-stationary" conditions, which might improve the understanding of the stress regulation.

Throughout this thesis, it was discussed that quantitative data or mathematical models on CO_2/HCO_3^- profiles in large scale bioreactor are lacking in the literature. Therefore, the experimental design for the application of 'high' CO_2/HCO_3^- oscillations considered an initial pCO_2 of 75 mbar, 150 mbar, and 315 mbar (MR, CR_1, and CR_2) that based on the estimation performed under "quasi-stationary" conditions and similar studies in the literature. pCO_2 oscillations in fermentations of *C. glutamicum* WT with a mean residence time of 3.55 min did not impair the process performance (no by-product formation), resulting in overall similar growth and substrate kinetics as obtained in reference MR experiments. This observation was further confirmed by substrate and biomass (mass) balancing of the individual compartments and revealed a high robustness of *C. glutamicum* not only to constantly 'high' but also dynamic CO_2/HCO_3^- levels. Comparative transcriptional analyses were performed at two time points (TP), relating both CRs to the MR: first, after initiation of the circulation process (highest ΔpCO_2 up to 240 mbar) and finally before pCO_2 equalization due to ongoing mixing of the CBS via total circulation (lowest ΔpCO_2 with 10 mbar). Similar to the results obtained previously, no general or acid stress gene expression was observed. Even though a comprehensive regulatory effect was not observed, the analyses revealed a short time transcriptional response, whose intensity can be directly correlated to (i) the strength of the ΔpCO_2 stimulus and (ii) the time of the cellular exposure. Therefore, the highest number of differently expressed genes (66) was observed after about 3.55 min for CR_2 vs. MR (TP1), which significantly decreased about six-fold for CR_1 vs. MR (TP2) with the mean residence time being reduced by 50 %. In addition, a gradual expression pattern was observed for the amplified genes decreasing from TP1 to TP2, finally leading to a clear restoration of the transcriptional state as revealed by the comparison of the state of the MR at both TP (TP2 vs. TP1).

The obtained amplification rates were compared and in agreement to theoretical estimations on the basis of polymerase elongation rates and in its extent similar to previous scale-down studies. The results thereby suggest a quick transcriptional response of the cells in reaction to the applied, oscillatory CO_2/HCO_3^- stimulus. With regard to a potential biologically-motivated scale-up criterion, one might deduce that mixing times at industrial scale higher than 1.8 min should be avoided to prevent a first transcriptional response of the cells. However, as the literature shows, this would be a challenging task for vessels sizes beyond (100–300) m^3. To further address this question, an additional

CBS cultivation under identical conditions was carried out with the L-lysine producer *C. glutamicum* DM1933. Similar to the WT studies, growth was not impaired and the overall productivity was equivalent to the productivity in the reference conditions; a first indication even hints at a stimulating effect of pCO_2 oscillations on the L-lysine formation. Even though further studies are necessary to corroborate the results with transcriptional analyses potentially leading to a deeper understanding, these preliminary experiments indicate that the 'high' pCO_2 oscillations not necessarily interfere with the process performance despite showing a responsive effect on the transcriptional level.

The general concept of this thesis is embedded in the multifaceted efforts to improve the understanding of (microbial) biotechnological processes in bioreactors. Therefore it focused on research aspects that derive from the classical interface of scale-up and scale-down questions that intends to provide tools and information to support the rational improvement and development of industrial processes.

The established CBS provides therefore a suitable platform for future scale-down studies not only limited to *C. glutamicum* and pCO_2 gradients, but also for all platform organisms or model strains and a broad range of inhomogeneity factors, especially dissolved gases. While the presented results on the application of 'high' oscillatory CO_2/HCO_3^- gradients clearly demonstrate the robustness of *C. glutamicum*, it would be highly interesting to determine critical pCO_2 gradients (upper pCO_2 boundary) in future analyses.

Even though the lack of suitable and extensive data on industrial bioreactors and their quantitative description is critically remarked in the public, it remains unlikely that such information will be available for the broad scientific community in the future. The acquisition of more in-depth information will depend, most presumably, on the development of powerful computational models and methods. Until then, experimental scale-down studies will continue to focus on the identification of distinct regulatory patterns, potential stress responses, and mechanisms of action to improve the fundamental understanding of the interaction between cell kinetics and large scaled-derived stimuli.

From a practical point of view, a higher degree of large scale abstraction might be achieved by implementing stochastic flow patterns into extended, multi-compartment scale-down devices[1]. Also, the superimposition of all relevant, process influencing gradients would contribute to a more accurate model of actual process environments. However, as a drawback, such applications would make the identification of regulatory

[1]Derived from contributions of Henk Noorman and Matthias Reuss at the international 3rd BioProScale Symposium 2014, Berlin, Germany.

responses and patterns in reaction to distinct stimuli significantly more complex. Here, the interest of fundamental and corporate research diverges at some point during the analyses and investigations.

The CBS offers, next to classical scale-up and scale-down motivated applications as discussed above, further opportunities to focus on the emerging research field of population heterogeneities. Future studies could therefore investigate if the application of CO_2/HCO_3^- gradients that might function as stress factors cause or stimulate the formation of sub-populations. These experiments would then link environmental to cellular inhomogeneities, which would be a further important step to capture (all relevant) influencing factors that determine the total (large scale) bioreactor performance.

CHAPTER 6
AUTHOR CONTRIBUTION

This chapter summarizes my (Jens Buchholz) contribution to the manuscripts that were either already published or at least submitted to international peer reviewed journals. The contents of the manuscripts I–IV are supplementary provided (appendix A–D).

Manuscript I

Buchholz, J, Schwentner, A, Brunnenkan, B, Gabris, C, Grimm, S, Gerstmeir, R, Takors, R, Eikmanns, BJ & Blombach, B (2013). Platform engineering of *C. glutamicum* with reduced pyruvate dehydrogenase complex activity for improved production of L-valine, and 2-ketoisovalerate. *Appl. Environ. Microbiol.* 79(18), 5566–5575.

Jens Buchholz (J.B.) performed the fed-batch fermentation experiments for 2-ketoisovalerate and L-valine production, participated in the data analysis, and carried out the corresponding product analytics.

Manuscript II

Blombach[#], B, **Buchholz[#], J**, Busche, T, Kalinowski, J & Takors, R (2013). Impact of different CO_2/HCO_3^- levels on metabolism and regulation in *Corynebacterium glutamicum*. *J. Biotechnol.* 168, 331–340.

#Both authors contributed equally to this work.

J.B. designed and performed all experiments in this work except for (i) the transcriptional analysis (DNA microarray processing and statistics), (ii) the determination of enzyme activities, and (iii) the *C. glutamicum* mutant construction. J.B. further participated in data analysis, data interpretation, and in the preparation of the manuscript.

Manuscript III

Buchholz, J, Graf, M, Blombach, B & Takors, R (2014). Improving the carbon balance of fermentations by total carbon analyses. *Biochem. Eng. J.*, DOI: 10.1016/j.bej.2014.06.007 — accepted.

J.B. designed and performed all experiments in this work, participated in data analysis, data interpretation, and in the preparation of the manuscript.

Manuscript IV

Buchholz, J, Graf, M, Freund, A, Busche, T, Kalinowski, J, Blombach, B & Takors, R (2014). CO_2/HCO_3^- perturbations imposed by simulated large-scale gradients in a novel scale-down device cause fast transcriptional responses in *Corynebacterium glutamicum*. — Manuscript submitted.

J.B. designed and performed all experiments in this work except for the transcriptional analysis (DNA microarray processing and statistics). J.B. further participated in data analysis, data interpretation, and in the preparation of the manuscript.

REFERENCES

Aboka, F (2008). *Short term step responses of central carbon and storage metabolism in* Saccharomyces cerevisiae*: Novel minibioreactors and ^{13}C studies*. PhD thesis, Technical University of Delft (cit. on p. 23).

Aboka, FO, H Yang, LP de Jonge, R Kerste, WA van Winden, WM van Gulik, R Hoogendijk, A Oudshoorn & JJ Heijnen (2006). Characterization of an experimental miniature bioreactor for cellular perturbation studies. *Biotechnol. Bioeng.* 95(6), 1032–1042 (cit. on p. 23).

Aguilera, J, T Petit, JH de Winde & JT Pronk (2005). Physiological and genome-wide transcriptional responses of *Saccharomyces cerevisiae* to high carbon dioxide concentrations. *FEMS Yeast Res.* 5(6-7), 579–593 (cit. on pp. 5, 7, 30, 158).

Aich, S, F Imabayashi & LT Delbaere (2003). Expression, purification, and characterization of a bacterial GTP-dependent PEP carboxykinase. *Protein Expression Purif.* 31(2), 298–304 (cit. on pp. 160, 176).

Ajinomoto Co., I (2013). Food products and feed-use amino acid business, URL lastly retrieved 05 May, 2014. URL: `www.ajinomoto.com/en/ir/pdf/FY13Q1_data_E.pdf` (cit. on p. 13).

Amanullah, A, CM McFarlane, AN Emery & AW Nienow (2001). Scale-down model to simulate spatial pH variations in large-scale bioreactors. *Biotechnol. Bioeng.* 73(5), 390–399 (cit. on pp. 5, 10, 18, 212).

Amoabediny, G & J Büchs (2010). Determination of CO_2 sensitivity of micro-organisms in shaken bioreactors. I. Novel method based on the resistance of sterile closure. *Biotechnol. Appl. Biochem.* 57(4), 157–166 (cit. on pp. 7, 30, 158, 212).

Amoabediny, G, MPH Abbas & J Büchs (2010). Determination of CO_2 sensitivity of micro-organisms in shaken bioreactors. II. Novel online monitoring method. *Biotechnol. Appl. Biochem.* 57(4), 167–175 (cit. on pp. 7, 30, 158, 212).

An, SJ, SS Yim & KJ Jeong (2013). Development of a secretion system for the production of heterologous proteins in *Corynebacterium glutamicum* using the Porin B signal peptide. *Protein Expr. Purif.* 89(2), 251–257 (cit. on p. 136).

Aoki, R, M Wada, N Takesue, K Tanaka & A Yokota (2005). Enhanced glutamic acid production by a H^+-ATPase-defective mutant of *Corynebacterium glutamicum*. *Biosci., Biotechnol., Biochem.* 69(8), 1466–1472 (cit. on p. 152).

Baez, A, N Flores, F Bolívar & OT Ramírez (2009). Metabolic and transcriptional response of recombinant *Escherichia coli* to elevated dissolved carbon dioxide concentrations. *Biotechnol. Bioeng.* 104(1), 102–110 (cit. on pp. 5, 7, 30, 31, 63, 67, 89, 91, 158, 170, 212, 224).

Baez, A, N Flores, F Bolívar & OT Ramírez (2011). Simulation of dissolved CO_2 gradients in a scale-down system: A metabolic and transcriptional study of recombinant *Escherichia coli*. *Biotechnol. J.* 6(8), 959–967 (cit. on pp. 7, 11, 30, 31, 89, 91, 158, 212, 224).

Ballestra, P, AA Da Silva & JL Cuq (1996). Inactivation of *Escherichia coli* by carbon dioxide under pressure. *J. Food Sci.* 61(4), 829–831 (cit. on pp. 30, 158).

Bartek, T, P Makus, B Klein, S Lang & M Oldiges (2008). Influence of L-isoleucine and pantothenate auxotrophy for L-valine formation in *Corynebacterium glutamicum* revisited by metabolome analyses. *Bioprocess. Biosyst. Eng.* 31(3), 217–225 (cit. on pp. 51, 136).

Bates, RL, PL Fondy & RR Corpstein (1963). Examination of some geometric parameters of impeller power. *Ind. Eng. Chem. Process Des. Dev.* 2(4), 310–314 (cit. on pp. 45, 216).

Bäumchen, C, A Knoll, B Husemann, J Seletzky, B Maier, C Dietrich, G Amoabediny & J Büchs (2007). Effect of elevated dissolved carbon dioxide concentrations on growth of *Corynebacterium glutamicum* on D-glucose and L-lactate. *J. Biotechnol.* 128(4), 868–874 (cit. on pp. 5, 7, 30, 62, 63, 158, 168, 170).

Becker, J & C Wittmann (2012). Bio-based production of chemicals, materials and fuels – *Corynebacterium glutamicum* as versatile cell factory. *Curr. Opin. Biotechnol.* 23(4), 631–640 (cit. on p. 14).

Becker, J, C Klopprogge, O Zelder, E Heinzle & C Wittmann (2005). Amplified expression of fructose 1,6-bisphosphatase in *Corynebacterium glutamicum* increases in vivo flux through the pentose phosphate pathway and lysine production on different carbon sources. *Appl. Environ. Microbiol.* 71(12), 8587–8596 (cit. on pp. 14, 51, 138).

Becker, J, C Klopprogge, A Herold, O Zelder, CJ Bolten & C Wittmann (2007). Metabolic flux engineering of L-lysine production in *Corynebacterium glutamicum*—Over expression and modification of G6P dehydrogenase. *J. Biotechnol.* 132(2), 99–109 (cit. on pp. 14, 51, 138).

Becker, J, O Zelder, S Häfner, H Schröder & C Wittmann (2011). From zero to hero—Design-based systems metabolic engineering of *Corynebacterium glutamicum* for L-lysine production. *Metab. Eng.* 13(2), 159–168 (cit. on pp. 14, 51, 138).

Becker, J, R Schäfer, M Kohlstedt, BJ Harder, NS Borchert, N Stöveken, E Bremer & C Wittmann (2013). Systems metabolic engineering of *Corynebacterium glutamicum* for production of the chemical chaperone ectoine. *Microb. Cell Fact.* 12, 110 (cit. on p. 14).

Betts, JI & F Baganz (2006). Miniature bioreactors: Current practices and future opportunities. *Microb. Cell Fact.* 5, 21 (cit. on p. 17).

Blankschien, MD, JM Clomburg & R Gonzalez (2010). Metabolic engineering of *Escherichia coli* for the production of succinate from glycerol. *Metab. Eng.* 12(5), 409–419 (cit. on p. 208).

Bloemen, H, L Wu, W Van Gulik, J Heijnen & M Verhaegen (2003). Reconstruction of the O_2 uptake rate and CO_2 evolution rate on a time scale of seconds. *AIChE J.* 49(7), 1895–1908 (cit. on pp. 56, 197).

Blombach, B & GM Seibold (2010). Carbohydrate metabolism in *Corynebacterium glutamicum* and applications for the metabolic engineering of L-lysine production strains. *Appl. Microbiol. Biotechnol.* 86(5), 1313–22 (cit. on p. 154).

Blombach, B, ME Schreiner, M Moch, M Oldiges & BJ Eikmanns (2007a). Effect of pyruvate dehydrogenase complex deficiency on L-lysine production with *Corynebacterium glutamicum*. *Appl. Microbiol. Biotechnol.* 76(3), 615–23 (cit. on pp. 52, 137, 152, 154, 155).

Blombach, B, ME Schreiner, J Holatko, T Bartek, M Oldiges & BJ Eikmanns (2007b). L-Valine production with pyruvate dehydrogenase complex-deficient *Corynebacterium glutamicum*. *Appl. Environ. Microbiol.* 73(7), 2079–84 (cit. on pp. 136, 152).

Blombach, B, J Buchholz, T Busche, J Kalinowski & R Takors (2013). Impact of different CO_2/HCO_3^- levels on metabolism and regulation in *Corynebacterium glutamicum*. *J. Biotechnol.* 168, 331–340 (cit. on pp. 33, 199, 204, 213–215).

Blombach, B & BJ Eikmanns (2011). Current knowledge on isobutanol production with *Escherichia coli*, *Bacillus subtilis* and *Corynebacterium glutamicum*. *Bioeng. Bugs*, 2(6), 346–350 (cit. on p. 13).

Blombach, B, ME Schreiner, T Bartek, M Oldiges & BJ Eikmanns (2008). *C. glutamicum* tailored for high-yield L-valine production. *Appl. Microbiol. Biotechnol.* 79(3), 471–479 (cit. on pp. 52, 54, 137, 151–153, 174).

Blombach, B, S Hans, B Bathe & BJ Eikmanns (2009a). Acetohydroxyacid synthase, a novel target for improvement of L-lysine production by *Corynebacterium glutamicum*. *Appl. Environ. Microbiol.* 75(2), 419–427 (cit. on pp. 33, 139, 198, 213).

Blombach, B, A Cramer, BJ Eikmanns & M Schreiner (2009b). RamB is an activator of the pyruvate dehydrogenase complex subunit E1p gene in *Corynebacterium glutamicum*. *J. Mol. Microbiol. Biotechnol.* 16(3-4), 236–239 (cit. on pp. 52, 153).

Blombach, B, A Arndt, M Auchter & BJ Eikmanns (2009c). L-Valine production during growth of pyruvate dehydrogenase complex-deficient *Corynebacterium glutamicum* in the presence of ethanol or by inactivation of the transcriptional regulator SugR. *Appl. Environ. Microbiol.* 75(4), 1197–1200 (cit. on pp. 52, 136, 138, 152).

Blombach, B, T Riester, S Wieschalka, C Ziert, JW Youn, VF Wendisch & BJ Eikmanns (2011). *Corynebacterium glutamicum* tailored for efficient isobutanol production. *Appl. Environ. Microbiol.* 77(10), 3300–3310 (cit. on pp. 13, 52, 136, 137, 152, 174).

Bothun, GD, BL Knutson, JA Berberich, HJ Strobel & SE Nokes (2004). Metabolic selectivity and growth of *Clostridium thermocellum* in continuous culture under elevated hydrostatic pressure. *Appl. Microbiol. Biotechnol.* 65(2), 149–157 (cit. on pp. 6, 30, 158).

Bott, M (2007). Offering surprises: TCA cycle regulation in *Corynebacterium glutamicum*. *Trends Microbiol.* 15(9), 417–425 (cit. on p. 14).

Bremer, H & PP Dennis (1996). *Escherichia coli* and *Salmonella*: Cellular and Molecular Biology. In: ed. by **Neidhardt, FC**. Washington, DC: ASM Press.

Chap. Modulation of chemical composition and other parameters of the cell by growth rate. 1553–1569 (cit. on pp. 95, 226).

Brognaux, A, S Han, S Sorensen, F Lebeau, P Thonart & F Delvigne (2013). A low-cost, multiplexable, automated flow cytometry procedure for the characterization of microbial stress dynamics in bioreactors. *Microb. Cell Fact.* 12(1), 100 (cit. on p. 24).

Brown, DAR, PN Jones, JC Middleton, G Papadopoulos & EB Arik (2004). Handbook of Industrial Mixing: Science and Practice. In: ed. by **Paul EL Atiemo-Obeng VA, KS**. New Jersey: Joh. Chap. Experimental Methods, 145–256 (cit. on pp. 42, 216).

Brune, I, H Werner, A Hüser, J Kalinowski, A Pühler & A Tauch (2006). The DtxR protein acting as dual transcriptional regulator directs a global regulatory network involved in iron metabolism of *Corynebacterium glutamicum*. *BMC Genomics*, 7(1), 21 (cit. on pp. 33, 67, 159, 166, 170).

Buchholz, J, A Schwentner, B Brunnenkan, C Gabris, S Grimm, R Gerstmeir, R Takors, BJ Eikmanns & B Blombach (2013). Platform engineering of *Corynebacterium glutamicum* with reduced pyruvate dehydrogenase complex activity for improved production of L-lysine, L-valine, and 2-ketoisovalerate. *Appl. Environ. Microbiol.* 79(18), 5566–5575 (cit. on pp. 33, 160, 174, 175).

Burkovski, A (2008). *Corynebacteria: Genomics and Molecular Biology*. Norfolk, UK: Caister Academic Press (cit. on pp. 14, 51).

Buziol, S, I Bashir, A Baumeister, W Claassen, N Noisommit-Rizzi, W Mailinger & M Reuss (2002). New bioreactor-coupled rapid stopped-flow sampling technique for measurements of metabolite dynamics on a subsecond time scale. *Biotechnol. Bioeng.* 80(6), 632–636 (cit. on p. 23).

Bylund, F, E Collet, SO Enfors & G Larsson (1998). Substrate gradient formation in the large-scale bioreactor lowers cell yield and increases by-product formation. *Bioprocess. Biosyst. Eng.* 18(3), 171–180 (cit. on pp. 8, 18, 20, 212).

Bylund, F, F Guillard, SO Enfors, C Trägårdh & G Larsson (1999). Scale down of recombinant protein production: A comparative study of scaling performance. *Bioprocess. Biosyst. Eng.* 20(5), 377–389 (cit. on p. 20).

Bylund, F, A Castan, R Mikkola, A Veide & G Larsson (2000). Influence of scale-up on the quality of recombinant human growth hormone. *Biotechnol. Bioeng.* 69(2), 119–128 (cit. on p. 21).

Carroll, JJ, JD Slupsky & AE Mather (1991). The solubility of carbon dioxide in water at low pressure. *J. Phys. Chem. Ref. Data*, 20(6), 1201–1209 (cit. on pp. 29, 196).

Caspeta, L, N Flores, NO Pérez, F Bolívar & OT Ramírez (2009). The effect of heating rate on *Escherichia coli* metabolism, physiological stress, transcriptional response, and production of temperature-induced recombinant protein: A scale-down study. *Biotechnol. Bioeng.* 102(2), 468–482 (cit. on p. 18).

Castan, A, A Näsman & SO Enfors (2002). Oxygen enriched air supply in *Escherichia coli* processes: Production of biomass and recombinant human growth hormone. *Enzyme Microb. Technol.* 30(7), 847–854 (cit. on pp. 7, 30, 158, 212).

Chamsartra, S, C Hewitt & A Nienow (2005). The impact of fluid mechanical stress on *Corynebacterium glutamicum* during continuous cultivation in an agitated bioreactor. *Biotechnol. Lett.* 27(10), 693–700 (cit. on p. 28).

de Kok, A, AF Hengeveld, A Martin & AH Westphal (1998). The pyruvate dehydrogenase multi-enzyme complex from Gram-negative bacteria. *Biochim. Biophys. Acta*, 1385(2), 353–366 (cit. on p. 152).

De Jonge, LP, NAA Buijs, A ten Pierick, A Deshmukh, Z Zhao, JAKW Kiel, JJ Heijnen & WM van Gulik (2011). Scale-down of penicillin production in *Penicillium chrysogenum*. *Biotechnol. J.* 6(8), 944–958 (cit. on pp. 22, 23).

Delvigne, F, J Destain & P Thonart (2006). A methodology for the design of scale-down bioreactors by the use of mixing and circulation stochastic models. *Biochem. Eng. J.* 28(3), 256–268 (cit. on p. 20).

Delvigne, F & P Goffin (2014). Microbial heterogeneity affects bioprocess robustness: Dynamic single-cell analysis contributes to understanding of microbial populations. *Biotechnol. J.* 9(1), 61–72 (cit. on p. 24).

Delvigne, F, M Boxus, S Ingels & P Thonart (2009). Bioreactor mixing efficiency modulates the activity of a prpoS::GFP reporter gene in *E. coli*. *Microb. Cell Fact.* 8, 15 (cit. on pp. 10, 24, 212).

Delvigne, F, S Ingels & P Thonart (2010). Evaluation of a set of *E. coli* reporter strains as physiological tracer for estimating bioreactor hydrodynamic efficiency. *Process Biochem.* 45(11), 1769–1778 (cit. on pp. 10, 24, 212).

Delvigne, F, A Brognaux, F Francis, JC Twizere, N Gorret, SJ Sorensen & P Thonart (2011). Green fluorescent protein (GFP) leakage from microbial

biosensors provides useful information for the evaluation of the scale-down effect. *Biotechnol. J.* 6(8), 968–978 (cit. on pp. 10, 24, 212).

Dixon, NM & DB Kell (1989). The inhibition by CO_2 of the growth and metabolism of micro-organisms. *J. Appl. Microbiol.* 67(2), 109–136 (cit. on pp. 7, 30, 158).

Dondrup, M, SP Albaum, T Griebel, K Henckel, S Jünemann, T Kahlke, CK Kleindt, H Küster, B Linke, D Mertens, V Mittard-Runte, H Neuweger, KJ Runte, A Tauch, F Tille, A Pühler & A Goesmann (2009). EMMA 2 – A MAGE-compliant system for the collaborative analysis and integration of microarray data. eng. *BMC Bioinf.* 10, 50 (cit. on p. 160).

Dower, WJ, JF Miller & CW Ragsdale (1988). High efficiency transformation of *E. coli* by high voltage electroporation. *Nucleic Acids Res.* 16(13), 6127–6145 (cit. on p. 141).

Du, Q, H Wang & J Xie (2011). Thiamin (vitamin B1) biosynthesis and regulation: A rich source of antimicrobial drug targets? *Int. J. Biol. Sci.* 7(1), 41–52 (cit. on p. 169).

Eggeling, L & O Reyes (2005). Experiments. In: *Handbook of Corynebacterium glutamicum*. Ed. by **Eggeling, L & Bott, M**. Boca Raton: CRC Press (cit. on pp. 13, 14, 51).

Eikmanns, BJ (2005). Handbook of *Corynebacterium glutamicum*. In: *Handbook of* Corynebacterium glutamicum. Ed. by **Eggeling, L & Bott, M**. Boca Raton: CRC Press. Chap. Central metabolism: Tricarboxylic acid cycle and anaplerotic reactions. 243–278 (cit. on p. 14).

Eikmanns, BJ, M Metzger, D Reinscheid, M Kircher & H Sahm (1991). Amplification of three threonine biosynthesis genes in *Corynebacterium glutamicum* and its influence on carbon flux in different strains. *Appl. Microbiol. Biotechnol.* 34(5), 617–622 (cit. on pp. 141, 159, 173, 198, 227).

Eikmanns, BJ, N Thum-Schmitz, L Eggeling, KU Lüdtke & H Sahm (1994). Nucleotide sequence, expression and transcriptional analysis of the *C. glutamicum gltA* gene encoding citrate synthase. *Microbiology*, 140, 1817–1828 (cit. on pp. 140, 174).

Eikmanns, BJ, D Rittmann & H Sahm (1995). Cloning, sequence analysis, expression, and inactivation of the *Corynebacterium glutamicum icd* gene encoding isocitrate dehydrogenase and biochemical characterization of the enzyme. *J. Bacteriol.* 177(3), 774–782 (cit. on pp. 160, 176).

Eikmanns, BJ & B Blombach (2014). The pyruvate dehydrogenase complex of *Corynebacterium glutamicum*: An attractive target for metabolic engineering. *J. Biotechnol.* —in press. (cit. on pp. 15, 55).

El-Sabbagh, N, B McNeil & LM Harvey (2006). Dissolved carbon dioxide effects on growth, nutrient consumption, penicillin synthesis and morphology in batch cultures of *Penicillium chrysogenum*. *Enzyme Microb. Technol.* 39(2), 185–190 (cit. on pp. 5, 7, 30, 158, 212).

El-Sabbagh, N, LM Harvey & B McNeil (2008). Effects of dissolved carbon dioxide on growth, nutrient consumption, cephalosporin C synthesis and morphology of *Acremonium chrysogenum* in batch cultures. *Enzyme Microb. Technol.* 42(4), 315–324 (cit. on pp. 7, 30, 158, 213).

Elisáková, V, M Pátek, J Holátko, J Nesvera, D Leyval, JL Goergen & S Delaunay (2005). Feedback-resistant acetohydroxy acid synthase increases valine production in *Corynebacterium glutamicum*. *Appl. Environ. Microbiol.* 71(1), 207–213 (cit. on p. 152).

Enfors, SO, M Jahic, A Rozkov, B Xu, M Hecker, B Jurgen, E Kruger, T Schweder, G Hamer, D O'Beirne, N Noisommit-Rizzi, M Reuss, L Boone, C Hewitt, C McFarlane, A Nienow, T Kovacs, C Tragardh, L Fuchs, J Revstedt, PC Friberg, B Hjertager, G Blomsten, H Skogman, S Hjort, F Hoeks, HY Lin, P Neubauer, R van der Lans, K Luyben, P Vrabel & A Manelius (2001). Physiological responses to mixing in large scale bioreactors. *J. Biotechnol.* 85(2), 175–185 (cit. on pp. 8, 17–20, 81, 212).

Engels, V & VF Wendisch (2007). The DeoR-type regulator SugR represses expression of *ptsG* in *Corynebacterium glutamicum*. *J. Bacteriol.* 189(8), 2955–2966 (cit. on p. 52).

Ezraty, B, M Chabalier, A Ducret, E Maisonneuve & S Dukan (2011). CO_2 exacerbates oxygen toxicity. *EMBO Rep.* 12(4), 321–326 (cit. on pp. 7, 67, 171).

Festel, G (2010). Industrial biotechnology: Market size, company types, business models, and growth strategies. *Ind. Biotechnol.* 6(2), 88–94 (cit. on pp. 17, 156, 211).

Follmann, M, I Ochrombel, R Krämer, C Trötschel, A Poetsch, C Rückert, A Hüser, M Persicke, D Seiferling, J Kalinowski & K Marin (2009). Functional genomics of pH homeostasis in *Corynebacterium glutamicum* revealed novel links between pH response, oxidative stress, iron homeostasis and methionine synthesis. *BMC Genomics*, 10, (cit. on pp. 67, 171).

Follonier, S, I Escapa, P Fonseca, B Henes, S Panke, M Zinn & MA Prieto (2013). New insights on the reorganization of gene transcription in *Pseudomonas putida* KT2440 at elevated pressure. *Microb. Cell Fact.* 12(1), 30 (cit. on pp. 6, 29, 67, 69, 158, 170).

Garcia-Gonzalez, L, AH Geeraerd, S Spilimbergo, K Elst, L Van Ginneken, J Debevere, JF Van Impe & F Devlieghere (2007). High pressure carbon dioxide inactivation of microorganisms in foods: The past, the present and the future. *Int. J. Food Microbiol.* 117(1), 1–28 (cit. on pp. 30, 158).

Garcia-Ochoa, F & E Gomez (2009). Bioreactor scale-up and oxygen transfer rate in microbial processes: An overview. *Biotechnol. Adv.* 27(2), 153–176 (cit. on pp. 8, 17, 19, 212).

George, S, G Larsson & SO Enfors (1993). A Scale-down 2- ompartment reactor with ontrolled substrate oscillations: Metabolic response of *Saccharomyces-Cerevisiae*. *Bioprocess. Eng.* 9(6), 249–257 (cit. on pp. 21, 22, 26, 212).

Georgi, T, D Rittmann & VF Wendisch (2005). Lysine and glutamate production by *Corynebacterium glutamicum* on glucose, fructose and sucrose: roles of malic enzyme and fructose-1,6-bisphosphatase. *Metab. Eng.* 7(4), 291–301 (cit. on p. 139).

Gill, NK, M Appleton, F Baganz & GJ Lye (2008). Quantification of power consumption and oxygen transfer characteristics of a stirred miniature bioreactor for predictive fermentation scale-up. *Biotechnol. Bioeng.* 100(6), 1144–1155 (cit. on pp. 8, 19).

Goudar, CT, R Matanguihan, E Long, C Cruz, C Zhang, JM Piret & KB Konstantinov (2007). Decreased pCO_2 accumulation by eliminating bicarbonate addition to high cell-density cultures. *Biotechnol. Bioeng.* 96(6), 1107–1117 (cit. on p. 157).

Graf, M (2014). *Characterization and Application of a Cascade Bioreactor to Analyze the Scale-Up dependent CO_2/HCO_3^- Stimulus in* Corynebacterium glutamicum. MA thesis, IBVT, University of Stuttgart (cit. on p. 50).

Grosz, R & G Stephanopoulos (1983). Statistical mechanical estimation of the free energy of formation of E. coli biomass for use with macroscopic bioreactor balances. *Biotechnol. Bioeng.* 25(9), 2149–2163 (cit. on pp. 196, 201).

Guest, JR & IT Creaghan (1974). Further studies with lipoamide dehydrogenase mutants of *Escherichia coli* K12. *J. Gen. Microbiol.* 81(1), 237–245 (cit. on p. 143).

Gutknecht, J, M Bisson & F Tosteson (1977). Diffusion of carbon dioxide through lipid bilayer membranes: Effects of carbonic anhydrase, bicarbonate, and unstirred layers. *J. Gen. Physiol.* 69(6), 779–794 (cit. on pp. 6, 16, 30, 158).

Han, S, F Delvigne, A Brognaux, GE Charbon & SJ Sorensen (2013). Design of growth-dependent biosensors based on destabilized GFP for the detection of physiological behavior of *Escherichia coli* in heterogeneous bioreactors. *Biotechnol. Prog.* 29(2), 553–563 (cit. on p. 24).

Hanahan, D (1983). Studies on transformation of *Escherichia coli* with plasmids. *J. Mol. Biol.* 166(4), 557–580 (cit. on p. 139).

Hasegawa, S, K Uematsu, Y Natsuma, M Suda, K Hiraga, T Jojima, M Inui & H Yukawa (2012). Improvement of the redox balance increases L-valine production by *Corynebacterium glutamicum* under oxygen deprivation conditions. *Appl. Environ. Microbiol.* 78(3), 865–875 (cit. on p. 152).

Hasegawa, S, M Suda, K Uematsu, Y Natsuma, K Hiraga, T Jojima, M Inui & H Yukawa (2013). Engineering of *Corynebacterium glutamicum* for high-yield L-valine production under oxygen deprivation conditions. *Appl. Environ. Microbiol.* 79(4), 1250–1257 (cit. on p. 152).

Heider, SAE, P Peters-Wendisch & VF Wendisch (2012). Carotenoid biosynthesis and overproduction in *Corynebacterium glutamicum*. *BMC Microbiol.* 12, 198 (cit. on p. 14).

Heider, SAE, P Peters-Wendisch, R Netzer, M Stafnes, T Brautaset & VF Wendisch (2014). Production and glucosylation of C_{50} and C_{40} carotenoids by metabolically engineered *Corynebacterium glutamicum*. *Appl. Microbiol. Biotechnol.* 98(3), 1223–1235 (cit. on p. 14).

Henderson, J & A Brooks (2010). *Improved amino acid methods using Agilent ZORBAX Eclipse Plus C18 columns for a variety of Agilent LC instrumentation and separation goals*. Tech. rep. Agilent Technologies (cit. on pp. 144, 199).

Hermann, T (2003). Industrial production of amino acids by coryneform bacteria. *J. Biotechnol.* 104(1-3), 155–172 (cit. on p. 157).

Hewitt, CJ, G Nebe-Von Caron, B Axelsson, CM McFarlane & AW Nienow (2000). Studies related to the scale-up of high-cell-density *E. coli* fed-batch fermentations using multiparameter flow cytometry: Effect of a changing microenvironment with respect to glucose and dissolved oxygen concentration. *Biotechnol. Bioeng.* 70(4), 381–390 (cit. on pp. 8, 20, 212).

Hewitt, C & A Nienow (2007). The scale-up of microbial batch and fed-batch fermentation processes. *J. Biotechnol.* 131(2), 134–135 (cit. on pp. 8, 17, 19, 20, 212).

Hewitt, CJ, H Onyeaka, G Lewis, IW Taylor & AW Nienow (2007). A comparison of high cell density fed-batch fermentations involving both induced and non-induced recombinant *Escherichia coli* under well-mixed small-scale and simulated poorly mixed large-scale conditions. *Biotechnol. Bioeng.* 96(3), 495–505 (cit. on pp. 10, 24, 212).

Ho, CS, MD Smith & JF Shanahan (1987). Carbon dioxide transfer in biochemical reactors. *Adv. Biochem. Eng. Biotechnol.* 35, 83–125 (cit. on pp. 29, 198).

Holátko, J, V Elisáková, M Prouza, M Sobotka, J Nesvera & M Pátek (2009). Metabolic engineering of the L-valine biosynthesis pathway in *Corynebacterium glutamicum* using promoter activity modulation. *J. Biotechnol.* 139(3), 203–210 (cit. on pp. 14, 51, 138, 152).

Hopkins, MJ, AJ Sheppard & P Eisenklam (1969). The use of transfer functions in evaluating residence time distribution curves. *Chemical Engineering Science*, 24(7), 1131–1137 (cit. on pp. 49, 82).

Hüser, AT, A Becker, I Brune, M Dondrup, J Kalinowski, J Plassmeier, A Puhler, I Wiegrabe & A Tauch (2003). Development of a *Corynebacterium glutamicum* DNA microarray and validation by genome-wide expression profiling during growth with propionate as carbon source. *J. Biotechnol.* 106(2-3), 269–86 (cit. on p. 160).

Ikeda, M & R Katsumata (1999). Hyperproduction of tryptophan by *Corynebacterium glutamicum* with the modified pentose phosphate pathway. *Appl. Environ. Microbiol.* 65(6), 2497–2502 (cit. on p. 208).

Inui, M, H Kawaguchi, S Murakami, AA Vertès & H Yukawa (2004). Metabolic engineering of *Corynebacterium glutamicum* for fuel ethanol production under oxygen-deprivation conditions. *J. Mol. Microbiol. Biotechnol.* 8(4), 243–254 (cit. on pp. 14, 136).

Isenschmid, A, IW Marison & U von Stockar (1995). The influence of pressure and temperature of compressed CO_2 on the survival of yeast cells. *J. Biotechnol.* 39(3), 229–237 (cit. on pp. 5, 6, 30, 158).

Jenzsch, M, R Simutis, G Eisbrenner, I Stückrath & A Lübbert (2006a). Estimation of biomass concentrations in fermentation processes for recombinant protein production. *Bioprocess. Biosyst. Eng.* 29(1), 19–27 (cit. on p. 55).

Jenzsch, M, S Gnoth, M Kleinschmidt, R Simutis & A Lübbert (2006b). Improving the batch-to-batch reproducibility in microbial cultures during recombinant protein production by guiding the process along a predefined total biomass profile. *Bioprocess. Biosyst. Eng.* 29(5-6), 315–321 (cit. on p. 55).

Jones, RP & PF Greenfield (1982). Effect of carbon-dioxide on yeast growth and fermentation. *Enzyme Microb. Technol.* 4(4), 210–222 (cit. on pp. 6, 29, 30, 158, 213).

Junker, BH & HY Wang (2006). Bioprocess monitoring and computer control: Key roots of the current PAT initiative. *Biotechnol. Bioeng.* 95(2), 226–261 (cit. on p. 55).

Junker, BH (2004). Scale-up methodologies for *Escherichia coli* and yeast fermentation processes. *J. Biosci. Bioeng.* 97(6), 347–364 (cit. on pp. 8, 18, 19, 156, 157, 212).

Junne, S, A Klingner, J Kabisch, T Schweder & P Neubauer (2011). A two-compartment bioreactor system made of commercial parts for bioprocess scale down studies: Impact of oscillations on *Bacillus subtilis* fed-batch cultivations. *Biotechnol. J.* none, 1009–1017 (cit. on pp. 9, 10, 21, 22, 28, 212).

Junne, S, A Klingner, D Itzeck, E Brand & P Neubauer (2012). Consistency of Scale-Up from Bioprocess Development to Production. In: *Biopharmaceutical Production Technology*. Ed. by **Subramanian, G**. Weinheim: Wiley-VCH Verlag GmbH & Co. KGaA, 511–543 (cit. on pp. 17, 212).

Käß, F, I Hariskos, A Michel, HJ Brandt, R Spann, S Junne, W Wiechert, P Neubauer & M Oldiges (2013). Assessment of robustness against dissolved oxygen/substrate oscillations for *C. glutamicum* DM1933 in two-compartment bioreactor. *Bioprocess Biosyst. Eng.* 1–12, (cit. on pp. 10, 11, 28, 92, 212, 224).

Käß, F, S Junne, P Neubauer, W Wiechert & M Oldiges (2014). Process inhomogeneity leads to rapid side product turnover in cultivation of *Corynebacterium glutamicum*. *Microb. Cell Fact.* 13, 6 (cit. on pp. 10, 11, 28, 92, 212, 224).

Kalinowski, J, B Bathe, D Bartels, N Bischoff, M Bott, A Burkovski, N Dusch, L Eggeling, BJ Eikmanns, L Gaigalat, A Goesmann, M Hartmann, K Huthmacher, R Krämer, B Linke, AC McHardy, F Meyer, B Möckel, W Pfefferle, A Pühler, DA Rey, C Rückert, O Rupp, H Sahm, VF Wendisch, I Wiegräbe & A Tauch (2003). The complete *Corynebacterium glutamicum* ATCC13032 genome sequence and its impact on the production of L-aspartate-derived amino acids and vitamins. *J. Biotechnol.* 104(1–3), 5–25 (cit. on pp. 69, 170, 183, 189, 193).

Katoh, S & F Yoshida (2009). *Biochemical Engineering: A Textbook for Engineers, Chemists and Biologists* . Weihnheim: Wiley-VCH (cit. on p. 37).

Kelle, R (2005). Handbook of *Corynebacterium glutamicum*. In: *Handbook of* Corynebacterium glutamicum. Ed. by **Eggeling, L & Bott, M**. Boca Raton: CRC Press. Chap. L-Lysine Production, 465–488 (cit. on pp. 6, 17, 154, 156, 211).

Kelly, WJ (2008). Using computational fluid dynamics to characterize and improve bioreactor performance. *Biotechnol. Appl. Biochem.* 49, 225–238 (cit. on p. 20).

Kern, DM (1960). The hydration of carbon dioxide. *J. Chem. Educ.* 37(1), 14–23 (cit. on pp. 16, 158).

Kind, S, WK Jeong, H Schröder, O Zelder & C Wittmann (2010a). Identification and elimination of the competing *N*-acetyldiaminopentane pathway for improved production of diaminopentane by *Corynebacterium glutamicum*. *Appl. Environ. Microbiol.* 76(15), 5175–5180 (cit. on pp. 14, 136).

Kind, S, WK Jeong, H Schröder & C Wittmann (2010b). Systems-wide metabolic pathway engineering in *Corynebacterium glutamicum* for bio-based production of diaminopentane. *Metab. Eng.* 12(4), 341–351 (cit. on pp. 14, 136).

Kirchner, O & A Tauch (2003). Tools for genetic engineering in the amino acid-producing bacterium *Corynebacterium glutamicum*. *J. Biotechnol.* 104(1–3), 287–299 (cit. on pp. 14, 51, 153).

Klaffl, S & BJ Eikmanns (2010). Genetic and functional analysis of the soluble oxaloacetate decarboxylase from *Corynebacterium glutamicum*. *J. Bacteriol.* 192(10), 2604–2612 (cit. on pp. 16, 157).

Klapa, MI, JC Aon & G Stephanopoulos (2003). Systematic quantification of complex metabolic flux networks using stable isotopes and mass spectrometry. *Eur. J. Biochem.* 270(17), 3525–3542 (cit. on pp. 14, 16, 157).

Knoll, A, B Maier, H Tscherrig & J Büchs (2005). The oxygen mass transfer, carbon dioxide inhibition, heat removal, and the energy and cost efficiencies of high pressure fermentation. *Adv. Biochem. Eng. Biotechnol.* 92, 77–99 (cit. on p. 31).

Knoll, A, S Bartsch, B Husemann, P Engel, K Schroer, B Ribeiro, C Stöckmann, J Seletzky & J Büchs (2007). High cell density cultivation of recombinant yeasts and bacteria under non-pressurized and pressurized conditions in stirred tank bioreactors. *J. Biotechnol.* 132(2), 167–179 (cit. on pp. 5, 7, 31, 62, 63, 89).

Kovács, R, F Házi, Z Csikor & P Miháltz (2007). Connection between oxygen uptake rate and carbon dioxide evolution rate in aerobic thermophilic sludge digestion. *Chem. Eng.* 51(1), 17–22 (cit. on pp. 56, 197).

Kozliak, EI, JA Fuchs, MB Guilloton & PM Anderson (1995). Role of bicarbonate/CO_2 in the inhibition of *Escherichia coli* growth by cyanate. *J. Bacteriol.* 177(11), 3213–3219 (cit. on pp. 64, 171).

Kraume, M (2012). *Transportvorgänge in der Verfahrenstechnik: Grundlagen und apparative Umsetzungen*. Berlin: Springer Vieweg (cit. on pp. 45, 216).

Krause, FS, A Henrich, B Blombach, R Krämer, BJ Eikmanns & GM Seibold (2010a). Increased glucose utilization in *Corynebacterium glutamicum* by use of maltose, and Its application for the improvement of L-valine productivity. *Appl. Environ. Microbiol.* 76(1), 370–374 (cit. on pp. 52, 138).

Krause, FS, B Blombach & BJ Eikmanns (2010b). Metabolic engineering of *Corynebacterium glutamicum* for 2-ketoisovalerate production. *Appl. Environ. Microbiol.* 76(24), 8053–8061 (cit. on pp. 52, 54, 136, 137, 140, 142, 149, 152, 154).

Kuriyama, H, W Mahakarnchanakul, S Matsui & H Kobayashi (1993). The effects of pCO_2 on yeast growth and metabolism under continuous fermentation. *Biotechnol. Lett*, 15(2), 189–194 (cit. on pp. 6, 30, 158).

Lamprecht, W & F Heinz (1983). Pyruvate. In: *Methods of Enzymatic Analysis*. Ed. by **Bergmeyer, HU**. 3rd. Weinheim: Verlag Chemie, 570–577 (cit. on pp. 144, 176).

Langheinrich, C & AW Nienow (1999). Control of pH in large-scale, free suspension animal cell bioreactors: Alkali addition and pH excursions. *Biotechnol. Bioeng.* 66(3), 171–179 (cit. on p. 18).

Lapin, A, D Müller & M Reuss (2004). Dynamic behavior of microbial populations in stirred bioreactors simulated with Euler-Lagrange methods: Traveling along the lifelines of single cells. *Ind. Eng. Chem. Res.* 43(16), 4647–4656 (cit. on pp. 9, 20).

Lapin, A, J Schmid & M Reuss (2006). Modeling the dynamics of *E. coli* populations in the three-dimensional turbulent field of a stirred-tank bioreactor—A structured-segregated approach. *Chem. Eng. S*, 61(14), 4783–4797 (cit. on pp. 9, 20).

Lara, AR, E Galindo, OT Ramirez & LA Palomares (2006a). Living with heterogeneities in bioreactors. *Mol. Biotechnol.* 34(3), 355–381 (cit. on pp. 6, 8, 9, 17, 21–23, 28, 86, 212).

Lara, AR, L Leal, N Flores, G Gosset, F Bolívar & OT Ramírez (2006b). Transcriptional and metabolic response of recombinant *Escherichia coli* to spatial dissolved oxygen tension gradients simulated in a scale-down system. *Biotechnol. Bioeng.* 93(2), 372–385 (cit. on pp. 10, 21, 24, 95, 212, 226).

Lara, AR, H Taymaz-Nikerel, MR Mashego, WM van Gulik, JJ Heijnen, OT Ramírez & WA van Winden (2009). Fast dynamic response of the fermentative metabolism of *Escherichia coli* to aerobic and anaerobic glucose pulses. *Biotechnol. Bioeng.* 104(6), 1153–1161 (cit. on pp. 22, 23).

Larsson, G & SO Enfors (1988). Studies of insufficient mixing in bioreactors: Effects of limiting oxygen concentrations and short term oxygen starvation on *Penicillium chrysogenum*. *Bioprocess Eng.* 3(3), 123–127 (cit. on pp. 9, 20–22, 212).

Leuchtenberger, W, K Huthmacher & K Drauz (2005). Biotechnological production of amino acids and derivatives: Current status and prospects. *Appl. Microbiol. Biotechnol.* 69(1), 1–8 (cit. on pp. 13, 136, 157).

Levenspiel, O (2012). *Tracer Technology: Modeling the Flow of Fluids*. Ed. by **Moreau, R**. New York: Springer (cit. on pp. 24, 47, 79, 82, 216, 217).

Levenspiel, O (1999). *Chemical Reaction Engineering*. John Wiley & Sons (cit. on pp. 28, 47).

Liao, JC (1989). Fermentation data analysis and state estimation in the presence of incomplete mass balance. *Biotechnol. Bioeng.* 33(5), 613–622 (cit. on p. 196).

Liebl, W (1991). The Prokaryotes. In: *The Prokaryotes*. Ed. by **Balows, A, Trüper, H, Dworkin, M, Harder, W & Schleifer, K**. Vol. 2. New York: Springer. Chap. Corynebacterium—Nonmedical, 1157–1171 (cit. on pp. 13, 57, 60, 136, 157, 208, 211).

Lin, HY & P Neubauer (2000). Influence of controlled glucose oscillations on a fed-batch process of recombinant *Escherichia coli*. *J. Biotechnol.* 79(1), 27–37 (cit. on p. 19).

Lindner, SN, GM Seibold, A Henrich, R KrÃ¤mer & VF Wendisch (2011). Phosphotransferase system-independent glucose utilization in *Corynebacterium glutamicum* by inositol permeases and glucokinases. *Appl. Environ. Microbiol.* 77(11), 3571–3581 (cit. on pp. 37, 248).

Lindroth, P & K Mopper (1979). High performance liquid chromatographic determination of subpicomole amounts of amino acids by precolumn fluorescence

derivatization with *o*-phthaldialdehyde. *Anal. Chem.* 51(11), 1667–1674 (cit. on p. 144).

Litsanov, B, A Kabus, M Brocker & M Bott (2012). Efficient aerobic succinate production from glucose in minimal medium with *Corynebacterium glutamicum*. *Microb. Biotechnol.* 5(1), 116–128 (cit. on p. 208).

MacMullin, R & M Weber (1935). The theory of short-circuiting in continuous-flow mixing vessels in series and kinetics of chemical reactions in such systems. *Trans. AIChE*, 31(2), 409–458 (cit. on p. 27).

Magnus, JB, D Hollwedel, M Oldiges & R Takors (2006). Monitoring and modeling of the reaction dynamics in the valine/leucine synthesis pathway in *Corynebacterium glutamicum*. *Biotechnol. Prog.* 22(4), 1071–1083 (cit. on p. 23).

Marienhagen, J, N Kennerknecht, H Sahm & L Eggeling (2005). Functional analysis of all aminotransferase proteins inferred from the genome sequence of *Corynebacterium glutamicum*. *J. Bacteriol.* 187(22), 7639–7646 (cit. on pp. 139, 155).

Marx, A, AA de Graaf, W Wiechert, L Eggeling & H Sahm (1996). Determination of the fluxes in the central metabolism of *Corynebacterium glutamicum* by nuclear magnetic resonance spectroscopy combined with metabolite balancing. *Biotechnol. Bioeng.* 49(2), 111–129 (cit. on p. 208).

Mashego, MR, WM van Gulik, JL Vinke, D Visser & JJ Heijnen (2006). In vivo kinetics with rapid perturbation experiments in *Saccharomyces cerevisiae* using a second-generation BioScope. *Metab. Eng.* 8(4), 370–383 (cit. on p. 23).

Mauch, K, S Vaseghi & M Reuss (2000). Quantitative Analysis of Metabolic and Signaling Pathways in *Saccharomyces cerevisiae*. In: *Bioreaction Engineering*. Ed. by **Schügerl, K & Bellgardt, KH**. Berlin: Springer, 435–477 (cit. on p. 23).

Mayr, B, A Moser, E Nagy & P Horvat (1994). Scale-up on basis of structured mixing models: A new concept. *Biotechnol. Bioeng.* 43(3), 195–206 (cit. on pp. 18, 212).

McIntyre, M & B McNeil (1997). Effects of elevated dissolved CO_2 levels on batch and continuous cultures of *Aspergillus niger* A60: An evaluation of experimental methods. *Appl. Environ. Microbiol.* 63(11), 4171–4177 (cit. on pp. 6, 7, 30, 157, 158, 212, 213).

Merlin, C, M Masters, S McAteer & A Coulson (2003). Why is carbonic anhydrase essential to *Escherichia coli*? *J. Bacteriol.* 185(21), 6415–6424 (cit. on pp. 69, 172).

Mersmann, A, WD Einenkel & M Käppel (1975). Auslegung und Maßstabsvergrößerung von Rührapparaten. *Chem. Ing. Tech.* 47(23), 953–964 (cit. on pp. 44, 72, 73, 216, 218).

Mimitsuka, T, H Sawai, M Hatsu & K Yamada (2007). Metabolic engineering of *Corynebacterium glutamicum* for cadaverine fermentation. eng. *Biosci. Biotechnol. Biochem.* 71(9), 2130–2135 (cit. on p. 136).

Mitsuhashi, S, J Ohnishi, M Hayashi & M Ikeda (2004). A gene homologous to β-type carbonic anhydrase is essential for the growth of *Corynebacterium glutamicum* under atmospheric conditions. *Appl. Microbiol. Biotechnol.* 63(5), 592–601 (cit. on pp. 16, 69, 158, 172).

Monod, J (1949). The growth of bacterial cultures. *Annu. Rev. Microbiol.* 3, 371–394 (cit. on p. 37).

Mori, M & I Shiio (1985). Purification and some properties of phosphoenolpyruvate carboxylase from *Brevibacterium flavum* and its aspartate-overproducing mutant. *J. Biochem.* 97(4), 1119–1128 (cit. on pp. 160, 176).

Moritz, B, K Striegel, AA De Graaf & H Sahm (2000). Kinetic properties of the glucose-6-phosphate and 6-phosphogluconate dehydrogenases from *Corynebacterium glutamicum* and their application for predicting pentose phosphate pathway flux in vivo. *Eur. J. Biochem.* 267(12), 3442–3452 (cit. on pp. 160, 176).

Nauman, E (2002). *Chemical Reactor Design, Optimization, and Scaleup.* New York: McGraw-Hill (cit. on pp. 48, 217).

Netzer, R, M Krause, D Rittmann, PG Peters-Wendisch, L Eggeling, VF Wendisch & H Sahm (2004). Roles of pyruvate kinase and malic enzyme in *Corynebacterium glutamicum* for growth on carbon sources requiring gluconeogenesis. *Arch. Microbiol.* 182(5), 354–363 (cit. on pp. 16, 157).

Neubauer, P, L Häggström & SO Enfors (1995a). Influence of substrate oscillations on acetate formation and growth yield in *Escherichia coli* glucose limited fed-batch cultivations. *Biotechnol. Bioeng.* 47(2), 139–146 (cit. on pp. 10, 21).

Neubauer, P, M Ahman, M Törnkvist, G Larsson & SO Enfors (1995b). Response of guanosine tetraphosphate to glucose fluctuations in fed-batch cultivations of *Escherichia coli*. *J. Biotechnol.* 43(3), 195–204 (cit. on p. 21).

Neubauer, P (2011). Towards faster bioprocess development. *Biotechnol. J.* 6(8), 902–903 (cit. on pp. 17, 156, 211).

Neubauer, P & S Junne (2010). Scale-down simulators for metabolic analysis of large-scale bioprocesses. *Curr. Opin. Biotechnol.* 21(1), 114–121 (cit. on pp. 9, 23, 212).

Neubauer, P, N Cruz, F Glauche, S Junne, A Knepper & M Raven (2013). Consistent development of bioprocesses from microliter cultures to the industrial scale. *Eng. Life Sci.* 13(3), 224–238 (cit. on pp. 8, 17, 212).

Neveling, U, S Bringer-Meyer & H Sahm (1998). Gene and subunit organization of bacterial pyruvate dehydrogenase complexes. *Biochim. Biophys. Acta*, 1385(2), 367–372 (cit. on p. 152).

Nielsen, J, J Villadsen & G Lidén (2003). *Bioreaction Engineering Principles*. 2nd. New York: Kluwer Academic (cit. on p. 55).

Nishimura, T, AA Vertes, Y Shinoda, M Inui & H Yukawa (2007). Anaerobic growth of *Corynebacterium glutamicum* using nitrate as a terminal electron acceptor. *Appl. Microbiol. Biotechnol.* 75(4), 889–897 (cit. on pp. 13, 136, 157, 211).

Noorman, H (2011). An industrial perspective on bioreactor scale-down: What we can learn from combined large-scale bioprocess and model fluid studies. *Biotechnol. J.* 6(8), 934–943 (cit. on pp. 6, 8, 81, 89).

Okada, S & S Iwamatu (1997). Scale-up production of milbemycin by *Streptomyces hygroscopicus* subsp. *aureolacrimosus* with control of internal pressure, temperature, aeration and agitation. *J. Chem. T echnol. Biotechnol.* 70(2), 179–187 (cit. on p. 17).

Okino, S, M Inui & H Yukawa (2005). Production of organic acids by *Corynebacterium glutamicum* under oxygen deprivation. *Appl. Microbiol. Biotechnol.* 68(4), 475–80 (cit. on p. 136).

Okino, S, R Noburyu, M Suda, T Jojima, M Inui & H Yukawa (2008a). An efficient succinic acid production process in a metabolically engineered *Corynebacterium glutamicum* strain. *Appl. Microbiol. Biotechnol.* 81(3), 459–464 (cit. on p. 136).

Okino, S, M Suda, K Fujikura, M Inui & H Yukawa (2008b). Production of L-lactic acid by *Corynebacterium glutamicum* under oxygen deprivation. *Appl. Microbiol. Biotechnol.* 78(3), 449–454 (cit. on p. 136).

Oldiges, M & R Takors (2005). Applying metabolic profiling techniques for stimulus-response experiments: Chances and pitfalls. *Adv. Biochem. Eng. Biotechnol.* 92, 173–196 (cit. on p. 23).

Oldiges, M, S Lütz, S Pflug, K Schroer, N Stein & C Wiendahl (2007). Metabolomics: Current state and evolving methodologies and tools. *Appl. Microbiol. Biotechnol.* 76(3), 495–511 (cit. on p. 23).

Oldshue, JY (1966). Fermentation mixing scale-up techniques. *Biotechnol. Bioeng.* 8(1), 3–24 (cit. on p. 19).

Onyeaka, H, AW Nienow & CJ Hewitt (2003). Further studies related to the scale-up of high cell density *Escherichia coli* fed-batch fermentations: The additional effect of a changing microenvironment when using aqueous ammonia to control pH. *Biotechnol. Bioeng.* 84(4), 474–484 (cit. on pp. 10, 18).

Oosterhuis, NMG (1984). *Scale-up of bioreactors: A scale-down approach.* PhD thesis, Technical University of Delft (cit. on pp. 21, 22).

Oosterhuis, NMG & NWF Kossen (1983). Dissolved oxygen concentration profiles in a production-scale bioreactor. *Chem. Eng. Res. Des.* 61(5), none, 308–312 (cit. on p. 20).

Oosterhuis, NM, NW Kossen, AP Olivier & ES Schenk (1985). Scale-down and optimization studies of the gluconic acid fermentation by *Gluconobacter oxydans*. *Biotechnol. Bioeng.* 27(5), 711–720 (cit. on pp. 21, 22, 212).

Palomares, LA, AR Lara, OT Ramírez & MC Flickinger (2009). Bioreactor scale-down. In: *Encyclopedia of Industrial Biotechnology*. New York: John Wiley & Sons (cit. on p. 44).

Park, JH & SY Lee (2010). Metabolic pathways and fermentative production of L-aspartate family amino acids. *Biotechnol. J.* 5(6), 560–577 (cit. on p. 154).

Park, JH, YS Jang, JW Lee & SY Lee (2011). *Escherichia coli* W as a new platform strain for the enhanced production of L-valine by systems metabolic engineering. *Biotechnol. Bioeng.* 108(5), 1140–1147 (cit. on pp. 54, 153).

Peters-Wendisch, PG, VF Wendisch, S Paul, BJ Eikmanns & H Sahm (1997). Pyruvate carboxylase as an anaplerotic enzyme in *Corynebacterium glutamicum*. *Microbiology*, 143(4), 1095–1103 (cit. on pp. 160, 176).

Peters-Wendisch, PG, C Kreutzer, J Kalinowski, M Pátek, H Sahm & BJ Eikmanns (1998). Pyruvate carboxylase from *Corynebacterium glutamicum*: Characterization, expression and inactivation of the *pyc* gene. *Microbiology*, 144(4), 915–927 (cit. on pp. 16, 66, 157).

Petersen, S, AA de Graaf, L Eggeling, M Möllney, W Wiechert & H Sahm (2000). In vivo quantification of parallel and bidirectional fluxes in the anaplerosis

of *Corynebacterium glutamicum*. *J. Biol. Chem.* 275(46), 35932–35941 (cit. on p. 16).

Petersen, S, C Mack, AA De Graaf, C Riedel, BJ Eikmanns & H Sahm (2001). Metabolic consequences of altered phosphoenolpyruvatecarboxykinase activity in *Corynebacterium glutamicum* reveal anaplerotic regulation mechanisms in vivo. *Metab. Eng.* 3(4), 344–361 (cit. on pp. 14, 16, 157).

Radmacher, E, A Vaitsiková, U Burger, K Krumbach, H Sahm & L Eggeling (2002). Linking central metabolism with increased pathway flux: L-valine accumulation by *Corynebacterium glutamicum*. *Appl. Environ. Microbiol.* 68(5), 2246–2250 (cit. on pp. 51, 136, 139, 152).

Reuss, M, S Schmalzriedt & M Jenne (2000). Bioreaction Engineering. In: ed. by **Schügerl, K & Bellgardt, KH**. Berlin: Springer. Chap. Application of Computational Fluiddynamics (CFD) to Modeling Stirred Tank Bioreactors, 207–246 (cit. on p. 20).

Reuss, M, L Aguilera-Vázquez & K Mauch (2007). Reconstruction of dynamic network models from metabolite measurements. In: *Metabolomics*. Ed. by **Nielsen, J & Jewett, M**. Vol. 18. Topics in Current Genetics. Berlin: Springer, 97–127 (cit. on p. 23).

Riedel, C, D Rittmann, P Dangel, B Möckel, S Petersen, H Sahm & BJ Eikmanns (2001). Characterization of the phosphoenolpyruvate carboxykinase gene from *Corynebacterium glutamicum* and significance of the enzyme for growth and amino acid production. *J. Mol. Microbiol. Biotechnol.* 3(4), 573–83 (cit. on pp. 16, 157, 174).

Rodionov, DA, AG Vitreschak, AA Mironov & MS Gelfand (2002). Comparative genomics of thiamin biosynthesis in procaryotes: New genes and regulatory mechanisms. *J. Biol. Chem.* 277(50), 48949–48959 (cit. on p. 169).

Royce, PN (1992). Effect of changes in the pH and carbon dioxide evolution rate on the measured respiratory quotient of fermentations. *Biotechnol. Bioeng.* 40(10), 1129–1138 (cit. on pp. 56, 196).

Royce, PN & NF Thornhill (1991). Estimation of dissolved carbon dioxide concentrations in aerobic fermentations. *AIChE J.* 37(11), 1680–1686 (cit. on pp. 56, 196).

Rückert, C, J Milse, A Albersmeier, DJ Koch, A Pühler & J Kalinowski (2008). The dual transcriptional regulator CysR in *Corynebacterium glutamicum*

ATCC 13032 controls a subset of genes of the McbR regulon in response to the availability of sulphide acceptor molecules. *BMC Genomics*, 9, 483 (cit. on p. 160).

Sahm, H & L Eggeling (1999). D-Pantothenate synthesis in *Corynebacterium glutamicum* and use of *panBC* and genes encoding L-valine synthesis for *d*-pantothenate overproduction. *Appl. Environ. Microbiol.* 65(5), 1973–1979 (cit. on p. 139).

Sambrook, J, D Russel, N Irwin & U Janssen (2001). *Molecular Cloning: A Laboratory Manual*. 3rd ed. Cold Spring Harbor, NY: Cold Spring Harbor Laboratory (cit. on pp. 141, 159, 198, 213).

San, KY & G Stephanopoulos (1984). Studies on on-line bioreactor identification. II. Numerical and experimental results. *Biotechnol. Bioeng.* 26(10), 1189–1197 (cit. on p. 196).

Sandoval-Basurto, EA, G Gosset, F Bolívar & OT Ramírez (2005). Culture of *Escherichia coli* under dissolved oxygen gradients simulated in a two-compartment scale-down system: Metabolic response and production of recombinant protein. *Biotechnol. Bioeng.* 89(4), 453–463 (cit. on pp. 10, 21, 24, 31, 81, 212, 224).

Sasaki, M, T Jojima, M Inui & H Yukawa (2010). Xylitol production by recombinant *Corynebacterium glutamicum* under oxygen deprivation. *Appl. Microbiol. Biotechnol.* 86(4), 1057–1066 (cit. on pp. 14, 136).

Sauer, U & BJ Eikmanns (2005). The PEP-pyruvate-oxaloacetate node as the switch point for carbon flux distribution in bacteria. *FEMS Microbiol. Rev.* 29(4), 765–794 (cit. on pp. 7, 14, 16, 51, 65, 157, 172).

Schädel, F & E Franco-Lara (2009). Rapid sampling devices for metabolic engineering applications. *Appl. Microbiol. Biotechnol.* 83(2), 199–208 (cit. on p. 23).

Schaefer, U, W Boos, R Takors & D Weuster-Botz (1999). Automated sampling device for monitoring intracellular metabolite dynamics. *Anal. Biochem.* 270(1), 88–96 (cit. on pp. 22, 23).

Schäfer, A, A Tauch, W Jäger, J Kalinowski, G Thierbach & A Pühler (1994). Small mobilizable multi-purpose cloning vectors derived from the *Escherichia coli* plasmids pK18 and pK19: Selection of defined deletions in the chromosome of *Corynebacterium glutamicum*. *Gene*, 145(1), 69–73 (cit. on pp. 139, 142).

Schäpper, D, MNHZ Alam, N Szita, A Eliasson Lantz & KV Gernaey (2009). Application of microbioreactors in fermentation process development: A review. *Anal. Bioanal. Chem.* 395(3), 679–695 (cit. on p. 17).

Scheele, S, D Oertel, J Bongaerts, S Evers, H Hellmuth, KH Maurer, M Bott & R Freudl (2013). Secretory production of an FAD cofactor-containing cytosolic enzyme (sorbitol-xylitol oxidase from *Streptomyces coelicolor*) using the twin-arginine translocation (Tat) pathway of *Corynebacterium glutamicum*. *Microb. Biotechnol.* 6(2), 202–206 (cit. on p. 136).

Schilling, BM, W Pfefferle, B Bachmann, W Leuchtenberger & WD Deckwer (1999). A special reactor design for investigations of mixing time effects in a scaled-down industrial L-lysine fed-batch fermentation process. *Biotechnol. Bioeng.* 64(5), 599–606 (cit. on pp. 10, 22, 28, 212).

Schmalzriedt, S, M Jenne, K Mauch & M Reuss (2003). Integration of physiology and fluid dynamics. *Adv. Biochem. Eng. Biotechnol.* 80, 19–68 (cit. on pp. 9, 20).

Schmidt, FR (2005). Optimization and scale up of industrial fermentation processes. *Appl. Microbiol. Biotechnol.* 68(4), 425–435 (cit. on pp. 8, 17, 19, 212).

Schneider, J & VF Wendisch (2010a). Putrescine production by engineered *Corynebacterium glutamicum*. *Appl. Microbiol. Biotechnol.* 88(4), 859–868 (cit. on pp. 14, 136).

Schneider, J & VF Wendisch (2010b). Putrescine production by engineered *Corynebacterium glutamicum*. *Appl. Microbiol. Biotechnol.* 88(4), 859–868 (cit. on p. 14).

Schneider, J & VF Wendisch (2011). Biotechnological production of polyamines by bacteria: Recent achievements and future perspectives. *Appl. Microbiol. Biotechnol.* 91(1), 17–30 (cit. on p. 14).

Schneider, J, D Eberhardt & VF Wendisch (2012). Improving putrescine production by *Corynebacterium glutamicum* by fine-tuning ornithine transcarbamoylase activity using a plasmid addiction system. *Appl. Microbiol. Biotechnol.* 95(1), 169–178 (cit. on pp. 14, 136, 153).

Schreiner, ME & BJ Eikmanns (2005). Pyruvate:quinone oxidoreductase from *Corynebacterium glutamicum*: Purification and biochemical characterization. *J. Bacteriol.* 187(3), 862–871 (cit. on p. 157).

Schreiner, ME, D Fiur, J Holátko, M Pátek & BJ Eikmanns (2005). E1 Enzyme of the pyruvate dehydrogenase complex in *Corynebacterium glutamicum*: Molecular analysis of the gene and phylogenetic aspects. *J. Bacteriol.* 187(17), 6005–6018 (cit. on pp. 52, 136, 139, 145, 157).

Schreiner, ME, C Riedel, J Holáko, M Pátek & BJ Eikmanns (2006). Pyruvate:quinone oxidoreductase in *Corynebacterium glutamicum*: Molecular analysis of the *pqo* gene, significance of the enzyme, and phylogenetic aspects. *J. Bacteriol.* 188(4), 1341–1350 (cit. on pp. 139, 140, 142, 157).

Schröder, J & A Tauch (2010). Transcriptional regulation of gene expression in *Corynebacterium glutamicum*: The role of global, master and local regulators in the modular and hierarchical gene regulatory network. *FEMS Microbiol. Rev.* 34(5), 685–737 (cit. on pp. 67, 171).

Schweder, T (2011). Bioprocess monitoring by marker gene analysis. *Biotechnol. J.* 6(8), 926–933 (cit. on p. 24).

Schweder, T, E Krüger, B Xu, B Jürgen, G Blomsten, SO Enfors & M Hecker (1999). Monitoring of genes that respond to process-related stress in large-scale bioprocesses. *Biotechnol. Bioeng.* 65(2), 151–159 (cit. on pp. 10, 19, 21, 23, 95, 212, 226).

Smith, KM, KM Cho & J Liao (2010). Engineering *Corynebacterium glutamicum* for isobutanol production. *Appl. Microbiol. Biotechnol.* 87(3), 1045–1055 (cit. on pp. 14, 136).

Soini, J, K Ukkonen & P Neubauer (2011). Accumulation of amino acids deriving from pyruvate in *Escherichia coli* W3110 during fed-batch cultivation in a two-compartment scale-down bioreactor. *Adv. Biosci. Biotechnol.* 2(5), 336–339 (cit. on p. 10).

Song, Y, K Matsumoto, T Tanaka, A Kondo & S Taguchi (2013). Single-step production of polyhydroxybutyrate from starch by using α-amylase cell-surface displaying system of *Corynebacterium glutamicum*. *J. Biosci. Bioeng.* 115(1), 12–14 (cit. on p. 14).

Spérandio, M & E Paul (1997). Determination of carbon dioxide evolution rate using on-line gas analysis during dynamic biodegradation experiments. *Biotechnol. Bioeng.* 53(3), 243–252 (cit. on pp. 56, 197).

Spilimbergo, S & A Bertucco (2003). Non-thermal bacterial inactivation with dense CO_2. *Biotechnol. Bioeng.* 84(6), 627–638 (cit. on pp. 30, 158).

Stephanopoulos, G, AA Aristidou & J Nielsen (1998). *Metabolic Engineering: Principles and Methodologies*. San Diego: Academic Press (cit. on p. 195).

Stumm, W & J Morgan (1996). *Aquatic Chemistry: Chemical Equilibria and Rates in Natural Waters*. New York: John Wiley & Sons (cit. on pp. 29, 197).

Sweere, APJ, L Janse, KCAM Luyben & NWF Kossen (1988). Experimental simulation of oxygen profiles and their influence on baker's yeast production: II. Two-fermentor system. *Biotechnol. Bioeng.* 31(6), 579–586 (cit. on p. 21).

Takeno, S, J Ohnishi, T Komatsu, T Masaki, K Sen & M Ikeda (2007). Anaerobic growth and potential for amino acid production by nitrate respiration in *Corynebacterium glutamicum*. *Appl. Microbiol. Biotechnol.* 75(5), 1173–1182 (cit. on p. 13).

Takors, R (2012). Scale-up of microbial processes: Impacts, tools and open questions. *J. Biotechnol.* 160(1-2), 3–9 (cit. on pp. 9, 18, 21, 23, 157, 212).

Takors, R, B Bathe, M Rieping, S Hans, R Kelle & K Huthmacher (2007). Systems biology for industrial strains and fermentation processes—Example: Amino acids. *J. Biotechnol.* 129(2), 181–190 (cit. on pp. 13, 14, 51, 136, 157, 211).

Tateno, T, Y Okada, T Tsuchidate, T Tanaka, H Fukuda & A Kondo (2009). Direct production of cadaverine from soluble starch using *Corynebacterium glutamicum* coexpressing alpha-amylase and lysine decarboxylase. *Appl. Microbiol. Biotechnol.* 82(1), 115–121 (cit. on p. 136).

Teramoto, H, M Inui & H Yukawa (2011). Transcriptional regulators of multiple genes involved in carbon metabolism in *Corynebacterium glutamicum*. *J. Biotechnol.* 154(2–3), 114–125 (cit. on pp. 14, 51).

Teramoto, H, M Inui & H Yukawa (2013). OxyR acts as a transcriptional repressor of hydrogen peroxide-inducible antioxidant genes in *Corynebacterium glutamicum* R. *FEBS J.* 280(14), 3298–3312 (cit. on pp. 67, 171).

Uy, D, S Delaunay, JM Engasser & JL Goergen (1999). A method for the determination of pyruvate carboxylase activity during the glutamic acid fermentation with *Corynebacterium glutamicum*. *J. Microbiol. Methods*, 39(1), 91–96 (cit. on pp. 160, 176).

Vallino, JJ & G Stephanopoulos (2000). Metabolic flux distributions in *Corynebacterium glutamicum* during growth and lysine overproduction. *Biotechnol. Bioeng.* 67(6), 872–885 (cit. on p. 208).

van der Rest, ME, C Lange & D Molenaar (1999). A heat shock following electroporation induces highly efficient transformation of *C. glutamicum* with xenogeneic plasmid DNA. eng. *Appl. Microbiol. Biotechnol.* 52(4), 541–545 (cit. on pp. 141, 174).

van Ooyen, J, S Noack, M Bott, A Reth & L Eggeling (2012). Improved L-lysine production with *Corynebacterium glutamicum* and systemic insight into citrate synthase flux and activity. *Biotechnol. Bioeng.* 109(8), 2070–2081 (cit. on pp. 139, 154).

Vasicová, P, M Pátek, J Nesvera, H Sahm & B Eikmanns (1999). Analysis of the *Corynebacterium glutamicum dapA* promoter. *J. Bacteriol.* 181(19), 6188–6191 (cit. on pp. 52, 138, 145, 153, 154).

Vertès, AA, M Inui & H Yukawa (2012). Postgenomic approaches to using corynebacteria as biocatalysts. *Annu. Rev. Microbiol.* 66, 521–550 (cit. on pp. 14, 51).

Villadsen, J, J Nielsen & G Lidén (2011). Scale-up of bioprocesses. In: *Bioreaction Engineering Principles*. New York: Springer, 497–546 (cit. on p. 20).

Visser, D, GA van Zuylen, JC van Dam, A Oudshoorn, MR Eman, C Ras, WM van Gulik, J Frank, GWK van Dedem & JJ Heijnen (2002). Rapid sampling for analysis of in vivo kinetics using the BioScope: A system for continuous-pulse experiments. *Biotechnol. Bioeng.* 79(6), 674–681 (cit. on p. 23).

Vrábel, P, RGJM van der Lans, KCAM Luyben, L Boon & AW Nienow (2000). Mixing in large-scale vessels stirred with multiple radial or radial and axial up-pumping impellers: Modelling and measurements. *Chem. Eng. Sci.* 55(23), 5881–5896 (cit. on p. 157).

Vrábel, P, RG van der Lans, FN van der Schot, KC Luyben, B Xu & SO Enfors (2001). CMA: Integration of fluid dynamics and microbial kinetics in modelling of large-scale fermentations. *Chem. Eng. J.* 84(3), 463–474 (cit. on pp. 9, 20).

Wada, M, N Hijikata, R Aoki, N Takesue & A Yokota (2008). Enhanced valine production in Corynebacterium glutamicum with defective H^+-ATPase and C-terminal truncated acetohydroxyacid synthase. *Biosci. Biotechnol. Biochem.* 72(11), 2959–2965 (cit. on p. 152).

Wang, NS & G Stephanopoulos (1983). Application of macroscopic balances to the identification of gross measurement errors. *Biotechnol. Bioeng.* 25(9), 2177–2208 (cit. on p. 196).

Wang, NS, GN Stephanopoulos & LE Erickson (1984). Computer applications to fermentation processes. *Crit. Rev. Biotechnol.* 2(1), 1–103 (cit. on pp. 196, 201).

Weiss, R (1970). The solubility of nitrogen, oxygen and argon in water and seawater. *Deep Sea Res. Oceanog. Abstr.* 17(4), 721–735 (cit. on pp. 29, 196).

Wendisch, VF, M Bott, J Kalinowski, M Oldiges & W Wiechert (2006). Emerging *Corynebacterium glutamicum* systems biology. *J. Biotechnol.* 124(1), 74–92 (cit. on pp. 14, 51).

Wennerhold, J & M Bott (2006). The DtxR Regulon of *Corynebacterium glutamicum*. *J. Bacteriol.* 188(8), 2907–2918 (cit. on pp. 67, 166, 170).

Wennerhold, J, A Krug & M Bott (2005). The AraC-type regulator RipA represses aconitase and other iron proteins from *Corynebacterium* under iron limitation and is itself repressed by DtxR. *J. Biol. Chem.* 280(49), 40500–40508 (cit. on pp. 68, 169).

Weuster-Botz, D (2005). Parallel reactor systems for bioprocess development. *Adv. Biochem. Eng. Biotechnol.* 92, 125–143 (cit. on p. 17).

Wiechert, W (2001). ^{13}C Metabolic flux analysis. *Metab. Eng.* 3(3), 195–206 (cit. on p. 195).

Wieschalka, S, B Blombach & BJ Eikmanns (2012). Engineering *Corynebacterium glutamicum* for the production of pyruvate. *Appl. Microbiol. Biotechnol.* 94(2), 449–59 (cit. on pp. 52, 136, 137, 152).

Wieschalka, S, B Blombach, M Bott & BJ Eikmanns (2013). Bio-based production of organic acids with *Corynebacterium glutamicum*. *Microb. Biotechnol.* 6(2), 87–102 (cit. on pp. 13, 52).

Wu, L, H Lange, W Van Gulik & J Heijnen (2003). Determination of in vivo oxygen uptake and carbon dioxide evolution rates from off-gas measurements under highly dynamic conditions. *Biotechnol. Bioeng.* 81(4), 448–458 (cit. on pp. 56, 197).

Yamamoto, S, W Gunji, H Suzuki, H Toda, M Suda, T Jojima, M Inui & H Yukawa (2012). Overexpression of genes encoding glycolytic enzymes in *Corynebacterium glutamicum* enhances glucose metabolism and alanine production under oxygen deprivation conditions. *Appl. Environ. Microbiol.* 78(12), 4447–4457 (cit. on p. 152).

Yamuna Rani, K & VS Ramachandra Rao (1999). Control of fermenters—A review. *Bioprocess. Eng.* 21(1), 77–88 (cit. on p. 55).

Zamboni, N, SM Fendt, M Ruhl & U Sauer (2009). ^{13}C-based metabolic flux analysis. *Nat. Protocols*, 4(6), 878–892 (cit. on p. 195).

Zhu, MM, A Goyal, DL Rank, SK Gupta, TV Boom & SS Lee (2005). Effects of elevated pCO_2 and osmolality on growth of CHO cells and production of antibody-fusion protein B1: A case study. *Biotechnol. Progr.* 21(1), 70–77 (cit. on p. 5).

Ziegler, J & NB Nichols (1942). Optimum settings for automatic controllers. *Trans. ASME*, 64, 759–768 (cit. on pp. 239, 240).

APPENDICES

A Manuscript I

Exchange of the native *Corynebacterium glutamicum* promoter of the *aceE* gene, encoding the E1p subunit of the pyruvate dehydrogenase complex (PDHC), with mutated *dapA* promoter variants led to a series of *C. glutamicum* strains with gradually reduced growth rate and PDHC activity. Upon overexpression of the L-valine biosynthetic genes *ilvBNCE*, all strains produced L-valine. Among these strains, *C. glutamicum aceE* A16 (pJC4 *ilvBNCE*) showed the highest biomass and product yields and thus, was further improved by additional deletion of the *pqo* and *ppc* genes, encoding pyruvate:quinone oxidoreductase and phosphoenolpyruvate carboxylase, respectively. In fed-batch fermentations at high cell densities, *C. glutamicum aceE* A16 Δ*pqo*Δ*ppc* (pJC4 *ilvBNCE*) produced up to 738 mM (i.e., 86.5 g L^{-1}) L-valine with an overall yield (Y_{PS}) of 0.36 mol mol^{-1} of glucose and a volumetric productivity (Q_P) of 13.6 mM h^{-1} (1.6 g L^{-1} h^{-1}). Additional inactivation of the transaminase B gene (*ilvE*) and overexpression of *ilvBNCD* instead of *ilvBNCE* transformed the L-valine-producing strain into a 2-ketoisovalerate producer, excreting up to 303 mM (35 g L^{-1}) 2-ketoisovalerate with a Y_{PS} of 0.24 mol mol^{-1} of glucose and a Q_P of 6.9 mM h^{-1} (0.8 g L^{-1} h^{-1}). The replacement of the *aceE* promoter by the *dapA*-A16 promoter in the two *C. glutamicum* L-lysine producers DM1800 and DM1933 improved the production by 100 % and 44 %, respectively. These results demonstrate that *C. glutamicum* strains with reduced PDHC activity are an excellent platform for the production of pyruvate-derived products.

[1]This chapter has been published as:
Buchholz, J, Schwentner, A, Brunnenkan, B, Gabris, C, Grimm, S, Gerstmeir, R, Takors, R, Eikmanns, BJ & Blombach, B (2013). Platform engineering of *C. glutamicum* with reduced pyruvate dehydrogenase complex activity for improved production of L-lysine, L-valine, and 2-ketoisovalerate. *Appl. Environ. Microbiol.* 79(18), 5566–5575.

A.1 Introduction

Corynebacterium glutamicum is a Gram-positive, facultative anaerobic organism that grows on a variety of sugars and organic acids and is the workhorse for the production of a number of amino acids, e.g., L-glutamate, L-lysine, and also L-valine (Leuchtenberger et al., 2005; Liebl, 1991; Nishimura et al., 2007; Takors et al., 2007). Recent studies also showed the successful employment of *C. glutamicum* for the production of the diamines putrescine and cadaverine (Kind et al., 2010a,b; Mimitsuka et al., 2007; Schneider & Wendisch, 2010a; Schneider et al., 2012; Tateno et al., 2009), the organic acids D-lactate, succinate, 2-ketoisovalerate, and pyruvate (Krause et al., 2010b; Okino et al., 2005; Okino et al., 2008a,b; Wieschalka et al., 2012), the biofuels ethanol and isobutanol (Blombach et al., 2011; Inui et al., 2004; Smith et al., 2010), xylitol (Sasaki et al., 2010), and heterologous proteins (An et al., 2013; Scheele et al., 2013).

Since the common precursor of the products mentioned above is pyruvate (with the exception of xylitol and proteins), the optimization of its availability has a high potential to improve microbial production processes. Radmacher et al. (2002) showed that inactivation of the D-pantothenate biosynthesis by deleting the *panBC* genes in combination with plasmid-bound overexpression of the genes encoding acetohydroxyacid synthase (AHAS; *ilvBN* gene product), acetohydroxyacid isomeroreductase (AHAIR; *ilvC* gene product), dihydroxyacid dehydratase (DHAD; *ilvD* gene product), and/or transaminase B (TA; *ilvE* gene product; Fig. A.1) led to increased L-valine production of *C. glutamicum* when cultivated under D-pantothenate limiting conditions. Later on, Bartek et al. (2008) showed that this limitation results in a drastically increased cytoplasmatic pyruvate pool, due to reduced coenzyme A availability for the reaction of the PDHC. Schreiner et al. (2005) identified and functionally characterized the E1p subunit of the PDHC in *C. glutamicum* and showed that the activity of this multi-enzyme complex is essential for growth of this organism on glucose, pyruvate, or L-lactate. Deletion of the *aceE* gene encoding the E1p subunit caused PDHC deficiency and the resulting strain *C. glutamicum* Δ*aceE* strain required either acetate or ethanol as additional carbon source for growth (Blombach et al., 2009c; Schreiner et al., 2005). Further characterization of the PDHC-deficient strain *C. glutamicum* Δ*aceE* showed that the mutant forms significant amounts of L-valine, L-alanine, and pyruvate from glucose when acetate was exhausted from the medium and growth stopped (Blombach et al., 2007b). Plasmid-bound overexpression of the L-valine biosynthesis genes *ilvBNCE* shifted the product spectrum towards L-valine (Blombach et al., 2007b), and inactivation of the

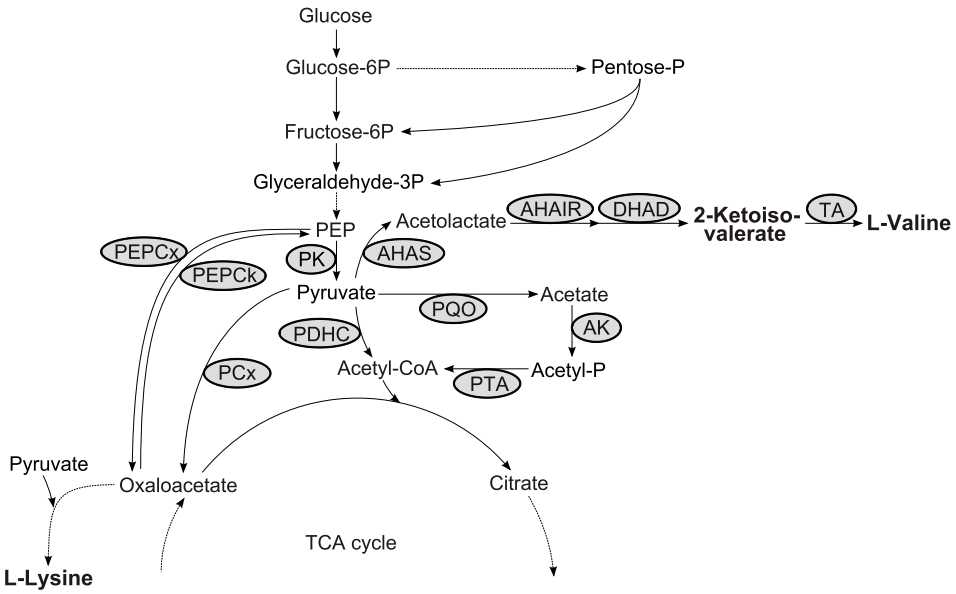

Fig. A.1: Enzymes of the central metabolism with the biosynthetic pathway of 2-ketoisovalerate/L-valine and L-lysine in *C. glutamicum*. Abbreviations: AHAIR, acetohydroxyacid isomeroreductase; AHAS, acetohydroxyacid synthase; AK, acetate kinase; DHAD, dihydroxyacid dehydratase; PCx, pyruvate carboxylase; PDHC, pyruvate dehydrogenase complex; PEP, phosphoenolpyruvate; PEPCk, PEP carboxykinase; PEPCx, PEP carboxylase; PK, pyruvate kinase; PTA, phosphotransacetylase; PQO, pyruvate:quinone oxidoreductase; TA, transaminase B; TCA, tricarboxylic acid.

pyruvate:quinone oxidoreductase (PQO; *pqo* gene product; Fig. A.1) and phosphoglucose isomerase (*pgi* gene product) in *C. glutamicum* Δ*aceE* (pJC4 *ilvBNCE*) resulted in even more efficient L-valine production [up to 410 mM, with a maximum yield of 0.86 mol mol^{-1} of glucose in the production phase (Blombach et al., 2008)]. Based on these results, we engineered the wild type of *C. glutamicum* for the aerobic, growth-decoupled production of 2-ketoisovalerate (KIV) from glucose by deletion of the *aceE*, *pqo* and *ilvE* genes, and additional overexpression of the *ilvBNCD* genes (Krause et al., 2010b). In fed-batch fermentations at high cell densities, *C. glutamicum* Δ*aceE* Δ*pqo* Δ*ilvE* (pJC4 *ilvBNCD*) produced up to 188 mM KIV and showed a volumetric productivity of about 4.6 mM h^{-1} the overall production phase (Krause et al., 2010b). In further approaches, we used the PDHC-deficient *C. glutamicum* strain as platform for the efficient production of about 500 mM pyruvate (i.e. 45 g L^{-1}) or 175 mM isobutanol (i.e. 13 g L^{-1}) and also to improve L-lysine production with *C. glutamicum* (Blombach et al., 2007a; Blombach et al., 2011; Wieschalka et al., 2012).

As stated above, a common feature of all PDHC-deficient *C. glutamicum* strains is the start of the production phase only after complete consumption of the acetate required for growth. Although the addition of maltose instead of glucose, the use of

ethanol instead of acetate, or the inactivation of the transcriptional regulator SugR led to growth-coupled production of L-valine, all strains still require the use of acetate (or ethanol) as essential carbon sources (Blombach et al., 2009c; Krause et al., 2010a), resulting in a more laborious production process compared to approaches with glucose as a single carbon source. This holds true especially in large scale production processes which always prefer rather simple approaches.

Promoter engineering is a suitable metabolic engineering strategy to carefully modulate transcription and to alter the resulting enzyme activity avoiding deletion of a corresponding gene and its unwanted effects such as auxotrophies. Holátko et al. (2009) reduced activity of the *ilvA* (encoding threonine deaminase), and *leuA* (encoding isopropylmalate synthase) promoters and increased the activities of the *ilvD* and *ilvE* promoters by site directed mutagenesis of the respective (extended) −10 regions. These modifications in combination with the deletion of *panB* (see above) and expression of *ilvBN* alleles encoding a feedback resistant variant of the AHAS resulted in a L-isoleucine bradytrophy and improved production strain, which is, however, still auxothrophic for D-pantothenate (Holátko et al., 2009). To improve L-lysine production with *C. ,glutamicum*, several studies employed the strong promoters of the superoxide dismutase gene or of the elongation factor TU gene to replace the native chromosomal promoters of target genes (Becker et al., 2005, 2007, 2011).

By site-directed mutagenesis of the (extended) −10 region of the dihydrodipicolinate synthase gene (*dapA*) promoter, Vasicová et al. (1999) engineered a library with gradually differing promoter activity. Here we make use of this *dapA* promoter library and show that the replacement of the native promoter of the *aceE* gene by mutated *dapA* promoters led to a series of *C. ,glutamicum* strains with gradually reduced PDHC activity and growth on glucose, without requirement of additional carbon sources. These strains were investigated for their ability to produce L-valine and the most promising strain was then further engineered for high titer L-valine and 2-ketoisovalerate production. Finally, the novel *C. glutamicum* platform with reduced PDHC activity was employed for improving L-lysine production.

A.2 Materials and methods

A.2.1 Bacterial strains and plasmids

All bacterial strains, plasmids, and oligonucleotides used and their relevant characteristics, sequences and sources or purposes are listed in Tab. A.1.

Tab. A.1: Strains, plasmids, and oligonucleotides used in this study

Strain, plasmid, or oligonucleotide	Relevant characteristic(s) or sequence	Source, reference, or purpose
Strain		
E. coli DH5α	F$^-$Φ80*lacZ*ΔM15 Δ(*lacZYA-argF*) U169 *endA*1 *recA*1 *hsdR*17 (r_κ^-, m_κ^+) *supE*44 *thi*-1 *gyrA*96 *relA*1 *phoA*	Hanahan (1983)
C. glutamicum WT	Wild-type (WT) strain ATCC13032, biotin-auxotrophic	American Type Culture Collection
C. glutamicum Δ*aceE*	*C. glutamicum* WT with deletion of the E1p gene (*aceE*) of the pyruvate dehydrogenase complex	Schreiner et al. (2005)
C. glutamicum DM1800	L-Lysine producer; *pyc*^{P458S}, *lys*^{CT311I}, derived from *C. glutamicum* WT	Georgi et al. (2005)
C. glutamicum DM1800 aceE A16	*C. glutamicum* DM1800 in which the native *aceE* promoter was replaced by the *dapA*-A16 promoter	This work
C. glutamicum DM1933	L-Lysine producer; Δ*pck*,*pyc*^{P458S}; *hom*^{V59A}; 2× *lys*^{CT311I}, 2× *asd*, 2× *dapA*, 2× *dapB*, 2× *ddh*, 2× *lysA*, 2× *lysE*, derived from *C. glutamicum* WT	Blombach et al. (2009a)
C. glutamicum DM1933 aceE A16	*C. glutamicum* DM1933 in which the native *aceE* promoter was replaced by the *dapA*-A16 promoter	This work
C. glutamicum aceE L1, A23, A25, A16	*C. glutamicum* WT in which the native *aceE* promoter was replaced by the *dapA*-L1, A23, A25, or A16 promoter, respectively	This work
C. glutamicum aceE A16 Δ*pqo*	*C. glutamicum aceE* A16 with deleted *pqo*-gene, encoding pyruvate:quinone oxidoreductase	This work
C. glutamicum aceE A16 Δ*pqo* Δ*ppc*	*C. glutamicum aceE* A16 Δ*pqo* with deleted *ppc* gene, encoding phosphoenolpyruvate carboxylase	This work
C. glutamicum aceE A16 Δ*pqo* Δ*ppc* Δ*ilvE*	*C. glutamicum aceE* A16 Δ*pqo* Δ*ppc* with deleted *ilvE* gene, encoding transaminase B	This work
Plasmids		
pK18/19*mobsacB*	Km^R, mobilizable (*oriT*), *oriV*	Schäfer et al. (1994)
pK18*mobsacB*aceE-rAc	pK18*mobsacB* carrying a truncated promoter region of the *aceE* gene, encoding the E1 subunit of the PDHC	This work
pK18*mobsacB* P*aceE* *dapA*-L1, A23, A25, A16	pK19*mobsacB* P*aceE* carrying the *dapA*-L1, A23, A25, or A16 promoter, respectively	This work
pK19*mobsacB* Δ*ppc*	pK19*mobsacB* carrying a truncated *ppc* gene, encoding phosphoenolpyruvate carboxylase	This work
pK19*mobsacB* Δ*pqo*	pK19*mobsacB* carrying a truncated *pqo* gene, encoding pyruvate:quinone oxidoreductase	Schreiner et al. (2006)
pK19*mobsacB* Δ*ilvE*	pK19*mobsacB* carrying a truncated *ilvE* gene, encoding transaminase B	Marienhagen et al. (2005)
pK19*mobsacB* dP*gltA*540-P*dapA*- L1, A23, A25, A16	pK19*mobsacB* carrying a truncated promoter region of the *gltA* gene and the *dapA*-L1, A23, A25, or A16 promoter, respectively	van Ooyen et al. (2012)
pJC4 *ilvBNCD*	Kan^R; plasmid carrying the *ilvBNCD* genes encoding the L-valine biosynthetic enzymes acetohydroxyacid synthase, isomeroreductase, and dihydroxyacid dehydratase	Sahm & Eggeling (1999)
pJC4 *ilvBNCE*	Kan^R; plasmid carrying the *ilvBNCE* genes encoding the L-valine biosynthetic enzymes acetohydroxyacid synthase, isomeroreductase, and transaminase B	Radmacher et al. (2002)

. . . to be continued on the following page

Tab. A.1: Strains, plasmids, and oligonucleotides used in this study (continued)

Strain, plasmid, or oligonucleotide	Relevant characteristic(s) or sequence	Source, reference, or purpose
Oligonucleotides		
dapAfow	5'-AACTGCAGAACCAATGCATTGGTTC TGCAGTTATCACACCC-3'	Amplification of *dapA* promoters, NsiI site underlined
dapArev2	5'-GGGAATTCCATATGAGGCTCCTTTT AAATCGAGCGGCTCCGGTCTTAGCTG TTAAACC-3'	Amplification of *dapA* promoters/verification of promoter exchange, NdeI site underlined
ace1	5'-CCCAAGCTTGCACATTACCGTCCAACC-3'	Sequencing of *dapA* promoters/verification of promoter exchange
ace2	5'-CGCGGATCCCGACGGTAACGCTTCTCC-3'	Sequencing of *dapA* promoters
ilvE1	5'-GCGTTGACTGATTCTTGGTC-3'	Primer to verify deletion of *ilvE* (Krause et al., 2010b)
ilvE2	5'-CGAGTTCGATGGAATCTTCG-3'	Primer to verify deletion of *ilvE* (Krause et al., 2010b)
pqodel1	5'-AAGGAATTCGTTTTCGAGGCGACCAGA CAG-3'	Primer to verify deletion of *pqo* (Schreiner et al., 2006)
pqodel4	5'-TGGCACAAGCTTGTTAAGCGCTCGCGG TCAATG-3'	Primer to verify deletion of *pqo* (Schreiner et al., 2006)
ppc1	5'-CCCAAGCTTGAGTTGCGCAGCGCAGTG-3'	Primer for deletion of *ppc*, HindIII site underlined
ppc2	5'-GTGCTGCGCAATGCTGAGGGCATTA GAGCAGTGGATTGG-3'	Primer for deletion of *ppc*, crossover overlap underlined
ppc3	5'-CCTCAGCATTGCGCAGCACATCGGC CACAGCTTCTGC-3'	Primer for deletion of *ppc*, crossover overlap underlined
ppc4	5'-CGCGGATCCCGATGACATCAGGTTC CTC-3'	Primer for deletion of *ppc*, BamHI site underlined
ppcdel1	5'-GGAATAGACTCGCTCGGC-3'	Primer to verify deletion of *ppc*
ppcdel2	5'-GTGAACAGGCTCTCGATGC-3'	Primer to verify deletion of *ppc*
aceEup-fw	5'-CGGGATCCCGACCCAATGCGTACCG ATGTG-3'	Primer for deletion of aceE promoter region, BamHI site underlined
aceE-intrev	5'-GCGCTAGCGCCACCATCGGAGGTGT TGTTC-3'	Primer for deletion of *aceE* promoter region, NheI site underlined
aceE-rAC-soeleft	5'-TTGATCGGCC*ATATG*TATT*ATGCAT* CTCTCACGTTTGACGCGAATCG-3'	Primer for deletion of *aceE* promoter region, crossover overlap underlined; NsiI and NdeI in italic
aceE-rAC-soeright	5'-CAAACGTGAGAG*ATGCAT*AATACA*TATG* GCCGATCAAGCAAAACTTGG-3'	Primer for deletion of *aceE* promoter region, crossover overlap underlined; NsiI and NdeI in italic

A.2.2 DNA preparation and transformation

Isolation of plasmids from *Escherichia coli* was performed as described (Eikmanns et al., 1994). Plasmid DNA transfer into *C. glutamicum* was carried out by electroporation and recombinant strains were selected on Luria-Bertani Brain Heart Infusion (LB-BHI) agar plates containing 0.5 M sorbitol, 85 mM potassium acetate, and appropriate

concentrations of kanamycin (50 µg mL^{-1}) (van der Rest et al., 1999). Isolation of chromosomal DNA from *C. glutamicum* was performed as described (van der Rest et al., 1999). Electroporation of *E. coli* was carried out with competent cells according to the method of Dower et al. (1988).

A.2.3 Culture conditions

E. coli was grown aerobically in 2× TY complex medium (Sambrook et al., 2001) at 37 °C as 50 mL cultures in 500 mLl baffled Erlenmeyer flasks on a rotary shaker at 120 min^{-1}. Pre-cultures of the different *C. glutamicum* strains were grown in 2× TY medium containing 0.5 % (w/v) potassium acetate. The L-lysine producer strains *C. glutamicum* DM1800, DM1933 and its derivatives were grown in BHI medium (Becton, Dickinson, 37 g L^{-1}) containing 1 % (w/v) glucose. For growth and amino acid fermentations in shake-flasks, cells of an overnight pre-culture were washed with 0.9 % (w/v) NaCl and inoculated into CGXII minimal medium [pH 7.4; Eikmanns et al. (1991)] with 222 mM glucose to give an optical density at 600 nm (OD_{600}) of about 1. The plasmid-carrying strains were grown in the presence of kanamycin (50 µg mL^{-1}). *C. glutamicum* was grown aerobically at 30 °C as 50 mL cultures in 500 mL baffled Erlenmeyer flasks on a rotary shaker at 120 min^{-1}.

Fed-batch fermentations for L-valine production were performed at 30 °C in 300 mL cultures in a fed-batch pro fermentation system from DASGIP (Jülich, Germany) and for 2-ketoisovalerate production as 1,500 mL cultures in a Bioengineering (Wald, Switzerland) stirred tank reactor with a head pressure of 1.5 bar. Batch fermentations for L-lysine production were performed in glass reactors as 600 mL cultures. The pH was maintained at 7.3 by online measurement using a standard pH-probe (Mettler Toledo, Giessen, Germany) and addition of 10 % NH_3 and 5 M H_2SO_4 (for L-valine and L-lysine) or 5 M KOH and 5 M H_2SO_4 (for 2-ketoisovalerate). Foam development was prohibited by manual injection of about 20 µL of struktol 674 antifoam (Schill und Seilacher, Hamburg, Germany). Dissolved oxygen was measured online using a polarometric oxygen electrode (Mettler Toledo, Giessen, Germany) and adjusted to ≥ 20 % of saturation in a cascade by stirring at (300–1.500) min^{-1} and aeration up to 1 vvm. The fermentations were carried out in CGXII minimal medium (pH 7.4; Eikmanns et al. (1991)) initially containing 222 mM or 333 mM glucose. For 2-ketoisovalerate fermentations 1 % (w/v) yeast extract and 10 mM L-valine, L-isoleucine, and L-leucine and for L-lysine fermentations 0.5 % (w/v) BHI powder was additionally added. Antibiotics were added appropriately (kanamycin

50 µg mL^{-1}). During the fed-batch processes, adequate amounts of 50 % (w/v) glucose were injected.

A.2.4 Construction of *Corynebacterium glutamicum* deletion and promoter exchange mutants

Chromosomal inactivation of the phosphoenolpyruvate carboxylase gene *ppc* in *C. glutamicum aceE* A16 Δ*pqo* was performed using crossover PCR and the suicide vector pK19*mobsacB*. DNA fragments were generated using the primer pairs ppc1/ppc2 and ppc3/ppc4, respectively. The two fragments were purified, mixed in equal amounts, and subjected to crossover PCR using primers ppc1 and ppc4. The resulting fusion product (containing the *ppc* gene with an internal deletion of 1,922 bp) was ligated into BamHI/HindIII-restricted plasmid pK19*mobsacB* and transformed into *E. coli*. After isolation and sequencing (MWG Biotech), the recombinant plasmid was electroporated into *C. glutamicum aceE* A16 Δ*pqo*. Using the method described by Schäfer et al. (1994), the intact chromosomal *ppc* gene was replaced by the truncated *ppc* gene via homologous recombination (double crossover). The screening of the *ppc* mutants was done on 2× TY agar plates containing 10 % (w/v) sucrose and 0.5 % (w/v) potassium acetate. The replacement at the chromosomal locus was verified by PCR using primers ppcdel1/ppcdel2.

Chromosomal inactivation of the pyruvate:quinone oxidoreductase gene *pqo* in *C. glutamicum aceE* A16 and of the transaminase B gene *ilvE* in *C. glutamicum aceE* A16 Δ*pqo* Δ*ppc* was performed as described before (Krause et al., 2010b; Schreiner et al., 2006). The replacement at the chromosomal locus was verified by PCR using primers pqodel1/pqodel4 or ilvE1/ilvE2, respectively.

Chromosomal replacement of the native *aceE* promoter by mutated *dapA* promoters *in C. glutamicum* WT was performed using the suicide vector pK18*mobsacB*. DNA fragments were generated using primer pairs aceEup-fw/aceE-rAC-soeleft and aceE-intrev/aceE-rAC-soeright respectively. The two fragments were purified, mixed in equal amounts, and subjected to crossover PCR using primers aceEup-fw and aceE-intrev. The resulting fusion product (containing the *aceE* promoter region shortened by 338 bp) was ligated into BamHI/XbaI-restricted plasmid pK18*mobsacB* and transformed into *E. coli*. After isolation, the nucleotide sequence of the insert region in the recombinant plasmid pK18*mobsacBaceE*-rAC was verified (MWG Biotec). Then, the mutated *dapA* promoters (A16, A23, A25, L1) were amplified via PCR with the primers dapAfow and dapArev2 from plasmids pK19*mobsacB* dP*gltA*540-P*dapA*-L1, -A23, -A25, and -A16, respectively,

and ligated into NsiI/NdeI-restricted pK18*mobsacBaceE*-rAC. All nucleotide sequences of the inserts in the newly constructed plasmids were verified by sequencing (MWG Biotech). Double crossover and screening for the correct mutants was performed as described above. The replacement of the native *aceE* promoter by the *dapA*-L1, -A16, -A23, and -A25 promoter, respectively, at the chromosomal locus was verified by PCR using primers ace1/dapArev2.

A.2.5 Determination of pyruvate dehydrogenase complex activities

For determination of PDHC activities, the relevant strains were cultivated aerobically in shake-flasks to an OD_{600} of about 5. The cells were harvested by centrifugation for 10 min at $4,500 \times g$ and 4 °C, washed once with 25 mL 0.2 M Tris-HCL (pH 7.4), centrifuged again, and resuspended in 0.5 mL 0.2 M Tris-HCL (pH 7.4), 10 mM $MgCl_2$, 3 mM L-cysteine, and 10 % (v/v) glycerol. The cell suspension was transferred into 2 mL screw-cap vials together with 250 mg of glass beads (0.1 mm diameter; Roth) and subjected to mechanical disruption three times for 30 s at 6,500 min^{-1} with a Precellys 24 (Peqlab) at RT with intermittent cooling on ice for 5 min. Intact cells and cell debris were removed by centrifugation for 15 min at $12,100 \times g$ and 4 °C. Then, the resulting cell-free extract was subjected to ultracentrifugation for 45 min at $45,000 \times g$ and 4 °C, and the supernatant was directly used to determine the PDHC activity according to Guest & Creaghan (1974).

For all tested strains, three biological and two technical replicates were performed. The protein concentration was quantified with the Pierce BCA protein assay (Thermo Scientific) with bovine serum albumin as standard. Assays were linear over time and proportional to the protein concentration. One unit of activity is defined as 1 µmol NADH formed per min at 30 °C.

A.2.6 Analytics

Biomass formation was either followed by determining the OD_{600} or the cell dry weight (CDW in g L^{-1}) at a given time point. Both techniques were correlated for several independent fermentations resulting in CDW = OD_{600} ×0.3.

For determination of glucose, organic and amino acid concentrations in the culture fluid, 1 mL of the culture was harvested by centrifugation [$12,100 \times g$, 10 min, room temperature (RT)] and the supernatant was analyzed. Glucose concentrations were determined by enzymatic tests (Roche Diagnostics). The phosphate concentration was

analysed by the phosphate kit LCK 348 (Hach Lange). The pyruvate concentrations were determined enzymatically according to Lamprecht & Heinz (1983) or by high pressure liquid chromatography (HPLC; see below).

The amino acid concentration was determined by reversed-phase HPLC (on a HP 1100 instrument; Hewlett-Packard) with fluorimetric detection (excitation at 230 nm and emission at 450 nm) after automatic precolumn derivatization with *ortho*-phthaldialdehyde (Lindroth & Mopper, 1979). Separation was carried out at 40 °C on a Multohyp octyldecylsilane column (particle size, 5 µm; 125× 4 mm; CS-Chromatographie). The elution buffer consisted of a polar phase (0.1 M sodium acetate, pH 7.2) and methanol as nonpolar phase. Quantification was done by calculation of the concentration using an internal standard (L-ornithine at 100 µm) and by a 10-point calibration curve for each amino acid. Amino acid concentrations were also determined using an Agilent 1200 Series apparatus (Agilent Technologies) equipped with an Agilent ZORBAX Eclipse Plus C18 column (250× 4.6 mm, 5 µm) protected by an Agilent ZORBAX Eclipse Plus C18 guard column (12.5× 4.6 mm, 5 µm). Fluorometric detection (excitation at 230 nm and emission at 450 nm) was carried out after automatic pre-column derivatization with *ortho*-phthaldialdehyde. The elution buffer consisted of a polar phase (10 mM Na_2HPO_4, 10 mM $Na_2B_4O_7$, 0.5 mM NaN_3, pH 8.2) and a non-polar phase (45 % (v/v) acetonitril, 45 % (v/v) methanol). Protocol details are given in Henderson & Brooks (2010). Quantification of the analytes was conducted by using L-norvaline as internal standard to correct for analyte variability and by an 8-point calibration curve for each component as external reference standard.

Organic acid concentrations were measured via HPLC using an Agilent 1200 Series apparatus equipped with a Rezex ROA organic acid column H^+ (8 %) column (300× 7.8 mm, 8 µm), protected by a Rezex ROA organic acid column H^+ (8 %) guard column (50 × 7.8 mm). A protocol for phosphate precipitation was applied to each sample and standard prior to measurement. Thus, 45 µL 4 M NH_3 and 100 µL 1.2 M $MgSO_4$ were added to 1,000 µL sample. After 5 min of incubation, the sample was centrifuged for 5 min at $18,000 \times g$ and RT. 500 µL supernatant were then transferred to 500 µL 0.1 M H_2SO_4. After thorough mixing and 15 min of incubation at RT, samples were finally centrifuged for 15 min at $18,000 \times g$ at RT. Subsequently, the supernatant was provided for HPLC injection (10 µL injection volume). Separation was performed under isocratic conditions at 50 °C (column temperature) for 45 min with 5 mM H_2SO_4 as mobile phase at a constant flow rate of 0.4 mL min^{-1}. Detection of glucose and organic acids was achieved via an Agilent 1200 Series refractive index detector at 32 °C. Quantification

of the analytes was conducted by using L-rhamnose as internal standard to correct for analyte variability and by an 8-point calibration curve for each component as external reference standard.

A.3 Results

A.3.1 Replacement of the *aceE* promoter by mutated *dapA* promoters results in reduced growth and pyruvate dehydrogenase complex activity

Recently, we identified and functionally characterized the E1p subunit of the PDHC in *C. glutamicum*, located the promoter region and identified the transcriptional start site of the *aceE* gene 121 nucleotides upstream of the translational start (Schreiner et al., 2005). To replace the native *aceE* promoter, we firstly cloned the flanking promoter regions into the suicide vector pK18mobsacB, deleting 338 nucleotides upstream of translational start site. Then, we cloned the four *dapA* promoter variants A16, A23, A25, and L1 (Vasicová et al., 1999) between the flanking regions. Applying homologous recombination, we were able to replace the native *aceE* promoter in *C. glutamicum* WT by the mutated *dapA* promoters (see also materials and methods section). Subsequently, the growth of the resulting strains *C. glutamicum aceE* A16, A23, A25, and L1 was compared with that of *C. glutamicum* WT and the PDHC-deficient strain *C. glutamicum* Δ*aceE* in minimal medium with 4 % (w/v) glucose (Fig. A.2 A). As already shown by Schreiner et al. (2005), *C. glutamicum* Δ*aceE* showed almost no growth (OD_{600} of 2.8 after 24 h), whereas *C. glutamicum* WT reached an OD_{600} about 61 after 24 h with a growth rate of $(0.32 \pm 0.01)\,h^{-1}$. *C. glutamicum* strains with the exchanged *dapA* promoters A16, A25, A23, and L1 reached significantly lower final OD_{600} of about 14.5, 12.3, 7.4, and 7.0, respectively. When compared to the parental WT strain, the growth rates of the mutant strains were gradually decreased to μ = 0.22, 0.20, 0.15, and $0.14\,h^{-1}$ for strains A16, A25, A23, and L1, respectively.

To further analyze the replacement of the native *aceE* promoter by mutated *dapA* promoters, we determined the overall PDHC activities in the respective strains grown in minimal medium with 4 % (w/v) glucose. *C. glutamicum* WT showed in the exponential growth phase a PDHC activity of $(64 \pm 7)\,mU\,mg^{-1}$ protein. In agreement with the decreased growth rates, *C. glutamicum aceE* A16, A25, A23, and L1 showed significantly lower PDHC activities of 13, 10, 5, and $3\,mU\,mg^{-1}$ protein, respectively (Fig. A.2 B).

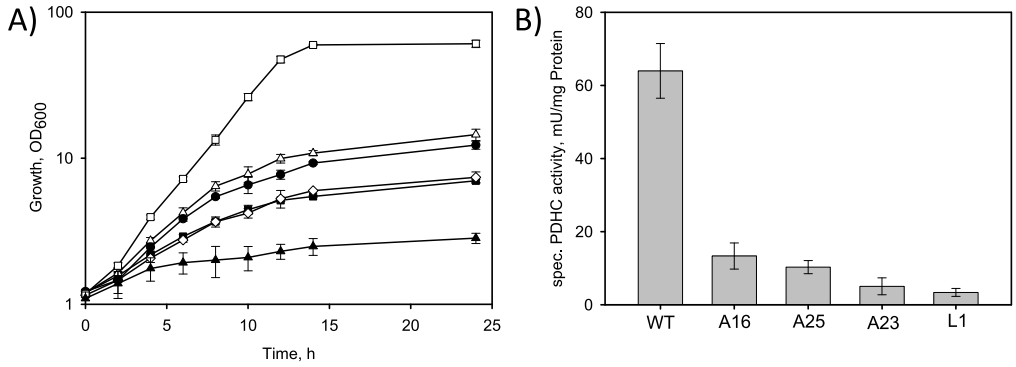

Fig. A.2: Growth of *C. glutamicum* WT and its derivatives with reduced (A16, A23, A25, L1) or abolished (*C. glutamicum* Δ*aceE*) PDHC activity in shake-flasks containing CGXII medium with 222 mM glucose. □, *C. glutamicum* WT; ▲, *C. glutamicum* Δ*aceE*; △, *C. glutamicum aceE* A16; ●, *C. glutamicum aceE* A25; ◇, *C. glutamicum aceE* A23; ■, *C. glutamicum aceE* L1. (B) Specific PDHC activities of *C. glutamicum* WT and its derivatives with reduced PDHC activity grown in shake-flasks containing CGXII medium with 222 mM mM glucose. Three independent fermentations were performed. Error bars show standard deviation.

A.3.2 Overexpression of the *ilvBNCE* genes in strains with reduced pyruvate dehydrogenase complex activity results in improved L-valine overproduction

To analyze the suitability of the engineered *C. glutamicum* strains with reduced PDHC activity for L-valine production, we transformed *C. glutamicum aceE* A16, A25, A23, L1, and the WT strain with plasmid pJC4 *ilvBNCE*, carried out shake-flask cultivations in minimal medium with 222 mM glucose, and investigated growth, substrate consumption, and amino acid formation (Tab. A.2). Overexpression of the L-valine biosynthetic pathway genes resulted in L-alanine and L-valine overproduction in all strains. *C. glutamicum* WT (pJC4 *ilvBNCE*) showed a substrate-specific biomass yield (Y_{XS}) of about 0.066 g mmol^{-1}, a biomass specific glucose consumption rate (q_S) of about 0.80 g g^{-1} h^{-1}, a substrate-specific L-alanine yield of about 0.02 mol mol^{-1} and a substrate-specific L-valine yield (Y_{PS}) of about 0.11 mol mol^{-1}. Interestingly, among the modified *C. glutamicum* strains the one with lowest Y_{XS} but with the uppermost q_S did not exhibit the highest Y_{PS}. With stepwise increasing Y_{XS} (L1, A23, A25, A16) the Y_{PS} increased from about 0.21 (L1) to 0.37 mol mol^{-1} (A16) and the substrate-specific L-alanine yield dropped from about 0.06 (L1) to 0.02 mol mol^{-1} (A16; Tab. A.2).

Tab. A.2: Substrate-specific biomass yield (Y_{XS}), biomass specific glucose consumption rate (q_S), substrate-specific L-alanine and L-valine yield (Y_{PS}) of *C. glutamicum* L-valine producer strains cultivated in CGXII medium with 4 % (w/v) glucose in shake flasks.[†]

Strain	Y_{XS}, g mmol^{-1}	q_S, g g^{-1} h^{-1}	Y_{PS}, mol mol^{-1}	
			L-Alanine	L-Valine
C. glutamicum WT (pJC4 *ilvBNCE*)	0.066 ± 0.012	0.80 ± 0.15	0.02 ± 0.01	0.11 ± 0.04
C. glutamicum aceE L1 (pJC4 *ilvBNCE*)	0.024 ± 0.004	1.00 ± 0.17	0.06 ± 0.01	0.21 ± 0.01
C. glutamicum aceE A23 (pJC4 *ilvBNCE*)	0.027 ± 0.003	0.91 ± 0.10	0.07 ± 0.01	0.25 ± 0.01
C. glutamicum aceE A25 (pJC4 *ilvBNCE*)	0.040 ± 0.003	0.80 ± 0.06	0.04 ± 0.01	0.35 ± 0.02
C. glutamicum aceE A16 (pJC4 *ilvBNCE*)	0.042 ± 0.002	0.77 ± 0.04	0.02 ± 0.01	0.37 ± 0.01
C. glutamicum aceE A16 Δ*pqo* (pJC4 *ilvBNCE*)	0.042 ± 0.003	0.72 ± 0.05	0.02 ± 0.01	0.40 ± 0.03
C. glutamicum aceE A16 Δ*pqo* Δ*ppc* (pJC4 *ilvBNCE*)	0.039 ± 0.005	0.80 ± 0.11	0.02 ± 0.01	0.42 ± 0.02

[†] Given values represent the arithmetic mean ± standard deviation of at least three independent experiments.

A.3.3 Inactivation of the pyruvate:quinone oxidoreductase and phosphoenolpyruvate carboxylase further improves L-valine production

Among the engineered *C. glutamicum* L-valine producers, *C. glutamicum aceE* A16 (pJC4 *ilvBNCE*) showed the best performance, i.e., highest Y_{XS} and Y_{PS} combined with the lowest substrate-specific L-alanine yield (Tab. A.2). In shake-flask experiments, this strain consumed 245 mM glucose within 30 h and produced about 90 mM L-valine after 48 h (Fig. A.3). Thus, *C. glutamicum aceE* A16 (pJC4 *ilvBNCE*) formed the optimal basis for further improvement and therefore, we stepwise deleted the *pqo* and *ppc* genes to further increase pyruvate availability. Both modifications did not significantly alter the Y_{XS}, q_S or the substrate-specific L-alanine yield, but cumulatively led to an about 14 % increased Y_{PS} from 0.37 to 0.42 mol mol^{-1} (Tab. A.2).

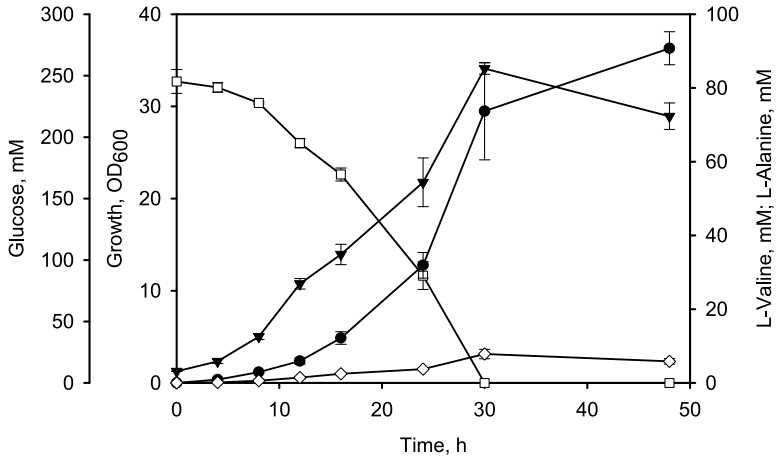

Fig. A.3: Growth, glucose consumption, and L-alanine and L-valine formation of *C. glutamicum aceE* A16 (pJC4 *ilvBNCE*) cultivated in shake-flasks with CGXII medium containing 222 mM glucose. ▼, OD_{600}; □, glucose; ◇, L-alanine; ●, L-valine. Three independent fermentations were performed. Error bars show standard deviation

A.3.4 Fed-batch fermentations with *Corynebacterium glutamicum aceE* A16 Δ*pqo* Δ*ppc* (pJC4 *ilvBNCE*)

In order to test the suitability of *C. glutamicum aceE* A16 Δ*pqo* Δ*ppc* (pJC4 *ilvBNCE*) for an improved L-valine production process, we carried out fed-batch fermentations in minimal medium initially containing about 333 mM glucose (Fig. A.4). Under these conditions, *C. glutamicum aceE* A16 Δ*pqo* Δ*ppc* (pJC4 *ilvBNCE*) grew exponentially with a growth rate of 0.15 h^{-1} to an OD_{600} of about 158 (i.e., 47.4 g L^{-1}) and produced about 378 mM L-valine (i.e., 44.3 g L^{-1}) within 33.5 h. Then, phosphate in the medium became limiting, however, despite transition to the stationary phase, the cells continued to metabolize glucose and to produce L-valine (Fig. A.4). Until the end of the fermentation after 55 h, *C. glutamicum aceE* A16 Δ*pqo* Δ*ppc* (pJC4 *ilvBNCE*) produced about 41 mM L-alanine and up to 738 mM L-valine (86.5 g L^{-1}) with a Y_{PS} of 0.36 mol mol^{-1} of glucose and a volumetric productivity of about 13.6 mM h^{-1} (1.6 g L^{-1} h^{-1}). Taken together, *C. glutamicum aceE* A16 Δ*pqo* Δ*ppc* (pJC4 *ilvBNCE*) with reduced PDHC activity represents an excellent production platform. In contrast to the previously developed producer strains, *C. glutamicum aceE* A16 Δ*pqo* Δ*ppc* (pJC4 *ilvBNCE*) did not require any additional carbon source (such as acetate or ethanol) for growth (see introduction).

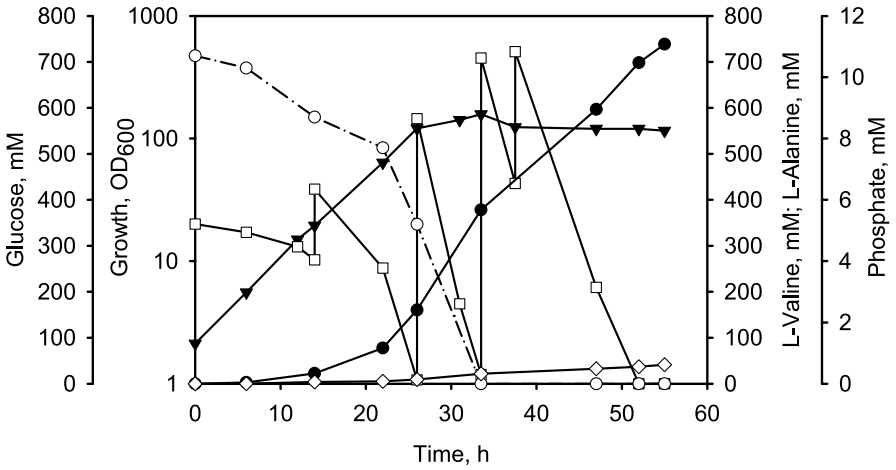

Fig. A.4: Representative fed-batch fermentation of *C. glutamicum aceE* A16 Δ*pqo* Δ*ppc* (pJC4 *ilvBNCE*) in CGXII medium initially containing about 333 mM glucose. ▼, OD_{600}; □, glucose; ◇, L-alanine; ●, L-valine; ○, phosphate.

A.3.5 Inactivation of the transaminase B and overexpression of *ilvBNCD* in *Corynebacterium glutamicum aceE* A16 Δ*pqo* Δ*ppc* results in efficient 2-ketoisovalerate production

Recently, we demonstrated the ability of PDHC-deficient *C. glutamicum* strains to produce 2-ketoisovalerate from glucose when acetate was exhausted from the culture broth (Krause et al., 2010b). To investigate the applicability of the novel production platform for 2-ketoisovalerate production, we inactivated the transaminase B by deletion of the *ilvE* gene in *C. glutamicum aceE* A16 Δ*pqo* Δ*ppc* and transformed the resulting strain with plasmid pJC4 *ilvBNCD*. With the final strain *C. glutamicum aceE* A16 Δ*pqo* Δ*ppc* Δ*ilvE* (pJC4 *ilvBNCD*), we carried out fed-batch fermentations in minimal medium initially containing 333 mM glucose, 1 % (w/v) yeast extract, and 10 mM L-valine, L-isoleucine, and L-leucine, respectively. In contrast to the corresponding (transaminase B-positive) L-valine producer, *C. glutamicum aceE* A16 Δ*pqo* Δ*ppc* Δ*ilvE* (pJC4 *ilvBNCD*) showed no exponential growth, but a steadily decreasing growth rate. After 29 h and at an OD_{600} of about 84 (25.2 g L^{-1}; Fig. A.5) growth stopped, although neither phosphate nor LL-valine, LL-isoleucine, or LL-leucine became limiting in the culture broth (not shown). In the growth phase, *C. glutamicum aceE* A16 Δ*pqo* Δ*ppc* Δ*ilvE* (pJC4 *ilvBNCD*) produced about 228 mM (26 g L^{-1}) 2-ketoisovalerate. After the growth arrest, the strain continued to consume glucose and further excreted 2-ketoisovalerate into the medium. At the end of the fermentation after 44 h, the strain reached an OD_{600} of about 88 (26.4 g L^{-1}) and produced about 30 mM pyruvate, 33 mM L-valine, and up to 303 mM (35 g L^{-1})

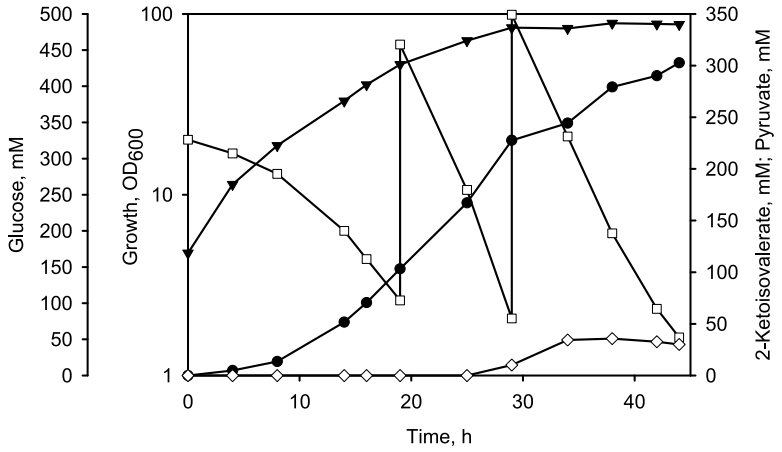

Fig. A.5: Representative fed-batch fermentation of *C. glutamicum aceE* A16 Δ*pqo* Δ*ppc* Δ*ilvE* (pJC4 *ilvBNCD*) in CGXII medium initially containing about 333 mM glucose, 1 % (w/v) yeast extract and 10 mM L-valine, L-isoleucine and L-leucine, respectively. ▼, OD_{600}; □, glucose; ◇, pyruvate; ●, 2-ketoisovalerate.

2-ketoisovalerate (Fig. A.5), with a Y_{KS} 0.24 mol mol^{-1} and a volumetric productivity of about 6.9 mM h^{-1} (0.8 g L^{-1} h^{-1}).

A.3.6 Reducing pyruvate dehydrogenase complex activity improves L-lysine production

Since pyruvate is also the precursor for L-lysine synthesis (see Fig. A.1), we analyzed the effect of reduced PDHC activity on L-lysine production with *C. glutamicum*. For this purpose, we replaced the native *aceE* promoter in the defined L-lysine producer *C. glutamicum* DM1800 by the *dapA*-A16 promoter. With the resulting strain *C. glutamicum* DM1800 *aceE* A16, we carried out shake-flask cultivations in minimal medium with 222 mM glucose and 0.5 % (w/v) BHI, and analyzed growth and L-lysine production. In comparison to the parental strain *C. glutamicum* DM1800, the newly constructed *C. glutamicum* DM1800 *aceE* A16 showed a 34 % reduced Y_{XS} of about 0.048 g mmol^{-1}, however, it produced two times more L-lysine and showed a 34 % increased biomass specific production rate (q_P) (Tab. A.3). We also introduced the *dapA* A16 promoter in *C. glutamicum* DM1933, which produces about 60 % more L-lysine than strain DM1800, and carried out batch fermentations in aerated and stirred bioreactors. Under these conditions, *C. glutamicum* DM1933 *aceE* A16 reached a Y_{XS} of about 0.043 g mmol^{-1}, secreted the by-products L-valine (5 mM) and L-alanine (3 mM) and showed a Y_{PS} of 0.23 mol mol^{-1} and a q_P of 0.138 g g^{-1} h^{-1} (Tab. A.3), which are about 44 % and 77 % higher when compared to the parental *C. glutamicum* DM1933.

Tab. A.3: Substrate specific biomass yield (Y_{XS}), final titer, substrate specific L-lysine yield (Y_{PS}), and biomass specific production rate (q_P) of *C. glutamicum* L-lysine producers cultivated in CGXII medium with 4 % (w/v) glucose and 0.5 % (w/v) BHI in shake flasks (DM1800) or in bioreactors (DM1933).[†]

Strain	Y_{XS}, g mol^{-1}	Titer, mM	Y_{PS}, mol mol^{-1}	q_P, g g^{-1} h^{-1}
C. glutamicum DM1800	0.072 ± 0.001	22 ± 2	0.10 ± 0.01	0.068 ± 0.007
C. glutamicum DM1800 *aceE* A16	0.048 ± 0.001	45 ± 2	0.20 ± 0.02	0.091 ± 0.009
C. glutamicum DM1933	0.069 ± 0.004	35 ± 3	0.16 ± 0.03	0.078 ± 0.016
C. glutamicum DM1933 *aceE* A16	0.043 ± 0.006	52 ± 6	0.23 ± 0.04	0.138 ± 0.028

[†] Given values represent the arithmetic mean ± standard deviation of at least three independent experiments.

A.3.7 Platform comparison: pyruvate dehydrogenase complex deficiency vs. reduction of pyruvate dehydrogenase complex activity

Tab. A.4 gives an overview on the production characteristics of L-valine and 2-ketoisovalerate producers based on PDHC deficiency or on PDHC with reduced activity. The genetic background of the respective strains is not completely identical, however, as shown above, the additional deletion of the *ppc* gene did improve the Y_{PS} of L-valine production with *C. glutamicum aceE* A16 Δ*pqo* Δ*ppc* (pJC4 *ilvBNCE*) only by 5 % compared to the parental strain with an active PEPCx. With the given improvements taken into account, the contribution of the *ppc* deletion is low and therefore, a comparison of the respective producers is acceptable.

For L-valine production, the reduction of the PDHC activity in *C. glutamicum* in combination with the deletion of the *pqo* and *ppc*, and overexpression of the *ilvBNCE* genes led to growth-coupled L-valine production of 83.6 g L^{-1} in fed-batch fermentations. Compared to *C. glutamicum* Δ*aceE* Δ*pqo* (pJC4 *ilvBNCE*) (Blombach et al., 2008), this titer is 3.4-times higher. Furthermore, *C. glutamicum aceE* A16 Δ*pqo* Δ*ppc* (pJC4 *ilvBNCE*) showed a 43 % higher overall Y_{PS} and a 3-times higher volumetric productivity (Q_P; Tab. A.4).

For 2-ketoisovalerate, the effect is not as drastic as for L-valine production. When compared to Y_{PS} of the PDHC-deficient producer strain, that of *C. glutamicum aceE* A16 Δ*pqo* Δ*ppc* Δ*ilvE* (pJC4 *ilvBNCD*) was reduced by about 19 %, however, the final titer and the Q_P were improved by 55 % and 40 %, respectively (Tab. A.4).

Taken together, our results demonstrate that the novel engineered *C. glutamicum* platform with reduced PDHC activity has characteristics which are superior compared to its PDHC-deficient counterpart.

Tab. A.4: Final product concentrations (c_P), substrate specific product yields (Y_{PS}), and volumetric productivities (Q_P) of fed-batch fermentations of *C. glutamicum* L-valine and 2-ketoisovalerate producers with either inactivated PDHC or PDHC with reduced activity.[†]

Condition and strain	c_P, g L^{-1}	Y_{PS}, mol mol^{-1}	Q_P, g L^{-1} h^{-1}
L-Valine overproduction			
C. glutamicum Δ*aceE* Δ*pqo* (pJC4 *ilvBNCE*)[‡]	24.6 ± 2.6	0.23 ± 0.02	0.5 ± 0.1
C. glutamicum aceE A16 Δ*pqo* Δ*ppc* (pJC4 *ilvBNCE*)	83.6 ± 2.6	0.33 ± 0.01	1.5 ± 0.1
2-Ketoisovalerate overproduction			
C. glutamicum Δ*aceE* Δ*pqo* Δ*ilvE* (pJC4 *ilvBNCD*)[*]	21.8 ± 3.2	0.26 ± 0.02	0.5 ± 0.1
C. glutamicum aceE A16 Δ*pqo* Δ*ppc* Δ*ilvE* (pJC4 *ilvBNCD*)	33.7 ± 1.0	0.21 ± 0.04	0.7 ± 0.1

[†] Given values represent the arithmetic mean ± standard deviation of at least three independent experiments.
[‡] Data are from reference Blombach et al. (2008)
[*] Data are from reference Krause et al. (2010b)

A.4 Discussion

Several recent studies with *C. glutamicum* aimed to improve the pyruvate availability for L-valine, L-lysine, L-alanine, 2-ketoisovalerate, or isobutanol production or to engineer *C. glutamicum* for the production of pyruvate itself. These approaches included (i) inactivating enzymes of D-pantothenate synthesis to limit CoA availability for the PDHC reaction (Elisáková et al., 2005; Holátko et al., 2009; Radmacher et al., 2002), (ii) applying anaerobic conditions to abolish/reduce oxidative TCA flux (Hasegawa et al., 2012, 2013; Yamamoto et al., 2012), (iii) using an ATPase defective mutant leading to increased pyruvate availability (Aoki et al., 2005; Wada et al., 2008), and (iv) deleting the *aceE* gene encoding the E1p subunit of the PDHC (Blombach et al., 2007a,b; Blombach et al., 2008, 2009c, 2011; Krause et al., 2010b; Wieschalka et al., 2012). However, all these approaches did either result in a requirement for D-pantothenate, ethanol, or acetate, did not allow an adequate adjustment of the PDHC activity and the carbon flux into the TCA, and/or required a cleverly devised redox state of the cell (under anaerobic conditions). In this study, we applied promoter engineering to develop *C. glutamicum* strains with gradually decreased PDHC activity by exchange of the native *aceE* promoter by a series of mutated *dapA* promoters, allowing the screening of the most promising variant for further optimization by metabolic engineering. Since the PDHC is a multi-enzyme complex consisting of three subunits (AceE, AceF, Lpd), which are arranged in a tightly defined stoichiometric composition (de Kok et al., 1998; Neveling et al., 1998), it is difficult to predict the effects of tuning the promoter activity of one of the respective

genes (*aceE*, *aceF* or *lpd*) on the overall PDHC activity. Therefore, we randomly choose four *dapA* promoter variants [A16, A23, A25, L1; Vasicová et al. (1999)] to replace the native *aceE* promoter and analyzed growth and overall PDHC activity. Shake flask cultivations of the different engineered strains (*C. glutamicum aceE* A16, A23, A25, L1) revealed that with decreasing PDHC activity coherently the growth rate decreased, but also the final biomass concentration (Fig. A.2) although glucose was still present in the medium (data not shown). The reduced biomass formation is surprising, but might be attributed to metabolic inhibition since all strains excreted significant amounts of L-valine, L-alanine, and pyruvate (data not shown). However, overexpression of the *ilvBNCE* genes in these strains leading to a drain-off of pyruvate towards L-valine did not improve the final biomass concentration (data not shown). Moreover, compared to the wildtype, *C. glutamicum aceE* A23 and L1 (pJC4 *ilvBNCE*) showed a 14 % and 25 % increased q_S (Tab. A.2) indicating energy limitation, which might led to the observed growth.

For the promoter variants *dapA*-A16, A23, A25 we found a linear correlation of the overall PDHC and the respective promoter activity (data not shown). However, the *dapA*-A16 promoter showed the highest activity (Vasicová et al., 1999), but interestingly this promoter was unable to completely compensate the activity of the native *aceE* promoter, since *C. glutamicum aceE* A16 showed 79 % lower PDHC activity and a 31 % decreased growth rate when compared to *C. glutamicum* WT (Fig. A.2). It is noteworthy to mention that the −10 region (TATCCT) of the native *aceE* promoter corresponds to that of the *dapA*-A14 promoter, which shows lower activity compared to that of *dapA*-A16 promoter (Vasicová et al., 1999). As a consequence, other enhancing elements such as the extended −10 region or the action of transcriptional regulators such as RamB (Blombach et al., 2009b) give the *aceE* promoter its strength. Since *C. glutamicum aceE* A16 showed the highest Y_{PS} and Y_{XS}, it might be anticipated that other promoters, stronger than the *dapA*-A16 but weaker than the native *aceE* promoter, might be even more suitable for production purposes. Alternatively or in combination to our approach, modulation of translation initiation by altering the sequence length between the ribosome binding site (RBS) and the translational start codon (TSC), using different TSCs or deleting the RBS as recently applied to improve putrescine production with *C. glutamicum* (Schneider et al., 2012) as well as self-cloning (Kirchner & Tauch, 2003) or deletion of repressor/activator binding sites (for e.g. RamB) might be promising strategies to adjust expression of the *aceE* gene more exactly. However, taking into account the numbers for current aerobic production processes for L-valine with *E. coli* [61 g L^{-1}; Park et al. (2011)] or *C. glutamicum* [48 g L^{-1}; Blombach et al.

(2008)] and for 2-ketoisovalerate with *C. glutamicum* [22 g L^{-1}; Krause et al. (2010b)], the novel engineered *C. glutamicum* platform with reduced PDHC activity (84 g L^{-1} L-valine; 34 g L^{-1} 2-ketoisovalerate; Tab. A.4) is highly competitive or even superior.

In contrast to the L-valine producer (Fig. A.4), the 2-ketoisovalerate producer *C. glutamicum aceE* A16 Δ*pqo* Δ*ppc* Δ*ilvE* (pJC4 *ilvBNCD*) showed no constant growth but a steadily decreasing growth rate (Fig. A.5). This phenomenon might be attributed to an inhibiting effect of the product, since neither phosphate nor one of the supplemented amino acids L-valine, L-isoleucine, or L-leucine became limiting (data not shown). However, the decreasing growth rate of the 2-ketoisovalerate producer discloses the general advantage of the PDHC-deficient platform (production starts not before acetate is depleted and growth stops) for the production of cytotoxic products. Anyhow, despite the continuously decreasing growth rate, *C. glutamicum aceE* A16 Δ*pqo* Δ*ppc* Δ*ilvE* (pJC4 *ilvBNCD*) reached a significantly higher 2-ketoisovalerate titer compared to the PDHC-deficient counterpart (Tab. A.4). For the production of more toxic/growth inhibiting products, the situation might be different and a growth-decoupled production process will then be advantageous.

C. glutamicum is the workhorse for industrial L-lysine production and several improvements have been made by metabolic engineering [overview in Blombach & Seibold (2010), Kelle (2005), and Park & Lee (2010)]. Recently, we inactivated the PDHC in the defined L-lysine producer *C. glutamicum* DM1729 which led to an auxotrophy for acetate, however, also to 44 % improved L-lysine production when compared to the parental strain (Blombach et al., 2007a). Here we found that introduction of the *dapA*-A16 promoter in *C. glutamicum* DM1800, which shows the identical Y_{PS} as DM1729, led to prototrophic growth and increased the Y_{PS} by 100 %, indicating that reduction of PDHC activity might be more useful to optimize L-lysine production with *C. glutamicum* than a complete shutdown of the PDHC. The reason for reduced improvement of the PDHC-deficient counterpart might be attributed to reduced expression of relevant genes under non-growing conditions limiting efficient L-lysine production.

van Ooyen et al. (2012) also made use of the *dapA* promoter library from Vasicová et al. (1999) to adjust citrate synthase (encoded by *gltA*) flux for optimized L-lysine production with *C. glutamicum*. The most promising variant, *C. glutamicum* DM1800 Δ*prpC*1 Δ*prpC*2 with *gltA* under control of the C7-*dapA* promoter improved L-lysine production by 82 % compared to the parental strain (van Ooyen et al., 2012), which is in the same range as the improvement by reduction of PDHC activity (see above). Anyway, both examples demonstrate that reducing the TCA flux with optimizing

pyruvate and oxaloacetate supply is highly beneficial for efficient L-lysine production with *C. glutamicum*. *C. glutamicum* DM1933 *aceE* A16 excreted in batch fermentations L-alanine and L-valine in significant amounts. L-alanine formation is mainly catalysed by the aminotransferase AlaT from pyruvate (Marienhagen et al., 2005). This reaction is in equilibrium and therefore formation of L-alanine and also L-valine is a good indicator for an increased intracellular pyruvate concentration, adumbrating that L-lysine production in this strain is limited by the reactions from pyruvate to L-lysine and not by pyruvate availability. Also the PDHC-deficient L-lysine producer DM1729 Δ*aceE* excreted L-alanine, L-valine and pyruvate into the medium and the additional overexpression of the *ddh* gene (encoding diaminopimelate dehydrogenase) reduced the formation of these by-products and increased the Y_{PS} by 60 % (Blombach et al., 2007a). Here, we found that introducing a second copy of the *ddh* gene and additionally of all L-lysine biosynthetic genes (*lysC*^{T311I}, *asd*, *dapA*, *dapB*, *ddh*, *lysA*, *lysE*) in *C. glutamicum* DM1800 *aceE* A16 did only result in an about 15 % improved Y_{PS} (DM1800 *aceE* A16 vs. DM1933 *aceE* A16), indicating that either *ddh* expression is still too low or other obstacles such as a sufficient NADPH availability have to be overcome in C. glutamicum DM1933 *aceE* A16. However, the surplus of the precursor pyruvate in *C. glutamicum* DM1933 *aceE* A16 opens the possibility for further optimization of L-lysine production by metabolic engineering.

Acknowledgments

Plasmids pJC4 *ilvBNCD* and pJC4 *ilvBNCE* were kindly provided by Lothar Eggeling (Research Center Jülich). We thank Andreas Freund, Salaheddine Laghrami, Mira Lenfers-Lücker, Ulrike Hillemann, and Yasmin Kalmbach for technical assistance. The support of the Fachagentur Nachwachsende Rohstoffe (FNR) of the BMELV (FNR grant 220-095-08A; BioProChemBB project in the frame of the ERA-IB programme) is gratefully acknowledged.

B Manuscript II

We investigated the growth kinetics and transcriptional responses of *Corynebacterium glutamicum* in environments with low (pCO_2 < 40 mbar) and high (pCO_2 ≥ 300 mbar) CO_2/HCO_3^- levels compared to standard conditions. When cultivated at high CO_2/HCO_3^- levels, *C. glutamicum* showed increased (63 %) biomass to substrate yields during the initial growth phase. Other kinetic parameters such as growth rate (μ), specific glucose consumption rate (q_S), and selected enzymatic activities of anaplerotic reactions, the pentose phosphate pathway and the tricarboxylic acid cycle were similar to standard conditions. However, microarray hybridization disclosed a complex transcriptional response involving 117 differentially expressed genes. Among those, 60 genes were assigned to the complete DtxR/RipA regulon controlling iron homeostasis in *C. glutamicum*. Impaired growth of a $\Delta dtxR$ mutant at high CO_2/HCO_3^- levels validated the relevance of this master regulator to cope with excessive CO_2/HCO_3^- availability. At low CO_2/HCO_3^- levels, *C. glutamicum* grew in a bi-level manner with three distinct growth phases. Differential analyses revealed approximately doubled activities of glucose-6-phosphate dehydrogenase and 6-phosphogluconate dehydrogenase accompanied by the formation of L-alanine and L-valine during the lowest μ occurring in mid-phase of the cultivation. DNA microarray analysis revealed more than 100 differentially expressed genes in growth phase II compared to phase I including almost all thiamin pyrophosphate (TPP) biosynthesis genes, which were significantly up regulated. Concluding, we hypothesize that *C. glutamicum* counteracts the lack of CO_2/HCO_3^- by triggering TPP biosynthesis for increasing the activities of TPP-dependent enzymes involved in CO_2 formation.

B.1 Introduction

Industrial biotechnology is regarded as one of the current key technologies with an expected market volume of more than $300 billion by 2030, only considering microbial, non-biopharmaceutical products (Festel, 2010; Neubauer, 2011). To achieve this goal, new production approaches are steadily developed yielding at the minimization of production costs and the increase of productivity. Following the economy-of-scale principle, low price/high volume products sooner or later must be produced in large scales, i.e. in (250–750) m^3 (Junker, 2004; Kelle, 2005). However, increasing reactor dimensions typically

[1]This chapter has been published as:
Blombach, B, Buchholz, J, Busche, T, Kalinowski, J & Takors, R (2013). Impact of different CO_2/HCO_3^- levels on metabolism and regulation in *Corynebacterium glutamicum*. *J. Biotechnol.* 168, 331–340.

coincides with insufficient bulk mixing that results in mixing times of ≈ 240 s (Junker, 2004; Vrábel et al., 2000). Consequently, unintended reactor inhomogeneities occur that are mirrored by radial and vertical gradients e.g. for substrates, pH, temperature, etc. (Takors, 2012). Notably, dissolved gases such as O_2 or CO_2 are affected by large-scale manifold: operating head pressures and hydrostatic pressure increase gas solubilities (compared to typical laboratory-scale set-ups), while large-scale mixing adjacent to technical gas transfer limitations cause radial gradients (Junker, 2004; McIntyre & McNeil, 1997).

This contribution concentrates on one explicit large-scale impact factor – namely the dissolved CO_2 (pCO_2) level. Its generic influence on metabolic and transcriptional regulation is presented – a topic that has been rarely addressed so far. As a prominent example, the Gram-positive, facultatively anaerobic bacterium *Corynebacterium glutamicum* (Liebl, 1991; Nishimura et al., 2007) is chosen. This industrial workhorse is responsible for large-scale amino acid production (such as L-glutamate and L-lysine) with > 2 million tons-per-year (Ajinomoto "Food products and feed-use amino acid business" 2010, 2011) (Hermann, 2003; Leuchtenberger et al., 2005; Takors et al., 2007).

In central metabolism, CO_2 is released via conserved decarboxylation activity in pentose phosphate pathway (PPP; oxidative phosphorylation) and in TCA, basically decarboxylating the C_6 skeleton of citrate to the C_4 body of oxaloacetate (OAA). In contrast to many other organisms, *C. glutamicum* comprises two anaplerotic reactions that are able to replenish TCA intermediates, namely the phosphoenolpyruvate (PEP) carboxylase (PPC) and the pyruvate carboxylase (PYC, Fig. B.4). According to Peters-Wendisch et al. (1998), Klapa et al. (2003), and Petersen et al. (2001), PYC dominates anaplerotic flux under non-gluconeogenic conditions. Additionally, *C. glutamicum* is able to decarboxylate pyruvate to acetyl-CoA via pyruvate dehydrogenase complex [PDHC; Schreiner et al. (2005)], or alternately, via pyruvate:quinone oxidoreductase [PQO; Schreiner & Eikmanns (2005) and Schreiner et al. (2006)] followed by acetate kinase and phosphotransacetylase. Moreover, three C_4-decarboxylating enzymes [oxaloacetate decarboxylase (OAD) (Klaffl & Eikmanns, 2010), malic enzyme (MalE) (Goudar et al., 2007; Netzer et al., 2004), and PEP carboxykinase (PCK)] facilitate the backward reaction of OAA or malate to PEP or pyruvate (Riedel et al., 2001). Despite intensive studies [reviewed in Sauer & Eikmanns (2005)] the complex interplay of *C. glutamicum*'s anaplerosis is still not completely unraveled and has not yet been studied with respect to different CO_2/HCO_3^- levels.

CO_2 is not only actively produced by decarboxylating reactions, but its hydrated form (bicarbonate) is of essential importance for the bicarbonate-dependent carboxylating reactions (e.g. PYC and PPC). Due to the diffusive potential of CO_2 and its rather slow interconversion rate to bicarbonate (Kern, 1960), depletion of the latter can be circumvented by carbonic anhydrase (CA) activity, which catalyzes the reversible hydration of CO_2. Mitsuhashi et al. (2004) identified two genes encoding putative β-type and γ-type carbonic anhydrases in *C. glutamicum*. However, only the β-type enzyme was shown to carry out essential functionality under normal growth and ordinary atmospheric conditions.

CO_2/HCO_3^- may not only serve as co-substrate/-product for enzymes, the species may also alter physico-chemical properties of proteins, acidify the internal pH, and regulate virulence and toxin production in pathogens (Follonier et al., 2013) as well. On the one hand, CO_2 not only freely diffuses through the cellular membrane (Gutknecht et al., 1977), it may also accumulate in the same (Bothun et al., 2004; Jones & Greenfield, 1982; Kuriyama et al., 1993), thus increasing its fluidity and permeability finally leading to the potentially lethal "anaesthesia effect" (Isenschmid et al., 1995). Additionally, detrimental bearings of high CO_2 pressures on vitality, growth, metabolism, and productivity of many industrially relevant bacteria and fungi were reported (Amoabediny & Büchs, 2010; Amoabediny et al., 2010; Baez et al., 2009, 2011; Castan et al., 2002; Dixon & Kell, 1989; El-Sabbagh et al., 2006, 2008; Jones & Greenfield, 1982; McIntyre & McNeil, 1997), being advantageous for emerging non-thermal pasteurization methods of foodstuffs (Ballestra et al., 1996; Garcia-Gonzalez et al., 2007; Spilimbergo & Bertucco, 2003).

So far, Bäumchen et al. (2007) were the first who studied the impact of high CO_2/HCO_3^- levels on the growth of *C. glutamicum*. When grown on glucose in turbidostat cultures, the maximum growth rate decreased with CO_2 partial pressures above (200–300) mbar (exhaust gas), whereas the same CO_2-level enhanced growth with lactate as carbon source. Even though numerous studies dealing with the effect of scale-up dependent reactor inhomogeneities, e.g. O_2, substrate, and pH exist, CO_2-specific reports on the basis of comprehensive physiological and transcriptional investigations are rare (Aguilera et al., 2005; Baez et al., 2009, 2011), or in case of *C. glutamicum* are not available. Thus, we systematically analyzed growth kinetics and regulatory consequences of the industrially highly relevant bacterium *C. glutamicum* in response to different CO_2/HCO_3^- levels in this study.

B.2 Materials and methods

Methods details and associated information are provided in the supplementary data.

B.2.1 Bacterial strain, pre-culture and media

The wild-type strain *C. glutamicum* ATCC 13032 obtained from the American Type Culture Collection (ATCC, Manassas, VA, USA) and its derivatives *C. glutamicum* $\Delta dtxR$ (Brune et al., 2006) and *C. glutamicum* Δppc, $\Delta malE$, Δpyc, and Δpck (constructed in this study; supplementary data) were used in this study. Glycerol stock seed cultures were grown on tryptone-yeast extract [2 × TY; Sambrook et al. (2001)] agar plates and used to inoculate first pre-cultures of 5 mL 2 × TY medium in glass reaction tubes. Second pre-cultures were grown in 50 mL 2 × TY medium supplemented with 1 % (w/v) glucose in 500 mL baffled shaking flasks overnight at 30 °C, harvested by centrifugation, washed with 0.9 % (w/v) NaCl solution and used to inoculate modified CGXII minimal medium (Eikmanns et al., 1991) main cultures (bioreactor) to give an initial optical density at 600 nm (OD_{600}) of about $OD_{600} \geq 1$.

B.2.2 Bioreactor cultivation

Fermentations were carried out at $T = 30\,°C$ at a total pressure of $p = 1.5$ bar in stainless steel 1.5 L bench-top bioreactors with six-blade Rushton-type impellers and standard sensor equipment. Additionally installed were dissolved CO_2 (pCO_2) potentiometric sensors (InPro®5000, Mettler-Toledo, Gießen, Germany). Fermentations were performed under three distinct CO_2/HCO_3^- environments defined as (i) standard (S), (ii) high (H), and (iii) low (L). For the standard setup, the volumetric gas flow rate (Q/V_R) was set to $Q/V = 0.1$ vvm. High CO_2/HCO_3^- levels were achieved with 20 % CO_2 in the inlet gas flow ($Q/V = 0.5$ vvm) and low CO_2/HCO_3^- levels were installed by intensive stripping at $Q/V = 3$ vvm. Unless otherwise stated all fermentation were performed at least as biological triplicates.

B.2.3 Biomass and growth characterization

Biomass formation was either followed by measuring OD_{600} (spectrophotometer DR 2800, Dr. Lange, Berlin, Germany) or by determining the cell dry weight (CDW in $g\,L^{-1}$) using the correlation $CDW = OD_{600} \times 0.3\ g\,L^{-1}$. Maximum specific growth rates μ_{max} (h^{-1}) were estimated in batch cultures via linear regression and least squares fitting of $\ln X(t)$ courses. The fitting quality of linear $\ln(X)$ courses and Y_{XS} derivations were used to

distinguish the three characteristic growth phases at low CO_2/HCO_3^- levels. Related Y_{XS} were deduced from individual biomass and substrate balancing.

B.2.4 HPLC analyses

The determination of amino acids, glucose, and organic acids was performed as described previously by Buchholz et al. (2013).

B.2.5 Determination of enzyme activities

Cells were harvested from the bioreactor at an OD_{600} of about 4, 15, and 41 corresponding to growth phase I, phase II, and phase III, respectively. All enzymes activities were determined by following the NAD(P)H consumption or formation at 340 nm in a spectrophotometer (Ultrospec 2100 *pro*, Biochrom, Cambridge, UK) at 30 °C. Determination of PYC, PPC, PCK, isocitrate dehydrogenase (ICD), glucose-6-phosphate dehydrogenase (GPDH), and 6-phosphogluconate dehydrogenase (PGDH) activities were performed according to modified protocols of Peters-Wendisch et al. (1997), Uy et al. (1999), Mori & Shiio (1985), Aich et al. (2003), Eikmanns et al. (1995), and Moritz et al. (2000), respectively. The protein concentration was quantified with the Pierce BCA protein assay (Thermo Scientific, Waltham, MA, USA).

B.2.6 DNA microarray analysis

For DNA microarray analyses, technical duplicates were sampled from each of the biologically duplicated fermentations $OD_{600} \approx 4$ (phase I) and at $OD_{600} \approx 15$ and 41 in low CO_2/HCO_3^- fermentations corresponding to phases II and III, respectively. Sample preparation was performed following the protocol of Hüser et al. (2003). RNA was finally quantified with a NanoDrop ND-1000 spectrophotometer (Thermo Scientific, Wilmington, DE, USA). The hybridization of whole-genome oligonucleotide microarrays was performed as described by Rückert et al. (2008), using 15 µg of total RNA for cDNA synthesis. For each experiment two biological and two technical replicates were used for microarray-hybridization including a dye-swap. The latter was applied to account for dye-specific bias by reciprocal labeling of cDNA with Cy3 and Cy5. Scanned arrays were analyzed with IMAGENE v6.0 (BioDiscovery Inc., El Segundo, CA, USA). Normalization and evaluation of the hybridization data was performed with EMMA 2 (Dondrup et al., 2009) using a signal intensity (A-value) cut-off of ≥ 7.0 and a signal intensity ratio (M-value) cut-off of ± 1, which corresponds to relative expression changes equal to or

larger than twofold. Students *t*-test statistics was performed with a probability cut-off of $P = 0.05$.

Cohybridization of cDNA samples obtained from low CO_2/HCO_3^- and standard conditions ($OD_{600} \approx 4$) identified two genes (*citB* and cg1082) with increased and one gene (*purU*) with decreased mRNA level that just passed the applied mRNA fold-change filtering with 2.22, 2.00, and 0.41, respectively (supplementary data, Tab. BS.2). The physiological and transcriptional state of *C. glutamicum* under the two conditions for growth phase I was therefore considered as equal, permitting (i) further transcriptional analyses of growth phase II, and phase III in reference to RNA samples of phase I (low CO_2/HCO_3^-) as new reference pool and (ii) the cross-comparability of these results to the expression levels determined for the reference process under standard conditions.

B.3 Results

B.3.1 Growth kinetics

To characterize the growth behavior of *C. glutamicum* WT at various CO_2/HCO_3^- levels, batch fermentations with glucose as sole carbon source were carried out (Fig. B.1). To adjust the CO_2/HCO_3^- concentration in the liquid phase during the fermentation process, different aeration rates and compositions of the inlet gas were applied (Fig. B.1 A). The reference (standard, S) condition considered initial volumetric gas flow rates of Q/V = 0.1 vvm (air) and a maximum pCO_2 evolution of 180 mbar in the late exponential phase. Additional setups allowed enhanced CO_2 partial pressures (high, H) and significantly reduced pCO_2 levels (low, L; Fig. B.1 A). As a precondition of high level studies, the culture medium was aerated with $Q/V = 0.5$ vvm consisting of 20 % CO_2 resulting in high initial CO2 partial pressures of about 300 mbar. Along with biomass formation, pCO2 values up to 380 mbar were found (Fig. B.1 A). On the contrary, stripping conditions (L) considered increased gas flow rates ($Q/V = 3$ vvm, air) to keep CO_2 levels low. As a consequence, CO_2 partial pressures did not exceed 40 mbar (Fig. B.1 A). To ensure comparability of the experiments, other process conditions that may influence cellular growth or CO_2/O_2 availability were kept constant, i.e. total pressure, pH, temperature, and pO_2 levels.

When cultivated under standard and enhanced CO_2/HCO_3^- levels, *C. glutamicum* WT showed exponential growth with rates of $(0.40 \pm 0.02)\,h^{-1}$ and $(0.41 \pm 0.01)\,h^{-1}$ (Fig. B.2 A; Tab. B.5), respectively. Final biomass concentrations reached about (20–22 ± 2) $g\,L^{-1}$ (Fig. B.1 B). Besides, *C. glutamicum* wild-type showed similar q_S of

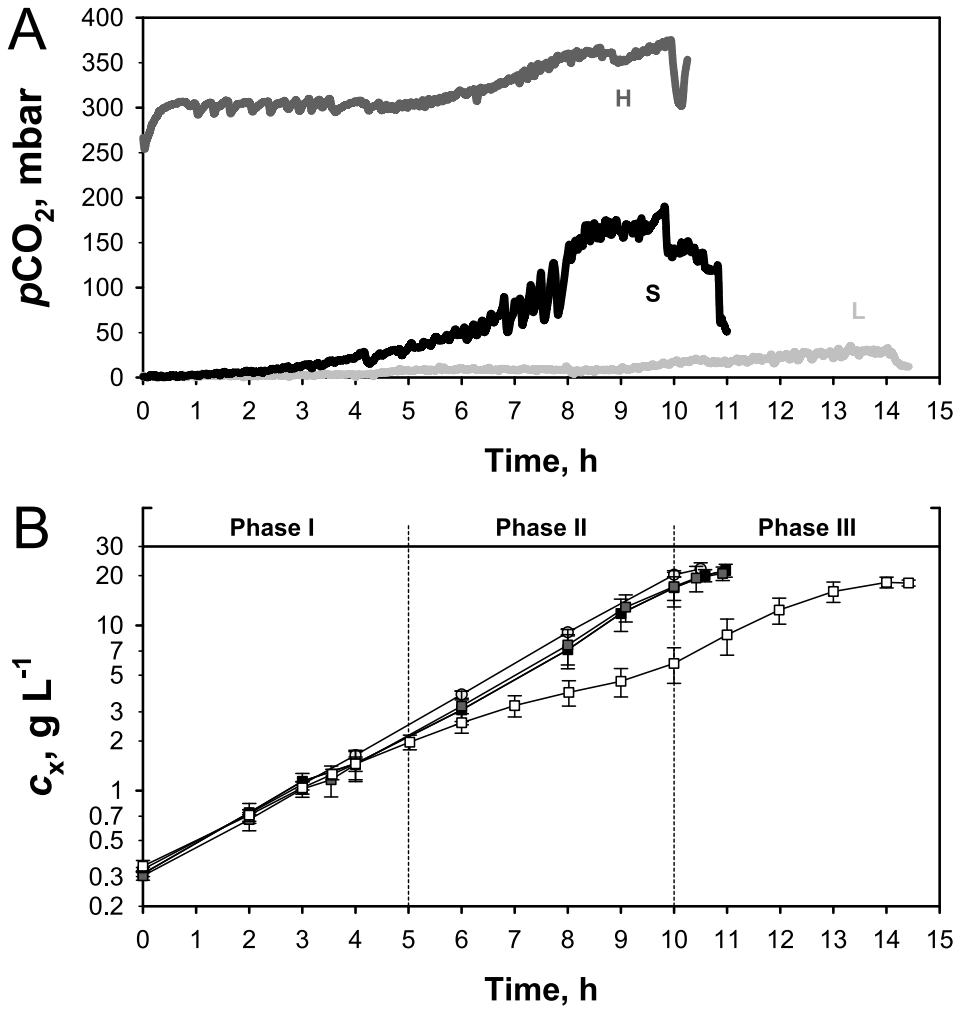

Fig. B.1: Illustration of *C. glutamicum* wild-type batch fermentations carried out at $T = 30\,°C$, pH = 7.4, $p = 1.5\,bar$ in $V = (1.0–1.1)\,L$ modified CGXII minimal salt medium containing 4 % (w/v) glucose. **(A)** Evolution of the dissolved CO_2 concentrations during CO_2-specific batch fermentations. Variable process conditions refer to standard/reference fermentations with volumetric gas flow rates of $Q/V = 0.1\,vvm$ (S, black line), elevated CO_2/HCO_3^- levels using $Q/V = 0.5\,vvm$ with 20 % CO_2 in the inlet gas flow (H, dark gray line), as well as low CO_2/HCO_3^- levels by stripping with $Q/V = 3\,vvm$ (L, light gray line). **(B)** Biomass formation of *C. glutamicum* under standard/reference conditions (black squares), elevated CO_2/HCO_3^- levels (dark gray squares), low CO_2/HCO_3^- levels (open squares), and complemented conditions with high volumetric gas flow rates ($Q/V = 3\,vvm$) and 20 % CO_2 in the inlet gas flow (light gray circle), respectively. At least three independent experiments were performed showing the statistical mean with error bars that represent ±SD.

Tab. B.5: Summary of process characteristics in CO_2-relevant batch cultivations of *C. glutamicum* ATCC13032 WT under standard, high, low or complemented CO_2/HCO_3^- levels. Aeration conditions, compositions, and corresponding process phase(s) are indicated. Fermentations were carried out at $T = 30\,°C$, pH = 7.4, $p = 1.5\,bar$ in $V = (1.0–1.1)\,L$ modified CGXII minimal salt medium containing 4 % (w/v) glucose. Values represent the statistical mean ±SD of at least three independent experiments.

Condition	Standard	High	Low			Complemented
Gas	Air	Air, 20 % CO_2	Air	Air	Air	Air, 20 % CO_2
Q/V, vvm	0.1	0.5	3	3	3	3
Process phase	I–III	I–III	I	II	III	I–III
μ_{max}, h^{-1}	0.40 ± 0.02	0.41 ± 0.01	0.35 ± 0.01	0.19 ± 0.03	0.30 ± 0.04	0.42 ± 0.00
Y_{XS}, $g\,g^{-1}$	0.56 ± 0.02	0.61 ± 0.02	0.71 ± 0.10	0.32 ± 0.03	0.50 ± 0.03	0.56 ± 0.01
q_S, $g\,g^{-1}\,h^{-1}$	0.71 ± 0.03	0.68 ± 0.04	0.48 ± 0.05	0.64 ± 0.03	0.60 ± 0.04	0.74 ± 0.01

$(0.71 \pm 0.03)\,g\,g^{-1}\,h^{-1}$ and $(0.68 \pm 0.04)\,g\,g^{-1}\,h^{-1}$, respectively (Tab. B.5). However, Y_{XS} differed significantly in presence of elevated CO_2/HCO_3^- levels during the first half of the cultivation (Fig. B.2 B). While standard conditions resulted at Y_{XS} of $(0.42 \pm 0.06)\,g\,g^{-1}$, high CO_2/HCO_3^- levels yielded a 63 % increased Y_{XS} of $(0.69 \pm 0.04)\,g\,g^{-1}$ within the first 6 h of the cultivation. For the second half of the fermentation, comparable Y_{XS} of about $(0.58 \pm 0.03)\,g\,g^{-1}$ were determined for both conditions (Fig. B.2 B).

Notably, at low pCO_2 levels growth kinetics of *C. glutamicum* WT showed a three phasic behavior (Fig. B.1 B). Initial growth resembled growth kinetics at high and standard conditions (phase I) revealing a μ of $(0.35 \pm 0.01)\,h^{-1}$ (Fig. B.3 A; Tab. B.5). Between 5 h to 10 h (phase II), the growth rate decreased considerably by almost 50 % to $(0.19 \pm 0.03)\,h^{-1}$ but subsequently re-increased to $(0.30 \pm 0.04)\,h^{-1}$ in phase III (Fig. B.3 A; Tab. B.5). Under this condition *C. glutamicum* WT reached a final biomass concentrations of about $(18.03 \pm 0.76)\,g\,L^{-1}$, which is 19 % lower compared to standard conditions (Fig. B.1 B). Y_{XS} and μ courses showed similar profiles starting with high Y_{XS} of $(0.71 \pm 0.10)\,g\,g^{-1}$ in phase I, a reduction to $(0.32 \pm 0.03)\,g\,g^{-1}$ in phase II, and finally, a re-increase to $(0.50 \pm 0.03)\,g\,g^{-1}$ in phase III (Fig. B.3 C; Tab. B.5). In contrast, q_S ramped up from phase I at $(0.48 \pm 0.05)\,g\,g^{-1}$ to steady high levels during phases II of $(0.64 \pm 0.03)\,g\,g^{-1}$ and $(0.60 \pm 0.04)\,g\,g^{-1}$ in phase III (Tab. B.5). To verify the reduced CO_2/HCO_3^- availability as the only reason for the observed bi-level growth under stripping conditions, control experiments cultivating *C. glutamicum* WT in CO_2/HCO_3^- enriched environments under stripping conditions ($Q/V = 3$ vvm, air with 20 % CO_2) were performed. These experiments complemented the bi-level phenotype and led to exponential growth identical to standard and high CO_2/HCO_3^- levels with μ of $(0.42 \pm 0.00)\,h^{-1}$

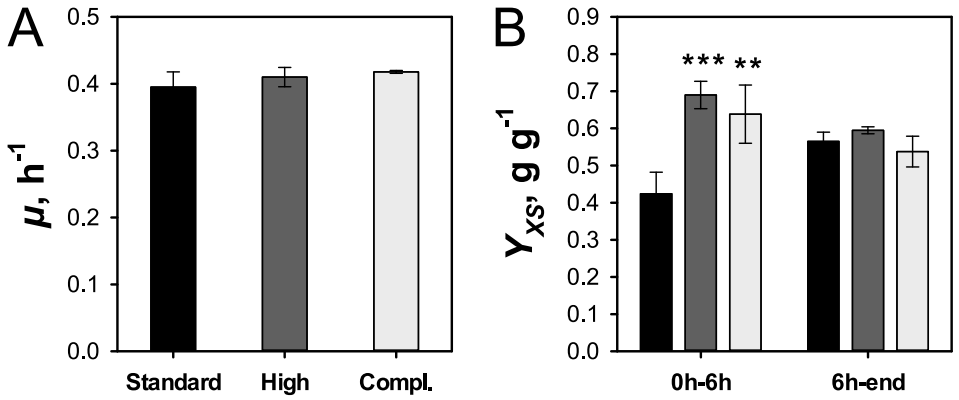

Fig. B.2: Illustration of selected process parameters (μ and Y_{XS}) calculated for the *C. glutamicum* wild-type batch fermentations. Cultivations under standard (Q/V = 0.1 vvm, black bars), high CO_2/HCO_3^- levels (Q/V = 0.5 vvm with 20 % CO_2, dark gray bars) and complemented conditions (Q/V = 3 vvm with 20 % CO_2, light gray bars) are indicated. **(A)** Growth rates (μ) were calculated for the exponential phase. **(B)** Biomass yields (Y_{XS}) were determined within the first 6 h of cultivation and for the remaining period of the fermentation. At least three independent experiments were performed showing the statistical mean with error bars that represent ± SD. Pairwise *t*-tests were performed for each process parameter compared to the corresponding standard condition. *P*-values indicate levels of significance as follows: $^{*}P < 0.05$, $^{**}P < 0.01$ and $^{***}P < 0.001$.

(Fig. B.2 A; Tab. B.5), a final biomass concentration of about $(22 \pm 2)\,\mathrm{g\,L^{-1}}$ with an overall Y_{XS} of $(0.56 \pm 0.01)\,\mathrm{g\,g^{-1}}$, and q_S of $(0.74 \pm 0.01)\,\mathrm{g\,g^{-1}\,h^{-1}}$ (Tab. B.5). Additional control experiments considered oxygen stress as a potential reason for the observed growth phenotype under stripping conditions. At high CO_2 stripping rates of 3 vvm, about 97 % of the original air volumes were initially replaced by N_2, still installing the same dissolved oxygen levels. As result, coincidently to conditions with air as sole stripping gas, equal bi-level growth curves were obtained (data not shown).

To analyze the relevance of selected enzymes of the anaplerotic node under different CO_2/HCO_3^- levels, we deleted the genes encoding PCK, PPC, MalE, and PYC in *C. glutamicum* WT, and recorded the growth kinetics of *C. glutamicum* Δ*pck*, Δ*ppc*, Δ*malE*, and Δ*pyc* in environments with a $pCO_2 < 40$ mbar and a $pCO_2 = 300$ mbar compared to standard conditions (supplementary data, Tab. BS.1). Under the latter condition, compared to the WT all mutant strains showed a reduced μ of $(0.30–0.34)\,\mathrm{h^{-1}}$ which significantly re-increased to $(0.36–0.39)\,\mathrm{h^{-1}}$ when *C. glutamicum* Δ*pck*, Δ*malE*, and Δ*pyc* were exposed to high CO_2/HCO_3^- conditions, respectively. At low pCO_2 levels the mutant strains showed the bi-level growth behavior similar to the WT, with *C. glutamicum* Δ*pyc* exhibiting pronounced growth retardation in phase II with a μ of $0.09\,\mathrm{h^{-1}}$, which is two times lower compared to *C. glutamicum* WT (supplementary data, Tab. BS.1).

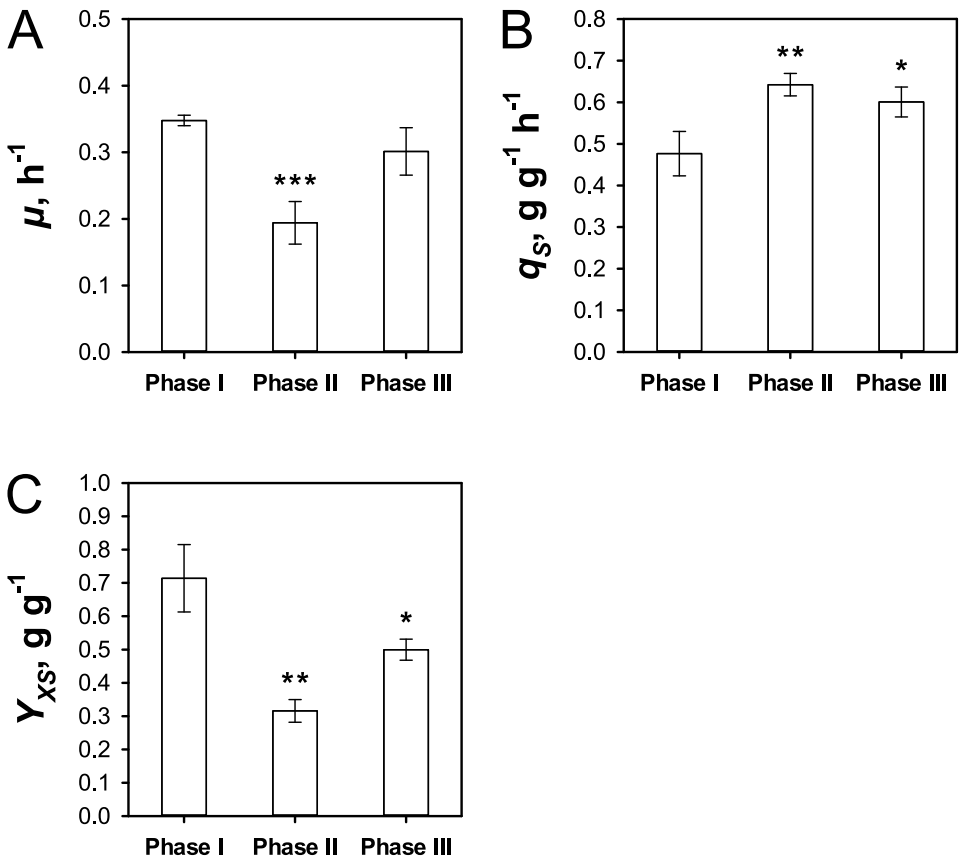

Fig. B.3: Characterization of process parameters (μ, q_S, and Y_{XS}) for *C. glutamicum* wild-type obtained under low CO_2/HCO_3^- concentrations illustrated for the three distinct growth phases indicated in Fig. B.1 B. **(A)** Growth rates (μ) were calculated for the exponential phase. Equivalently, **(B)** biomass specific glucose uptake rates (q_S) and **(C)** yield coeffcients of biomass per unit of consumed substrate (Y_{XS}) were calculated for each growth phase (I, II, and III) respectively. At least three independent experiments were performed showing the statistical mean with error bars that represent ±SD. Pairwise t-tests were performed for each process parameter of phase II and phase III compared to phase I. P-values indicate levels of significance as follows: $^{*}P < 0.05$, $^{**}P < 0.01$ and $^{***}P < 0.001$.

B.3.2 Enzyme activities and by-product formation

Enzyme activities were determined for selected carboxylating and decarboxylating reactions of the central metabolism of *C. glutamicum* WT including the PPP, the TCA, and the anaplerotic node (ANA; Fig. B.4 A). For at least three biological replicates, all three fermentation conditions (standard, high, and low CO_2/HCO_3^-) were sampled to calculate enzymatic reaction rates for growth phase I ($OD_{600} \approx 4$), phase II ($OD_{600} \approx 15$), and phase III ($OD_{600} \approx 41$). A threshold of 1.5 fold change compared to the reference state was defined as significant. In general, most activities remained unchanged. Also PPP-related enzyme activities of GPDH and PDGH were almost identical under standard and high CO_2/HCO_3^- levels. However GPDH and PDGH

activities were found to be changed most significantly: at low CO_2/HCO_3^- levels they almost doubled from $(0.079 \pm 0.009)\,U\,mg^{-1}$ and $(0.25 \pm 0.03)\,U\,mg^{-1}$ in phase I to $(0.15 \pm 0.01)\,U\,mg^{-1}$ and $(0.40 \pm 0.04)\,U\,mg^{-1}$ in phase II, respectively, and remained constantly high [$(0.12 \pm 0.01)\,U\,mg^{-1}$ and $(0.33 \pm 0.04)\,U\,mg^{-1}$, respectively] in phase III.

To elucidate whether different CO_2/HCO_3^- conditions induced by-product formation in *C. glutamicum* WT, sample supernatants were analyzed with respect to organic (data not shown) and amino acids (Fig. B.4 B). Organic acids were not secreted into the medium under any of the tested conditions. Only under low CO_2/HCO_3^- levels, L-alanine and L-valine production was observed (Fig. B.4 B), beginning at the transition from growth phase I to II with maximum concentrations after 10 h of $(3.86 \pm 0.59)\,mM$ and $(1.18 \pm 0.26)\,mM$, respectively. With increasing growth rates in phase III (Fig. B.3 A), L-alanine and L-valine concentrations decreased to $(1.23 \pm 0.71)\,mM$ and $(0.41 \pm 0.25)\,mM$ at the end of the fermentation.

B.4 Transcriptional analysis

B.4.1 Analysis under high carbon dioxide/bicarbonate levels

Following the protocol explained in the 'Material and Method' section, 117 genes (of which 33 encode membrane proteins) turned out to be significantly differentially transcribed in presence of high CO_2/HCO_3^- levels compared to standard conditions (supplementary data, Tab. BS.2). Among others, functional grouping identified the regulons RipA/DtxR, AcnR, LtbR, and respiration-specific genes, with a maximum 7.62-fold (sdhB) increased and about 14-fold (cg0471) decreased mRNA level. Interestingly, we observed a significant activation of the complete DtxR/RipA regulon (60 genes), controlled by DtxR as (dual transcriptional) master regulator involved in control of iron homeostasis in *C. glutamicum* (Fig. B.5 A). As suggested by Brune et al. (2006) and Wennerhold & Bott (2006), DtxR performs its global function also by altering expression of transcriptional regulators as *ripA*, which in turn trigger multiple responses. At high CO_2/HCO_3^- conditions, mRNA levels of *ripA* were about sixfold decreased (0.17). In accordance with results of Brune et al. (2006) and Wennerhold & Bott (2006) the repression of *ripA* by DtxR led to a derepression of target genes, which encode phosphotransacetylase and acetate kinase, and several iron-containing proteins, such as aconitase, isopropylmalate dehydratase, succinate dehydrogenase, nitrate reductase, catalase, and catechol 1,2-dioxygenase (Fig. B.5 A). To verify these findings, growth experiments at high CO_2/HCO_3^- levels were repeated with *C. glutamicum* $\Delta dtxR$ (Brune et al., 2006) and its parental WT. Under standard

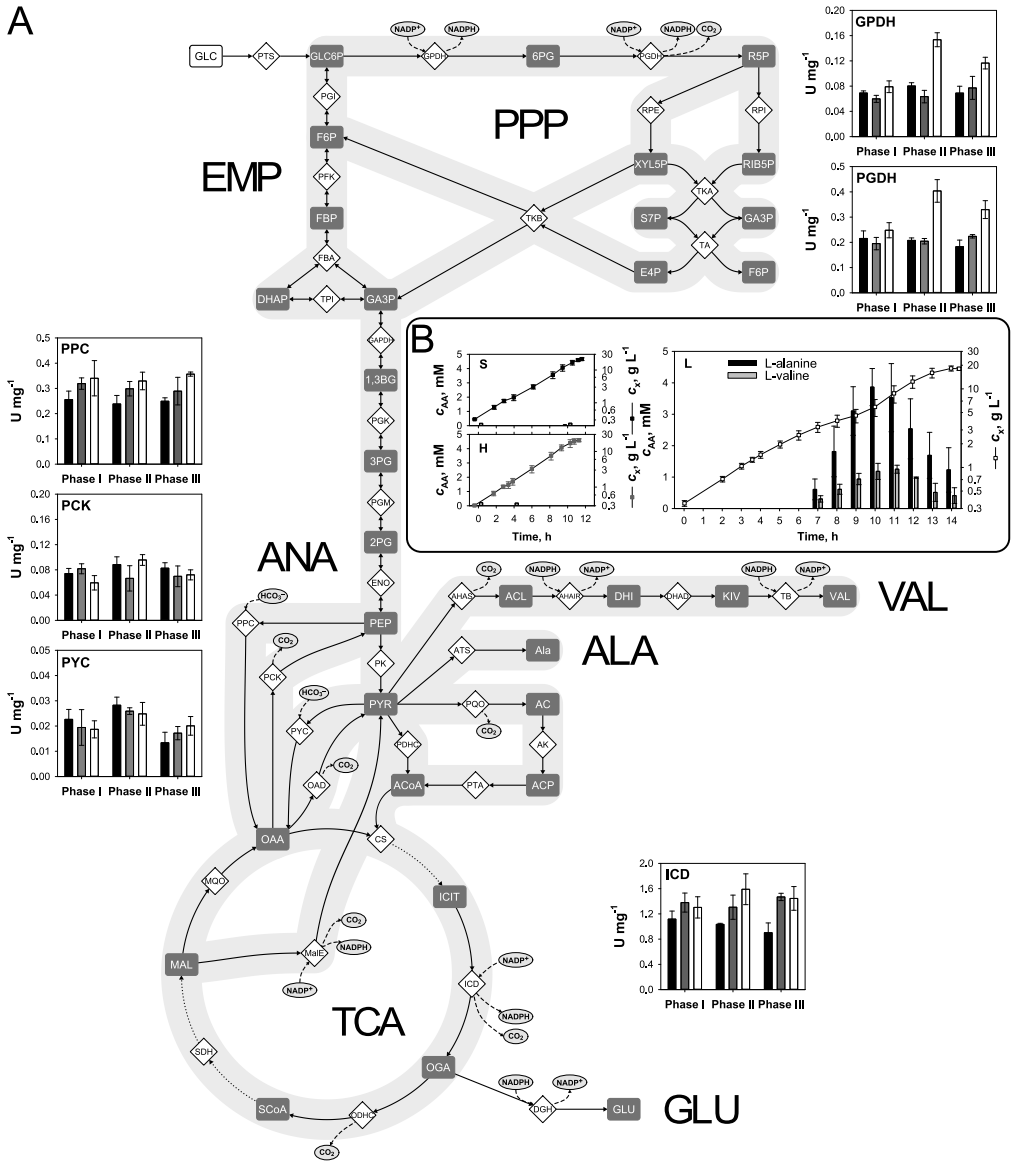

Fig. B.4: Schematic presentation of the central metabolism of *C. glutamicum* wild-type showing the Embden-Meyerhof-Parnas pathway (EMP), pentose phosphate pathway (PPP) and tricarboxylic acid cycle (TCA) connected by the various anaplerotic reactions (ANA). Besides, amino acid pathways are indicated for L-alanine (ALA), L-glutamate (GLU), and L-valine (VAL) biosynthesis. **(A)** Determined enzyme activities cover the anaplerotic branch from phosphoenolpyruvate (PEP) by carboxylating/decarboxylating reactions as PEP carboxylase (PPC), PEP carboxykinase (PCK) and pyruvate carboxylase (PYC). As representative of TCA and PPP, isocitrate dehydrogenase (ICD), as well as glucose-6-phosphate dehydrogenase (GPDH), and 6-phosphogluconate dehydrogenase (PGDH) activities were measured. Activities were determined under standard CO_2/HCO_3^- (black bars), high CO_2/HCO_3^- (dark gray bars) and low CO_2/HCO_3^- (open bars) levels, and are given for each growth phase (Fig. B.1 B). **(B)** By-product formation was followed for all three CO_2/HCO_3^--related fermentation conditions (S, standard; H, high; L, low). Where detectable, L-alanine (black bars) and L-valine (gray bars) concentrations are illustrated with the corresponding growth curve. At least three independent experiments were performed showing the statistical mean with error bars that represent ±SD.

conditions, both mutant and WT performed equivalently to the WT strain used in this study (data not shown). However, under enhanced CO_2/HCO_3^- conditions, a significant growth phenotype could be detected for *C. glutamicum* $\Delta dtxR$ with a 40 % decreased μ_{max} of $(0.29 \pm 0.03)\,h^{-1}$ compared to the wild-type (Fig. B.5 B). This result corroborates the findings of the transcriptional studies by implying the importance of DtxR and its regulative function in presence of increased CO_2/HCO_3^- conditions.

B.4.2 Analysis under low carbon dioxide/bicarbonate levels

Transcript analysis of phase I of low CO_2/HCO_3^- versus standard conditions only identified two genes (*citB* and cg1082) with increased and one gene (*purU*) with decreased mRNA level that just passed the predefined mRNA fold-change filtering with 2.22, 2.00, and 0.41, respectively (supplementary data, Tab. BS.3). Next, transcript patterns of phase II were compared with phase I. The analysis revealed 140 differentially expressed genes (of which 46 encode membrane proteins; 80 genes with increased and 60 genes with decreased mRNA level) belonging to the regulons Zur, McbR, Lrp, AcnR, PdxR, NrtR, ArnR, ArgR, AmrR, respiration-specific genes, and others (supplementary data, Tab. BS.4). Interestingly, we also found that almost all genes assigned to thiamin biosynthesis showed an increased mRNA level in phase II compared to phase I, including assembling pathways (*thiC*, *thiF*, *thiO*, *hmpK*, *thiD*, *thiG*, *thiM*, and *thiE*), putative transporter subunits (*ykoCDE*), and other genes potentially involved in thiamin biosynthesis (*chaA* and *oarX*; Fig. B.5 C; supplementary data, Tab. BS.4). Among them, *thiC* showed the highest expression rise (33-fold).

Finally, transcript levels of phase III were compared with measurements of phase I. In total, 102 genes showed a differential expression, ranging from a 53.08-fold (cg0041) increase to an about 4-fold (*fpr2*) decrease. Genes involved in respiration and in the regulons Zur, McbR, SsuR, and CysR were found to exhibit twofold expression changes or higher. Notably, the same gene setup of thiamin biosynthesis was found to be increased in phase III as in phase II (see above), even though, the overall level of over-expression generally decreased compared to phase II (Fig. B.5 C; supplementary data, Tab. BS.5).

B.5 Discussion

In large-scale fermentations, *C. glutamicum* is typically exposed to varying CO_2/HCO_3^- levels. Despite their putative impact on growth kinetics and cellular regulation, different CO_2/HCO_3^- levels were rarely investigated so far. Bäumchen et al. (2007) outlined

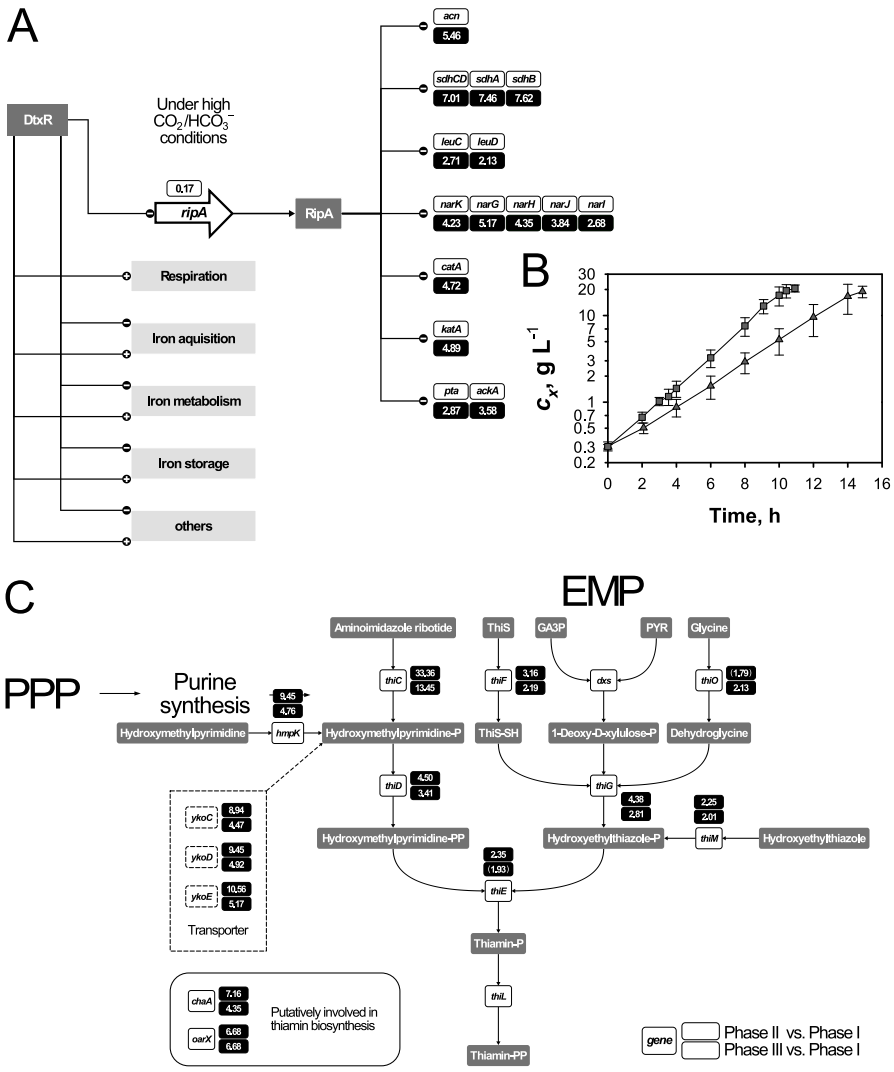

Fig. B.5: **(A)** Schematic presentation of the DtxR/RipA regulon. Transcriptional activation (+) and repression (−) are indicated. **(B)** *C. glutamicum* wild-type (dark gray squares) and *C. glutamicum* Δ*dtxR* (dark gray triangles) batch fermentations carried out at T = 30 °C, pH = 7.4, p = 1.5 bar in V = (1.0–1.1) L modified CGXII minimal salt medium containing 4 % (w/v) glucose in an elevated CO_2/HCO_3^- environment using Q/V = 0.5 vvm with 20 % CO_2 in the inlet gas flow. At least three independent experiments were performed showing the statistical mean with error bars that represent ±SD. **(C)** Schematic presentation of thiamin biosynthesis deduced from the genomic information of *C. glutamicum*. **(A/C)** Numbers in boxes give expressional changes (filled black box, increased mRNA level; open box, decreased mRNA level) of relevant genes identified by DNA microarray analysis from cells grown under high **(A)** and low **(C)** CO_2/HCO_3^- conditions in comparison to the standard approach, respectively. The figures represent a snapshot of the complete analysis. The detailed summary of all genes showing significantly altered expression is supplementary provided (Tab. BS.2–Tab. BS.5). The design for the DtxR/RipA regulon was modified after Wennerhold et al. (2005). The thiamin biosynthesis pathway in bacteria is illustrated corresponding to Du et al. (2011) and Rodionov et al. (2002). *Abbreviations*: *ackA*, acetate kinase; *acn*, aconitase; *catA*, catechol 1,2-dioxygenase; *chaA*, putative secondary Na^+/Ca_2^+ antiporter, Ca_2^+:cation antiporter (CaCA) family; *dxs*, probable 1-deoxyxylulose-5-phosphate synthase; GA3P, glyceraldehyde 3-phosphate; *hmpK*, predicted hydroxymethylpyrimidine kinase; *katA*, catalase; *leuCD*, 3-isopropylmalate dehydratase; *narKGHJI*, respiratory nitrate reductase; *oarX*, putative short chain dehydrogenase related to 3-oxoacyl-(acyl-carrier protein) reductase; PYR, pyruvate; *ripA*, transcriptional regulator; *sdhCDAB*, succinate dehydrogenase; *thiC*, phosphomethylpyrimidine synthase; *thiD*, phosphomethylpyrimidine kinase/thiamine-phosphate diphosphorylase; *thiE*, thiamine-phosphate diphosphorylase; *thiF*, sulfur carrier protein adenylyltransferase ThiF; *thiG*, thiazole synthase; *thiL*, thiamine-monophosphate kinase; *thiM*, hydroxyethylthiazole kinase; *thiO*, putative D-amino acid dehydrogenase; *thiS*, sulfur carrier protein; *ykoCDE*, thiamin-regulated ECF transporter for hydroxymethylpyrimidine.

that growth rates on glucose are almost unaffected up to 180 mbar pCO_2 showing a slight decrease of 10 % when 260 mbar pCO_2 were installed, and coherently decreased with further enhancing pCO_2 up to 800 mbar. We also observed constant growth rates of about 0.4 h^{-1} at pCO_2 between 40 mbar and 380 mbar, however, Bäumchen et al. (2007) observed higher growth rates (0.58 h^{-1}) at standard condition that are most likely the consequence of the different media composition and the experimental setup (turbidostatic culture). Besides, Y_{XS} values of our studies were slightly increased at high CO_2/HCO_3^- levels while q_S were almost unchanged. This phenomenon may mirror increased CO_2/HCO_3^- incorporation rates. However, additional enzyme activity measurements of anaplerotic reactions, the PPP, and the TCA did not unravel significant changes compared to standard conditions (Tab. B.5; Fig. B.1 B; Fig. B.2 A; Fig. B.4 A, B). The cellular response on the transcriptional level disclosed a complex adaptation to elevated CO_2/HCO_3^- levels – revealing a different regulation regime than found in e.g. *E. coli* (Baez et al., 2009) or *Pseudomonas putida* (Follonier et al., 2013): with the exception of *mez* encoding malic enzyme, neither genes coding for de-/carboxylating enzymes nor genes involved in acid or the general sigma factor-dependent stress response were significantly affected. However, we found a remarkable fraction of genes (28 %; i.e. 33 of 117 altered genes) coding for membrane proteins with altered expression levels. This portion is higher than the total fraction of annotated membrane proteins of the genome [22 %; Kalinowski et al. (2003)] and might mirror the cellular response on elevated CO_2/HCO_3^- levels with changes in membrane permeability and fluidity. Accordingly, Follonier et al. (2013) also observed this effect in microarrays with *P. putida* KT2440 exposed to increased pressure causing high CO_2/HCO_3^- levels. Noteworthy, significant expression changes are not restricted to high CO_2/HCO_3^- levels. At low CO_2/HCO_3^- conditions, about 33 % (i.e. 46 of 140 altered genes) of differentially expressed genes code for (putative) membrane proteins. This in turn indicates that low CO_2/HCO_3^- concentrations also affect the membrane properties leading to the observed transcriptional pattern. In this context we identified the intersection of commonly expressed genes encoding membrane proteins under high and low CO_2/HCO_3^- conditions of 39 % and 28 %, respectively (Fig. BS.1).

One striking observation is the transcriptional activation of the whole DtxR/RipA regulon in the presence of high CO_2/HCO_3^- concentrations. DtxR/RipA are controlling iron homeostasis in *C. glutamicum* (Brune et al., 2006; Wennerhold & Bott, 2006). According to the common understanding, the applied high CO_2/HCO_3^- level led to a regulatory response similar to iron excess with DtxR-mediated repression of several

genes encoding, e.g., siderophore uptake systems as well as *ripA*, which in turn results in a de-repression of genes encoding iron containing enzymes (with the exception of PTA and AK). Besides, expression of *katA* encoding catalase was found to be 5-fold increased anticipating oxidative stress, which was shown to occur at low pH conditions accompanied by activation of the iron starvation response (Follmann et al., 2009). However, no extracellular acid stress was installed in our experiments and in contrast to Follmann et al. (2009), we observed a transcriptional pattern similar to iron excess conditions, excluding the occurrence of intracellular acidic stress caused by the high CO_2/HCO_3^- environment. It might be speculated that enhanced transcription of *katA* points to oxidative stress caused by an increased TCA flux and respiration enforced by high CO_2/HCO_3^- levels, as proposed for *E. coli* where elevated CO_2 concentrations led to increased death rates due to exacerbated H_2O_2 stress (Ezraty et al., 2011). Accordingly, we found a slightly increased activity of ICD and significantly higher mRNA levels under high CO_2/HCO_3^- conditions of genes encoding succinate dehydrogenase, succinate-CoA ligase, aconitase, nitrate reductase, and cytochrome c oxidase (supplementary data, Tab. BS.2). However, other genes known to be involved in the SigM/SigH-dependent (Schröder & Tauch, 2010) or OxyR-related [*C. glutamicum* R; Teramoto et al. (2013)] oxidative stress response were not differently expressed. Noteworthy, we found 63 % increased Y_{XS} under high CO_2/HCO_3^- in the first half of the fermentation compared to standard conditions, which underlines the elevated cellular demand for TCA-based precursor supply for biomass formation. Besides, the impaired growth of the $\Delta dtxR$ mutant under elevated CO_2/HCO_3^- levels demonstrates that the master regulator DtxR is of importance for dealing with the applied conditions.

Low CO_2/HCO_3^- conditions ($pCO_2 < 40$ mbar) caused bi-level growth separated in three phases (I–III; Fig. B.1 B; Fig. B.3 B). This observation agrees with similar results of Kozliak et al. (1995) who found that growth of *E. coli* BUM015 was drastically reduced when aerated with CO_2 depleted air but which could be restored by addition of malate, succinate, or 2-ketoglutarate. The conclusion was drawn that biomass precursor supply via anaplerotic reactions was limiting at low CO_2/HCO_3^- levels and thus compensated by organic acid supply. To investigate which reaction of the anaplerotic node might be of relevance under low CO_2/HCO_3^- conditions, we deleted the genes encoding PCK, PPC, MalE, and PYC in *C. glutamicum* WT, respectively. All strains showed bi-level growth similar to the WT (supplementary data, Tab. BS.1). However, compared to the other strains *C. glutamicum* Δpyc showed a two times lower μ in phase II indicating an important role of PYC to replenish oxaloacetate under low pCO_2 conditions. Also the

significantly reduced μ of *C. glutamicum* Δ*pyc* under standard conditions underlines its importance for optimal growth as already shown by e.g. flux analysis [reviewed in Sauer & Eikmanns (2005)]. However, also the growth perturbation of the PCK, PPC, and MalE mutants under standard and high conditions indicates that the rather complex anaplerotic node of *C. glutamicum* represents a sensible and tightly balanced enzymatic network. Applying high CO_2/HCO_3^- conditions led to significantly re-increased growth rates of the mutant strains (excepting *C. glutamicum* Δ*ppc*), but not to WT level.

Notably, at equilibrium conditions of pH 7.4, HCO_3^- levels are about > 10-fold higher than those of dissolved CO_2. Decarboxylating reactions release CO_2 while HCO_3^- is typically incorporated via carboxylations. Due to the slow hydration reaction to HCO_3^-, high interexchange rates are required to meet cellular demands for growth not only in *E. coli* (Merlin et al., 2003) but also in *C. glutamicum* (Mitsuhashi et al., 2004). *C. glutamicum* possesses two genes (*bca* and *gca*) encoding β-type and γ-type carbonic anhydrases, respectively, with the former being essential during growth on glucose under ordinary atmospheric conditions (Mitsuhashi et al., 2004). Transcriptional analysis showed that expression of the *bca* gene is higher in the exponential growth phase than in the stationary and that in two L-lysine overproducing *C. glutamicum* strains the *bca* transcript is significantly more abundant than in the wild-type. This leads to the assumption that the higher demand of HCO_3^- for anaplerosis results in a transcriptional activation of the *bca* gene (Mitsuhashi et al., 2004). In contrast, in our study neither high nor low CO_2/HCO_3^- conditions including altering growth phases/rates under the low CO_2/HCO_3^- environment resulted in changed transcript levels of the *bca* or *gca* genes, indicating that both genes are constitutively expressed in *C. glutamicum* independent of the CO_2/HCO_3^- availability. The bi-level growth of *C. glutamicum* at low CO_2/HCO_3^- conditions was also characterized by a reduced Y_{XS} but significantly increased q_S during the transition phase between 5 h and 10 h (phase II; Tab. B.5). Obviously, carbon is rerouted from biomass formation to the excretion of L-alanine and L-valine (Fig. B.4 B). Maximum titers of about 1.5 mM L-alanine and 4 mM L-valine were determined at minimum growth before by-products decreased towards the end of the fermentation. Concurrently, about twofold increased GPDH and PGDH activities were detected in growth phase II compared to phase I (Fig. B.4 A) while the overexpression of almost all thiamin biosynthesis genes was determined (Fig. B.5 C) during the same period. Summarizing, the observed results indicate an increased flux into PPP ensuring improved precursor provision for the purine synthesis branch of the thiamin biosynthesis. As a consequence, not only CO_2 formation via PGDH but also exceptional amounts of

NADPH via GPDH and PGDH would be released that may be readily regenerated via the production of L-alanine and L-valine as described above (Fig. B.4 B). The excretion of both amino acids also anticipates an increased intracellular pyruvate pool, which serves as precursor for thiamin biosynthesis of the EMP branch as well (Fig. B.5 C). In summary, these results indicate that the lack of CO_2/HCO_3^- availability in *C. glutamicum* triggers transcriptional activation of thiamin biosynthesis probably leading to improved TPP availability. As a consequence TPP-dependent reactions such as acetohydroxyacid synthase, pyruvate and 2-ketoglutarate dehydrogenase complex, and pyruvate:quinone oxidoreductase are reinforced. Notably, these conversions release CO_2, which can be regarded as the cellular countermeasure to prevent too low CO_2/HCO_3^- levels finally limiting cell growth. Obviously this regulatory regime is part of *C. glutamicum* portfolio rendering the strain a robust industrial producer.

Acknowledgments

We thank Mira Lenfers-Lücker for the assistance with the HPLC analyses, Michaela Graf, Michael Ghosh, and Andreas Ulmer for the support in the bioreactor studies and the strain construction, Michael Kraml and Salaheddine Laghrami for the technical support, as well as Andreas Freund for the technical advice in carrying out the fermentation experiments. We also thank Eva Schulte-Berndt for the technical assistance in the microarray analyses. The authors further gratefully acknowledge the funding of this work by the Deutsche Forschungsgemeinschaft (DFG), grant TA 241/5-1.

BS.1 Supplementary methods

BS.1.1 Bacterial strain, pre-culture and media

Glycerol stocks were stored at −70 °C and 2 × TY agar plates were incubated at 30 °C for (48–60) h. A colony was then used to inoculate the first pre-culture of 5 mL 2 × TY medium incubated in glass reaction tubes for 8 h. All pre-cultures were incubated on a bench-top rotary shaker (Infors HT, Bottmingen, Switzerland) at 120 min^{-1} and 30 °C. 50 mL of overnight cultures were harvested at $4,500 \times g$ at 4 °C for 15 min (Eppendorf 5804 R, Eppendorf, Hamburg, Germany), prior to washing and inoculation of the bioreactor. Changes of the original composition of the CGXII medium after Eikmanns et al. (1991) were as follows: urea and 3-(*N*-morpholino)propanesulfonic acid (MOPS) were omitted and the concentrations of $(NH_4)SO_4$, K_2HPO_4, and KH_2PO_4 increased to

$10\,g\,L^{-1}$, $1\,g\,L^{-1}$, and $1\,g\,L^{-1}$, respectively. Besides, the medium contained 4 % (w/v) glucose as single carbon source, if not indicated otherwise.

BS.1.2 Strain construction

Isolation of plasmids from *E. coli* was performed as described previously (Eikmanns et al., 1994). Plasmid DNA transfer into *C. glutamicum* was carried out by electroporation and recombinant strains were selected on Luria-Bertani Brain Heart Infusion agar plates containing appropriate concentrations of kanamycin [$50\,\mu g\,mL^{-1}$; van der Rest et al. (1999)]. Chromosomal inactivation of the PPC gene *ppc*, the MalE gene *malE*, the PYC gene *pyc*, and the PCK gene *pck* in *C. glutamicum* WT was performed as described before using the plasmids pK19*mobsacB*-Δ*ppc*, pK19*mobsacB*-Δ*malE*, pK19*mobsacB*-Δ*pyc*, and pK19*mobsacB*-Δ*pck*. The replacement at the chromosomal locus was verified by Colony-PCR using primers ppcdel1/ppcdel2, Co-malE1/Co-malE1, pycfow1/pycrev1, and pckdel1/pckdel2, respectively (Blombach et al., 2008, 2011; Buchholz et al., 2013; Riedel et al., 2001).

BS.1.3 Bioreactor cultivation

Process conditions were set to $T = 30\,°C$ at a total pressure of $p = 1.5\,bar$ (piezoresistive probe PR-35 X HT, KELLER Druckmesstechnik, Jestetten, Germany) with initial starting volumes of $V = (1.0–1.1)\,L$ using 4 % inoculumn. The modified CGXII medium (see above) was set to pH 7.4 by adding 25 % (w/w) NH_4OH. The pH was maintained constant throughout the fermentation (pH probe: 405-DPAS-SC-K8S, Mettler-Toledo, Gießen, Germany). The bioreactor was sterilized in situ with 50 mM phosphate buffer for 20 min at 121 °C. After cooling, the buffer was removed, the CO_2 probe calibrated and the bioreactor aseptically filled with separately sterilized modified CGXII medium. Dissolved oxygen (pO_2) concentrations were recorded with on-line polarographic sensors (InPro®6800, Mettler-Toledo, Gießen, Germany) as percentage of air saturation. The levels were kept at $pO_2 \geq 20\,\%$ by cascadic increase of the agitation speed between $N = (300–1.500)\,min^{-1}$ and additionally by enhancing the volumetric gas flow rate (Q/V) if necessary (see below). Dissolved partial CO_2 pressures (pCO_2) were quantified after calibration by flushing the empty bioreactor with a defined CO_2 containing gas mixture between (10–20) %. In case of high CO_2/HCO_3^- level fermentations, the inoculation was delayed until the modified CGXII medium was equilibrated at pH 7.4 with the air/CO_2 gas mixture (indicated by constant pO_2/pCO_2 levels and pH titration stop). Notably, in

all cases, aeration rates were proportionally reduced to consider volume losses e.g. via sampling. Antifoam agent Struktol® J 647 (Schill + Seilacher, Hamburg, Germany) was added manually when required. Process control and data recording was performed by LabVIEW® 2009 SP1 (National Instruments, Austin, USA).

BS.1.4 Determination of the biomass concentration

CDW was detected in triplicate by pelleting 10 mL culture suspension in previously dried and measured glass centrifuge tubes at $4,000 \times g$ and 4 °C for 15 min (Megafuge 1.0R, Heraeus, Hanau, Germany). The cells were washed twice in 10 mL deionized water. Subsequently, the pellet was dried for at least 48 h in a convection drying oven (Heraeus, Hanau, Germany) at 120 °C, before it was finally weighed again.

BS.1.5 HPLC sample preparation

For the determination of amino acids, glucose, and organic acids, 1 mL of culture suspension was withdrawn from the bioreactor and centrifuged for 5 min at $13,000 \times g$ (Eppendorf 5417 R, Eppendorf, Hamburg, Germany). Then, the supernatant was filtered through 0.22 µm syringe filters (Rotilabo®, Carl Roth, Karlsruhe, Germany) and stored at −20 °C until further analysis. The determination of amino acids, glucose, and organic acids was performed as described previously by Buchholz et al. (2013), facilitating the quantification of amino acids reliably above about 0.5 mM in this study.

BS.1.6 Determination of enzyme activities

For determination of PPC, PCK, isocitrate dehydrogenase (ICD), glucose-6-phosphate dehydrogenase (GPDH), and 6-phosphogluconate dehydrogenase (PGDH) activities, cells from the bioreactor experiments were harvested by centrifugation for 10 min at $4,500 \times g$ at an OD_{600} of about 4, 15, and 41 corresponding to growth phase I, phase II, and phase III, respectively. Then, the cells were washed once with 25 mL 0.2 M Tris-HCL (pH 7.4), centrifuged again and resuspended in 0.5 mL of the same buffer. The cell suspension was transferred into 2 mL screw-cap vials together with 250 mg glass beads (diameter, 0.1 mm; Roth, Karlsruhe, Germany) and subjected to mechanical disruption three times for 30 s at 6,500 min^{-1} with a Precellys 24 (Peqlab, Erlangen, Germany) at room temperature with intermittent cooling on ice for 5 min. Intact cells and cell debris were removed by centrifugation for 15 min at $4,500 \times g$ and 4 °C. The supernatant was used for determination of the enzyme activities. Cells for determination of PYC

activity were re-suspended after washing (see above) in 0.1 M 4-(2-hydroxyethyl)-1-piperazineethanesulfonic acid (HEPES; pH 7.5) containing 20 % (v/v) glycerol to give an OD_{600} of about 150 corresponding to 45 g CDW L^{-1}.

All enzymes activities were determined by following the NAD(P)H consumption or formation at 340 nm in a spectrophotometer (Ultrospec 2100 pro, Biochrom, Cambridge, UK) at 30 °C.

Determination of the ICD activity was performed in cell-free extracts with DS-threo-isocitrate as substrate according to Eikmanns et al. (1995) with the exception that 0.1 M Tris-HCL (pH 7.6) was used instead of 0.1 M triethanolamine buffer (pH 7.6). One unit of activity is defined as 1 µmol NADPH formed per min.

PPC and PCK activity were assayed as described before by Mori & Shiio (1985) and Aich et al. (2003), respectively. One unit of activity is defined as 1 µmol NADH consumed per min for both assays.

Determination of GPDH and PGDH activity was performed in cell-free extracts with glucose 6-phophate or 6-phosphogluconate as substrate according to Moritz et al. (2000) with the exception that 0.2 M potassium glutamate in the reaction mixture was omitted. One unit of activity is defined as 1 µmol NADPH formed per min for both assays.

For determination of PYC activity the prepared cells (see above) were permeabilized with N-cetyl-N,N,N-trimethylammonium bromide (CTAB) as described by Peters-Wendisch et al. (1997) and directly applied to the assay according to Uy et al. (1999) with the exception that the reaction was stopped by heat (95 °C, 10 min) instead of addition of 30 % (w/v) ortho-phosphoric acid. The remaining pyruvate concentrations were determined enzymatically according to Lamprecht & Heinz (1983). One unit of PYC activity is defined as 1 nmol pyruvate consumed per min.

For all tested conditions at least three biological and two technical replicates were performed. The protein concentration was quantified with the Pierce BCA protein assay (Thermo Scientific, Waltham, MA, USA) with bovine serum albumin as standard. Assays were linear over time and proportional to the protein concentration.

BS.1.7 DNA microarray sample preparation

1×10^9 cells were sampled in previously cooled reaction tubes and harvested by centrifugation for 15 s at 0 °C and $12,100 \times g$ (Eppendorf MiniSpin, Eppendorf, Hamburg, Germany). After centrifugation, the supernatant was quickly discarded, the pellet immediately shock

frozen and stored at −70 °C for further analysis. The second sampling was carried out 10 min later and pooled with the predecessor prior to microarray hybridization.

BS.2 Supplementary tables

Tab. BS.1: Summary of process characteristics in CO_2-relevant batch cultivations of *C. glutamicum* ATCC13032 mutants under standard, high, and low CO_2/HCO_3^- levels. Aeration conditions, compositions, and corresponding process phase(s) are indicated. Fermentations were carried out at T = 30 °C, pH = 7.4, p = 1.5 bar in V = (1.0–1.1) L modified CGXII minimal salt medium containing 2 % (w/v) glucose.

	Condition	Standard	High	Low		
	Gas	Air	Air, 20 % CO_2	Air	Air	Air
	Q/V, vvm	0.1	0.5	3	3	3
Strain	Process phase	I–III	I–III	I	II	III
C. glutamicum WT	μ_{max}, h^{-1}	0.40	0.41	0.35	0.19	0.30
	Y_{XS}, $g\,g^{-1}$	0.56	0.61	0.71	0.32	0.50
C. glutamicum Δ*pck*	μ_{max}, h^{-1}	0.30	0.36	0.29	0.17	0.34
	Y_{XS}, $g\,g^{-1}$	0.57	0.59	0.53	0.46	0.60
C. glutamicum Δ*pyc*	μ_{max}, h^{-1}	0.30	0.37	0.28	0.09	0.26
	Y_{XS}, $g\,g^{-1}$	0.57	0.61	0.70	0.21	0.50
C. glutamicum Δ*ppc*	μ_{max}, h^{-1}	0.34	0.34	0.33	0.18	0.38
	Y_{XS}, $g\,g^{-1}$	0.52	0.58	0.79	0.39	0.57
C. glutamicum Δ*malE*	μ_{max}, h^{-1}	0.34	0.39	0.34	0.17	0.36
	Y_{XS}, $g\,g^{-1}$	0.52	0.62	0.73	0.38	0.68

Tab. BS.2: Gene expression in *C. glutamicum* under high CO_2/HCO_3^- levels compared to standard conditions in growth phase I. Genes listed below exhibit relative expression changes equal to or larger than twofold.

Locus Tag	mRNA ratio	Gene	Function(s)†
			RipA/DtxR Regulation
cg0159	0.34		Hypothetical protein
cg0160	0.31		Hypothetical protein
cg0177	0.40		Hypothetical protein
cg0228	3.39		Two-component system, sensory histidine kinase, putative pseudogene
cg0310	4.89	*katA*	Catalase
cg0445	7.01	*sdhCD*	Succinate dehydrogenase, subunit CD
cg0446	7.46	*sdhA*	Succinate dehydrogenase, subunit A
cg0447	7.62	*sdhB*	Succinate dehydrogenase, subunit B
cg0448	2.41		Conserved putative membrane protein
cg0466	0.30		Conserved putative secreted protein
cg0467	0.41		ABC-type putative hemin transporter, substrate-binding lipoprotein
cg0469	0.43		ABC-type putative hemin transporter, ATPase subunit
cg0470	0.09		Conserved secreted protein
cg0471	0.07		Conserved secreted protein
cg0527	0.39	*glyR*	Transcriptional activator of glyA, ArsR-family
cg0589	0.31		ABC-type putative iron-siderophore transporter, ATPase subunit
cg0590	0.32		ABC-type putative iron-siderophore transporter, permease subunit
cg0767	0.24		Siderophore-interacting protein
cg0768	0.19		ABC-type putative iron-siderophore transporter, ATPase subunit
cg0769	0.22		ABC-type putative iron-siderophore transporter, permease subunit
cg0770	0.29		ABC-type putative iron-siderophore transporter, permease subunit
cg0771	0.23	*irp1*	ABC-type putative iron-siderophore transporter, substrate-binding lipoprotein
cg0834	2.46	*tusE*	ABC-type trehalose transporter, substrate-binding lipoprotein
cg0921	0.21		Siderophore-interacting protein
cg0922	0.19		ABC-type putative iron-siderophore transporter, substrate-binding lipoprotein
cg0924	0.41		ABC-type putative iron-siderophore transporter, substrate-binding lipoprotein
cg1120	0.17	*ripA*	Putative transcriptional regulator, AraC-family
cg1312	2.95		Putative membrane protein
cg1341	2.68	*narI*	Respiratory nitrate reductase 2, gamma chain

. . . to be continued on the following page

Tab. BS.2: Gene expression in *C. glutamicum* under high CO_2/HCO_3^- levels compared to standard conditions in growth phase I. (continued)

Locus Tag	mRNA ratio	Gene	Function(s)†
cg1342	3.84	*narJ*	Respiratory nitrate reductase 2, delta chain
cg1343	4.35	*narH*	Respiratory nitrate reductase 2, beta chain
cg1344	5.17	*narG*	Respiratory nitrate reductase 2, alpha chain
cg1345	4.23	*narK*	Putative nitrate/nitrite permease, MFS-type
cg1405	0.48		Siderophore-interacting protein
cg1418	0.31		ABC-type putative iron-siderophore transporter, substrate-binding lipoprotein
cg1487	2.71	*leuC*	3-Isopropylmalate dehydratase, large subunit
cg1488	2.13	*leuD*	3-Isopropylmalate dehydratase, small subunit
cg1612	4.03		Putative acetyltransferase
cg1737	5.46	*acn*	Aconitate hydratase
cg1930	0.20		Putative secreted hydrolase
cg1931	0.23		Putative secreted protein
cg2137	2.39	*gluB*	ABC-type glutamate transporter, substrate-binding lipoprotein (TC 3.A.1.3.9)
cg2138	2.10	*gluC*	ABC-type glutamate transporter, permease subunit (TC 3.A.1.3.9)
cg2181	2.46		ABC-type putative dipeptide/oligopeptide transporter, substrate-binding lipoprotein
cg2183	2.25		ABC-type putative dipeptide/oligopeptide transporter, permease subunit
cg2184	2.31		ABC-type putative dipeptide/oligopeptide transporter, ATPase subunit
cg2234	0.40		ABC-type putative iron(III) dicitrate transporter, substrate-binding lipoprotein
cg2283	0.25		Conserved hypothetical protein
cg2422	2.55	*lipB*	Lipoyltransferase
cg2445	0.43	*hmuO*	Heme oxygenase (decyclizing)
cg2636	4.72	*catA*	Catechol 1,2-dioxygenase
cg2707	2.11		Conserved hypothetical protein
cg2777	0.30		Conserved putative membrane protein
cg2796	0.23		Conserved hypothetical protein, MMGE/PRPD-family, putative involved in propoinate catabolism
cg2836	5.31	*sucD*	Succinate-CoA ligase (ADP-forming), alpha subunit
cg2837	4.35	*sucC*	Succinate-CoA ligase (ADP-forming), beta subunit
cg3047	3.58	*ackA*	Acetate kinase
cg3048	2.87	*pta*	Phosphate acetyltransferase
cg3404	0.39		ABC-type putative iron(III) dicitrate transporter, substrate-binding lipoprotein
cg3407	0.50		Putative membrane protein

. . . to be continued on the following page

Tab. BS.2: Gene expression in *C. glutamicum* under high CO_2/HCO_3^- levels compared to standard conditions in growth phase I. (continued)

Locus Tag	mRNA ratio	Gene	Function(s)†
			Respiration (aerobic, anaerobic)
cg0445	7.01	*sdhCD*	Succinate dehydrogenase, subunit CD
cg0446	7.46	*sdhA*	Succinate dehydrogenase, subunit A
cg0447	7.62	*sdhB*	Succinate dehydrogenase, subunit B
cg1341	2.68	*narI*	Respiratory nitrate reductase 2, gamma chain
cg1342	3.84	*narJ*	Respiratory nitrate reductase 2, delta chain
cg1343	4.35	*narH*	Respiratory nitrate reductase 2, beta chain
cg1344	5.17	*narG*	Respiratory nitrate reductase 2, alpha chain
cg1345	4.23	*narK*	Putative nitrate/nitrite permease, MFS-type
cg2404	2.11	*qcrA1*	Rieske iron-sulfur protein
cg2405	3.14	*qcrC*	Cytochrome c1
cg2406	2.73	*ctaE*	Cytochrome c oxidase subunit 3
cg2891	0.49	*pqo*	Pyruvate:quinone oxidoreductase
cg3369	2.16	*qcrA2*	Putative rieske iron-sulfur protein
			AcnR Regulon (repressor of aconitase gene)
cg1737	5.46	*acn*	Aconitate hydratase
cg1738	2.79	*acnR*	Transcriptional repressor AcnR, TetR-family
			LtbR Regulon (leucine and tryptophan biosynthesis regulator)
cg1487	2.71	*leuC*	3-Isopropylmalate dehydratase, large subunit
cg1488	2.13	*leuD*	3-Isopropylmalate dehydratase, small subunit
			Others
cg0405	0.12		ABC-type putative iron(III) dicitrate transporter, substrate-binding lipoprotein
cg0465	0.31		Conserved putative membrane protein
cg0508	2.1		ABC-type putative spermidine/putrescine/iron(III) transporter, substrate-binding lipoprotein
cg0591	0.34		ABC-type putative iron-siderophore transporter, permease subunit
cg0748	0.29		ABC-type putative iron-siderophore transporter, substrate-binding lipoprotein
cg0755	0.49	*metY*	O-Acetylhomoserine sulfhydrylase
cg0759	2.35	*prpD2*	2-Methylcitrate dehydratase, involved in propionate catabolism (prpR regulon)
cg0926	0.5		ABC-type putative iron-siderophore transporter, permease subunit
cg0961	2.3		Putative hydrolase, alpha/beta-fold
cg0992	3.51		Putative permease, sulfate permease (SulP) family
cg0993	3.71		Putative transcriptional regulator, ArsR-family

. . . to be continued on the following page

Tab. BS.2: Gene expression in *C. glutamicum* under high CO_2/HCO_3^- levels compared to standard conditions in growth phase I. (continued)

Locus Tag	mRNA ratio	Gene	Function(s)†
cg1218	0.43		ADP-ribose pyrophosphatase
cg1291	0.43		Putative membrane protein
cg1299	2.1	*cydD*	ABC-type putative multidrug/protein/lipid transporter, ATPase and permease subunit
cg1370	2.97		Conserved hypothetical protein
cg1373	2.71		Putative glyoxalase
cg1419	0.3		Putative secondary Na^+/bile acid symporter, bile acid:Na^+ symporter (BASS) family
cg1540	2		Putative secreted protein
cg1626	0.22		Conserved hypothetical protein
cg1628	0.19		Putative hydrolase, alpha/beta superfamily
cg1658	0.36		Putative metabolite permease, MFS-type
cg1673	0.5	*ppmN*	Polyprenol-phosphate-mannose synthase domain 2
cg1695	2.23		putative antidote protein, HTH-motif XRE family
cg1852	0.45	*sdaA*	L-Serine dehydratase
cg1906	2.01		Hypothetical protein
cg2002	2.43		Hypothetical protein
cg2135	2.69	*miaB*	tRNA methylthiotransferase
cg2139	2.03	*gluD*	ABC-type glutamate transporter, permease subunit (TC 3.A.1.3.9)
cg2182	2.3		ABC-type putative dipeptide/oligopeptide transporter, permease subunit
cg2467	2.08		ABC-type transporter, ATPase subunit
cg2468	2.31		ABC-type transporter, permease subunit
cg2610	5.31		ABC-type putative dipeptide/oligopeptide transporter, substrate-binding lipoprotein
cg2674	0.47		Alkylhydroperoxidase, AhpD-family core domain
cg2675	0.49		ABC-type putative dipeptide/oligopeptide transporter, ATPase subunit
cg2676	0.41		ABC-type putative dipeptide/oligopeptide transporter, permease subunit
cg2677	0.47		ABC-type putative dipeptide/oligopeptide transporter, permease subunit
cg2778	2		Conserved hypothetical protein
cg2797	0.23		Conserved hypothetical protein
cg2896	2.23		Putative secreted protein, hypothetical endoglucanase
cg2949	2.25		Putative secreted protein
cg2962	0.38		Hypothetical protein, uncharacterized enzyme involved in biosynthesis of extracellular polysaccharides
cg3040	0.47		Putative epimerase

. . . to be continued on the following page

Tab. BS.2: Gene expression in *C. glutamicum* under high CO_2/HCO_3^- levels compared to standard conditions in growth phase I. (continued)

Locus Tag	mRNA ratio	Gene	Function(s)†
cg3045	0.48		ABC-type putative glutamine transporter, substrate-binding lipoprotein
cg3088	0.5	*arr*	Putative rifampin ADP-ribosyl transferase, putative pseudogene (N-terminal fragment)
cg3156	0.19		Putative secreted protein
cg3195	4.47		Putative flavin-containing monooxygenase
cg3198	2.46	*glpK*	Glycerol kinase
cg3207	2.07	*pheA*	Prephenate dehydratase
cg3226	2.62		Putative MFS-type L-lactate permease
cg3335	3.32	*mez*	Malate dehydrogenase (oxaloacetate-decarboxylating) ($NADP^+$)
cg3365	0.49	*rmpC*	Phosphotransferase system (PTS), putative ribitol/mannitol-specific enzyme IIC component

† refer to Kalinowski et al. (2003)

Tab. BS.3: Gene expression in *C. glutamicum* under low CO_2/HCO_3^- levels compared to standard conditions in growth phase I. Genes listed below exhibit relative expression changes equal to or larger than twofold.

Locus Tag	mRNA ratio	Gene	Function(s)†
			Others
cg0090	2.22	*citB*	Two-component system, transcriptional response regulator involved in regulation of citrate utilization
cg0457	0.41	*purU*	Putative formyltetrahydrofolate deformylase
cg1082	2		Putative membrane protein

† refer to Kalinowski et al. (2003)

Tab. BS.4: Gene expression in *C. glutamicum* under CO_2/HCO_3^- levels (growth phase II) compared to standard conditions (growth phase I). Genes listed below exhibit relative expression changes equal to or larger than twofold. Genes with transcriptional fold-changes in parentheses (mRNA ratio < 2) are just indicated for functional clarification.

Locus Tag	mRNA ratio	Gene	Function(s)†
			Thiamin Biosynthesis
cg0825	6.68	*oarX*	Putative short chain dehydrogenase related to 3-oxoacyl-(acyl-carrier protein) reductase

. . . to be continued on the following page

Tab. BS.4: Gene expression in *C. glutamicum* under high CO_2/HCO_3^- levels (growth phase II) compared to standard conditions (growth phase I) (continued)

Locus Tag	mRNA ratio	Gene	Function(s)†
cg1227	10.56	*ykoE*	Substrate-specific component YkoE of thiamin-regulated ECF transporter for hydroxymethylpyrimidine
cg1228	9.45	*ykoD*	Duplicated ATPase component YkoD of energizing module of thiamin-regulated ECF transporter for hydroxymethylpyrimidine
cg1229	8.94	*ykoC*	Transmembrane component YkoC of energizing module of thiamin-regulated ECF transporter for hydroxymethylpyrimidine
cg1230	9.45	*hmpk*	Predicted hydroxymethylpyrimidine kinase
cg1231	7.16	*chaA*	Putative secondary Na^+/Ca_2^+ antiporter, Ca_2^+:cation antiporter (CaCA) Family
cg1476	33.36	*thiC*	Phosphomethylpyrimidine synthase
cg1654	4.5	*thiD1*	Phosphomethylpyrimidine kinase/thiamine-phosphate diphosphorylase
cg1655	2.25	*thiM*	Hydroxyethylthiazole kinase
cg2236	2.35	*thiE*	Thiamine-phosphate diphosphorylase
cg2237	-1.79	*thiO*	Glycine oxidase
cg2238	3.07	*thiS*	Sulfur transfer protein involved in thiamine biosynthesis, ThiS-like
cg2239	4.38	*thiG*	Thiazole synthase
cg2240	3.16	*thiF*	Sulfur carrier protein adenylyltransferase ThiF
			Respiration (aerobic, anaerobic)
cg0129	2.07	*putA*	Proline dehydrogenase/delta-1-pyrroline-5-carboxylate dehydrogenase
cg0445	4.11	*sdhCD*	Succinate dehydrogenase, subunit CD
cg0446	4.41	*sdhA*	Succinate dehydrogenase, subunit A
cg0447	4.41	*sdhB*	Succinate dehydrogenase, subunit B
cg1341	2.77	*narI*	Respiratory nitrate reductase 2, gamma chain
cg1342	2.2	*narJ*	Respiratory nitrate reductase 2, delta chain
cg1343	3.46	*narH*	Respiratory nitrate reductase 2, beta chain
cg1344	3.46	*narG*	Respiratory nitrate reductase 2, alpha chain
cg1345	2.19	*narK*	Putative nitrate/nitrite permease, MFS-type
cg1769	2.16	*ctaA*	Cytochrome oxidase assembly protein
cg2192	2.45	*mqo*	Malate:quinone oxidoreductase
cg2403	2.69	*qcrB*	Cytochrome b
cg2404	2.91	*qcrA1*	Rieske iron-sulfur protein
cg2405	2.45	*qcrC*	Cytochrome c1
cg2406	2.71	*ctaE*	Cytochrome c oxidase subunit 3
cg2409	2.04	*ctaC*	Cytochrome c oxidase subunit II

. . . to be continued on the following page

Tab. BS.4: Gene expression in *C. glutamicum* under high CO_2/HCO_3^- levels (growth phase II) compared to standard conditions (growth phase I) (continued)

Locus Tag	mRNA ratio	Gene	Function(s)†
			Zur Regulon
cg0793	0.44		Putative secreted protein
cg1109	0.42	*porB*	Hypothetical protein
cg2261	3.78	*amtB*	Putative secondary ammonium transporter, Amt-family
cg2560	2.58	*aceA*	Isocitrate lyase
cg2911	2.36	*znuA1*	ABC-type putative Mn/Zn transporter, substrate-binding lipoprotein
cg2925	0.27	*ptsS*	Phosphotransferase system (PTS), sucrose-specific enzyme IIBCA component
			McbR Regulon
cg0012	0.45	*ssuR*	Transcriptional activator of sulfonate(ester) utilization, ROK-family
cg0310	3.58	*katA*	Catalase
cg0755	0.48	*metY*	O-Acetylhomoserine sulfhydrylase
cg0899	0.39	*pdxT*	pyridoxal 5'-phosphate (PLP) synthase subunit, glutamine amidotransferase
cg1214	0.48	*nifS2*	Putative cysteine desulfurase, AT class IV
cg1216	0.46	*nadA*	Quinolinate synthetase, subunit A
cg1218	0.42		ADP-ribose pyrophosphatase
cg1290	2.1	*metE*	5-Methyltetrahydropteroyltriglutamate-homocysteine methyltransferase
cg1476	33.36	*thiC*	Thiamine biosynthesis protein ThiC
cg2677	0.43		ABC-type putative dipeptide/oligopeptide transporter, permease subunit
cg2678	0.44		ABC-type putative dipeptide/oligopeptide transporter, substrate-binding lipoprotein
cg2833	0.18	*cysK*	Cysteine synthase
cg2925	0.27	*ptsS*	Phosphotransferase system (PTS), sucrose-specific enzyme IIBCA component
cg3048	2	*pta*	Phosphate acetyltransferase
			Lrp Regulon (Val, Ile, Leu sensing)
cg0314	2.91	*brnF*	Secondary branched-chain amino acid efflux transporter, LIV-E family, large subunit
			AcnR Regulon (repressor of aconitase gene)
cg1737	4.2	*acn*	Aconitate hydratase
cg1738	3.46	*acnR*	Transcriptional repressor AcnR, TetR-family

. . . to be continued on the following page

Tab. BS.4: Gene expression in *C. glutamicum* under high CO_2/HCO_3^- levels (growth phase II) compared to standard conditions (growth phase I) (continued)

Locus Tag	mRNA ratio	Gene	Function(s)†
			PdxR Regulon (activator or pyridoxal phosphate synthase genes)
cg0899	0.39	*pdxT*	pyridoxal 5'-phosphate (PLP) synthase subunit, glutamine amidotransferase
			NrtR Regulon (repressor of NAD biosynthesis genes)
cg1214	0.48	*nifS2*	Putative cysteine desulfurase, AT class IV
cg1216	0.46	*nadA*	Quinolinate synthetase, subunit A
			ArnR Regulon (dual regulator of anaerobic respiration)
cg1343	3.46	*narH*	Respiratory nitrate reductase 2, beta chain
cg1344	3.46	*narG*	Respiratory nitrate reductase 2, alpha chain
cg1341	2.77	*narI*	Respiratory nitrate reductase 2, gamma chain
cg1342	2.2	*narJ*	Respiratory nitrate reductase 2, delta chain
cg1345	2.19	*narK*	Putative nitrate/nitrite permease, MFS-type
			ArgR Regulon (repressor of arginine and glutamate biosynthesis genes)/FarR Regulon (repressor and arginine and glutamate biosynthesis genes)
cg0229	6.59	*gltB*	Glutamate synthase (NADPH), large chain (only in ArgR regulon)
cg1580	4.32	*argC*	N-acetyl-gamma-glutamyl-phosphate reductase
cg1581	3.36	*argJ*	Glutamate N-acetyltransferase
cg1582	4.03	*argB*	Acetylglutamate kinase
cg1583	2.81	*argD*	Acetylornithine aminotransferase, AT class II
cg1584	3.1	*argF*	Ornithine carbamoyltransferase
cg1585	2.85	*argR*	Transcriptional repressor of arginine biosynthesis, ArgR-family
cg1586	2.38	*argG*	Argininosuccinate synthase
cg1588	2.35	*argH*	Argininosuccinate lyase (only in FarR regulon)
			AmtR Regulon (repressor of nitrogen metabolism)
cg0115	2	*ureC*	Urease alpha subunit
cg0229	6.59	*gltB*	Glutamate synthase (NADPH), large chain (only in ArgR regulon)
cg0825	6.68	*oarX*	Putative short chain dehydrogenase related to 3-oxoacyl-(acyl-carrier protein) reductase
cg1109	0.42	*porB*	Hypothetical protein
cg1214	0.48	*nifS2*	Putative cysteine desulfurase, AT class IV
cg1227	10.56	*ykoE*	Putative membrane protein
cg1228	9.45	*ykoD*	ABC-type putative cobalt transporter, ATPase subunit
cg1229	8.94	*ykoC*	ABC-type putative cobalt transporter, permease subunit

. . . to be continued on the following page

Tab. BS.4: Gene expression in *C. glutamicum* under high CO_2/HCO_3^- levels (growth phase II) compared to standard conditions (growth phase I) (continued)

Locus Tag	mRNA ratio	Gene	Function(s)†
cg1230	9.45	*hmpK*	Conserved hypothetical protein
cg1231	7.16	*chaA*	Putative secondary Na^+/Ca_2^+ antiporter, Ca_2^+:cation antiporter (CaCA) Family
cg1783	2.75	*soxA*	Putative oxidase, pseudogene (N-terminal fragment)
cg1784	2.6	*ocd*	Putative ornithine cyclodeaminase
cg2261	3.78	*amtB*	Putative secondary ammonium transporter, Amt-family
cg2911	2.36	*znuA1*	ABC-type putative Mn/Zn transporter, substrate-binding lipoprotein
cg3281	0.49	*copB*	Putative Cu_2^+ transporting P-type ATPase
			Others
cg0018	0.26		conserved hypothetical membrane protein
cg0105	0.49		Hypothetical protein
cg0120	2.31		Putative hydrolase
cg0159	0.44		Hypothetical protein
cg0160	0.48		Hypothetical protein
cg0303	2.01	*leuA*	2-Isopropylmalate synthase
cg0405	0.46		ABC-type putative iron(III) dicitrate transporter, substrate-binding lipoprotein
cg0415	0.49	*ptpA2*	Putative protein-tyrosine-phosphatase
cg0464	0.48	*ctpA*	Putative Cu_2^+ transporting P-type ATPase
cg0465	0.45		Conserved putative membrane protein
cg0519	2		Putative phosphoglycerate mutase
cg0534	2.04		Putative integral membrane protein
cg0544	0.46		Putative membrane protein
cg0590	0.47		ABC-type putative iron-siderophore transporter, permease subunit
cg0591	0.43		ABC-type putative iron-siderophore transporter, permease subunit
cg0701	3.32		Putative secondary drug/ metabolite transporter, drug/metabolite transporter (DMT) superfamily
cg0756	0.13	*cstA*	Putative carbon starvation protein A
cg0768	0.5		ABC-type putative iron-siderophore transporter, ATPase subunit
cg0808	0.37	*wbpC*	Conserved putative membrane protein
cg0858	0.35		Putative secreted protein
cg0921	0.42		Siderophore-interacting protein
cg0922	0.33		ABC-type putative iron-siderophore transporter, substrate-binding lipoprotein
cg0936	0.29	*rpf1*	RPF-protein precursor
cg0963	2.19		Hypothetical protein
cg0980	0.44		Putative secreted protein, related to metalloendopeptidases

. . . to be continued on the following page

Tab. BS.4: Gene expression in *C. glutamicum* under high CO_2/HCO_3^- levels (growth phase II) compared to standard conditions (growth phase I) (continued)

Locus Tag	mRNA ratio	Gene	Function(s)†
cg1083	2.38	*cgtS10*	Two-component system, sensory histidine kinase
cg1129	6.87	*aroF*	Putative phospho-2-dehydro-3-deoxyheptonate aldolase
cg1130	3.27	*uppS1*	Putative undecaprenyl pyrophosphate synthetase
cg1167	0.35		Putative acetyltransferase, GNAT-family
cg1169	0.46	*metP*	Na^+:methionine symporter, neurotransmitter:sodium symporter (NSS) family
cg1281	2.19		ABC-type putative multidrug transporter, ATPase and permease subunit
cg1292	0.37		Flavin-containing monooxygenase 3
cg1348	0.38		Putative membrane protein, containing a CBS domain
cg1349	0.42		Putative membrane protein, containing a CBS domain
cg1370	2.97		Conserved hypothetical protein
cg1373	2.91		Putative glyoxalase
cg1457	2.16	*dnaQ2*	Putative DNA polymerase III, epsilon subunit
cg1478	4.82		Hypothetical protein
cg1626	0.48		Conserved hypothetical protein
cg1639	0.36		Putative membrane protein, containing a CBS domain
cg1640	0.39		Putative membrane protein, containing a CBS domain
cg1642	5.39		Siderophore-interacting protein
cg1658	0.37		Putative metabolite permease, MFS-type
cg1660	0.38		Putative membrane protein
cg1665	2.99		Putative secreted protein
cg1832	3.03		ABC-type putative iron-siderophore transporter, substrate-binding lipoprotein
cg1884	2.06		Putative membrane protein
cg1905	2.71		Hypothetical protein
cg1906	2.73		Hypothetical protein
cg2125	2.2	*uraA*	Putative xanthine/uracil symporter, nucleobase:cation symporter-2 (NCS2) family
cg2135	2.89	*miaB*	tRNA methylthiotransferase
cg2211	2		Putative membrane protein
cg2283	0.5		Conserved hypothetical protein
cg2348	2.41		Putative secreted protein
cg2402	0.26		Secreted protein NLP/P60 family
cg2445	2.1	*hmuO*	Heme oxygenase (decyclizing)
cg2539	0.49	*ectP*	Putative secondary glycine betaine/choline transporter, betaine/carnitine/choline transporter (BCCT) family
cg2610	2.55		ABC-type putative dipeptide/oligopeptide transporter, substrate-binding lipoprotein
cg2676	0.37		ABC-type putative dipeptide/oligopeptide transporter, permease subunit
cg2747	0.45		Putative secreted peptidase, M23/M37-family

. . . to be continued on the following page

Tab. BS.4: Gene expression in *C. glutamicum* under high CO_2/HCO_3^- levels (growth phase II) compared to standard conditions (growth phase I) (continued)

Locus Tag	mRNA ratio	Gene	Function(s)†
cg2796	0.32		Conserved hypothetical protein, MMGE/PRPD-family, putative involved in propoinate catabolism
cg2797	0.36		Conserved hypothetical protein
cg2838	0.43		Putative dithiol-disulfide isomerase
cg2959	0.48		Putative secreted protein
cg3047	3.29	*ackA*	Acetate kinase
cg3083	0.33		Putative secondary $Co_2^+/Zn_2^+/Cd_2^+$ efflux transporter, cation diffusion facilitator (CDF) family
cg3126	2.81	*tctB*	citrate uptake transporter, membrane subunit (citB regulon)
cg3141	0.36	*hmp*	Globin-like flavohaemoprotein, putative nitric oxide dioxygenase
cg3169	2.31	*pck*	Phosphoenolpyruvate carboxykinase (GTP)
cg3274	0.46		Putative DNA invertase, putative pseudogene
cg3277	0.5		Hypothetical protein, containing double-stranded beta-helix domain
cg3283	0.48		Hypothetical protein
cg3340	2.07	*dadA*	D-Amino-acid dehydrogenase
cg3395	0.28	*proP*	Putative proline/betaine permease, MFS-type
cg3399	0.22		Permease, MFS-type
cg3402	0.36		Putative Hg_2^+ permease, MerTP-family

† refer to Kalinowski et al. (2003)

Tab. BS.5: Gene expression in *C. glutamicum* under CO_2/HCO_3^- levels (growth phase III) compared to standard conditions (growth phase I). Genes listed below exhibit relative expression changes equal to or larger than twofold. Genes with transcriptional fold-changes in parentheses (mRNA ratio < 2) are just indicated for functional clarification.

Locus Tag	mRNA ratio	Gene	Function(s)†
			Thiamin Biosynthesis
cg0825	6.68	*oarX*	Putative short chain dehydrogenase related to 3-oxoacyl-(acyl-carrier protein) reductase
cg1227	5.17	*ykoE*	Substrate-specific component YkoE of thiamin-regulated ECF transporter for hydroxymethylpyrimidine
cg1228	4.92	*ykoD*	Duplicated ATPase component YkoD of energizing module of thiamin-regulated ECF transporter for hydroxymethylpyrimidine
cg1229	4.47	*ykoC*	Transmembrane component YkoC of energizing module of thiamin-regulated ECF transporter for hydroxymethylpyrimidine

. . . to be continued on the following page

Tab. BS.5: Gene expression in *C. glutamicum* under high CO_2/HCO_3^- levels (growth phase III) compared to standard conditions (growth phase I) (continued)

Locus Tag	mRNA ratio	Gene	Function(s)†
cg1230	4.76	*hmpK*	Conserved hypothetical protein
cg1231	4.35	*chaA*	Putative secondary Na^+/Ca_2^+ antiporter, Ca_2^+:cation antiporter (CaCA) Family
cg1476	13.45	*thiC*	Phosphomethylpyrimidine synthase
cg1654	3.41	*thiD1*	Phosphomethylpyrimidine kinase/thiamine-phosphate diphosphorylase
cg1655	2.01	*thiM*	Hydroxyethylthiazole kinase.
cg2236	-1.93	*thiE*	Thiamine-phosphate diphosphorylase
cg2237	2.13	*thiO*	Glycine oxidase
cg2238	2.71	*thiS*	Sulfur transfer protein involved in thiamine biosynthesis, ThiS-like
cg2239	2.81	*thiG*	Thiazole synthase
cg2240	2.19	*thiF*	Sulfur carrier protein adenylyltransferase ThiF
			Respiration (aerobic, anaerobic)
cg0445	2.51	*sdhCD*	Succinate dehydrogenase, subunit CD
cg0446	2.48	*sdhA*	Succinate dehydrogenase, subunit A
cg0447	2.31	*sdhB*	Succinate dehydrogenase, subunit B
cg2405	2.17	*qcrC*	Cytochrome c1
cg2406	2.07	*ctaE*	Cytochrome c oxidase subunit 3
cg3227	2.95	*lldD*	Quinone dependent L-lactate dehydrogenase
			Zur Regulon
cg0041	53.08		ABC-type putative manganese/zinc transporter, substrate-binding lipoprotein
cg0040	26.35		Putative secreted protein
cg2911	15.89		ABC-type putative Mn/Zn transporter, substrate-binding lipoprotein
cg0795	12.47		Putative oxidoreductase
cg0042	8.88		ABC-type putative manganese/zinc transporter, permease subunit
cg2912	8.88		ABC-type putative Mn/Zn transporter, ATPase subunit
cg0043	7.46		ABC-type putative manganese/zinc transporter, ATPase subunit
cg2913	6.32		ABC-type putative Mn/Zn transporter, permease subunit
cg0794	3.81		Putative GTPase, G3E-family
cg0793	3.53		Putative secreted protein
cg3139	2.35		Conserved hypothetical protein
cg3140	2.08	*tagA1*	DNA-3-methyladenine glycosylase I
cg2181	2.16		ABC-type putative dipeptide/oligopeptide transporter, substrate-binding lipoprotein

. . . to be continued on the following page

Tab. BS.5: Gene expression in *C. glutamicum* under high CO_2/HCO_3^- levels (growth phase III) compared to standard conditions (growth phase I) (continued)

Locus Tag	mRNA ratio	Gene	Function(s)†
cg3138	2.28		Band 7 domain-containing protein, stomatin/prohibitin homolog
			McbR Regulon
cg0012	0.38	*ssuR*	Transcriptional activator of sulfonate(ester) utilization, ROK-family
cg0095	3.01	*bioB*	Biotin synthase
cg0737	0.43	*metQ*	ABC-type methionine transporter, substrate-binding lipoprotein (TC 3.A.1.24.1)
cg0754	0.49	*metX*	Homoserine O-acetyltransferase
cg0755	0.35	*metY*	O-Acetylhomoserine sulfhydrylase
cg1147	0.47	*ssuI*	NAD(P)H-dependent FMN reductase
cg1218	0.48		ADP-ribose pyrophosphatase
cg1290	2.1	*metE*	5-Methyltetrahydropteroyltriglutamate-homocysteine methyltransferase
cg1376	0.43	*ssuD1*	FMNH2-dependent aliphatic sulfonate monooxygenase
cg1379	0.43	*ssuB*	ABC-type aliphatic sulfonate transporter, ATPase subunit
cg1476	13.45	*thiC*	Thiamine biosynthesis protein ThiC
cg2181	2.16		ABC-type putative dipeptide/oligopeptide transporter, substrate-binding lipoprotein
cg2675	0.49		ABC-type putative dipeptide/oligopeptide transporter, ATPase subunit
cg2678	0.29		ABC-type putative dipeptide/oligopeptide transporter, substrate-binding lipoprotein
cg2833	0.43	*cysK*	Cysteine synthase
cg3048	2.13	*pta*	Phosphate acetyltransferase
cg3107	0.42	*adhA*	Alcohol dehydrogenase
cg3114	0.48	*cysN*	Sulfate adenylyltransferase subunit 1
cg3115	0.43	*cysD*	Sulfate adenylyltransferase subunit 2
cg3116	0.37	*cysH*	Adenosine phosphosulfate reductase
cg3118	0.29	*cysI*	Ferredoxin-sulfite reductase
cg3119	0.26	*fpr2*	Ferredoxin-$NADP^+$ reductase
cg3138	2.28		Band 7 domain-containing protein, stomatin/prohibitin homolog
cg3226	4.41		Putative MFS-type L-lactate permease
cg3372	0.41		Conserved hypothetical protein
cg3374	0.35		Putative NADH-dependent flavin oxidoreductase
			SsuR Regulon
cg0012	0.38	*ssuR*	Transcriptional activator of sulfonate(ester) utilization, ROK-family

. . . to be continued on the following page

Tab. BS.5: Gene expression in *C. glutamicum* under high CO_2/HCO_3^- levels (growth phase III) compared to standard conditions (growth phase I) (continued)

Locus Tag	mRNA ratio	Gene	Function(s)†
cg1147	0.47	*ssuI*	NAD(P)H-dependent FMN reductase
cg1376	0.43	*ssuD1*	FMNH2-dependent aliphatic sulfonate monooxygenase
cg1379	0.43	*ssuB*	ABC-type aliphatic sulfonate transporter, ATPase subunit
cg1380	0.49	*ssuA*	ABC-type aliphatic sulfonate transporter, substrate-binding lipoprotein
cg2678	0.29		ABC-type putative dipeptide/oligopeptide transporter, substrate-binding lipoprotein
cg3114	0.48	*cysN*	Sulfate adenylyltransferase subunit 1
cg3115	0.43	*cysD*	Sulfate adenylyltransferase subunit 2
			CysR Regulon
cg0012	0.38	*ssuR*	Transcriptional activator of sulfonate(ester) utilization, ROK-family
cg0445	2.51	*sdhCD*	Succinate dehydrogenase, subunit CD
cg2675	0.49		ABC-type putative dipeptide/oligopeptide transporter, ATPase subunit
cg2676	0.44		ABC-type putative dipeptide/oligopeptide transporter, permease subunit
cg2833	0.43	*cysK*	Cysteine synthase
cg3114	0.48	*cysN*	Sulfate adenylyltransferase subunit 1
cg3115	0.43	*cysD*	Sulfate adenylyltransferase subunit 2
cg3116	0.37	*cysH*	Adenosine phosphosulfate reductase
cg3117	0.31	*cysX*	Ferredoxin-like protein, involved in electron-transfer
cg3118	0.29	*cysI*	Ferredoxin-sulfite reductase
cg3119	0.26	*fpr2*	Ferredoxin-$NADP^+$ reductase
cg3372	0.41		Conserved hypothetical protein
			Others
cg0018	0.27		conserved hypothetical membrane protein
cg0159	0.44		Hypothetical protein
cg0177	0.31		Hypothetical protein
cg0371	0.48	*cspB*	Cold-shock protein B
cg0387	0.46		Putative NAD/mycothiol-dependent formaldehyde dehydrogenase
cg0388	0.37		Putative Zn-dependent hydrolase
cg0464	0.42	*ctpA*	Putative Cu_2^+ transporting P-type ATPase
cg0747	0.46		Conserved hypothetical protein
cg0756	0.48	*cstA*	Putative carbon starvation protein A
cg0792	2.58		Hypothetical protein
cg0825	6.68		Putative short chain dehydrogenase related to 3-oxoacyl-(acyl-carrier protein) reductase
cg1081	2.01		ABC-type putative daunorubicin transporter, ATPase subunit

. . . to be continued on the following page

Tab. BS.5: Gene expression in *C. glutamicum* under high CO_2/HCO_3^- levels (growth phase III) compared to standard conditions (growth phase I) (continued)

Locus Tag	mRNA ratio	Gene	Function(s)†
cg1082	2.16		Putative membrane protein
cg1120	0.49	*ripA*	Putative transcriptional regulator, AraC-family
cg1129	2.36	*aroF*	Putative phospho-2-dehydro-3-deoxyheptonate aldolase
cg1273	2		Putative twin arginine targeting (Tat) Preprotein translocase subunit
cg1325	2		Conserved hypothetical protein
cg1426	0.44	*gst*	Putative glutathione S-transferase
cg1478	0.34		Hypothetical protein
cg1628	0.43		Putative hydrolase, alpha/beta superfamily
cg1658	0.48		Putative metabolite permease, MFS-type
cg1737	2.13	*acn*	Aconitate hydratase
cg1833	2.58		ABC-type putative iron-siderophore transporter, ATPase subunit
cg1883	2.1		Putative secreted protein
cg1884	3.01		Putative membrane protein
cg1940	0.4		Putative secreted protein
cg2133	0.48		Acetyltransferase, GNAT-family
cg2182	2.3		ABC-type putative dipeptide/oligopeptide transporter, permease subunit
cg2183	2.01		ABC-type putative dipeptide/oligopeptide transporter, permease subunit
cg2184	2.31		ABC-type putative dipeptide/oligopeptide transporter, ATPase subunit
cg2430	2.2		Hypothetical protein
cg2434	2.36		Putative monooxygenase, luciferase
cg2556	2.3		Putative integral membrane protein
cg2610	2.17		ABC-type putative dipeptide/oligopeptide transporter, substrate-binding lipoprotein
cg3022	0.44		Conserved hypothetical protein
cg3047	2.25	*ackA*	Acetate kinase
cg3083	0.31		Putative secondary $Co_2^+/Zn_2^+/Cd_2^+$ efflux transporter, cation diffusion facilitator (CDF) family
cg3281	0.43		Putative Cu_2^+ transporting P-type ATPase
cg3375	0.49		Predicted nucleoside-diphosphate-sugar epimerase
cg3381	0.5		Putative twin arginine targeting (Tat) Preprotein translocase subunit
cg3399	0.34		Permease, MFS-type
cg3402	0.43		Putative Hg_2^+ permease, MerTP-family

† refer to Kalinowski et al. (2003)

BS.3 Supplementary figures

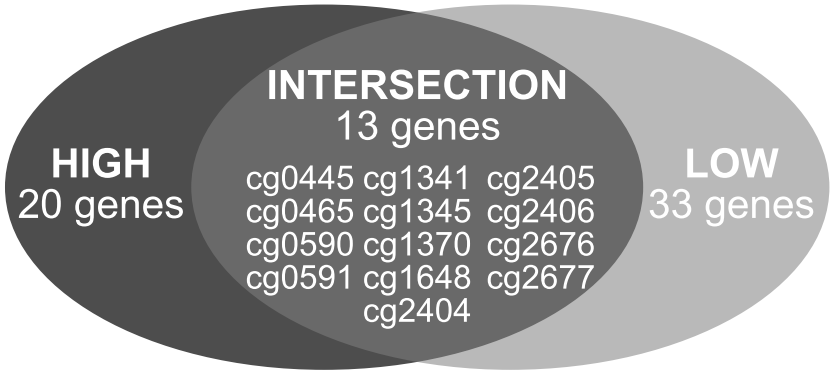

Fig. BS.1: This figure illustrates the intersection of genes encoding membrane proteins under high and low CO_2/HCO_3^- conditions.

C Manuscript III

Carbon balancing of microbial fermentations is a valuable tool for the evaluation of the process performance and to identify the presence of undesired by-products. In this study, we demonstrate the relevance of total carbon (TC) analysis for carbon balancing in fermentations with the wild-type of *Corynebacterium glutamicum* by (i) quantifying significant amounts of dissolved inorganic carbonic species (TIC) in the culture medium and (ii) determining the effective (mass) carbon content of the biomass fraction ($M_{C,X}$). In principle, TC based carbon balancing yielded at fully matching carbon balances. Thus, the application of our TC approach for the accurate detection of TIC and $M_{C,X}$ increased the total carbon recovery in standard batch fermentations with *C. glutamicum* on glucose from about 76 % to carbon closures of (94–100) % in contrast to conventional approaches. Besides, the origin of the missing 6 %-gap could be attributed to incomplete quantification of all carbon sources in the liquid phase. To conclude this study, the concept of TC-based balancing was transferred to an L-lysine production process, successfully quantifying relevant system carbon fractions, which resulted in matched carbon recoveries.

C.1 Introduction

Since its discovery by Lavoisier, the law of conservation of mass is an indispensable tool for balancing (bio-)chemical conversion processes. To analyze cultivations, for instance using microorganisms, particularly carbon (C-) balancing turned out to be a powerful approach for studying and evaluating the fate of C-containing educts (e.g. glucose) to C-containing products such as biomass, by-products, and gaseous carbon dioxide ($CO_{2,g}$). Accurate carbon balancing is essential for successful bioprocess development to qualify fermentation results properly. Based on closed C-balances, conclusions for optimizing strains and processes can be drawn, finally establishing high product yields and conversion rates. If carbon balances unravel gaps, they can point to non-balanced, maybe non-expected by-products or reveal the improper functioning of detection devices and analytics. Notably, C-balancing is not only a valuable reflection of the physiological understanding of any given process, but also the basis for advanced metabolic flux studies (Stephanopoulos et al., 1998; Wiechert, 2001; Zamboni et al., 2009).

[1]This chapter has been published as:
Buchholz, J, Graf, M, Blombach, B & Takors, R (2014). Improving the carbon balance of fermentations by total carbon analyses. *Biochem. Eng. J.* DOI: 10.1016/j.bej.2014.06.007 – in press.

Recovery calculations are based on mass balancing, consequently assuming that no further mass sinks or sources are considered except for those explicitly balanced. A commonly applied concept is the black box model balancing gaseous and liquid streams (containing cells) entering and leaving the boundary system as shown in Fig. C.1. Consequently, aerobic conversion of substrate to biomass and extracellular products can be written in C-mole notation as (Grosz & Stephanopoulos, 1983; Wang & Stephanopoulos, 1983; Wang et al., 1984):

$$\begin{aligned} \mathrm{C}_s\mathrm{H}_{a,s}\mathrm{O}_{b,s} + \lambda_n\mathrm{H}_{a,n}\mathrm{O}_{b,n}\mathrm{N}_{c,n} + \lambda\mathrm{O}_{2,g} - \lambda_x\mathrm{C}_x\mathrm{H}_{a,x}\mathrm{O}_{b,x}\mathrm{N}_{c,x} - \\ \sum_j \lambda_{p_j}\mathrm{C}_{p_j}\mathrm{H}_{a,p_j}\mathrm{O}_{b,p_j}\mathrm{N}_{c,p_j} - \lambda\mathrm{CO}_{2,g} - \lambda\mathrm{H}_2\mathrm{O} = 0 \end{aligned} \qquad [\mathrm{C.1}]$$

with s, n, x, and p_j encoding substrate, nitrogen source, biomass, and (by)-products, λ_i as (molar) stoichiometric coefficients and the subscripts (a, b, c, and d) as molar proportions of each element.

However, stoichiometric coefficients might be time-dependent, reflecting varying metabolic activities of the cells. Nevertheless, Eq. C.1 assumes that the elemental composition of the cell mass stays constant and that no further, unbalanced reactants or products occur (Liao, 1989; San & Stephanopoulos, 1984).

Usually, C-balancing is applied such that amounts of C-containing substrates are compared with measurements of liquid phase components (biomass and (by-)products) in addition to CO_2 of the exhaust gas. While this approach is commonly accepted and often applied, our contribution aims at pointing on the important aspect whether this balance fully covers all components.

One sensitive effector is the amount of CO_2 that is produced via cellular respiration. Unlike the rather poor solubility of O_2 in water, considerable amounts of CO_2 [which is about 30 times more soluble compared to O_2 at 30 °C (Carroll et al., 1991; Weiss, 1970)] are likely to dissolve in the fermentation medium during the cultivation process. Consequently, CO_2 and bicarbonate (HCO_3^-) levels may show significant accumulation and stripping dynamics, dependent on cellular metabolic activity and aeration conditions installed. To be precise, the inherent steady-state assumption of the C-balance may be invalid for a balancing interval due to transiently, non-balanced carbon sinks. Improper C-balance closures may be observed because measured carbon dioxide transfer rates (CTR) derived from exhaust analysis only give an incomplete picture of true carbon dioxide evolution rates (CER) of the biomass (Royce, 1992; Royce & Thornhill, 1991).

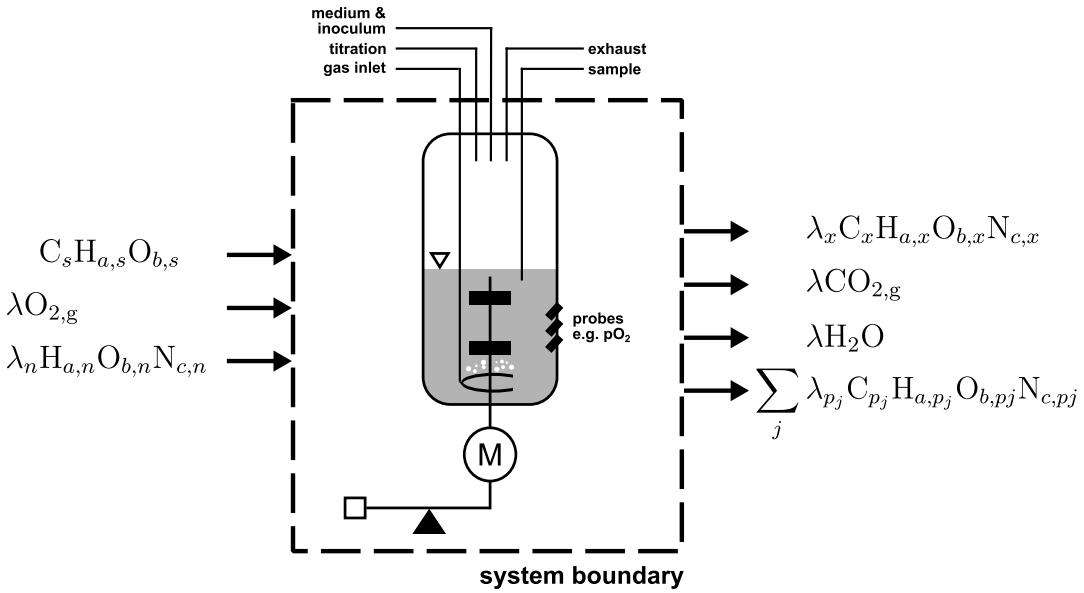

Fig. C.1: Flow sheet for the stoichiometry and mass balance of a routine (batch) fermentation with masses entering and leaving the system boundary on a C-mole basis. The chemical formulae of substrate, nitrogen source, biomass, and by-products are indicated by the corresponding identifier (s, n, x, and p_j) with λ_i as (molar) stoichiometric coefficient and the subscripts (a, b, c, and d) as molar proportion of each element.

This topic was basically addressed by analyzing exhaust gas signal dynamics (Bloemen et al., 2003; Wu et al., 2003) and elucidating physicochemical inter conversions of dissolved CO_2 to HCO_3^- and vice versa (Kovács et al., 2007; Spérandio & Paul, 1997). On that account, it should be considered that the dissociation equilibrium of CO_2 is complex, with the species carbonic acid (H_2CO_3), HCO_3^-, and the carbonate ion (CO_3^{2-}) being strongly pH dependent (Stumm & Morgan, 1996):

$$CO_{2,g} \rightleftarrows CO_{2,l} \qquad [C.2]$$

$$CO_{2,l} + H_2O \rightleftarrows H_2CO_3 \qquad [C.3]$$

$$H_2CO_3 \rightleftarrows HCO_3^- + H^+ \qquad [C.4]$$

commonly combining the hydration and protolysis of true H_2CO_3 to:

$$CO_{2,l} + H_2O \underset{k_{-1}}{\overset{k_1}{\rightleftarrows}} HCO_3^- + H^+ \quad , K_1 = \left(\frac{k_1}{k_{-1}}\right) = 10^{-6.3} \text{ mol L}^{-1} \qquad [C.5]$$

$$HCO_3^- \underset{k_{-2}}{\overset{k_2}{\rightleftarrows}} H^+ + CO_3^{2-} \quad , K_2 = \left(\frac{k_2}{k_{-2}}\right) = 10^{-10.3} \text{ mol L}^{-1} \qquad [C.6]$$

Hence, $CO_{2,l}$ forms the major portion at low pH < 5, whereas HCO_3^- is the dominating species at neutral pH 7–8. Consequently, a thorough C-balancing approach should consider all mentioned carbonic species, which can be achieved by total inorganic carbon (TIC) detection (Ho et al., 1987):

$$TIC = CO_{2,l} + H_2CO_3 + HCO_3^- + CO_3^{2-} \quad [C.7]$$

Notably, TIC measurement is an integral part of total carbon determination (TC) thus offering the opportunity to qualify carbon closures for the liquid phase (with and without biomass consideration) independent of additional $CO_{2,g}$ measurements.

Taken together, this contribution evaluates the improvement of TIC and TC measurements for total C-balancing. By studying representative batch fermentations with *Corynebacterium glutamicum* wild-type (WT) and L-lysine producer under highly dynamic conditions, it will be shown that TIC and TOC measurements significantly improve the balancing accuracy outlining that CO_2/HCO_3^- dynamics of the liquid phase and the quantification of the biomass carbon content severely affect carbon closure quality.

C.2 Materials and methods

C.2.1 Bacterial strain, pre-culture, media, and bioreactor cultivation

The WT strain *C. glutamicum* ATCC 13032 obtained from the American Type Culture Collection (ATCC, Manassas, VA, USA) and the L-lysine producer *C glutamicum* DM1933 (Blombach et al., 2009a) were used in this study. Glycerol stock seed cultures of the WT were grown on tryptone-yeast extract [2× TY; Sambrook et al. (2001)] agar plates and used to inoculate first pre-cultures of 5 mL 2× TY medium in glass reaction tubes, whereas 3.7 % (w/v) brain heart infusion (BHI) medium was used for the L-lysine producer, respectively. Subsequent seed cultures were grown overnight at 30 °C applying 100 mL modified CGXII minimal salt medium (see below) in 1,000 mL baffled shaking flasks at 140 min^{-1} on a bench-top rotary shaker (Infors HT, Bottmingen, Switzerland) and used to inoculate CGXII containing bioreactors, achieving initial biomass concentrations of $X_0 \geq 0.25\,g\,L^{-1}$. The modified CGXII minimal medium was prepared in accordance to Eikmanns et al. (1991) containing $10\,g\,L^{-1}$ $(NH_4)_2SO_4$, $5\,g\,L^{-1}$ urea, $21\,g\,L^{-1}$ 3-(*N*-morpholino)propanesulfonic acid (MOPS), $1\,g\,L^{-1}$ KH_2PO_4, $1\,g\,L^{-1}$ K_2HPO_4, $0.25\,g\,L^{-1}$ $MgSO_4 \cdot 7\,H_2O$, $10\,mg\,L^{-1}$ $CaCl_2 \cdot H_2O$, $10\,mg\,L^{-1}$ $MnSO_4 \cdot H_2O$,

16.4 mg L^{-1} Fe(II)$SO_4 \cdot 7\,H_2O$, 1 mg L^{-1} $ZnSO_4 \cdot 7\,H_2O$, 0.2 mg L^{-1} $CuSO_4 \cdot 5\,H_2O$, 0.02 mg L^{-1} $NiCl_2 \cdot 6\,H_2O$, and 0.2 mg L^{-1} biotin. *C. glutamicum* WT fermentations were carried out with 4 % (w/v), the L-lysine production process with 1 % (w/v) glucose. In both cases, urea and MOPS were omitted from bioreactor medium.

Duplicate batch fermentations of the WT and an exemplary L-lysine production process with initial starting volumes of V_R = 25 L using 2 % (v/v) inoculum were carried out at T = 30 °C at a total pressure of p = 1.5 bar in a stainless steel 100 L bioreactor (Bioengineering, Wald, Switzerland) with six-blade Rushton-type impellers and standard pH and dissolved oxygen (pO_2) sensor equipment (Blombach et al., 2013). Error bars of the respected state variables indicate their deviation from the mean, which was observed in the replicates. $pO_2 \geq 20\,\%$ was facilitated by cascadic increase of the agitation speed and initial volumetric gas flow rates of Q/V_R = 0.2 vvm. Exhaust gas analysis of O_2 and CO_2 was carried out with non-dispersive (photometric) infrared gas analyzers (BCP, BlueSens gas sensor GmbH, Herten, Germany). The antifoam agent Struktol® J 647 (Schill + Seilacher, Hamburg, Germany) with a carbon mass fraction of 61 % [(w/w) personal communication] was added manually when required. Process control and data recording was performed by LabVIEW® 2009 SP1 (National Instruments, Austin, USA).

C.2.2 Biomass determination, HPLC and total carbon analyses

Biomass (X) concentrations were quantified gravimetrically as cell dry weight (CDW in g L^{-1}) of triplicate samples as described previously (Blombach et al., 2013).

For the determination of amino and organic acids including glucose, culture suspension was withdrawn from the bioreactor and centrifuged for 5 min at 13,000 × g (Eppendorf 5417 R, Eppendorf, Hamburg, Germany). Then, the supernatant was filtered through 0.22 µm syringe filters (Rotilabo®, Carl Roth, Karlsruhe, Germany) and stored at −20 °C until further analysis.

The amino acid concentration was determined by reversed-phase HPLC using an Agilent 1200 Series apparatus (Agilent Technologies) equipped with an Agilent ZORBAX Eclipse Plus C18 column (250 × 4.6 mm, 5 µm) protected by an Agilent ZORBAX Eclipse Plus C18 guard column (12.5 × 4.6 mm, 5 µm). Fluorometric detection (excitation at 230 nm and emission at 450 nm) was carried out after automatic pre-column derivatization with *ortho*-phthaldialdehyde. The elution buffer consisted of a polar phase (10 mM Na_2HPO_4, 10 mM $Na_2B_4O_7$, 0.5 mM NaN_3, pH 8.2) and a non-polar phase (45 % (v/v) acetonitril, 45 % (v/v) methanol). Protocol details are given in Henderson & Brooks

(2010). Quantification of the analytes was conducted by using L-ornithine as internal standard to correct for analyte variability and by an 8-point calibration curve for each component as external reference standard.

Organic acid and glucose concentrations were measured via HPLC using an Agilent 1200 Series apparatus equipped with a Rezex ROA organic acid column H^+ (8 %) column (300 × 7.8 mm, 8 µm, Phenomenex), protected by a Rezex ROA organic acid column H^+ (8 %) guard column (50 × 7.8 mm). A protocol for phosphate precipitation was applied to each sample and standard prior to measurement. Thus, 45 µL 4 M NH_3 and 100 µL 1.2 M $MgSO_4$ were added to 1,000 µL sample. After 5 min of incubation, the sample was centrifuged for 5 min at 18,000 × g and RT. 500 µL supernatant were then transferred to 500 µL 0.1 M H_2SO_4. After thorough mixing and 15 min of incubation at RT, samples were finally centrifuged for 15 min at 18,000 × g at room temperature. Subsequently, the supernatant was provided for HPLC injection (10 µL injection volume). Separation was performed under isocratic conditions at 50 °C (column temperature) for 45 min with 5 mM H_2SO_4 as mobile phase at a constant flow rate of 0.4 mL min^{-1}. Detection of glucose and organic acids was achieved via an Agilent 1200 Series refractive index detector at 32 °C. Quantification of the analytes was conducted by using L-rhamnose as internal standard to correct for analyte variability and by an 8-point calibration curve for each component as external reference standard.

TIC and TOC contents in bioreactor samples were quantified with a TC analyzer (Multi N/C 2100s, Analytik Jena, Jena, Germany). The apparatus was operated in TOC mode using the differential detection method with the parallel measurement of (i) TIC and (ii) TC to determine the TOC amount of the sample (TOC = TC - TIC). First, 100 µL of diluted and prepared bioreactor samples (see below) were directly transferred to the TIC reactor freeing the carbonate-derived CO2 fraction by acidification with 10 % *ortho*-phosphoric acid. Second, 100 µL of the same sample were dosed into the combustion system operated with a furnace temperature of 750 °C converting both organic and inorganic carbon compounds to CO_2. For each detection, 3–4 individual measurements of 2–4 technical replicates were performed. CO_2 produced from thermal oxidation or acidification was then transferred into the measurement chamber by a constant carrier gas flow (O2) and was finally detected by non-dispersive infrared spectrometry (NDIR detector). For this purpose, the instrument was calibrated with a standard solution containing both 500 mg L^{-1} carbon from sodium carbonate and potassium hydrogen phthalate, producing a 14-point carbon calibration range of (0–500) mg L^{-1} for TIC and (0–1,000) mg L^{-1} for TC quantification.

To prevent the outgassing of $CO_{2,l}$ prior to detection, 1 mL of sample was immediately transferred to 20 mL graduated flasks containing 140 µL 5 N potassium hydroxide and deionized water, effectively increasing the basicity and thus shifting the carbonic acid equilibrium towards HCO_3^- and CO_3^{2-} (Grosz & Stephanopoulos, 1983; Wang et al., 1984).

For the quantification of biomass C-contents [$M_{C,X}$ in % (g g^{-1})] in the course of the fermentation, 2 mL samples were centrifuged for 10 min at 4 °C and 13,000 × g (Eppendorf 5417 R, Eppendorf, Hamburg, Germany) and were washed twice in 1 mL deionized water. The final pellet was subsequently re-suspended and transferred to 10 mL graduated flasks for volume correction.

C.2.3 Calculation of the carbon balance

C-recoveries [R_c in % (mol mol^{-1})] were calculated by balancing C-mole quantities (n) with regard to the boundaries depicted in Fig. C.1. For the analysis of the processes, three distinct quantifications were performed, applying the schematic overview of the C-species as illustrated in Fig. C.2.

Approach 'A': Integral substrate (S) based recoveries (R_c^S) covering the consumed glucose in the time interval from 0 to t were calculated as:

$$R_c^S = \frac{\Delta n_{X_{t-0}} + \Delta n_{TIC_{t-0}} + \Delta n_{other_{t-0}} + \Delta n_{\mathrm{CO_{2,g}}} + \left(\Delta n_{lys_{t-0}}\right)}{\Delta n_{S_{0-t}}} \times 100 \qquad [C.8]$$

with C-mole fractions of the liquid phase found in X, TIC, other (by-products), and L-lysine (*lys*; where applicable). Integral amounts of carbon in the exhaust gas were quantified from process start (t = 0 h) until process time t of the sample:

$$\Delta n_{\mathrm{CO_{2,g}}} = \int_0^t \left(\mathrm{CER}(t)\, V_R\right) dt \qquad [C.9]$$

with V_R = reaction volume (in L), and CER (in mmol L^{-1} h^{-1}).

Approach 'B': C-recoveries by TC analysis referenced the complete balance system (R_c^{Sys}) considering the gaseous (integral fraction in $n_{CO_{2,g}}$) and liquid phase ($n_{TC_{sample}}$ = $n_{TOC_t} + n_{TIC_t}$) of individual samples at process time t. R_c^{Sys} were calculated on the scale basis of TC amounts at process start t = 0 h ($n_{TC_{t=0}}$):

$$R_c^{Sys} = \frac{n_{TC_{sample}} + n_{\mathrm{CO_{2,g}}}}{n_{TC_{t=0}}} \times 100 \qquad [C.10]$$

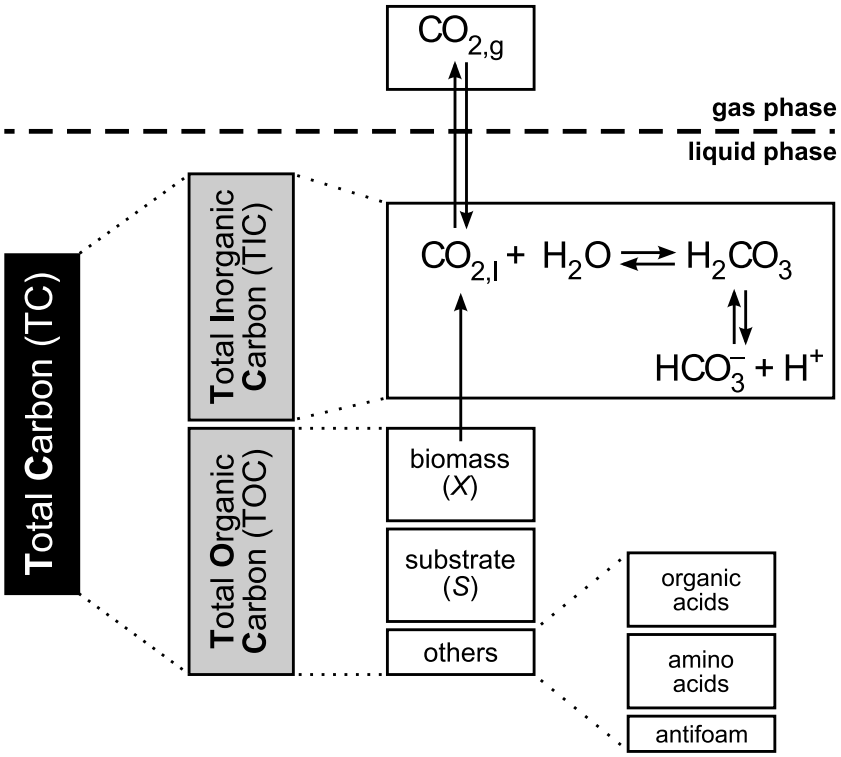

Fig. C.2: Schematic overview of the hierarchy of the different carbon species in the gas and liquid phase used to determine the carbon balances depicted in Fig. C.6.

Approach 'C': C-recoveries of individual samples were calculated with C-fractions found in the liquid phase only (R_c^L), setting the scale basis to the TC value of the corresponding sample equivalently withdrawn from the system at process time t ($n_{TC_{sample}}$):

$$R_c^L = \frac{n_{X_t} + n_{S_t} + n_{TIC_t} + n_{other_t} + \left(n_{lys_t}\right)}{n_{TC_{sample}}} \times 100 \qquad [C.11]$$

with 'other' indicating the sum of C-mole found in by-products and antifoam.

C.3 Results

Standard batch fermentations using *C. glutamicum* WT and L-lysine producer DM1933 were performed to investigate the potential of TC analysis for process characterization and C-recovery calculations. Duplicate bioreactor cultures (WT) were grown aerobically ($pO_2 > 20\,\%$; Fig. C.3) with rather low initial volumetric gas flow rates of $Q/V_R = 0.2\,\text{vvm}$ (Fig. C.4 B) in modified minimal CGXII medium with 4 % (w/v) glucose as sole C-source. After 10 h of cultivation, final biomass concentrations of about $X = 18.5\,\text{g}\,\text{L}^{-1}$

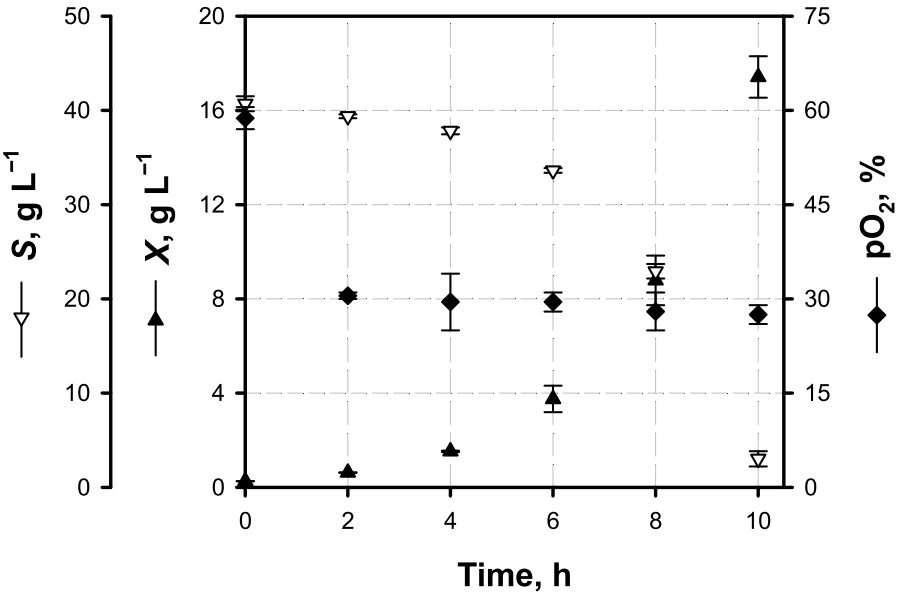

Fig. C.3: Illustration of the representative process parameters biomass (X), substrate concentration (S), and dissolved oxygen saturation (pO_2) in the course of both *C. glutamicum* WT batch fermentations performed under described condition. Process values obtained from both cultivations were averaged (symbols). Additionally, absolute deviations of the experimental measurements to the arithmetic mean of both fermentations (total range of measurements) were indicated by error bars.

were reached. During the exponential phase, growth rates of $\mu = 0.44\,h^{-1}$, biomass specific glucose consumption rates of $q_S = 0.91\,g\,g^{-1}\,h^{-1}$, and biomass to substrate yields of about $Y_{XS} = 0.48\,g\,g^{-1}$ were observed (data not shown). For the determination of the biomass-specific C-content $M_{C,X}$, a TOC in CDW vs. CDW correlation over the complete process was considered (Fig. C.5). A constant C-fraction in biomass of 51.4 % was found and used for all calculations.

To evaluate the impact of different balancing procedures on the quality of C-recovery closures, the following balancing approaches were performed (see section C.2.3): Procedure 'A' (Fig. C.6 A) compared the integral molar amounts of consumed glucose with liquid C-fractions found in X (n_X), total inorganic compounds (n_{TIC}), and (by)-products (n_{other}) and gaseous CO_2. Approach 'B' (Fig. C.6 B) based on liquid phase detection of total organic carbon (n_{TOC}) and n_{TIC}, plus the integral carbon from exhaust gas quantification ($n_{CO_{2,g}}$), whereas approach 'C' (Fig. C.6 C) omitted the latter, thereby focusing on the quantification of carbon in the liquid phase only. While the scale basis of 'A' was the total C-amount in S for a given time interval ($n_{S_{0-t}}$), 'B' and 'C' used TC values at process start $t = 0\,h$ ($n_{TC_{t=0}}$) or for individual samples at t as indicated ($n_{TC_{sample}}$), respectively.

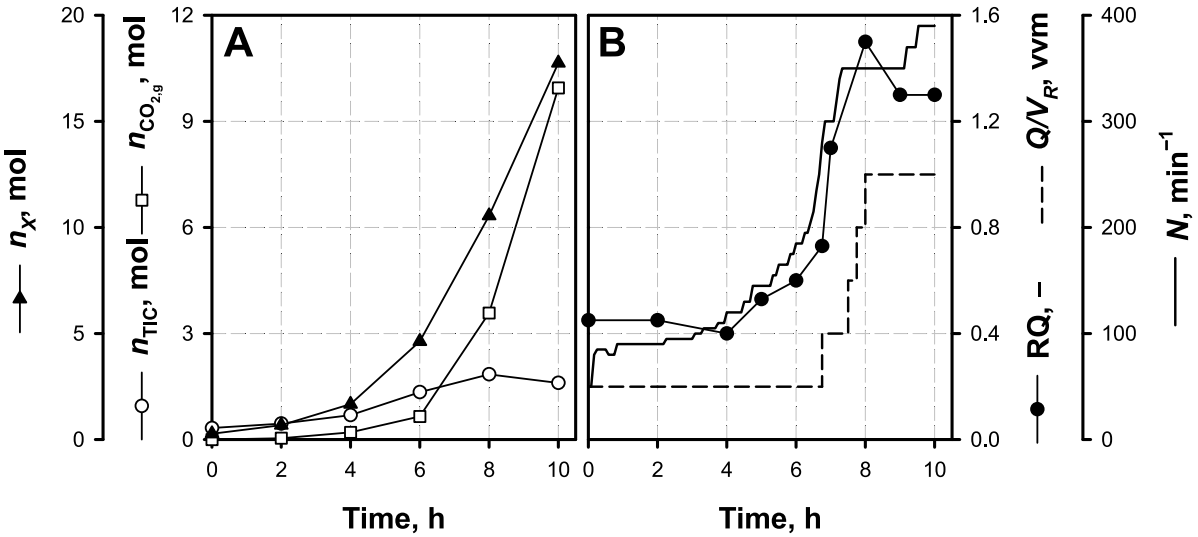

Fig. C.4: Illustration of selected process parameters of an exemplary *C. glutamicum* WT batch fermentation performed under described conditions. **(A)** Total molar carbon quantities (n) derived from biomass (n_X), total inorganic carbon (n_{TIC}), and exhaust gas analysis ($n_{CO_{2,g}}$). **(B)** Depiction of the volumetric gas flow rate (Q/V_R), agitation speed (N), and respiratory quotient (RQ).

Approach 'A': By analyzing the batch processes, C-recoveries (R_c^S) were calculated (Eq. C.8) covering the intervals from process start (t = 0 h) until 2 h, 6 h, and 10 h, respectively (Fig. C.6 A). As illustrated, the balancing considered the molar C-fractions of $n_{X_{t-0}}$, $n_{TIC_{t-0}}$, $n_{other_{t-0}}$, and $n_{\mathrm{CO_{2,g}}}$. C-closures achieved about (91–94) % match for all intervals. The C-fraction attributed to X comprised of (57–62) %, whereas the cumulative proportion of $n_{\mathrm{CO_{2,g}}}$ plus n_{TIC} was identified as (30–34) %. However, the fractions of liquid and gaseous CO_2 varied with time. During the first 6 h significantly high $\mathrm{CO_{2,l}}$ shares were identified via TIC analysis (Fig. C.4 A) contributing to (16–24) % of the total recovery (Fig. C.6 A). If balancing was expanded up to 10 h, the impact of the liquid species measured via TIC declined in favor of the gaseous amounts (Fig. C.4 A). This observation goes along with the low respiratory quotient (RQ) that was determined to be < 0.6 until 6 h of cultivation (Fig. C.4 B), followed by a sharp increase to levels > 1 after t = 7 h. Under aerobic conditions, *C. glutamicum* WT is known to produce no relevant amounts of by-products such as organic and amino acids (Blombach et al., 2013). Accordingly, only little side-product formation was detectable merely accounting for about <3 % of TC. At the end of the cultivation, about 2.5 mM of L-glutamate and <1.5 mM of e.g. L-cysteine and L-glycine were found.

Approach 'B': C-recoveries of the complete system were performed for individual samples on the basis of TC results at batch start (Eq. C.10). As illustrated in Fig. C.6 B,

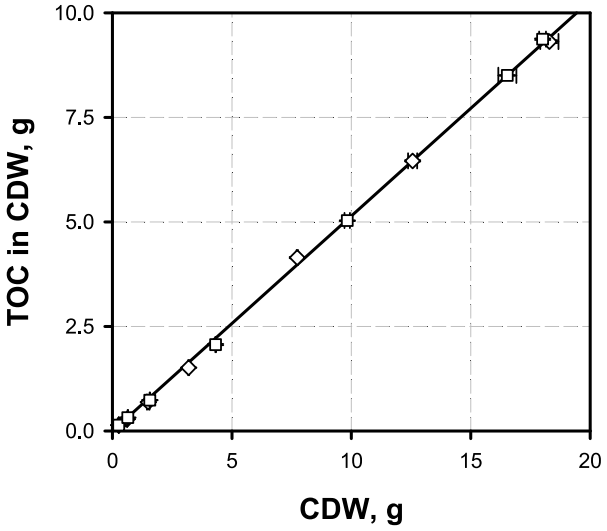

Fig. C.5: Correlation between the concentrations of total organic carbon (TOC) measured in washed biomass samples over the corresponding dried biomass (CDW) in the course of two *C. glutamicum* WT standard batch fermentation replicates (□/◇). The resulting mass fraction was determined to $M_{C,X}$ = 51.4 % and is indicated by the regression line (R^2 = 0.999). Error bars indicate the standard deviation of at least three technical replicates.

C-closures achieved high qualities between R_c^{Sys} = (97–100) % for all intervals. With increasing process time, the TOC covering C-fractions (represented by n_X, n_S, and n_{other}) decreased from >99 % to about 69 %, whereas the two CO_2-dependent C-fractions (n_{TIC} and $n_{CO_{2,g}}$) increased contrarily. These tendencies mirror increased cellular activities leading to enhanced (i) CO_2/HCO_3^- accumulation in the medium and (ii) CO_2 fractions in the exhaust gas, finally summing up to about 4 % and 26 %, respectively.

Approach 'C': For qualifying the C-closure of the biosuspension (i.e. the liquid phase) alone, we followed equation (Eq. C.11). Therefore, each sample was individually balanced (Fig. C.6 C) leading to distinct recoveries at 0 h, 2 h, 6 h, and 10 h. Similar to the TC based quantification of approach 'B' presented above, the complete C-amount measured via TC analysis served as reference. However, the scale basis was set to the TC value of the corresponding sample at process time t ($n_{TC_{sample}}$) and contrasted to C-fractions found in X, S, TIC, and by-products (other). Notably, antifoam also detectable via TC analysis was attributed to 'others' due to the individual distinction of the TOC-specific species in this case (Fig. C.2). Because C-amounts from exhaust gas quantification were omitted from consideration, the fractional percentages of the liquid categories n_{TIC} and n_{other} increased proportionally, resulting at final C-fractions of up to 6 %. As a mirror of biomass formation, the quantity of the C-fractions found in X and S almost reversed with time. While liquid C-recoveries of samples at 0 h, 2 h and 6 h can

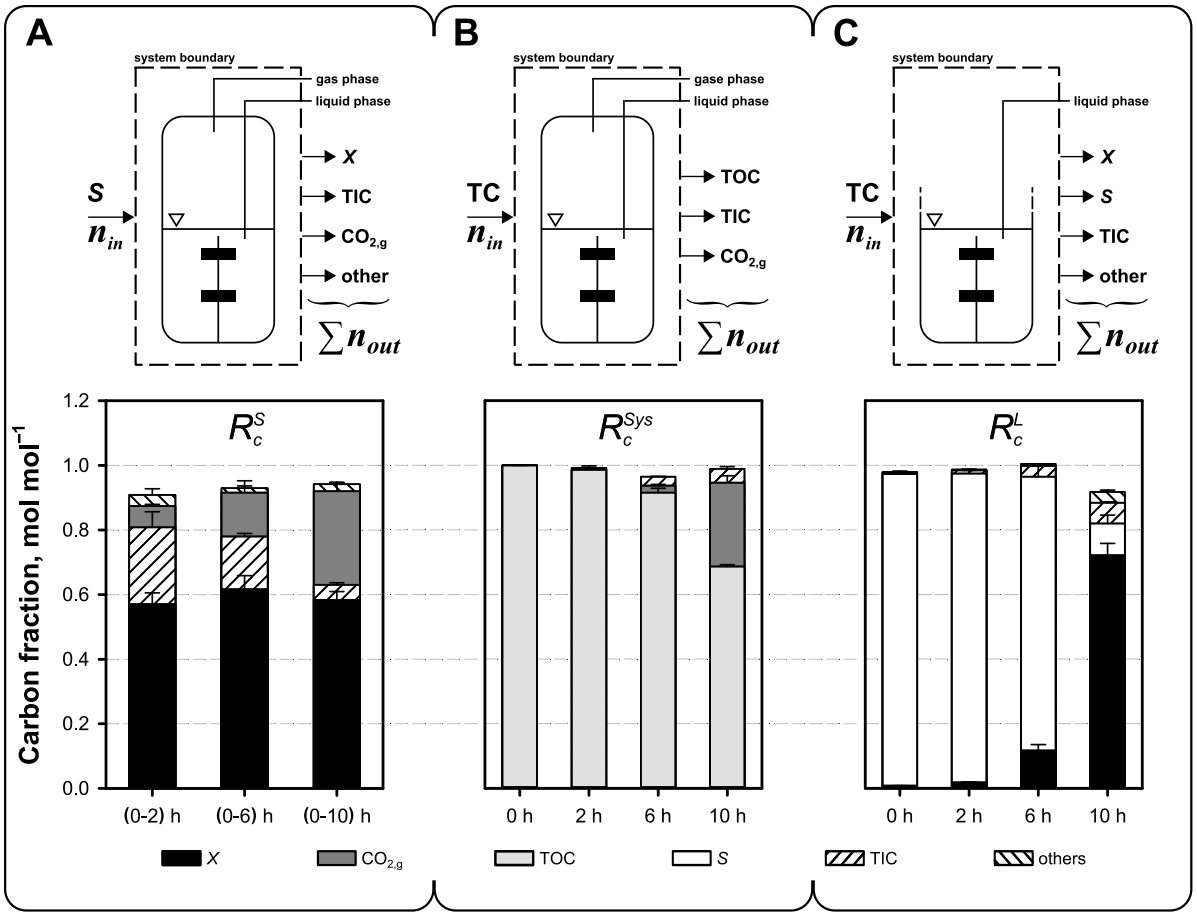

Fig. C.6: Carbon balancing calculated for both batch fermentations performed under described conditions. Recovery fractions obtained from both cultivations were averaged with error bars indicating the absolute deviation of the experimental measurements to the arithmetic mean (total range of measurements). **(A)** Balance (R_c^S) determined for recovered carbon found in biomass (X), exhaust gas ($CO_{2,g}$), total inorganic carbon (TIC), and by-products (others) on the basis of introduced substrate (glucose). **(B)** Carbon balance based on initially introduced TC (R_c^{Sys}) of the complete system for recovered carbon found in total organic carbon (TOC), TIC, and exhaust. **(C)** Recovery calculated for the liquid phase (R_c^L) on the basis of TC. Carbon fractions were recovered in X, substrate (S), TIC, and others (by-products and antifoam).

be qualified as successfully closed (R_c^L = (98–100) %), a balance gap of about 8 % was observed for the last sample (10 h).

We also applied the TC-based balancing approach on an L-lysine production process with *C. glutamicum* DM1933. The batch fermentation yielded an overall biomass to substrate yield of $Y_{XS} = 0.37\,\mathrm{g\,g^{-1}}$, a product to substrate yield of $Y_{PS} = 0.16\,\mathrm{g\,g^{-1}}$, and a growth rate of $\mu = 0.24\,\mathrm{h^{-1}}$ during the exponential phase (data not shown). The C-content of the biomass fraction was determined to $M_{C,X} = 44.0\,\%$ and all balancing approaches ('A', 'B', and 'C') as detailed above were identically applied. Closed overall R_c^S were

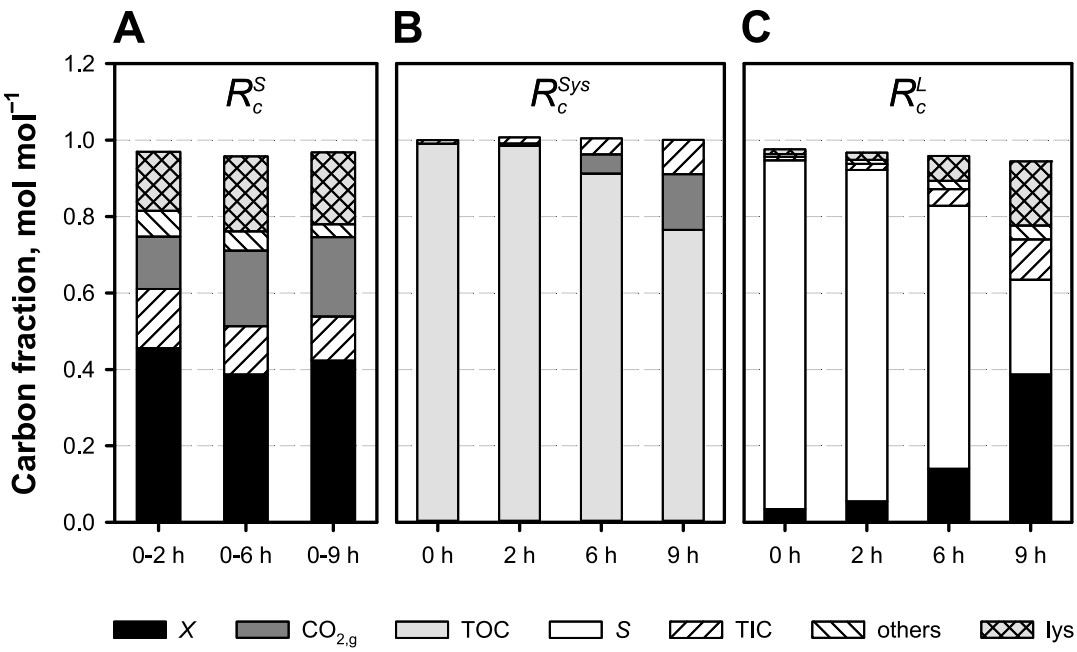

Fig. C.7: Exemplary carbon balancing of an L-lysine batch fermentation with *C. glutamicum* DM1933. **(A)** Balance (R_c^S) for recovered carbon found in biomass (X), exhaust gas ($CO_{2,g}$), total inorganic carbon (TIC), by-products (others), and L-lysine (lys) on the basis of applied substrate (glucose). **(B)** Carbon balance based on initially existing carbon detected via TC (R_c^{Sys}) and exhaust gas. **(C)** Recovery calculated for the liquid phase (R_c^L) on the basis of TC. Carbon fractions were determined in X, substrate (S), TIC, others (by-products and antifoam), and L-lysine.

determined to 97 % for time ranges until 2 h, 6 h, and 9 h of cultivation, respectively. With regard to the reduced Y_{XS} (compared to the WT), a decreased average C-fraction in X of about 42 % was found, whereas a similar cumulative proportion of $n_{CO_{2,g}}$ plus n_{TIC} with 31 % was identified (Fig. C.7 A). The highest TIC fraction with about 16 % was found at the beginning of the process, gradually decreasing until 12 % at the end of the culture. Contrarily, the C-fraction of the main product (L-lysine) reached a maximum of 19 % when balancing was expended to 9 h, whereas the by-product proportion accounts for about 3 %. In addition, calculated total system recoveries of individual samples between 0 h and 9 h were completely closed with an average of $R_c^{Sys} = (100 \pm 1)$ % (Fig. C.7 B). Similarly, by considering the n_{TIC} fraction in the liquid phase recovery, which accounts for a maximum proportion of >11 % at the end of the process (9 h), steadily decreasing balances from $R_c^L = 98$ % at process start (0 h) to about 94 % (9 h) were obtained (Fig. C.7 C). These results demonstrate that aside from biomass, CO_2 and L-lysine as main product, *C. glutamicum* DM1933 produces only minor amounts of by-products.

C.4 Discussion

A classical C-balance as demonstrated in Fig. C.6 A is a state-of-the-art tool to evaluate microbial production processes. Although the successful closure of the C-balance is occasionally demonstrated (Blankschien et al., 2010; Litsanov et al., 2012; Marx et al., 1996), the quality of the carbon match depends on the experimental framework: high cell density fed-batch or continuous cultivations usually benefit from high substrate quantities that are channeled through and converted by the cellular system within the fermenter. Therefore, in contrast to highly dynamic systems, common difficulties in the quantification of small deviations in uptake and production rates, and further inaccuracies of the detection facilities are of no or negligible consequence for the overall balance.

Furthermore, the use of accurate values for key parameters such as the C-fraction in biomass is crucial. For the wild-type strain *C. glutamicum* ATCC 13032, the common literature reference (Liebl, 1991) specifies the C-content with a rather large standard deviation of about 15 % to $M_{C,X} = (40.8–41.6)\,\%$. Notably, the data were derived from elemental analysis of cells grown in synthetic or complex medium different from that being used in this study. Besides, sampling details like cellular conditions, cell densities, or number of replicates were not indicated. In fact, the discrepancy of the literature data from the results in our experimental framework is about 25 % (Fig. C.5) and thus highly significant for the recovery calculation (Fig. C.6 A, C). Consequently, applying the 'standard' biomass composition leads to an underestimation of the biomass share in C-balancing. This effect is even more pronounced if the detection of TIC is omitted. Whether or not this TIC fraction plays a dominant role for C-balancing depends on the applied biological and technical environment. However, experimentalists should be aware of the potential impacts making it necessary to critically evaluate the experimental framework consisting of bacterial strains, medium, and process conditions individually. For instance, studies on the *C. glutamicum* strains ATCC 31833 and ATCC 21253 were reported with $M_{C,X} = (46.6–47.6)\,\%$ (Ikeda & Katsumata, 1999; Vallino & Stephanopoulos, 2000). In fact, the total C-recovery calculated for the interval of (0–10) h would significantly drop from 94 % to about 76 % corresponding to an absolute loss of carbon of about 18 %, if the additional information (measured TIC and $M_{C,X}$) generated in this study stays ignored.

Despite the enhancement of the conventional C-balance approach by TC analysis, about 6 % of all balanced carbon remains undetected ('A'). For this reason, approach 'B' referring to TC analysis of the complete system (Fig. C.6 B) was alternatively performed

to integrate the C-contents in liquid and gaseous phase. The results show that the quantification of the complete amount of carbon at any given process time in the liquid (via TC analysis) and gaseous phase [$CO_{2,g}$ integration (Eq. C.9)] is essential to achieve highly accurate C-closures during the course of the process. High C-recoveries averaging to about R_c^{Sys} = 99 % were achieved, which corroborates (i) the accurate integration of the data, (ii) the general capture of the total carbon in the system, and (iii) the functionality of exit gas and TC detection systems. Moreover, it could be shown that good matching recoveries of (98–102) % were achieved for the samples at 0 h, 2 h, 6 h, and 10 h if the scale basis of approach 'B' (Eq. C.10) was defined as total amount of carbon from substrate (n_{S_0}), data not shown).

Taken both previous approaches ('A', 'B') into account, to further investigate on the identification of the existing C-gap, balancing was solely focused on the liquid phase thus eliminating any additional impact of non-accurate n_{CO_2} quantification (Eq. C.11). This concept was followed by the balancing approach 'C' (Fig. C.6 C). The analysis of individual samples revealed closed balances of about R_c^L = (98–100) % until 6 h of cultivation. Sample analysis at 10 h showed that carbon could not be recovered completely resulting in a recovery loss of about 8 %, which corresponds to the observation obtained in the integral glucose based approach (Fig. C.6 A). Given that the thorough application of TIC and TOC measurements applied in approach 'B' succeeded in achieving complete C-recoveries, the conventional measurements for X, S, and by-products were identified as the source of non-complete C-detection. In this regard, TIC and TOC analysis not only enabled highest C-closure qualities but also pinpointed to necessary improvements of the conventional measurements of the liquid phase.

In the next step, we demonstrated the applicability of the different C-balancing approaches for an L-lysine production process using *C. glutamicum* DM1933. By integrating the TC analysis into the conventional C-balancing approach ('A'), the original C-gap of (12–16) % could now be successfully attributed to the n_{TIC} fraction finally achieving R_c^S = 97 % on average (Fig. C.7 A). In analogy to the WT studies, the accuracy of the approach was further confirmed by the determination of R_c^{Sys} to (100 ± 1) % (Fig. C.7 B). Finally, the findings of approach 'A' could be transferred to the quantification of the liquid phase ('C'). Via TC measurements, it was possible to quantify the otherwise missing C-fraction n_{TIC} in the liquid phase that accounts for >11 % (Fig. C.7 C), whereas undesired by-product formation was determined as a 4 % C-fraction. Notably, TC analysis prevents the false-positive allocation of C-gaps to by-product formation as well. Being able to assign and identify the n_{TIC} fraction prevents its putative consideration as a not

(yet) identified by-product that may cause additional research for its identification (3 %; Fig. C.7 A).

Taken together, this contribution demonstrates valuable insights acquired from TC analysis like the process quantification and monitoring of dissolved carbonic species in the fermentation medium and the determination of C-mass fraction of biomass throughout the cultivation. Moreover, TIC and TOC analyses are independent of conventional measurement techniques for X, S, and (by)-products, and can therefore serve to challenge, verify, and double-check respected findings. In case of existing C-gaps, the combination of all demonstrated approaches may be used to derive hints for advancing analytical approaches or point to targets for metabolic engineering. Concluding, the application of TC analysis is a valuable tool to improve the classical procedure of C-recovery calculations and is thus highly beneficial for the interpretation and determination of process data.

Acknowledgments

We thank Mira Lenfers-Lücker for the assistance with the HPLC analyses, as well as Salaheddine Laghrami and Andreas Freund for the technical support. The authors further gratefully acknowledge the funding of this work by the Deutsche Forschungsgemeinschaft (DFG), grant TA 241/5-1.

D Manuscript IV

The exploration of scale-down models to imitate the influence of large scale bioreactor inhomogeneities on cellular metabolism is a topic with increasing relevance. While gradients of substrates, pH, or dissolved oxygen are often investigated, oscillating CO_2/HCO_3^- levels, a typical scenario in large industrial bioreactors, is rarely addressed. Hereby, we investigate the metabolic and transcriptional response in Corynebacterium glutamicum wild type as well as the impact on L-lysine production in a model strain exposed to pCO_2 gradients of (75–315) mbar. A novel three-compartment cascade bioreactor system was developed and characterized that offers high flexibility for installing gradients and residence times to mimic industrial-relevant conditions, and provides the potential of accurate carbon balancing. The phenomenological analysis of cascade fermentations imposed to the pCO_2 gradients at industry-relevant residence times of about 3.55 min did not significantly impair the process performance, with growth and product formation being similar to control conditions. However, transcriptional analysis disclosed up to 66 differentially expressed genes already after 3.55 min under stimulus exposure, with the overall change in gene expression directly correlatable to the pCO_2 gradient intensity and the residence time of the cells.

D.1 Introduction

Industrial microbial biotechnology is regarded as a key technology with expected yearly revenues of more than $300 billion by 2030 (Festel, 2010; Neubauer, 2011). Following the economy-of-scale principle, the production of commodities yields at large scale production facilities in the range of (250–750) m^3 (Kelle, 2005). This scenario not only applies for already existing bioproducts such as amino and organic acids, vitamins or antibiotics serving the food, feed and pharma markets, but it is also likely to happen for newly developed products of the biofuel business. One industrial workhorse for large scale application is *Corynebacterium glutamicum*, a Gram-positive, facultative anaerobic bacterium (Liebl, 1991; Nishimura et al., 2007), which is used for large scale amino acid production (> 2 million tons-per-year) of L-glutamate and L-lysine [Ajinomoto "Food products and feed-use amino acid business", 2013; Takors et al. (2007)].

[1] This chapter has been submitted to *Applied Microbiology and Biotechnology* as:
Buchholz, J, Graf, M, Freund, A, Busche, T, Kalinowski, J, Blombach, B & Takors, R (2014). CO_2/HCO_3^- perturbations of simulated large scale gradients in a novel scale-down device cause fast transcriptional responses in *Corynebacterium glutamicum*.

Rapid bioprocess development is usually performed in bench-scale dimensions, thus the successful transfer of results from laboratory to industrial scale is of outmost importance. However, multiple biological, chemical, and physical impact factors are known that may severely hamper the successful scale-up (Garcia-Ochoa & Gomez, 2009; Hewitt & Nienow, 2007; Junne et al., 2012; Neubauer et al., 2013; Schmidt, 2005; Takors, 2012). Among those are dissolved gas levels in the micro-environment of the cells. Increased gas solubilities (compared to lab-scale) are found at the bottom of industrial bioreactors as the consequence of high operating head and hydrostatic pressures (Junker, 2004; McIntyre & McNeil, 1997). They lead to vertical gradients of dissolved oxygen (pO_2) and carbon dioxide (pCO_2) (Lara et al., 2006a), which are superimposed by radial gradients as the result of metabolic activities, limited transfer and mixing qualities with blend times of about 240 s commonly found at industrial scale (Junker, 2004; Mayr et al., 1994). Consequently, cells fluctuating in inhomogeneous large scale stirred tank reactors (STR) are continuously subjected to significant micro-environmental changes. In this regard, only few comprehensive studies aimed at identifying their impact on cellular performance *in-situ* (Bylund et al., 1998; Enfors et al., 2001; Hewitt et al., 2000; Larsson & Enfors, 1988).

Alternatively, various scale-down devices representing a multi-compartmented STR (Schilling et al., 1999), two-compartment STR-STR (Oosterhuis et al., 1985), or the most commonly applied STR-PFR [plug flow reactor; George et al. (1993); Hewitt et al. (2000); Junne et al. (2011)] were developed to simulate industrial-like conditions at lab-scale [reviewed in Lara et al. (2006a), Neubauer & Junne (2010), and Takors (2012)]. These systems were used to monitor metabolic responses like biomass-substrate yield, substrate uptake, and (by-) product formation while imposing inhomogeneities with respect to pO_2, pH, or substrate (Amanullah et al., 2001; Hewitt et al., 2007; Junne et al., 2011; Sandoval-Basurto et al., 2005). Furthermore, transcriptional and flow cytometry analyses were performed complementary (Delvigne et al., 2009, 2010, 2011; Käß et al., 2013, 2014; Lara et al., 2006b; Schweder et al., 1999).

Compared to these classical stimuli, the consequences of changing pCO_2 levels are rarely studied so far. This finding may surprise considering that dissolved CO_2 level together with the carbonic acid intermediate bicarbonate (HCO_3^-) are responsible for metabolic interactions (as substrates or products of de-/carboxylating reactions) and they are linked with detrimental effects concerning cell vitality, growth, membrane integrity, metabolism, and productivity as reported for high CO_2/HCO_3^- levels (Amoabediny & Büchs, 2010; Amoabediny et al., 2010; Baez et al., 2009, 2011; Castan et al., 2002;

El-Sabbagh et al., 2006, 2008; Jones & Greenfield, 1982; McIntyre & McNeil, 1997). Recently, our own studies outlined the fundamental impact of low ($pCO_2 < 40$ mbar) or high ($pCO_2 \geq 300$ mbar) CO_2/HCO_3^- levels on the transcriptional regulation in *C. glutamicum* (Blombach et al., 2013). While these effects were observed under pseudo-steady state conditions, the question arises whether transcriptional responses will also be found envisaging the typical dynamic heterogeneities of a large scale bioreactor. Studying this question demands for an experimental setup that enables to link unequivocally transcriptional responses to imposed CO_2 stimuli under large scale-like, dynamic bioreactor conditions. The classical STR-PFR approach is only partially suitable because it is limited in its ability to distinctly control multiple pCO_2 conditions and to balance the same in the PFR module. Consequently, we developed a novel three-compartment (STR-STR-STR) bioreactor cascade that allows to install multiple pCO_2 scenarios in the cascade, decoupled from metabolic activity additionally mimicking insufficient mixing qualities by applying pre-defined residence times.

Taken together, this contribution describes the novel technical approach and shows its successful application by identifying short-term transcriptional responses on dynamic pCO_2 levels in *C. glutamicum* for the first time.

D.2 Materials and methods

D.2.1 Bacterial strain, pre-culture and media

The wild-type (WT) strain *C. glutamicum* ATCC13032 obtained from the American Type Culture Collection (ATCC, Manassas, VA, USA) and the L-lysine producer *C. glutamicum* DM1933 (Blombach et al., 2009a) were used in this study. Glycerol stock seed cultures of the WT were grown on tryptone-yeast extract [2× TY; Sambrook et al. (2001)] agar plates and used to inoculate first pre-cultures of 5 mL 2× TY medium in glass reaction tubes, whereas 3.7 % (w/v) brain heart infusion (BHI) medium was used for the L-lysine producer, respectively. Subsequent seed cultures were grown overnight at 30 °C applying 100 mL modified CGXII minimal salt medium (see supplement for details) in 1,000 mL baffled shaking flasks at 140 min^{-1} on a bench-top rotary shaker (Infors HT, Bottmingen, Switzerland).

D.2.2 Main bioreactor cultivation

Batch fermentations in the main bioreactor (MR) with initial volumes of V_{MR} = 25 L using 2 % (v/v) inoculum on 1 % (w/v) or 4 % (w/v) glucose were carried out at T = 30 °C at

a total pressure of $p = 1.5\,\text{bar}$ in a stainless steel 100 L bioreactor (Bioengineering, Wald, Switzerland) with six-blade Rushton-type impellers, standard pH, pO_2, and pCO_2 sensor equipment (Blombach et al., 2013). $pO_2 \geq 20\,\%$ was controlled by cascadic increase of the agitation speed and initial volumetric gas flow rates of $Q/V_{MR} = 0.2\,\text{vvm}$. Antifoam agent (Struktol® J 647, Schill + Seilacher, Hamburg, Germany) was added when required.

D.2.3 Cascade bioreactor cultivation

Fermentations in the cascade bioreactor system (CBS), consisting of the MR and two 1 L-scale cascade reactors (CRs) arranged in a loop (Fig. D.1), were performed with an initial batch phase in the MR with starting volumes of $V_{MR} = 27.3\,\text{L}$, on 1 % (w/v) or 4 % (w/v) glucose, $T = 30\,°\text{C}$, and total pressure of $p = 2.0\,\text{bar}$. Cascade operation (total circulation) was started at $pCO_2 = 50\,\text{mbar}$ (in MR) with an initial biomass concentration of $X = (1.1 \pm 0.3)\,\text{g L}^{-1}$ and total pressures of $p = 0.6\,\text{bar}$ (in CR1) and 0.2 bar (in CR2). Biosuspension from the MR was pumped into both CRs, immediately adjusting the standard process parameters agitation speed (n), T, pH, and pO_2 as described above. Elevated CO_2/HCO_3^- levels in the CRs, initially set to $pCO_2 = 150\,\text{mbar}$ and 315 mbar, were achieved by CR gassing using high volumetric CO_2 fractions of (40–70) % installing $Q/V = 0.3\,\text{vvm}$ in CR1 and 1 vvm in CR2.

Unless otherwise stated, the circulation flow rate was set to $\nu = 0.58\,\text{L min}^{-1}$, continuously controlled by a motor diaphragm metering pump (Sigma/ 2 S2Ca, ProMinent GmbH, Heidelberg, Germany) and measured by a Coriolis-type flow-meter (Cubemass DCI 8CN, Endress+Hauser Messtechnik GmbH + Co. KG, Weil am Rhein, Germany). Filling and leveling of the CRs ($V_{CR} = 1\,\text{L}$) was continuously adjusted by pneumatic regulating diaphragm valves (type 2103 and 8696, Bürkert GmbH und Co. KG, Ingelfingen, Germany) based on V_{CR} detection (Combics 3, Sartorius AG, Göttingen, Germany). Prior to cultivations, the membrane pump and all connecting tubes and transfer sections consisting of stainless steel (grade 1.4571, (8–10) mm) inner diameter) and braided silicone pressure tubing (Thomafluid, (8–9.5) inner diameter, RCT Reichelt Chemietechnik GmbH + Co., Heidelberg, Germany) were in-situ steam sterilized. The switching procedure was controlled by on/off diaphragm valves (type 2031, Bürkert GmbH und Co. KG, Ingelfingen, Germany).

Overall raw data acquisition and processing was facilitated by an embedded controller (NI Compact-RIO, National Instruments, Austin, USA), whereas process control

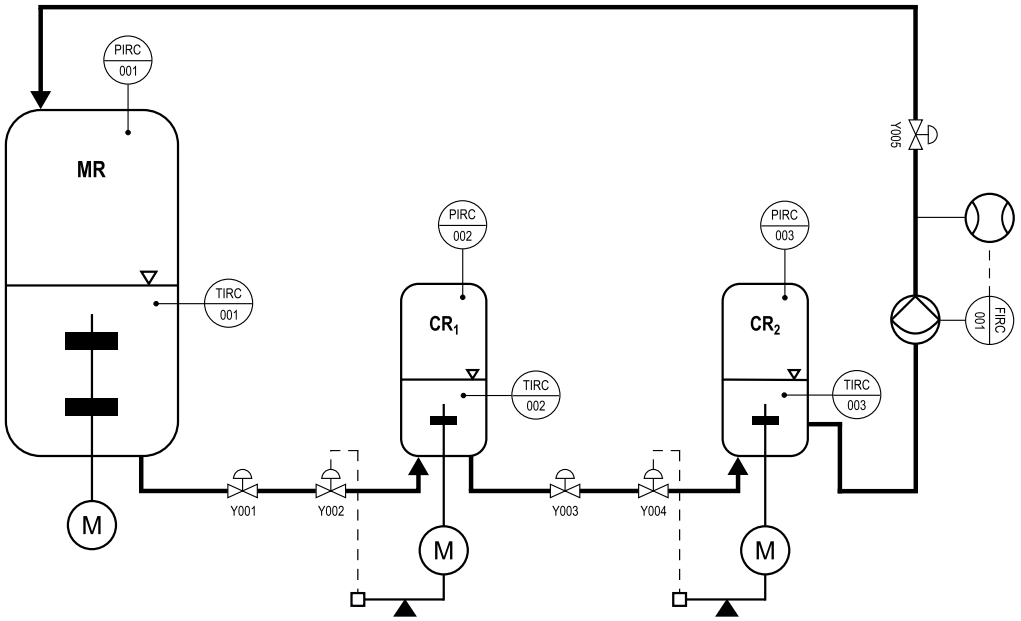

Fig. D.1: Flow sheet of the cascade bioreactor system (CBS) consisting of a 25 L working volume main (MR) and two 1 L cascade reactors (CRs) put in series. Forward liquid transport is facilitated by a pressure gradient (MR ⇒ CR_1 ⇒ CR_2) and total recirculation by a diaphragm metering pump controlled by a mass flow meter. Volumetric level control of both CRs was performed gravimetrically and through regulating valves as indicated.

and data handling was performed by LabVIEW® 2009 SP1 (National Instruments, Austin, USA).

D.2.4 Biomass determination, HPLC analysis, and DNA microarray experiments

Determination of biomass (X) concentrations (in g L^{-1}), amino acids, glucose and organic acids was performed as described previously (Blombach et al., 2013). Where indicated, X was derived by total organic carbon analysis (supplementary data). The transcriptional analysis of technical duplicates from samples withdrawn from the CBS was generally performed as described previously (Blombach et al., 2013) with an intensity ratio (M-value) cut-off set to ±0.5, corresponding to relative expression changes ≥ 1.5-fold. Samples were taken at two distinct time points (TP) that correspond to the initiation phase of the cascade showing the highest ΔpCO_2 between the reactors (TP1) and before equalization of the pCO_2 levels (TP2) given a Δt = 10 min between both TP. The microarray dataset was deposited at ArrayExpress (accession number E-MTAB-2585; `http://www.ebi.ac.uk/arrayexpress`).

D.2.5 Determination of the mixing time

Blend times of the individual bioreactors (MR and CR) to reach a 95 % degree of uniformity θ_{95} (in s), i.e. ±5 % of the final equilibrium, for varying n (in min^{-1}) were calculated as previously published (Brown et al., 2004). Response curves recorded with conductometers (LF 521, WTW Wissenschaftlich-Technische Werkstätten GmbH, Weilheim, Germany) were obtained from tracer pulse experiments using a 3 M di-potassium phosphate (K_2HPO_4) solution. Average mixing times with indicated standard deviations were derived from at least five technical replicates per experimental condition. The experimental results were contrasted to the empirical characteristics of baffled STR in the turbulent regime ($n\,\theta = const$) published by Mersmann et al. (1975):

$$\theta = \frac{6.7}{n}\left(\frac{d}{D}\right)^{-\frac{5}{3}} \mathrm{Ne}^{-\frac{1}{3}} \qquad [D.12]$$

with D (in m) as tank diameter, d (in m) as stirrer diameter, and Ne as dimensionless power number of the impeller in dependency of the Reynolds number, set to $\mathrm{Ne} = f(\mathrm{Re}) = 5$ for baffled STR with Rushton turbines at $\mathrm{Re} > 10^4$ (Bates et al., 1963; Kraume, 2012).

D.2.6 Determination of the residence time distribution

Equivalent to the mixing studies above, tracer experiments with 3 M K_2HPO_4 were performed to determine the residence time distribution (RTD) $E(t)$ (in min^{-1} of (i) the open CBS (MR ⇒ CR1 ⇒ CR2), (ii) the cascade section (CR1 ⇒ CR2), or (iii) the individual reactors (MR, CRs), respectively. $E(t)$ was derived from the response signal $c(t)$ as:

$$E(t) = \frac{c(t)}{\int_0^\infty c(t)\,dt} \approx \frac{c(t)}{\sum c(t)\,\Delta t} \qquad [D.13]$$

The average residence time $\bar{t}$ (in min) can be derived from the first moment of $E(t)$ (Levenspiel, 2012) as:

$$\bar{t} = \int_0^\infty t\,E(t)\,dt \qquad [D.14]$$

which was compared to the theoretical space time τ (in min) of the given system defined as:

$$\tau = \frac{V_R}{\nu} \qquad [D.15]$$

with V_R (in L) as reaction volume and ν (in $\mathrm{L\,min^{-1}}$ as circulation flow rate.

The second moment of $E(t)$ indicates the variance σ^2 (in $\mathrm{m^2}$) as degree of dispersion around the mean:

$$\sigma^2 = \int_0^\infty (t - \bar{t})^2 \, E(t) \, dt \qquad [D.16]$$

with the dimensionless variance σ^2_Θ derived from the dimensionless residence time $\Theta = t/\bar{t}$ according to:

$$\sigma^2_\Theta = \frac{\sigma^2}{\bar{t}^2} \qquad [D.17]$$

The RTD and mixing behavior of non-ideal (real) reactors can be described by the tanks-in-series (TIS) model (Levenspiel, 2012) defined as:

$$E(t) = \frac{1}{\bar{t}} \left(\frac{1}{\bar{t}}\right)^{N-1} \frac{N^N}{(N-1)!} \, e^{-\frac{t\,N}{\bar{t}}} \qquad [D.18]$$

with N as number of identical tanks.

The model reduces to the exponential distribution of a single reactor for $N = 1$ and approaches the delta distribution of piston flow with $N \longrightarrow \infty$ (Nauman, 2002). By fitting $E(t)$ to the experimental data using the method of least squares one derives N_{TIS}. Alternatively, N correlates to σ^2_Θ by:

$$N_{var} = \frac{1}{\sigma^2_\Theta} = \frac{\bar{t}^2}{\sigma^2} \qquad [D.19]$$

Calculations were performed using the MATLAB R2013b environment (MathWorks, Natick, MA, USA).

D.3 Results

To enable the monitoring of transcriptional responses on dynamically changing CO_2/ HCO_3^- levels, we developed a novel CBS mirroring the pCO_2-related reactor heterogeneity

that microbes are exposed to during their motion through different zones of a large scale industrial reactor. The compartmented bioreactor cascade consisted of three STRs connected in a loop: i.e. the MR at 25 L working volume, and two 1 L-scale CRs (Fig. D.1). Circulation in the CBS (MR ⇒ CR_1 ⇒ CR_2) was accomplished by a diaphragm metering pump along the pressure gradient of $p = 0.4$ bar allowing maximum flow rates of $\nu = 4\,\mathrm{L\,min^{-1}}$ controlled by a mass flow meter. Considering the total liquid volume of the cascade by-pass (2.3 L), the minimum theoretical space time was $\tau = 0.6$ min. Further technical details are provided in the supplement (Fig. DS.1, Tab. DS.1).

D.3.1 Technical characterization of the cascade bioreactor system

The mixing performance was evaluated within the operational agitation range of the MR (n = (50–390) $\mathrm{min^{-1}}$) and the CR (n = (300–1,500) $\mathrm{min^{-1}}$) by classical K_2HPO_4 tracer pulse experiments, setting a 95 % homogeneity criterion (Fig. D.2). For both reactors, an exponential decay of θ_{95} with increasing agitation rates was observed, resulting in $\theta_{95} = (2.60 \pm 0.36)$ s (MR) and (0.53 ± 0.05) s (CR) at maximum stirrer speeds. According to the empirical correlation (Eq. D.12) published by (Mersmann et al., 1975), theoretical blend times were calculated showing a good agreement within 10 % error margin to the experimental values.

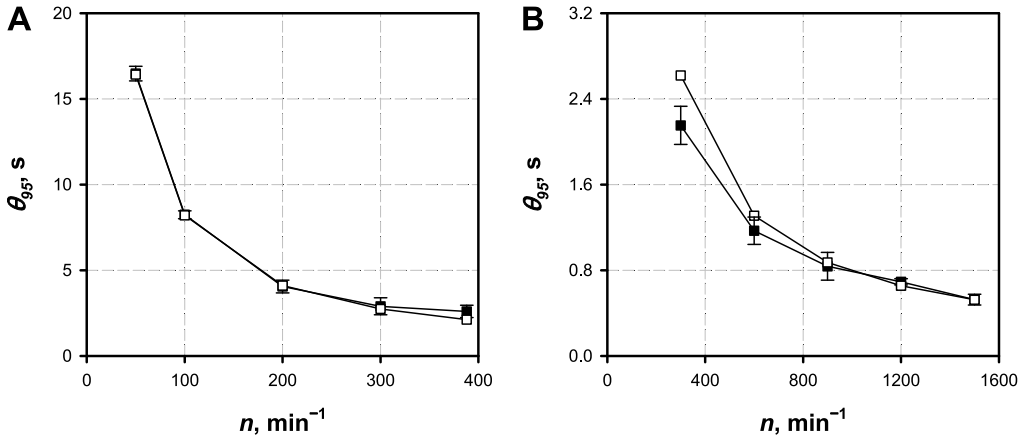

Fig. D.2: Mixing times reaching 95 % homogeneity (θ_{95}, closed symbols) after tracer experiments in dependency of the agitation speed (n) were determined for **(A)** the main and **(B)** cascade reactor with fill levels corresponding to the experimental condition. Additionally, theoretical mixing times derived from the empirical model introduced by Mersmann et al. (1975) are indicated (open symbols). θ_{95} values are given as statistical mean from at least four independent experiments ±SD.

Theoretical residence times $\tau = V_R/\nu$ (Eq. D.15) were compared to experimentally determined (real) mean residence times $\bar{t}$ (Eq. D.14) (Tab. D.6) analyzing typical operating

Tab. D.6: Residence time analysis for the bioreactor setups used in this study. Experiments were performed with a flow rate of about $\nu = 0.58\,\mathrm{L\,min^{-1}}$. Mean residence times ($\bar{t}$) , theoretical space times (τ), dimensionless variances (σ^2_Θ), and ideal tank numbers derived from the latter (N_{var}) or tank-in-series (TIS) fitting (N_{TIS}) are indicated. Results are given as statistical mean from at least four independent experiments ±SD. SD of τ was derived from error propagation assuming 1 % and 3 % error for V_R and ν, respectively.

System	τ, min	$\bar{t}$, min	σ^2_Θ, –	N_{var}, –	N_{TIS}, –
Cascade bioreactor system					
MR ⇒ CR_1 ⇒ CR_2	47.31 ± 1.50	45.66 ± 1.37	0.67 ± 0.03	1.50 ± 0.04	1.49 ± 0.02
Cascade section					
CR_1 ⇒ CR_2	3.60 ± 0.11	3.55 ± 0.05	0.48 ± 0.01	2.08 ± 0.06	1.99 ± 0.03
Cascade reactor					
CR_1	1.75 ± 0.06	1.74 ± 0.04	0.91 ± 0.05	1.10 ± 0.06	1.12 ± 0.01

conditions with the circulation flow rate $\nu = 0.58\,\mathrm{L\,min^{-1}}$. For the total CSB system, $\tau = 47.31\,\mathrm{min}$ was calculated which is in good agreement with the experimental finding of $\bar{t} = (45.66 \pm 1.37)\,\mathrm{min}$. Also the analysis of the separated cascade section and a single CR revealed high congruence levels >9 % between theoretical and experimental data ($\tau/\bar{t}$). From RTD determination according to (Eq. D.13), the number of (volumetrically identical) ideal tanks N of the CBS was derived. Therefore, we considered the dimensionless variance σ^2_Θ (Eq. D.17) following approach (Eq. D.19) or the TIS model fitted to experimental courses of $E(t)$ (Eq. D.18). Similar tank numbers N were obtained for the one- and two-compartment setups yielding at $N_{var} = 1.10 \pm 0.06$ and $N_{TIS} = 1.12 \pm 0.01$ for the CR and $N_{var} = 2.08 \pm 0.06$ and $N_{TIS} = 1.99 \pm 0.03$ for the cascade section, respectively. Additionally, both approaches characterized the total CSB system as 1.5 (ideal) tanks. Notably, this value of the realistic operating condition is about 1.3-fold higher than the sum of the theoretical volumetric cascade contribution and MR impact (Fig. DS.2) and underlines the technical success of artificially imposing tunable gradients inside the cascade section.

D.3.2 Cascade bioreactor system application with oscillating carbon dioxide/bicarbonate levels

An exemplary comparison of biomass and substrate courses of a *C. glutamicum* WT fermentation performed in the CBS under oscillating CO_2/HCO_3^- conditions compared to a reference single reactor process (in MR with 4 % (w/v) glucose) is given in Fig. D.3. Further relevant process parameters of an equivalent CBS cultivation (on 1 % (w/v)

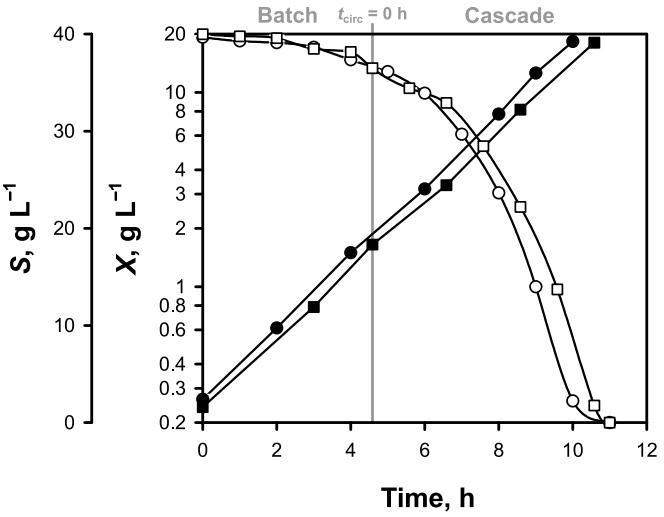

Fig. D.3: Biomass (X, black symbols) and substrate (S, white symbols) courses for an exemplary cascade bioreactor (squares) batch fermentation of *C. glutamicum* WT with 4 % (w/v) glucose compared to reference cultivation in the main reactor only (circles). The switch from batch to cascade mode (t_{circ} = 0 h) with initially applied pCO_2 levels of 75 mbar (MR), 150 mbar (CR_1), and 315 mbar (CR_2) for the CBS cultivation is indicated.

glucose) are provided in Fig. D.4. After the initial batch phase in the MR (Fig. D.4 A), the cascade was linked by circulating the culture with $\nu = 0.58\,\mathrm{L\,min^{-1}}$ representing a residence time of $\bar{t} = (3.55 \pm 0.05)$ min in the cascade section (Tab. D.6) with controlled CRs working volumes of $V_R = 1$ L (Fig. D.4 B). Setpoints for V_R and ν could be controlled highly accurate showing only small standard deviations of 1 % and 3 %. Despite the highly dynamic conditions installed in the CBS, essential process parameters such as pH, T, and p could be kept constant in all three reactors (Fig. D.4 A, C). To ensure aerobic conditions, saturating dissolved oxygen levels were installed in the total system. Thus, pO_2 levels were kept >20 % and >35 % in the MR and CRs, respectively (Fig. D.4 A, C). The start of the circulation (t_{circ} = 0 h) was set to pCO_2 = 50 mbar in the MR, which corresponds to biomass concentrations of about $X = (1.1 \pm 0.3)\,\mathrm{g\,L^{-1}}$. At the same time, pCO_2 levels of 150 mbar and 315 mbar were installed in CR_1 and CR_2, respectively (Fig. D.4D). Thereby, increasing pCO_2 levels were simulated for cells circulating in the MR ⇒ CR_1 ⇒ CR_2 loop before entering the MR again.

Process parameters obtained under reference and cascade conditions are summarized in Tab. D.7. Similar growth kinetics of *C. glutamicum* WT were observed in the presence of oscillating CO_2/HCO_3^- levels compared to standard conditions resulting in maximum specific growth rates of $\mu = (0.40\text{–}0.43)\,\mathrm{h^{-1}}$, biomass to substrate yields of $Y_{XS} = 0.48\,\mathrm{g\,g^{-1}\,h^{-1}}$, and biomass specific glucose uptake rates of $q_S = (0.84\text{–}0.88)\,\mathrm{g\,g^{-1}\,h^{-1}}$. Moreover, individual reactor (mass) balancing of glucose and biomass flows at cascade start with high pCO_2 gradients (time point 1, TP1) and right before pCO_2 level equilibrium (TP2) was performed for MR, CR_1, and CR_2, respectively (Fig. DS.3). As a result,

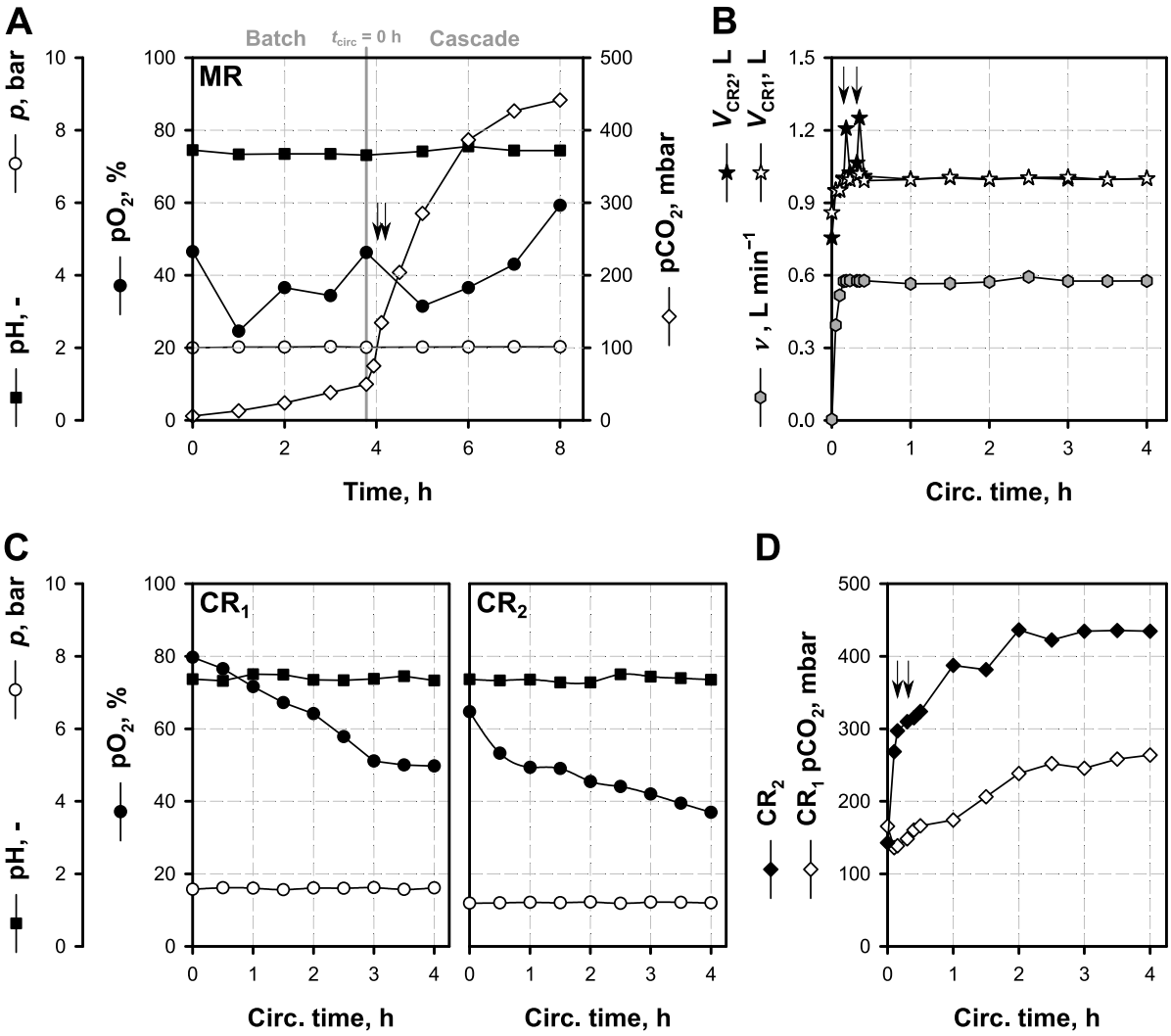

Fig. D.4: Overview of the selected process parameters pH, total pressure (p), dissolved O_2 and CO_2 (pO_2, pCO_2), obtained from an exemplary cascade bioreactor cultivation using *C. glutamicum* WT with 1 % (w/v) glucose. **(A)** Fermentation process in the main reactor (MR) indicating the switch from batch to cascade mode (t_{circ} = 0 h) with **(B)** relevant circulation characteristics as applied flow rate (ν) and controlled cascade reactors (CRs) volume levels (V_{CRs}). **(C/D)** Corresponding process parameters in the CRs during time of circulation are indicated. Additionally, both time points for DNA microarray analyses (TP1, 2) are illustrated (arrows).

derived glucose and biomass recoveries for all three reactors at both time points are fully closed and account for (100 ± 05) % and (100 ± 1) %, respectively.

To monitor the dynamic transcriptional response of *C. glutamicum* WT to the applied CO_2/HCO_3^- gradients, samples were withdrawn simultaneously from MR, CR_1, and CR_2 at the time points TP1 (array A.1, 2) and TP2 (array B.1, 2). Thereby, the cellular response to increased ΔpCO_2 levels at TP1 (75 mbar and 240 mbar) and TP2

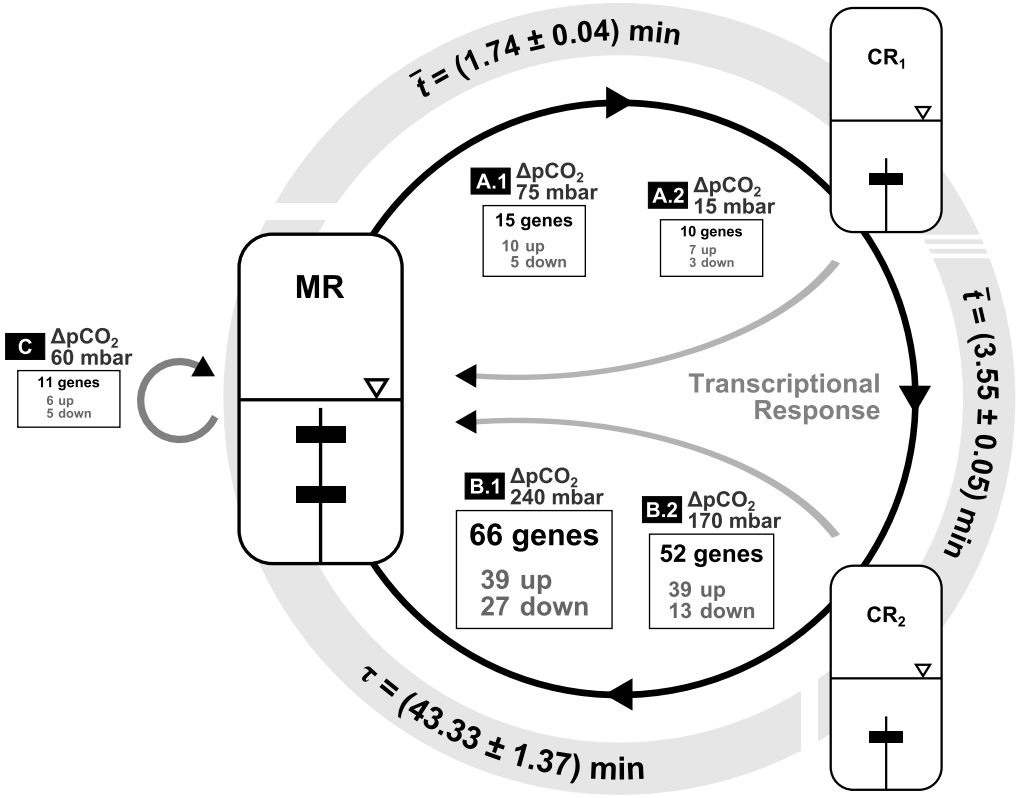

Fig. D.5: Illustration of the transcriptional short-time response of *C. glutamicum* WT during the batch fermentation in the cascade bioreactor system as a result of the exposure to the applied CO_2/HCO_3^- gradients as described. Mean residence ($\bar{t}$) and space times (τ) are indicated for the corresponding sections of the system. DNA microarray analyses for cascade reactor 1 (CR_1, A) and CR_2 (B) both referenced to the main reactor (MR), were performed after (i) cascade initiation, and (ii) before pCO_2 level equilibration (MR to CR_1). ΔpCO_2 gradients between MR and the individual CRs are indicated. Additionally, transcript differences were measured comparing MR samples between time points A and B (C).

(15 mbar and 170 mbar) was documented with respect to the reference status in MR (Fig. D.5; Tab. DS.2, arrays A and B). In addition, transcript levels of the MR at TP2 vs. TP1 (array C) were compared. Consequently, this procedure allows to quantify transcriptional responses in regard to speed (monitored by the cellular residence time in the CBS prior to sampling) and with respect to stimulus intensities (imposed by the artificial gradients inside the loop). As shown, the intensity of the transcriptional response can be linked directly to the strength of ΔpCO_2 stimulus (Fig. D.6). The largest number of differentially expressed genes, namely 66, was found for $\Delta pCO_2 = 240$ mbar comparing CR_2 vs. MR at TP1 (array B.1; Tab. DS.5). Notably, the transcriptional response occurred already $\bar{t} = (3.55 \pm 0.05)$ min after differential pCO_2 exposure. Slightly reduced transcript changes (52 genes) were found for the same stimulus duration at TP2

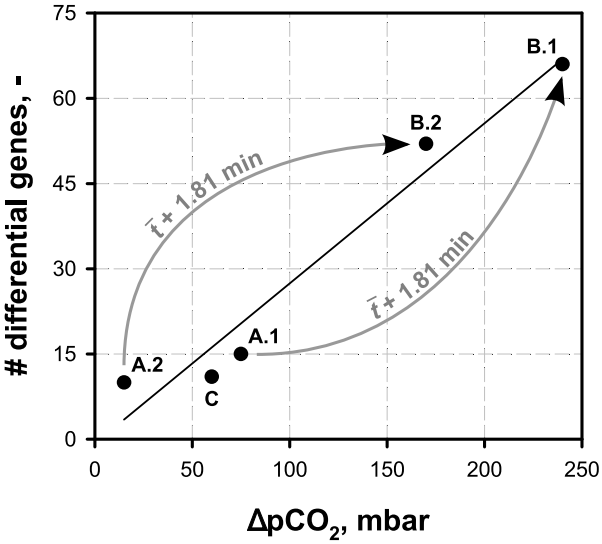

Fig. D.6: Total number of differentially expressed genes as a function of the imposed ΔpCO_2 gradients (see also Tab. DS.3–Tab. DS.7). Cells flowing from CR_1 to CR_2 are subjected to an additional residence time ($\bar{t}$) of about 1.81 min, which is indicated by arrows. The proportionality of gene expression and ΔpCO_2 stimulus is further indicated by linear regressions.

when the ΔpCO_2 level of the stimulus decreased to 170 mbar (array B.2, Tab. DS.6). Even faster transcriptional responses were detected when analyzing samples of CR_1. Already after $\bar{t} = (1.74 \pm 0.04)$ min, 15 (for ΔpCO_2 of 75 mbar) and 10 (for ΔpCO_2 of 15 mbar) differently expressed gene transcripts were observed (array A.1/2, Tab. DS.3, Tab. DS.4). Because CO_2-enrichment was used for the gassing of CR_1 and CR_2, pCO_2 levels accumulated in MR during the course of the experiment (Fig. D.4 A). Consequently, the relative increase of ΔpCO_2 = 60 mbar in MR was accompanied by the transcriptional change of 11 genes (Fig. D.5, Tab. DS.7).

In addition to the WT studies, the L-lysine producer *C. glutamicum* DM1933 was investigated in the CBS installing initial pCO_2 levels of 150 mbar (CR_1) and 300 mbar (CR_2). In analogy to the WT results, similar growth and production kinetics were determined under reference and oscillating CO_2/HCO_3^- levels (Tab. D.7). Additionally, integral (total process) L-lysine production rates of Q_P = (0.26–0.28) g L^{-1} h^{-1} were calculated for both process conditions (data not shown). Analysis of the first 48 min after cascade start revealed a very similar productivity ($Q_P = (0.27 \pm 0.03)$ g L^{-1} h^{-1}) for the backflow into MR (sampling of technical duplicates within 4 min intervals). Interestingly, the MR itself did not show equally high productivities during the same period. Instead, Q_P was found to be reduced to (0.21 ± 0.03) g L^{-1} h^{-1}.

D.4 Discussion

We developed a novel scale-down apparatus comprising of a three-compartment bioreactor system (Fig. D.1), which generally allows the implementation of distinct gradients such

as substrate, pH, T, and dissolved gases while leaving other operating factors constant (Fig. D.4). The given setup provides multiple opportunities to mimic the flow path of cells by imposing selected stimuli in the cascade. Corresponding dynamic responses can be resolved on the subcellular level even allowing mass balancing of individual CRs (Tab. DS.3). The present cascade-to-CBS volume ratio accounts for 8.4 %, which is at the lower end of previously published scale-down models (Sandoval-Basurto et al., 2005). However, RTD analyses showed that the relatively low volumetric impact is compensated by the hydrodynamic conditions applied, and that the system is thus applicable for various scale-down studies. The presented CBS approach provides the possibility to balance carbon flows for each individual cascade element which obviously is a prerequisite for future metabolic flux analyses and labeling experiments (Fig. DS.3).

Baez et al. (2009, 2011) performed CO_2-related experiments using a GFP producing *Escherichia coli* W3110 strain in batch fermentations in presence of constantly and dynamically applied pCO_2 levels up to 300 mbar. Unlike the results in this study, detrimental effects on growth and product formation (increased acetate production) was reported. Additionally, a weak transcriptional response involving e.g. up-regulation of acid resistance genes (constant condition) was observed. However, the time of exposure in the high pCO_2 environment had to be drastically elongated to $\bar{t} > 6$ min with a high volume ratio (scale-down approach) to significantly perturb the general metabolism, illustrating the adaptive potential of the microbial culture to oscillating environmental stress conditions.

Recently published scale-down studies using *C. glutamicum* WT and *C. glutamicum* DM1933 L-lysine producer were performed in a two-compartment STR-PFR system, revealing a strong robustness of the organism with respect to intensive pO_2 and substrate oscillations (Käß et al., 2013, 2014). Both strains were grown in glucose-limited fed-batch mode with maximum exposure in the un-aerated PFR compartment of $\bar{t}$ = (1.5–2.8) min. The comprehensive analysis of the proteome, metabolome, and transcriptome revealed a fairly limited impact on growth and subcellular regulation. In summary, lactate formation and re-metabolization after passing through the anaerobic PFR was observed, while growth rates, yield coefficients, and even L-lysine production remained unaffected. Similarly, the stimulus of fluctuating, high pCO_2 levels as reported in this study did not negatively affect the integral L-lysine formation and yield coefficients (Tab. D.7). However, by analyzing the first 48 min after cascade start, we observed L-lysine formation rates in the backflow of the CBS that corresponded to the final, integral values of the MR, but were about 25 % higher than those measured exclusively in the MR during this

Tab. D.7: Process parameters obtained in batch fermentations under described conditions using the *C. glutamicum* WT and L-lysine producer *C. glutamicum* DM1933. Single reactor reference cultivations were performed in the main reactor (MR) only. They are compared to the cascade bioreactor system (CBS) for initial pCO_2 levels of about 75 mbar, 150 mbar, and 315 mbar in the MR, CR_1 and CR_2, respectively. The circulation flow was set to about $\nu = 0.58\,\mathrm{L\,min^{-1}}$. Where applicable, values represent the arithmetic mean of two replicates ± total measurement range.

Strain	System	$\mu, \mathrm{h^{-1}}$	Y_{XS}, $\mathrm{g\,g^{-1}}$	$q_S, \mathrm{g\,g^{-1}\,h^{-1}}$	Y_{PS}, $\mathrm{g\,g^{-1}}$	Y_{PX}, $\mathrm{g\,g^{-1}}$	$q_P, \mathrm{g\,g^{-1}\,h^{-1}}$
C. glutamicum ATCC13032	MR	0.43 ± 0.00	0.48 ± 0.00	0.88 ± 0.01	—	—	—
	CBS	0.40 ± 0.01	0.47 ± 0.01	0.84 ± 0.04	—	—	—
C. glutamicum DM1933	MR	0.24	0.37	0.65	0.16	0.41	0.10
	CBS	0.22	0.35	0.63	0.15	0.42	0.09

starting period. Considering the fact that pCO_2 levels in the MR reached maximum values not before 2 h after cascade start and that the total CBS residence time was about 47 min (Tab. D.6), one may conclude that cells flowing back were already adapted to high pCO_2 levels while those still resting in the MR were not yet. However, more detailed studies are necessary to further elucidate these findings.

The comparative analysis of transcript levels revealed a fast transcriptional response of *C. glutamicum* WT to alternating CO_2/HCO_3^- perturbations (Fig. D.5). Already after a mean residence time of about 1.74 min in the CO_2-enriched CR_1, a first transcriptional response was observed, which was further amplified leading to about five times more differential genes (TP1, 2) by doubling the pCO_2 levels for additional 1.81 min in the CR_2. Notably, the transcriptional response appeared to be strongly correlated with (i) the strength of the pCO_2 stimulus, i.e. the higher the pCO_2 levels applied the more genes were affected, and (ii) also with $\bar{t}$ of the cells in the bypass (Fig. D.5, Fig. D.6). In summary, the levels of 29 gene transcripts (25 %) were collectively changed (CR_2 vs. MR) at TP1 and TP2 (Fig. DS.4). The majority of those, namely 24 (62 %) were up-regulated by an average factor of 2.14 for TP1 and 1.83 for TP2. Strongest amplification was documented for cg0992 (a putative sulfate permease), cg2810 (a DAACS type symporter) and cg0993 (a putative transcriptional regulator of the ArsR family) showing mRNA fold-changes of 3.58, 3.53, and 3.34 at TP1 and 2.00, 2.57, and 2.25 at TP2, respectively. Moreover, a gradual expression pattern was observed for about 83 % of all (collectively) amplified genes showing reduced mRNA fold-changes by 15 % on average with decreasing ΔpCO_2 levels from TP1 to TP2, respectively. Besides, the original transcriptional state

in the MR was obviously restored, as documented by the relatively small number of differentially expressed genes (Tab. DS.3–Tab. DS.7).

Similar to previous scale-down studies, which analyzed distinct genes by qPCR [e.g. Lara et al. (2006b) and Schweder et al. (1999)], we observed a fast and reproducible up-regulation in response to CO_2/HCO_3^- oscillations with residence times in the low digit minute-scale. Determined amplification rates were in agreement with expectations as corroborated by theoretical estimations of putative maximum gene amplifications (Fig. DS.5). In essence, all measured transcription rates, calculated as the number of transcribed nucleotides per second, were lower than the theoretical maxima. Calculations were performed on the basis of the individual gene length assuming an average RNA polymerase (one per gene) elongation rate of 35 nucleotides s^{-1}, which was deduced from *E. coli* studies at $\mu = 0.4\,h^{-1}$ and $T = 37\,°C$ [Fig. DS.5; Bremer & Dennis (1996)]. We qualify this finding as an additional hint that *C. glutamicum* quickly reacts on pCO_2 stimuli occurring in large scale bioreactors even on the transcriptional level. Notably, the transcriptional response is proportional to the strength of the pCO_2 stimulus imposed, not (yet) showing the transcriptional pattern observed under (pseudo-) steady-state pCO_2 exposure. Therefore, future studies need to clarify how short and long term transcriptional responses are connected.

Acknowledgments

We thank Mira Lenfers-Lücker for the assistance with the HPLC analyses, as well as Maria Rahnert, Jennifer Pfizenmaier, and Salaheddine Laghrami for the support with the cascade bioreactor fermentations. The authors further gratefully acknowledge the funding of this work by the Deutsche Forschungsgemeinschaft (DFG), grant TA 241/5-1.

DS.1 Supplementary methods

DS.1.1 Medium

The modified CGXII minimal medium was prepared in accordance to Eikmanns et al. (1991) containing 10 g L^{-1} $(NH_4)_2SO_4$, 5 g L^{-1} urea, 21 g L^{-1} 3-(*N*-morpholino)propanesulfonic acid (MOPS), 1 g L^{-1} KH_2PO_4, 1 g L^{-1} K_2HPO_4, 0.25 g L^{-1} $MgSO_4 \cdot 7H_2O$, 10 mg L^{-1} $CaCl_2 \cdot H_2O$, 10 mg L^{-1} $MnSO_4 \cdot H_2O$, 16.4 mg L^{-1} $Fe(II)SO_4 \cdot 7H_2O$, 1 mg L^{-1} $ZnSO_4 \cdot 7H_2O$, 0.2 mg L^{-1} $CuSO_4 \cdot 5H_2O$, 0.02 mg L^{-1} $NiCl_2 \cdot 6H_2O$, and 0.2 mg L^{-1} biotin. Urea and MOPS were omitted from the bioreactor medium.

DS.1.2 Total carbon analysis

Total organic carbon (TOC) and total inorganic carbon (TIC) contents in bioreactor samples were quantified with a TC analyzer (Multi N/C 2100s, Analytik Jena, Jena, Germany). The apparatus was operated in TOC mode using the differential detection method with the parallel measurement of (i) TIC and (ii) TC to determine the TOC amount of the sample (TOC = TC – TIC). First, 100 µL of diluted and prepared bioreactor samples (see below) were directly transferred to the TIC reactor freeing the carbonate-derived CO_2 fraction by acidification with 10 % *ortho*-phosphoric acid. Second, 100 µL of the same sample were dosed into the combustion system operated with a furnace temperature of 750 °C converting both organic and inorganic carbon compounds to CO_2. For each detection, 3–4 individual measurements of 2–4 technical replicates were performed. CO_2 produced from thermal oxidation or acidification was then transferred into the measurement chamber by a constant carrier gas flow (O_2) and was finally detected by non-dispersive infrared spectrometry (NDIR detector). For this purpose, the instrument was calibrated with a standard solution containing both 500 mg L^{-1} carbon from sodium carbonate and potassium hydrogen phthalate, producing a 14-point carbon calibration range of (0–500) mg L^{-1} for TIC and (0–1,000) mg L^{-1} for TC quantification.

To prevent the outgassing of CO_2 prior to detection, 1 mL of sample was immediately transferred to 20 mL graduated flasks containing 140 µL 5 N potassium hydroxide and deionized water, effectively increasing the basicity and thus shifting the carbonic acid equilibrium towards HCO_3^- and CO_3^{2-}.

DS.2 Supplementary tables

Tab. DS.1: Geometry and dimensions of the bioreactor systems used in this study.

	Bioreactor	
Description	Main reactor (MR)	Cascade reactors (CR_1, CR_2)
Working volume, V_R		
batch process	27.3 L	—
cascade process	25 L	1 L
Agitation, n	(100–400) min^{-1}	(1,000–1,500) min^{-1}
Gas flow rate, Q/V_R	(0.2–1) vvm	(0.3–1) vvm
Reactor height, H	835 mm	230 mm
Reactor diameter, D	413 mm	98 mm
Stirrer diameter, d	195 mm	47.5 mm
Agitator spacing,		
S_1	165 mm	75 mm
S_2	330 mm	—
Baffle width, B	43 mm	10 mm

Tab. DS.2: Number of differently expressed genes with relative expression changes equal or larger than 1.5-fold (twofold in parenthesis) obtained by DNA microarrays during cascade bioreactor operation of *C. glutamicum* WT under dynamic CO_2/HCO_3^- levels. Measurements were performed after initiation of the cascade at time point 1 (TP1) and right before equalization of the pCO_2 levels (difference at time of sampling indicated for each condition) between the main reactor (MR) and the first cascade reactor (CR_1) at TP2, respectively.

			Number of differentially expressed genes		
DNA Microarray	Comparison	ΔpCO_2	Decreased	Increased	Sum
A.1: TP1	CR_1 vs. MR	75 mbar	5 (1)	10 (2)	15 (3)
A.2: TP2		15 mbar	3 (0)	7 (0)	10 (0)
B.1: TP1	CR_2 vs. MR	240 mbar	27 (1)	39 (12)	66 (13)
B.2: TP2		170 mbar	13 (0)	39 (5)	52 (5)
C: TP2 vs. TP1	MR	60 mbar	5 (0)	6 (0)	11 (0)

Tab. DS.3: Gene expression in *C. glutamicum* ATCC 13032 under high CO_2/HCO_3^- levels in cascade reactor 1 compared to reference conditions in the main reactor at time point 1 (array A.1). Genes listed below exhibit relative expression changes equal to or larger than 1.5-fold.

Locus Tag	mRNA ratio	Gene	Function(s)
cg0040	0.49		Putative secreted protein
cg0047	0.65		Conserved hypothetical protein
cg0304	1.57		Putative membrane protein
cg0416	0.57		Putative secreted protein, carrying a eukaryotic domain
cg0535	1.71		Putative ketoglutarate semialdehyde dehydrogenase
cg0848	1.52	*wbbL*	Putative glycosyltransferase
cg0992	2.06		Putative permease, sulfate permease (SulP) family
cg0993	2.43		Putative transcriptional regulator, ArsR-family
cg1292	1.59		Flavin-containing monooxygenase 3
cg2745	0.64		Hypothetical protein
cg2810	1.65		Putative secondary H^+/Na^+:glutamate/dicarboxylate symporter, dicarboxylate/amino acid:cation symporter (DAACS) family
cg3118	1.72	*cysI*	Ferredoxin-sulfite reductase
cg3119	1.73	*fpr2*	Ferredoxin-$NADP^+$ reductase
cg3131	1.66		Acetylornithine deacetylase or related deacylase
cg3149	0.66	*alaT*	Putative aspartate aminotransferase, AT class I

Tab. DS.4: Gene expression in *C. glutamicum* ATCC 13032 under high CO_2/HCO_3^- levels in cascade reactor 1 compared to reference conditions in the main reactor at time point 2 (array A.2). Genes listed below exhibit relative expression changes equal to or larger than 1.5-fold.

Locus Tag	mRNA ratio	Gene	Function(s)
cg0037	1.62	*tnp22a/ ISCg22a*	Transposase, putative pseudogene
cg0181	1.67	*alkB*	Alkylated DNA repair protein AlkB
cg0205	0.66	*iolH*	Myo-inositol catabolism protein
cg0231	0.66		Putative membrane protein
cg0422	1.79	*murA*	UDP-N-acetylglucosamine 1-carboxyvinyltransferase
cg0826	0.59		Putative membrane protein
cg0992	1.68		Putative permease, sulfate permease (SulP) family
cg0993	1.71		Putative transcriptional regulator, ArsR-family
cg3118	1.6	*cysI*	Ferredoxin-sulfite reductase
cg3119	1.53	*fpr2*	Ferredoxin-NADP(+) reductase

Tab. DS.5: Gene expression in *C. glutamicum* ATCC 13032 under high CO_2/HCO_3^- levels in cascade reactor 2 compared to reference conditions in the main reactor at time point 1 (array B.1). Genes listed below exhibit relative expression changes equal to or larger than 1.5-fold.

Locus Tag	mRNA ratio	Gene	Function(s)
cg0013	1.53		Putative transcriptional regulator, TetR-family
cg0037	1.78	*tnp22a/ ISCg22a*	Transposase, putative pseudogene
cg0071	1.64		Metallo-beta-lactamase superfamily, RHOD domain
cg0075	1.68		Conserved hypothetical protein
cg0080	0.64		Magnesium/cobalt ion channel, CorA metal ion transporter (MIT) family
cg0219	0.65		O-methyl transferase, putative pseudogene (C-terminal fragment)
cg0422	1.59	*murA*	UDP-N-acetylglucosamine 1-carboxyvinyltransferase
cg0753	0.66		Putative secreted protein
cg0769	0.62		ABC-type putative iron-siderophore transporter, permease subunit
cg0848	0.66	*wbbL*	Putative glycosyltransferase
cg0855	0.57		Conserved hypothetical protein
cg0858	0.65		Putative secreted protein
cg0992	3.58		Putative permease, sulfate permease (SulP) family
cg0993	3.34		Putative transcriptional regulator, ArsR-family
cg1142	1.79		Putative Mn_2^+ transporter, metal ion (Mn_2^+-iron) transporter (Nramp) family
cg1279	1.69		Putative secreted protein
cg1291	1.62		Putative membrane protein
cg1292	2.14		Flavin-containing monooxygenase 3
cg1307	0.6		DNA/RNA helicase, superfamily II
cg1349	0.62		Putative membrane protein, containing a CBS domain
cg1475	0.66		Conserved hypothetical protein
cg1479	0.62	*glgP1*	Putative glycogen phosphorylase
cg1710	0.62	*bacA*	Putative undecaprenol kinase
cg1740	1.55		Putative nucleoside-diphosphate-sugar epimerase
cg1842	0.66		Putative secreted metalloprotease
cg1966	1.77		Hypothetical protein
cg1975	1.56		Conserved hypothetical protein
cg2102	1.74	*sigB*	RNA polymerase sigma factor rpoD (Sigma-A).
cg2136	0.62	*gluA*	ABC-type glutamate transporter, ATPase subunit (TC 3.A.1.3.9)
cg2261	1.55	*amtB*	Putative secondary ammonium transporter, Amt-family
cg2272	0.61	*mutM1*	Formamidopyrimidine-DNA glycosylase
cg2283	0.63		Conserved hypothetical protein
cg2336	0.64		Putative secreted protein
cg2391	0.44	*aroG*	3-Deoxy-7-phosphoheptulonate synthase
cg2437	0.6	*thrC*	Threonine synthase

. . . to be continued on the following page

Tab. DS.5: Gene expression in *C. glutamicum* under high CO_2/HCO_3^- levels in CR_1 vs. MR at TP2 (continued)

Locus Tag	mRNA ratio	Gene	Function(s)
cg2445	1.58	*hmuO*	Heme oxygenase (decyclizing)
cg2613	1.54	*mdh*	Malate dehydrogenase
cg2676	1.56		ABC-type putative dipeptide/oligopeptide transporter, permease subunit
cg2677	1.79		ABC-type putative dipeptide/oligopeptide transporter, permease subunit
cg2678	2.03		ABC-type putative dipeptide/oligopeptide transporter, substrate-binding lipoprotein
cg2783	1.57	*gntR1*	Transcriptional regulator, GntR-family
cg2796	2.1		Conserved hypothetical protein, MMGE/PRPD-family, putative involved in propoinate catabolism
cg2810	3.53		Putative secondary H^+/Na^+:glutamate/dicarboxylate symporter, dicarboxylate/amino acid:cation symporter (DAACS) family
cg2847	1.56	*mshD*	Putative 1-D-myo-inosityl-2-(L-cysteinyl)amido-2-deoxy-alpha-D-glucopyranoside *N*-acetyltransferase
cg2852	0.62		putative folate-binding protein implicated in RNA modification or replication initiation; YgfZ homolog
cg2857	0.53	*purF*	Amidophosphoribosyltransferase
cg2929	0.61	*nagA1*	N-acetylglucosamine-6-phosphate deacetylase
cg2962	2.53		Hypothetical protein, uncharacterized enzyme involved in biosynthesis of extracellular polysaccharides
cg3080	1.64		secondary Na^+/glutamate symporter
cg3116	1.6	*cysH*	Adenosine phosphosulfate reductase
cg3117	1.96	*cysX*	Ferredoxin-like protein, involved in electron-transfer
cg3118	2.19	*cysI*	Ferredoxin-sulfite reductase
cg3119	2.3	*fpr2*	Ferredoxin-$NADP^+$ reductase
cg3122	0.59	*phnB1*	Hypothetical protein, PhnB-like
cg3131	1.69		Acetylornithine deacetylase or related deacylase
cg3169	2.13	*pck*	Phosphoenolpyruvate carboxykinase (GTP)
cg3301	0.62		Putative sugar/metabolite permease, MFS-type
cg3329	2		Conserved hypothetical protein
cg3330	1.58		Putative secreted protein
cg3335	1.97	*mez*	Malate dehydrogenase (oxaloacetate-decarboxylating) ($NADP^+$)
cg3340	1.78	*dadA*	D-Amino-acid dehydrogenase
cg3372	1.69		Conserved hypothetical protein
cg3399	2.53		Permease, MFS-type
cg3404	0.62		ABC-type putative iron(III) dicitrate transporter, substrate-binding lipoprotein
cg3430	0.66		Conserved hypothetical protein

. . . to be continued on the following page

Tab. DS.5: Gene expression in *C. glutamicum* under high CO_2/HCO_3^- levels in CR_1 vs. MR at TP2 (continued)

Locus Tag	mRNA ratio	Gene	Function(s)
cg3431	0.65	*rnpA*	Ribonuclease P

Tab. DS.6: Gene expression in *C. glutamicum* ATCC 13032 under high CO_2/HCO_3^- levels in cascade reactor 2 compared to reference conditions in the main reactor at time point 2 (array B.2). Genes listed below exhibit relative expression changes equal to or larger than 1.5-fold.

Locus Tag	mRNA ratio	Gene	Function(s)
cg0033	0.62		Putative secreted protein
cg0120	1.6		Putative hydrolase
cg0173	0.66		Conserved hypothetical protein
cg0214	0.64		Hypothetical protein
cg0281	0.61		tRNA-specific adenosine deaminase
cg0412	0.66		Putative membrane protein
cg0449	0.66		Hypothetical protein
cg0519	0.64		Putative phosphoglycerate mutase
cg0604	1.68	*rpsQ*	30S ribosomal protein S17
cg0607	2.07		Putative secreted protein
cg0726	1.59		Putative secreted lipoprotein
cg0781	1.55		Putative membrane protein
cg0992	2		Putative permease, sulfate permease (SulP) family
cg0993	2.25		Putative transcriptional regulator, ArsR-family
cg1142	1.67		Putative Mn_2^+ transporter, metal ion (Mn_2^+-iron) transporter (Nramp) family
cg1279	1.77		Putative secreted protein
cg1291	1.73		Putative membrane protein
cg1292	1.96		Flavin-containing monooxygenase 3
cg1307	0.62		DNA/RNA helicase, superfamily II
cg1349	0.59		Putative membrane protein, containing a CBS domain
cg1636	1.59		Putative secreted protein
cg1710	0.65	*bacA*	Putative undecaprenol kinase
cg1966	1.96		Hypothetical protein
cg2051	1.72		Hypothetical protein
cg2102	1.67	*sigB*	RNA polymerase sigma factor rpoD (Sigma-A).
cg2159	1.52		Hypothetical protein
cg2223	0.64		Putative Secreted or membrane protein related to metalloendopeptidases
cg2380	1.54		Putative membrane protein
cg2391	0.51	*aroG*	3-Deoxy-7-phosphoheptulonate synthase
cg2458	1.53	*pgp2*	Putative phosphatase, HAD-family
cg2613	1.61	*mdh*	Malate dehydrogenase
cg2644	1.53	*clpP2*	Endopeptidase Clp, proteolytic subunit

... to be continued on the following page

Tab. DS.6: Gene expression in *C. glutamicum* under high CO_2/HCO_3^- levels in CR_2 vs. MR at TP2 (continued)

Locus Tag	mRNA ratio	Gene	Function(s)
cg2677	1.6		ABC-type putative dipeptide/oligopeptide transporter, permease subunit
cg2678	1.91		ABC-type putative dipeptide/oligopeptide transporter, substrate-binding lipoprotein
cg2796	1.67		Conserved hypothetical protein, MMGE/PRPD-family, putative involved in propoinate catabolism
cg2810	2.57		Putative secondary H^+/Na^+:glutamate/dicarboxylate symporter, dicarboxylate/amino acid:cation symporter (DAACS) family
cg2852	0.62		putative folate-binding protein implicated in RNA modification or replication initiation; YgfZ homolog
cg2962	2.14		Hypothetical protein, uncharacterized enzyme involved in biosynthesis of extracellular polysaccharides
cg3115	1.52	*cysD*	Sulfate adenylyltransferase subunit 2
cg3116	1.52	*cysH*	Adenosine phosphosulfate reductase
cg3117	1.87	*cysX*	Ferredoxin-like protein, involved in electron-transfer
cg3118	1.91	*cysI*	Ferredoxin-sulfite reductase
cg3119	1.88	*fpr2*	Ferredoxin-$NADP^+$ reductase
cg3131	1.65		Acetylornithine deacetylase or related deacylase
cg3159	1.52		Putative universal stress protein UspA or related nucleotide-binding protein
cg3169	1.78	*pck*	Phosphoenolpyruvate carboxykinase (GTP)
cg3219	1.59	*ldh*	L-Lactate dehydrogenase
cg3253	1.54	*mcbR*	Global transcriptional repressor of sulfur metabolism, TetR-family
cg3329	1.65		Conserved hypothetical protein
cg3335	1.52	*mez*	Malate dehydrogenase (OAA-decarboxylating) ($NADP^+$)
cg3372	1.66		Conserved hypothetical protein
cg3399	1.96		Permease, MFS-type

Tab. DS.7: Gene expression in *C. glutamicum* ATCC 13032 under high CO_2/HCO_3^- levels in the main reactor at time point 2 compared to reference conditions in the main reactor at time point 1 (array C). Genes listed below exhibit relative expression changes equal to or larger than 1.5-fold.

Locus Tag	mRNA ratio	Gene	Function(s)
cg0214	0.66		Hypothetical protein
cg0440	0.63		Hypothetical protein
cg0992	1.55		Putative permease, sulfate permease (SulP) family
cg0993	1.52		Putative transcriptional regulator, ArsR-family
cg1642	0.65		Siderophore-interacting protein

. . . to be continued on the following page

Tab. DS.7: Gene expression in *C. glutamicum* under high CO_2/HCO_3^- levels in the MR at TP2 vs. the MR at TP1 (continued)

Locus Tag	mRNA ratio	Gene	Function(s)
cg2444	1.69		Hypothetical protein
cg2445	1.58	*hmuO*	Heme oxygenase (decyclizing)
cg2887	0.62	*cgtS3*	Two-component system, sensory histidine kinase
cg2948	1.57	*cgtS5*	Two-component system, sensory histidine kinase
cg3275	1.91	*fdxA*	Putative ferredoxin
cg3402	0.65		Putative Hg_2^+ permease, MerTP-family

DS.3 Supplementary figures

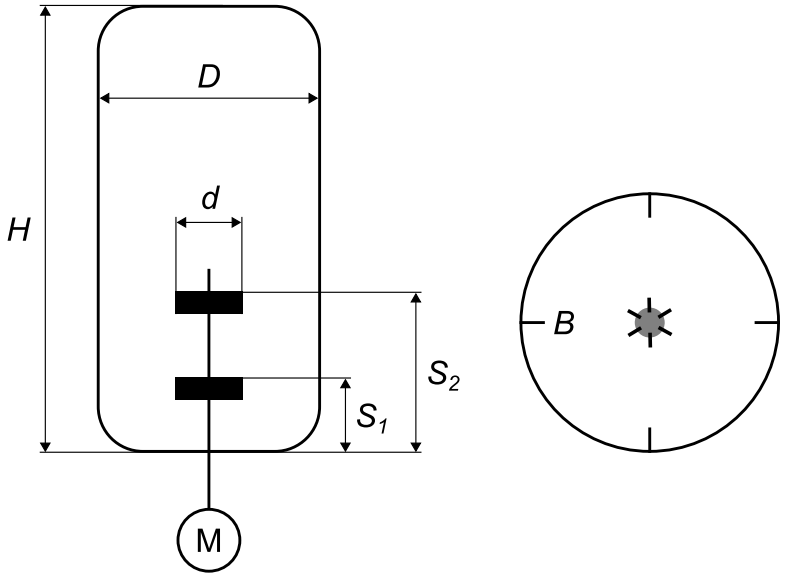

Fig. DS.1: Vessel geometry of bioreactors used in this study. Indicated are reactor height (H), tank (D) and stirrer diameter (d), spacing of the Rushton turbines (S_1, S_2), and baffle width (B).

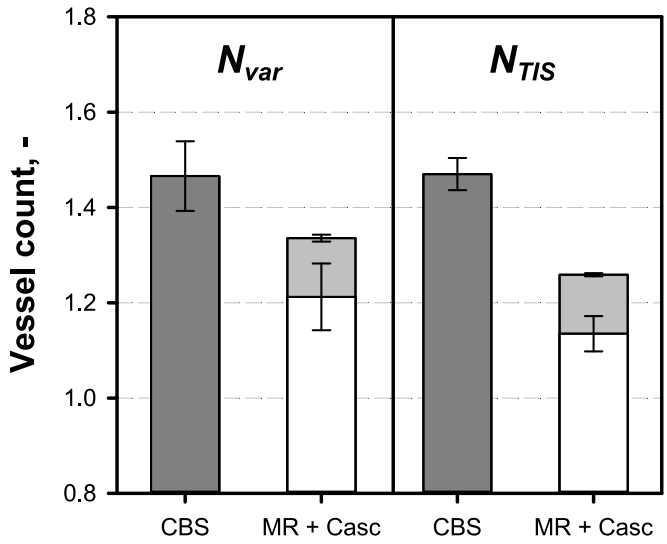

Fig. DS.2: Determined number of theoretical tanks of the cascade bioreactor system (CBS, dark grey bars) compared to the main reactor (MR, white bars) based on dimensionless variance calculations (N_{var}) and tanks-in-series model fitting (N_{TIS}) performed under described conditions at $\nu = 2.3\,\mathrm{L\,min^{-1}}$. Results are given as statistical mean ±SD from at least four independent experiments. The volumetric proportion of the cascade section on the CBS (light grey bars) was indicated assuming 1 % error for V_R ±SD derived from error propagation.

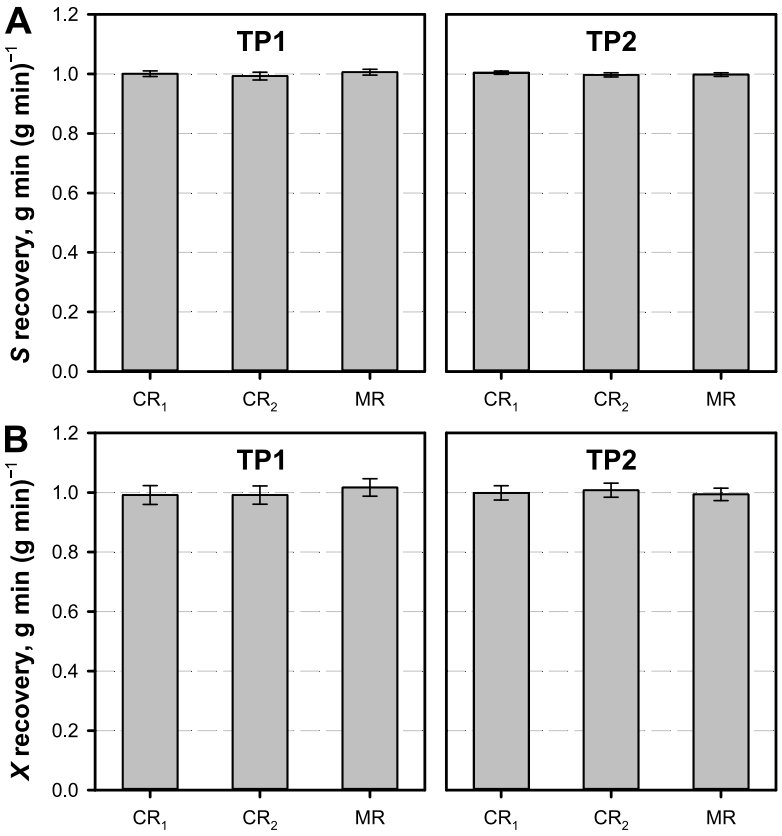

Fig. DS.3: Recovery calculations for the main reactor (MR) and both cascade reactors (CRs) at the two DNA microarray analyses time points (TP) of the *C. glutamicum* WT cascade fermentation with applied CO_2/HCO_3^- gradient. Simultaneous sampling was performed right before/after each reactor. Recoveries were determined on the basis of in- and outflow of **(A)** measured glucose (S) and **(B)** total carbon-dependent biomass (X) detection. Values represent the mean of at least four technical replicates ±SD derived from error propagation.

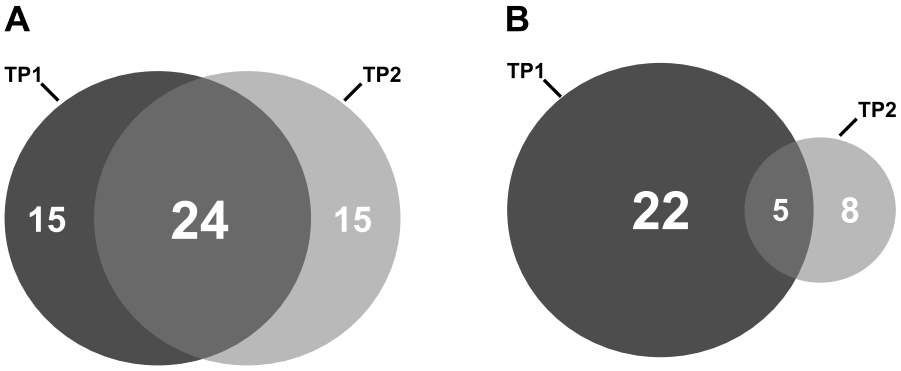

Fig. DS.4: Venn diagram of the number of genes showing **(A)** increased and **(B)** decreased transcription in the comparative DNA microarray analysis of cascade reactor 2 compared to the main reactor (array B.1, 2) between time point 1 and 2 (TP1 vs. TP2).

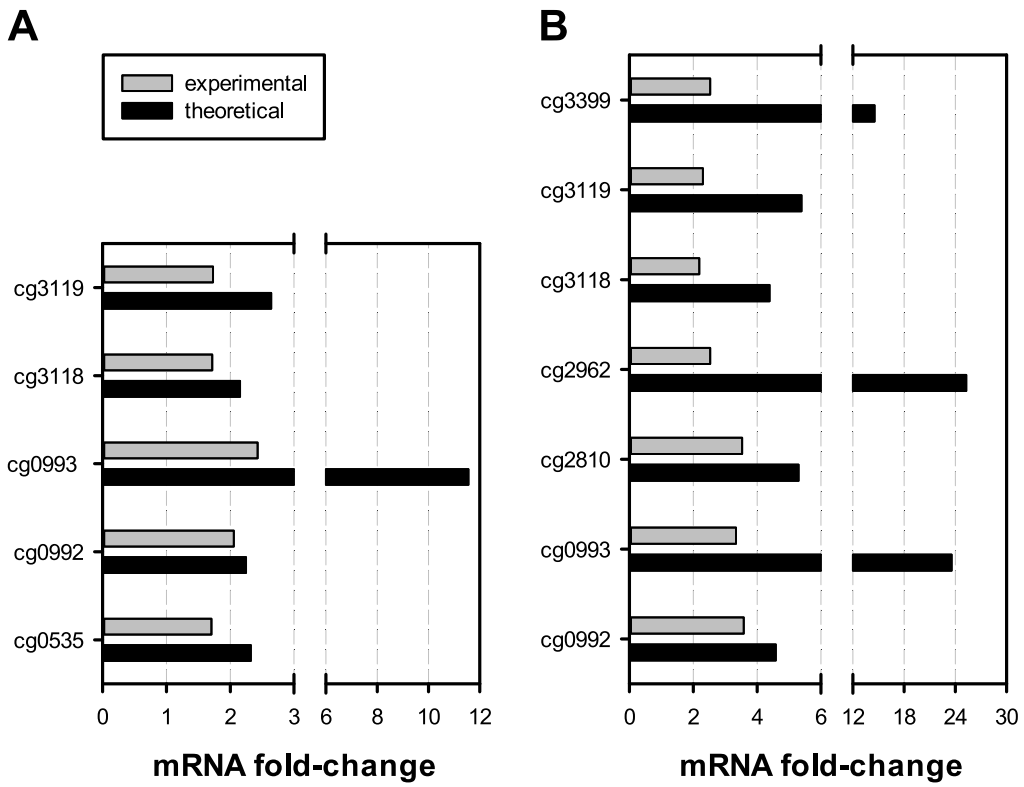

Fig. DS.5: Comparison of experimental and theoretical gene amplification of selected genes showing the highest mRNA fold-changes in **(A)** CR_1 vs. MR at TP1 (array A.1) and **(B)** CR_2 vs. MR at TP1 (array B.1). Maximum theoretical up-regulation was derived by considering the individual gene length and an average RNA polymerase (RNAP) transcription rate of 35 nucleotides s^{-1} (one RNAP per gene).

E Cascade bioreactor system settings and control

The following section provides detailed information on (i) essential cascade bioreactor system (CBS) settings, (ii) the characterization of the metering diaphragm pump and flow meter necessary for accurate circulation, and (iii) programming sequences of selected parts of the process and control system (PCS) in LabVIEW®.

Prior to the operation of the metering diaphragm pump for circulation experiments as during the characterization of the CBS or in cultivations, a characteristic pump profile was determined (Fig. E.1). Equivalently, the characterization of the regulating valves (RV) was followed (Fig. E.2). Both parameter sets were then incorporated into the PCS programmed in LabVIEW® to facilitate the direct switchover to circulation mode around the range of the desired flow speed at process start. In particular, the predefined operating range significantly simplifies the control of the volume level in both CRs due to potential restrictions of the control output right from the beginning; see the description of the circulation processing for the implementation of the RV illustrated in Fig. 4.12, the demonstration of the pump control sequence given in Fig. E.4, and the settings overview in Tab. E.8.

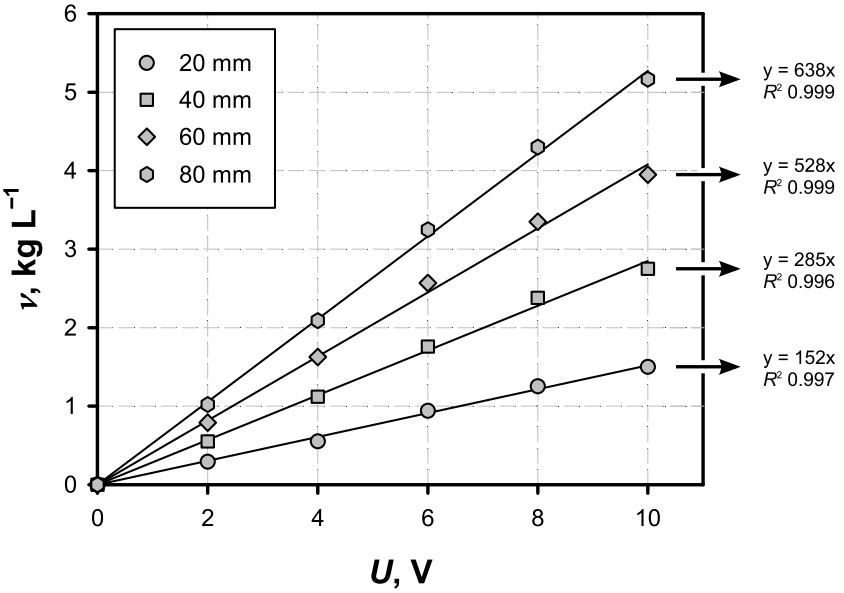

Fig. E.1: Characteristic curve of the metering diaphragm pump in dependency of the applied voltage and pump stroke. The flow rates (ν) were derived from the mass flow meter, the resulting curves fitted by linear regression as indicated and finally used for start-up of the circulation as described in Fig. 4.12.

The design and programming of the control units for temperature and pH regulation were performed according to the general control scheme depicted in Fig. E.3. It facilitates

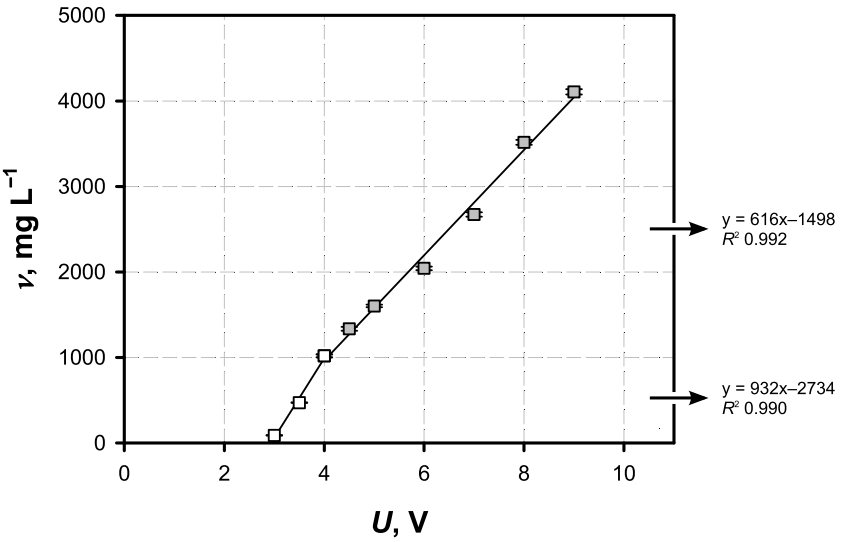

Fig. E.2: Characteristic curve of the regulating valve in dependency of the applied voltage. The flow rates (ν) were measured gravimetrically. Two characteristics were identified, the resulting curves fitted by linear regression as indicated and finally used for start-up of the circulation as described in Fig. E.7.

an adjustable control output of two independent control elements (e.g. heating and cooling devices, or acid and base pump) depending on the desired strength of the response. On the contrary, the pressure and RV control was implemented by regular PID controllers that were adjusted according the method of Ziegler & Nichols (1942). An overview of all control parameters is given in Tab. E.8

Tab. E.8: Parameter settings of the regulating valve (RV) control, the pressure valve control, the temperature control unit (Temp), and the pH control unit. Indicated are the proportional (K_p), integral (K_i), and derivate (K_d) parameters of the controller derived after Ziegler & Nichols (1942). Additionally, minimum (min. limit) and maximum (max. limit) factors were applied that function as multiplier of the original controller output signal for the RV. In case of temperature and pH control, t_{int} refers to the interval time of the control loop (Fig. E.3). Range of values are provided to adjust for varying fermentation and material conditions.

Controller	Parameter	Value	Controller	Parameter	Value
RV	K_p	15.52	**Pressure**	K_p	5
	K_i	0.881		K_i	0.055
	K_d	0.176		K_d	—
	min. limit	0.5×			
	max. limit	1.5×			
Temp	t_{int}	1	**pH**	t_{int}	1–7
	DB	0.02		DB	0.01–0.005
	PB	0.3		PB	0.05–0.15

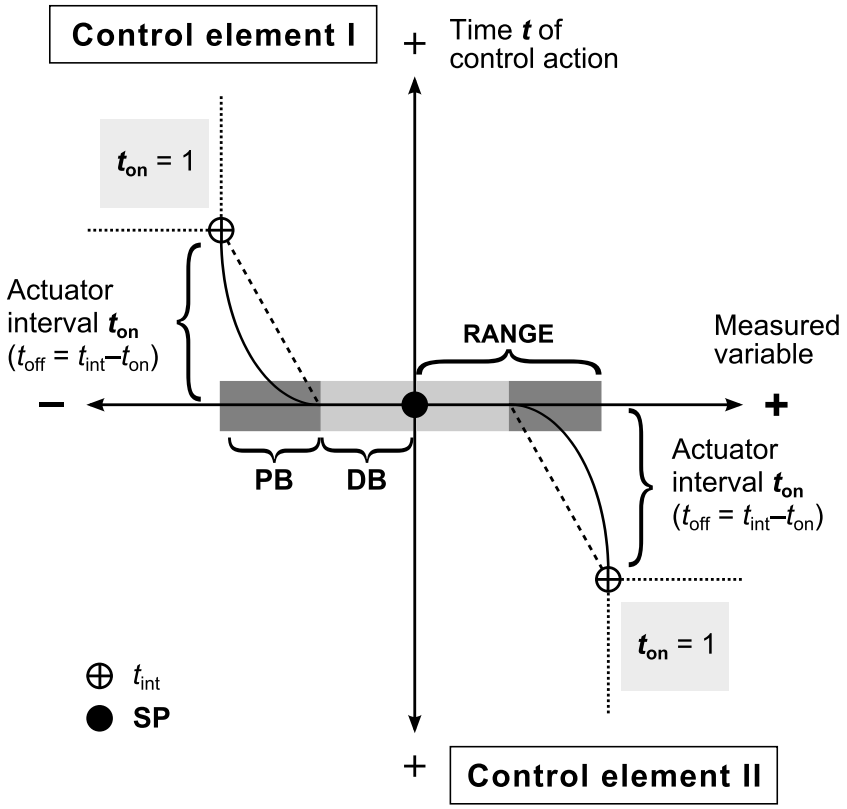

Fig. E.3: General control scheme that has been used for temperature and pH control in fermentations. The global control output was defined as the time the individual control element I and II (e.g. base and acid pump for pH control) were switched on (t_{on}). The latter depends on the interval time of the control loop (t_{int}) and whether a linear (····) or power function (——) was set for the proportional band (PB). As long as the actual measurement values lie out of the PB range, the corresponding control element is switched on continuously ($t_{on} = 1$). Further abbreviations are: DB, deadband; SP, setpoint.

The general concept of the circulation control is provided in Fig. E.4. Circulation initiation bases on the pump characteristics for the given flow speed and pump stroke as mentioned above. Further adjustment and flow control can be switched on separately, which leads to a timed control loop that facilitates the incremental approximation of the setpoint without harsh over- and underdrive, suspending the active control regime if a desired tolerance range is maintained.

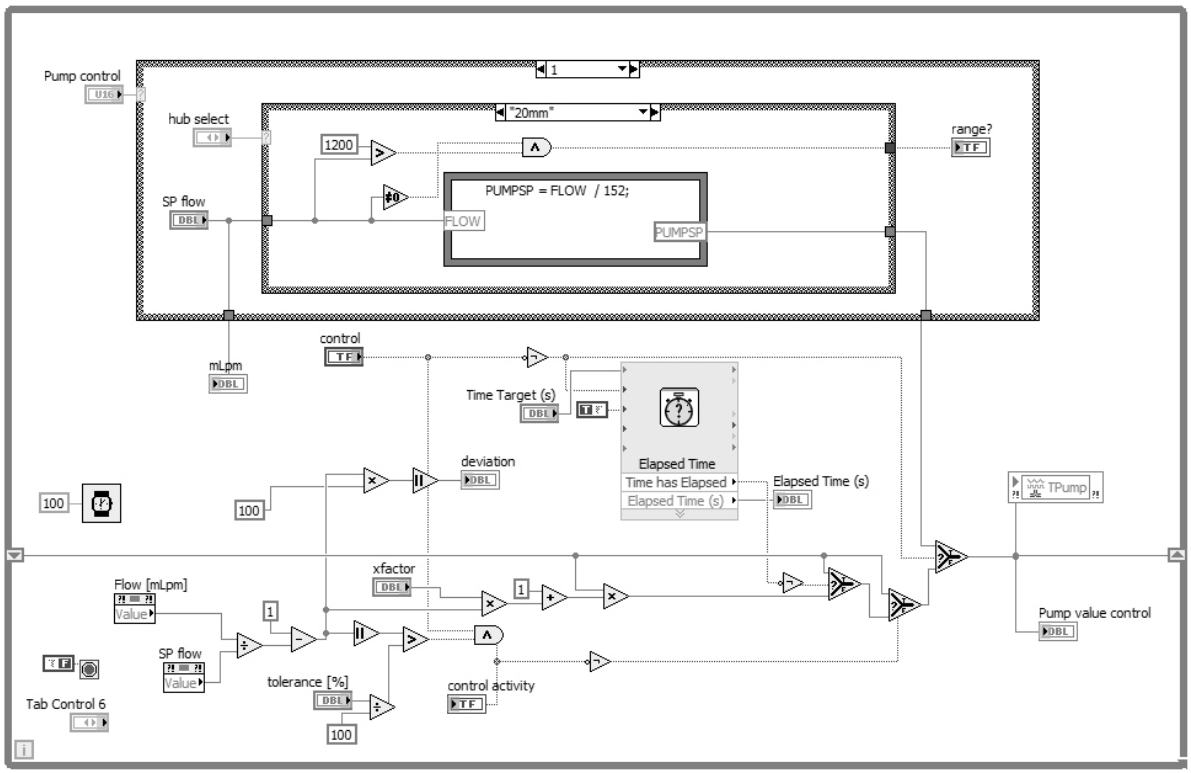

Fig. E.4: Block diagram of the metering diaphragm pump control sequence in LabVIEW®. Switching to the automatic mode (upper left hand side) applies a predefined voltage depending on the selected flow speed and on the selected stroke according to the pump characteristic as given in Fig. E.1. If the control mode is further activated (bottom section), desired and actual values are compared after each "time target" loop. Adjustment of the control deviation can further be refined by a control factor (usually set to 0.3) and is generally only performed if the offset is larger than the defined tolerance range (usually set to 0.7 %).

Setup of the frequency converter using the Engineer software (Lenze SE, Aerzen, Germany) is required for the adjustment and control of the motor speed by varying the input frequency and voltage. A snapshot of the adjusted parameters is given in Fig. E.5. The subsequent correlation between the applied voltage and the actual revolution of the stirrer was performed with a rev meter yielding a conversion factor of 2.6.

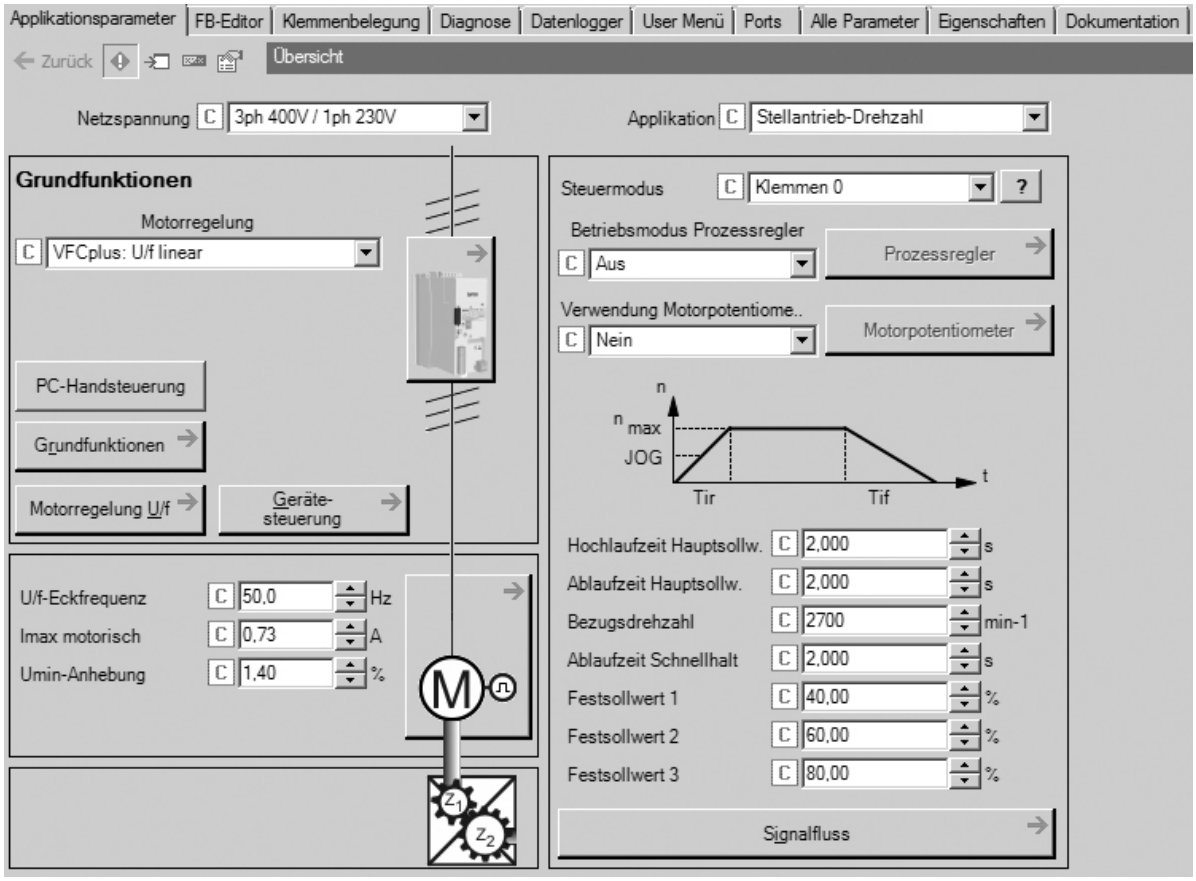

Fig. E.5: Overview of the settings applied for the frequency converter of both cascade reactors. The correlation between the applied voltage and the actual revolution of the stirrer per minute was performed with a rev meter (factor 2.6).

For the 'initiation', 'start-up', and 'shut-down' of the total recycle operation mode of the CBS, three distinct operating functions were implemented into the process and control system. Common procedure of all CBS cultivation was the initial batch phase in the main reactor (MR). Prior to cascade processing, the sterilization buffer was removed from both cascade reactors (CR), taring the balances for later level control. The successive culture transfer from the MR to the CR_2 was facilitated by the transfer sequence provided in Fig. E.6. Reference for the fill levels are the determined setpoints of the regulating valves (RV) and all necessary openings and closing of the intersections are automatically performed.

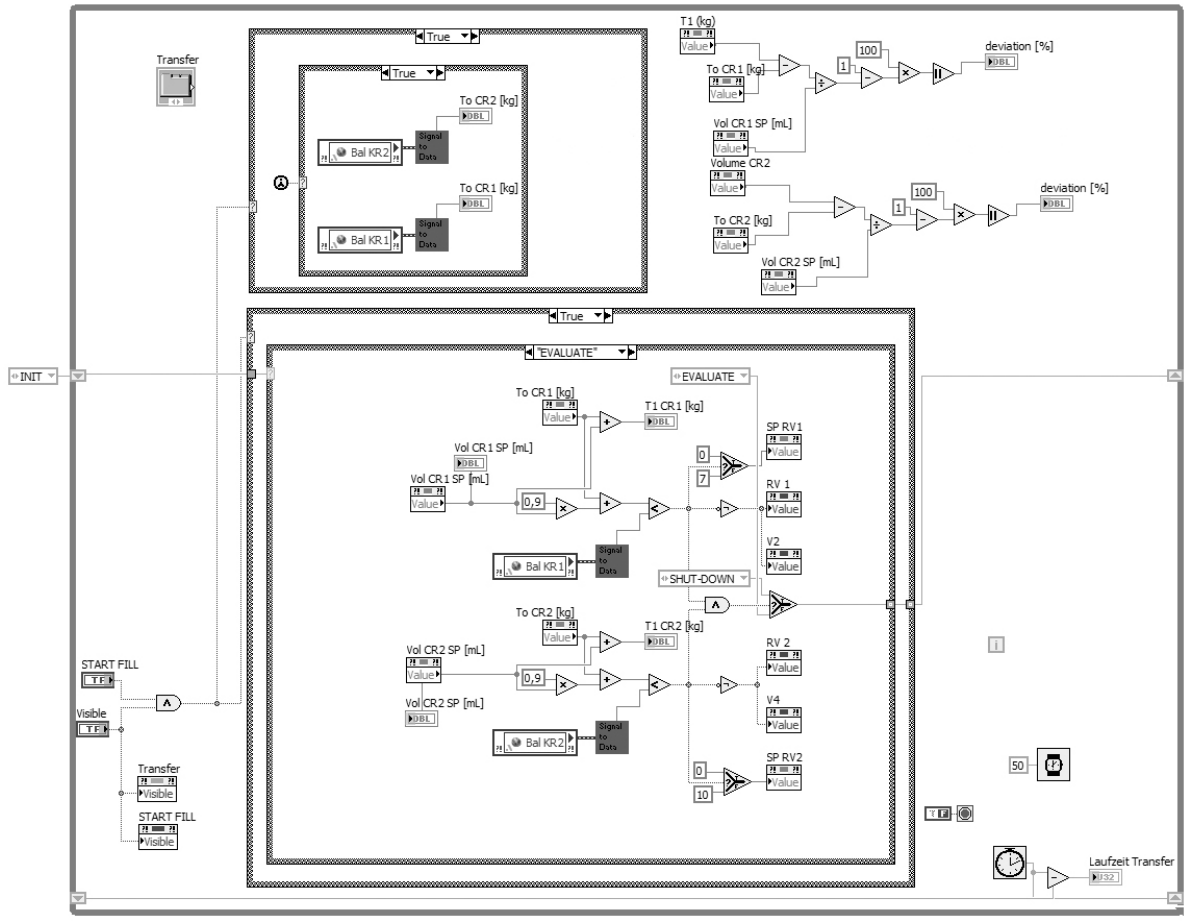

Fig. E.6: Block diagram of the transfer sequence in LabVIEW® used to fill up the cascade reactors (CR) prior start of the circulation process. The actual CRs volumes are read out continuously and compared to the setpoint provided to the regulating vales for level control (upper right hand side). The deviation of both values is then passed to the filling sequence (middle) that controls the incremental opening and closing of the relevant values in correct order. The complete sequence is terminated after reaching a corresponding CR fill level of 90 % of the setpoint to prevent overflow.

After the transfer is completed, the automatic initiation of the circulation is performed by the autostart sequence (Fig. E.7). For the beginning of the culture recycle, all necessary characteristics as the RV and metering diaphragm pump curve (Fig. E.1 and Fig. E.2) are selected according to the desired flow rate of the experiment. Level regulation and control is initiated automatically, whereas the pump speed is only set to the predefined value; regulation and setpoint control can be selected separately (see Fig. 4.12).

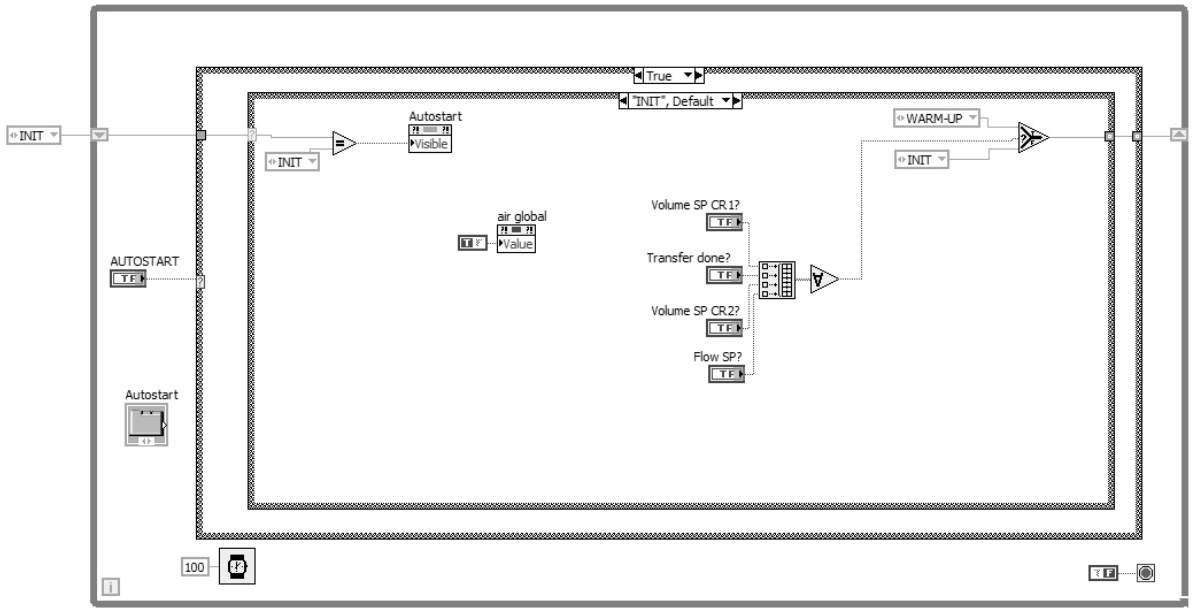

Fig. E.7: Block diagram of the autostart sequence for the initiation of the circulation in LabVIEW®. The sequence defines a "warm-up" phase in which both regulating valves (RV) are fully opened and closed consecutively to improve the accuracy of the starting procedure. Subsequently, the characteristic curves of the metering diaphragm pump and RVs are loaded with respect to the desired flow speed and pump stroke(Fig. E.1 and Fig. E.2), finally leading to the initiation of the circulation process.

Termination of the circulation process can be performed by the shut-down sequence (Fig. E.8) that considers the correct order of the close down, which is restricted to the pumping and RV operation. The standard operation of the three STR (agitation, pressure, pH and pO_2 control, etc.) is further maintained.

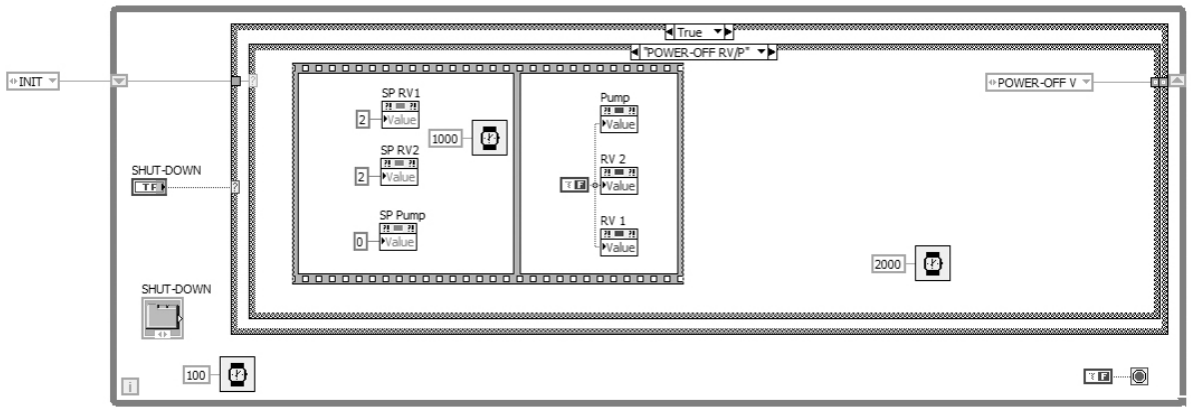

Fig. E.8: Block diagram of the shut-down sequence to terminate the circulation in LabVIEW®. After activation, the circulation mode is switched from automatic to manual processing, enabling the adjustment of the setpoints, and finally switching off all valves and the pump.

F Additional information on the cascade bioreactor system

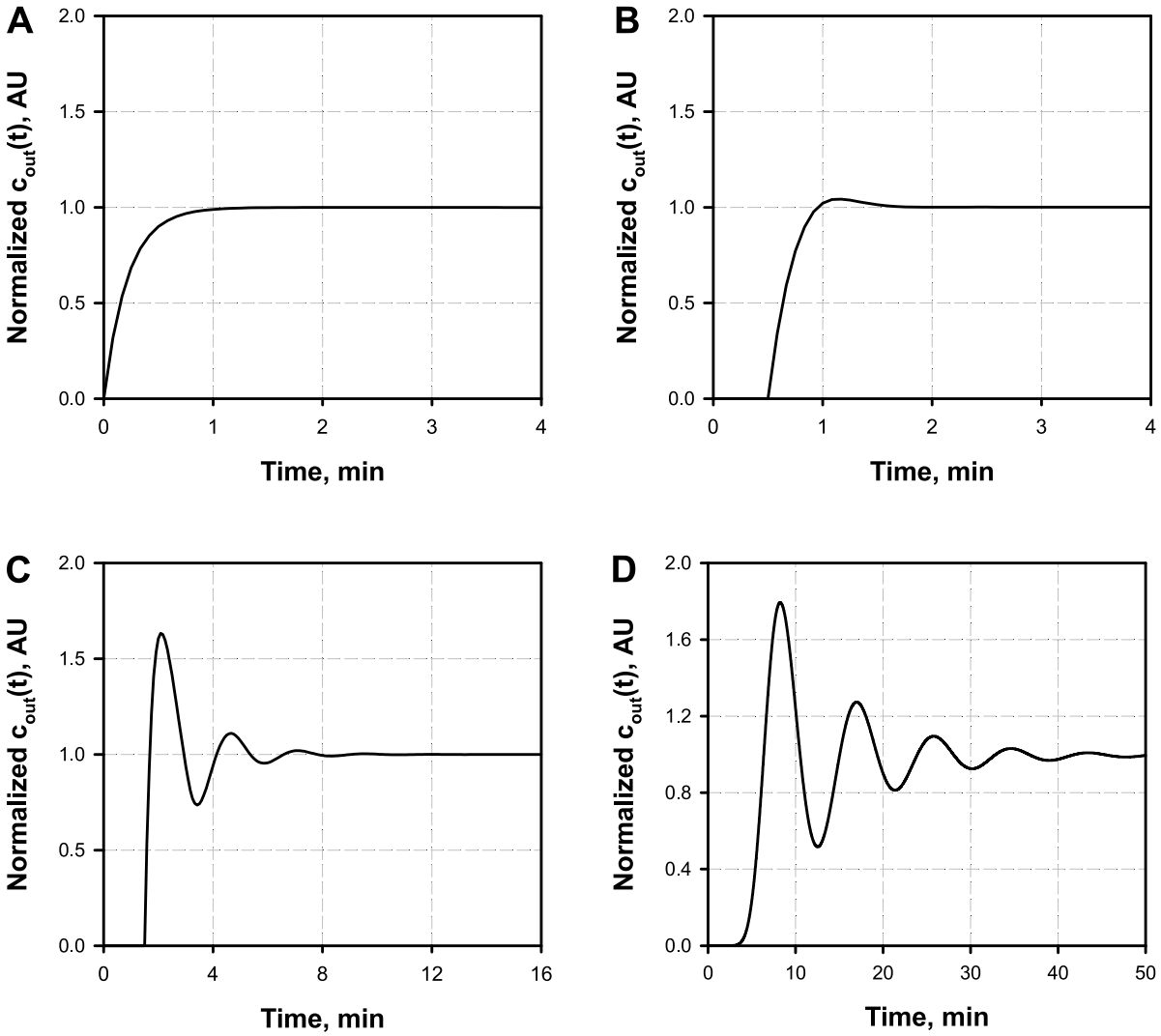

Fig. F.1: Simulation of the output signal of tracer experiments using both cascade reactors in total continuous recycle. **(A–B)** Modeling of ten passes through the two-compartment reactor system with the incremental increase of the dead time (t_{lag}) from 0 min, 0.5 min and 1 min. **(D)** Modeling of 20 passes for 20 CRs in series. (t_{lag} = 0 min). System poles were set equal to space times in all cases.

Tab. F.1: Overview of the theoretical (τ) and fitted ($\bar{t}$) systems poles, as well as dead times (t_{lag}) to determine the transfer function [$G(s)$] that were used to simulate the response curves $c_{out}(t)$ of the cascade bioreactor system under various circulation flows (ν) as illustrated in Fig. 4.18.

	Theoretical poles, min			Fitted poles, min			
ν, L min^{-1}	τ_{MR}	τ_{CR_1}	τ_{CR_2}	$\bar{t}_{MR}$	$\bar{t}_{CR_1}$	$\bar{t}_{CR_2}$	t_{lag}, min
0.58	43.48	1.74	1.74	48.33	1.73	1.73	0.27
2.30	10.87	0.43	0.43	12.10	0.43	0.43	0.13
3.95	6.33	0.25	0.25	7.50	0.25	0.25	0.03

Tab. F.2: Summary of process details of all performed cascade bioreactor system experiments in this study. Where applicable parameters are separately indicated for the main reactor (MR) and both cascade reactors (CR). Culture condition refers to the applied CO_2/HCO_3^- condition with 'standard' (S), 'high' (H), and 'low' (L) levels (section 3.1). All remaining process parameters as T or pH were kept constant throughout the process.

Experiment No.	Test #1	Test #2	#1	#2	#3
Condition †	S–H–L	S–L–L	S–H–H	S–H–H	S–H–H
V_{MR}, L	25	25	25	25	25
V_{CS}, L	2.3	2.3	2.3	2.3	2.3
V_{CR_1}, L	1	0.75	1	1	1
V_{CR_2}, L	0.7	0.75	1	1	1
p_{MR}, bar	2	2	2	2	2
p_{CR_1}, bar	0.6	0.6	0.6	0.6	0.6
p_{CR_2}, bar	0.2	0.2	0.2	0.2	0.2
Q/V_{MR}, vvm	0.3	0.2	0.2	0.2	0.2
Q/V_{CR_1}, vvm	1	2.5	0.3	0.3	0.3
Q/V_{CR_2}, vvm	4	5	1	1	1
CO_2 of CRs‡, % (v/v)	50–70	—	50–70	50–70	40–60
pCO_2 in CR_1*, mbar	≈400	−140	150–300	150–250	150–330
pCO_2 in CR_2§, mbar	≈140	−75	300–400	300–450	300–480

† The circulation experiments 'test run 1–2' and 'number 1–2' were performed with *C. glutamicum* WT and 'number 3' with the L-lysine producer *C. glutamicum* DM1933
‡ Portion of CO_2 in the inlet gas flow of the CRs when the H condition applies
* Detected pCO_2 in the course of the fermentation after initiation of the cascade circulation
§ Detected pCO_2 in the course of the fermentation after initiation of the cascade circulation

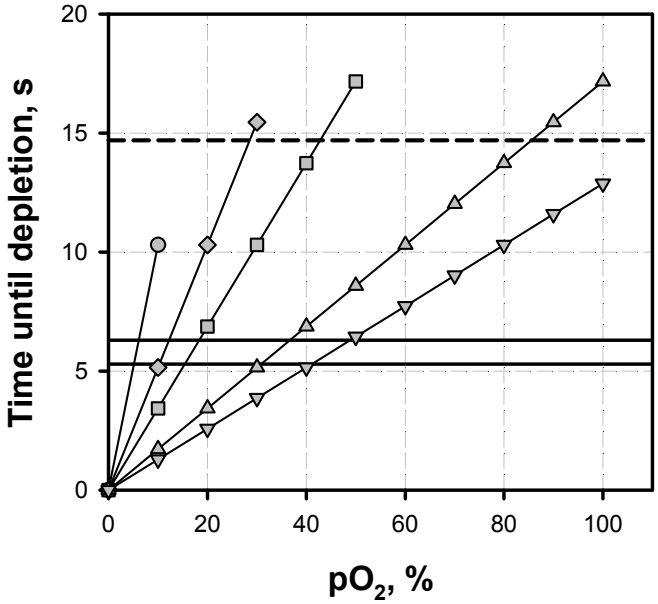

Fig. F.2: Estimated time period until oxygen depletion in the intersections of the cascade bioreactor system during circulation. All values were calculated with a flow rate of $\nu = 0.58\,\mathrm{L\,min^{-1}}$. The flow velocity was calculated on the basis of the pipe dimensions to determine the passage time between the main reactor, cascade reactor 1 (MR ⇒ CR_1; ——), and II (CR_1 ⇒ CR_2; ——), as well as for the backflow (CR_2 ⇒ MR; - - -). The oxygen depletion was estimated for given biomass concentrations of $2.5\,\mathrm{g\,L^{-1}}$ (○), $5\,\mathrm{g\,L^{-1}}$ (◇), $7.5\,\mathrm{g\,L^{-1}}$ (□), $15\,\mathrm{g\,L^{-1}}$ (△), and $20\,\mathrm{g\,L^{-1}}$ (▽). Dissolved oxygen (pO_2) courses (further mass transfer along the pipe neglected) were calculated at a total pressure of 1.5 bar using the Henry constant of oxygen in water at 30 °C, and the experimentally determined oxygen uptake rate of $0.25\,\mathrm{g\,g^{-1}\,h^{-1}}$. Biomass formation was modeled by Monod kinetics using a saturation constant of $K_S = 0.36\,\mathrm{g\,L^{-1}}$ as given by Lindner et al. (2011).

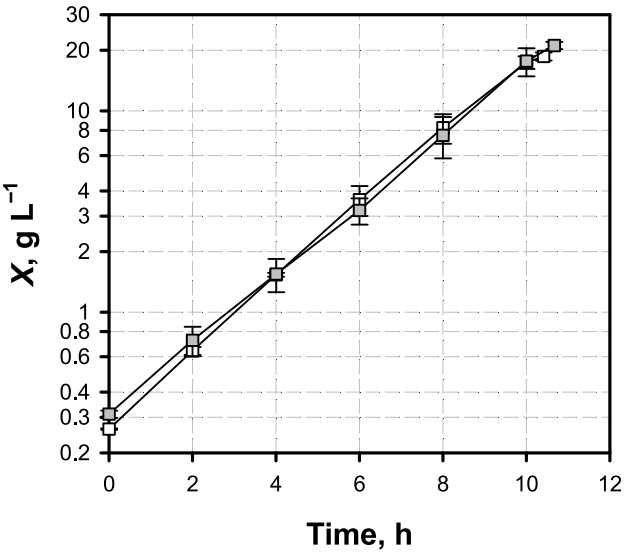

Fig. F.3: Growth comparison of *C. glutamicum* wild-type in batch fermentations performed in the cascade reactor (■) and in the main reactor (□) under described, standard CO_2/HCO_3^- conditions. Values represent the arithmetic mean ±SD of at least three independent experiments.